Vol. 133 No. 3, September 1, 1981 ISSN 0378-4304
(Computer Techniques and Optimization, Vol. 5 No. 3)

ANALYTICA CHIMICA ACTA

International journal devoted to all branches of analytical chemistry

COMPUTER TECHNIQUES AND OPTIMIZATION

ELSEVIER SCIENTIFIC PUBLISHING COMPANY

ANALYTICA CHIMICA ACTA

International journal devoted to all branches of analytical chemistry
Revue internationale consacrée à tous les domaines de la chimie analytique
Internationale Zeitschrift für alle Gebiete der analytischen Chemie

PUBLICATION SCHEDULE FOR 1981 (incorporating the section on Computer Techniques and Optimization)

	J	F	M	A	M	J	J	A	S	O	N	D
Analytica Chimica Acta	123	124/1	124/2	125	126	127	128	129	130/1	130/2	131	132
Section on Computer Techniques and Optimization		133/1			133/2			133/3			133/4	

Scope. *Analytica Chimica Acta* publishes original papers, short communications, and reviews dealing with every aspect of modern chemical analysis, both fundamental and applied. The section on *Computer Techniques and Optimization* is devoted to new developments in chemical analysis by the application of computer techniques and by interdisciplinary approaches, including statistics, systems theory and operation research. The section deals with the following topics: Computerized acquisition, processing and evaluation of data. Computerized methods for the interpretation of analytical data including chemometrics, cluster analysis, and pattern recognition. Storage and retrieval systems. Optimization procedures and their application. Automated analysis for industrial processes and quality control. Organizational problems.

Submission of Papers. Manuscripts (three copies) should be submitted as designated below for rapid and efficient handling:

Papers from the Americas to: Professor Harry L. Pardue, Department of Chemistry, Purdue University, West Lafayette, IN 47907, U.S.A.

Papers from all other countries to: Dr. A. M. G. Macdonald, Department of Chemistry, The University, P.O. Box 363, Birmingham B15 2TT, England.

For the section on *Computer Techniques and Optimization:* Dr. J. T. Clerc, Universität Bern, Pharmazeutisches Institut, Sahlistrasse 10, CH-3012 Bern, Switzerland.

American authors are recommended to send manuscripts and proofs by INTERNATIONAL AIRMAIL.

Submission of an article is understood to imply that the article is original and unpublished and is not being considered for publication elsewhere. Upon acceptance of an article by the journal, the author(s) resident in the U.S.A. will be asked to transfer the copyright of the article to the publisher. This transfer will ensure the widest dissemination of information under the U.S. Copyright Law.

Information for Authors. Papers in English, French and German are published. There are no page charges. Manuscripts should conform in layout and style to the papers published in this Volume. Authors should consult Vol. 121, p. 353 for detailed information. Reprints of this information are available from the Editors or from: Elsevier Editorial Services Ltd., Mayfield House, 256 Banbury Road, Oxford OX2 7DE (Great Britain).

Reprints. Fifty reprints will be supplied free of charge. Additional reprints (minimum 100) can be ordered. An order form containing price quotations will be sent to the authors together with the proofs of their article.

Advertisements. Advertisement rates are available from the publisher.

Subscriptions. Subscriptions should be sent to: Elsevier Scientific Publishing Company, P.O. Box 211, 1000 AE Amsterdam, The Netherlands. The section on *Computer Techniques and Optimization* can be subscribed to separately.

Publication. *Analytica Chimica Acta* (including the section on *Computer Techniques and Optimization*) appears in 11 volumes in 1981. The subscription for 1981 (Vols. 123–133) is Dfl. 1639.00 plus Dfl. 198.000 (postage) (total approx. U.S. $942.00). The subscription for the *Computer Techniques and Optimization* section only (Vol. 133) is Dfl. 149.00 plus Dfl. 18.00 (postage) (total approx. U.S. $86.00). Journals are sent automatically by airmail to the U.S.A. and Canada at no extra cost and to Japan, Australia and New Zealand for a small additional postal charge. All earlier volumes (Vols. 1–121) except Vols. 23 and 28 are available at Dfl. 164.00 (U.S. $84.00), plus Dfl. 13.00 (U.S. $6.50) postage and handling, per volume.

Claims for issues not received should be made within three months of publication of the issue, otherwise they cannot be honoured free of charge.

Customers in the U.S.A. and Canada who wish to obtain additional bibliographic information on this and other Elsevier journals should contact Elsevier/North Holland Inc., Journal Information Center, 52 Vanderbilt Avenue, New York, NY 10017. Tel: (212) 867-9040.

JOURNAL OF ANALYTICAL AND APPLIED PYROLYSIS

his new international journal ings together, in one source, ıalitative and quantitative sults relating to:

Controlled thermal degradation and pyrolysis of technical and biological macromolecules;
Environmental, geochemical, biological and medical applications of analytical pyrolysis;
- Basic studies in high temperature chemistry, reaction kinetics and pyrolysis mechanisms;
- Pyrolysis investigations of energy related problems, fingerprinting of fossil and synthetic fuels, coal extraction and liquefaction products.

The scope includes items such as the following:

1. Fundamental investigations of pyrolysis processes by chemical, physical and physicochemical methods.
2. Structural analysis and fingerprinting of synthetic and natural polymers or products of high molecular weight.
3. Technical developments and new instrumentation for pyrolysis techniques in combination with chromatographic or spectrometric methods, with special attention to automation, optimization and standardization.
4. Computer handling and processing of pyrolysis data.

Pyrolysis is applied in a wide range of disciplines. This journal is therefore of value to scientists in such diverse fields as polymer science, forensic science, soil science, geochemistry, environmental analysis, energy production, biochemistry, biology and medicine.

The journal publishes original papers, technical reviews, short communications, letters, book reviews and reports of meetings and committees. The language of the journal is English. Prospective authors should contact one of the editors.

Subscription Information:
1981: US $86.25/Dfl. 168.00, including postage.

Ask for a free sample copy.

P.O. Box 211,
1000 AE Amsterdam
The Netherlands

52 Vanderbilt Ave
New York, N.Y. 10017

The Dutch guilder price is definitive. US $ prices are subject to exchange rate fluctuations.

ELSEVIER

More and more primary literature? Less and less time to read it?

take TrAC

trends in analytical chemistr

A monthly publication of short, critical reviews and new on trends and developments in analytical chemist

low much better informed 'ou could be if only you had he time to keep up with the atest developments.

'ime we cannot give you, but ve can give you concise, ritical information on what s going on in the analytical ciences. Every month, as it appens.

t's all in TrAC – Trends in nalytical Chemistry – new or the 1980's from Elsevier nd yours now at a low ntroductory rate.

ntroductory Offer

SIXTEEN ISSUES FOR THE PRICE OF TWELVE!

olume 1 – 1981/82 – of **Trends in nalytical Chemistry** will have six- een issues: March 1981 and monthly om October 1981 to December 1982. rder the **Personal Edition** before ecember 1981 and receive all sixteen sues for US $42.50 (USA and Cana- a), £20.00 (UK), 91.50 Dutch guilders* Europe), 95.50 Dutch guilders (else- here). Or order the **Library Edition** r US $133.25 or 260.00 Dutch uilders* throughout the world.

ll issues of both editions are sent by r worldwide.

The Dutch guilder price is definitive.

Take just a minute to order either edition now – you will enjoy the time it saves you later.

ELSEVIER

TrAC is your opportunity to learn from researchers in related fields, to g first-hand, detailed reports on important developments in methodolo and instrumentation. **TrAC** brings you current information on trends a techniques from laboratories all over the world.

Lab managers will find in **TrAC** evaluations of new methods and tec niques which will enable them to make better-informed purchasi decisions. As a training aid **TrAC** is more up-to-date than any textboo

TrAC is written in clear, jargon-free language, avoiding highly specializ terminology and provides you with a working knowledge of relat methodology and techniques.

In every issue you will find:

- short critical reviews written for an interdisciplinary audience
- feature articles
- insights into the function, organization and operation of industria government or research laboratories
- news on topics of general interest
- teaching aids – TrAC is more up-to-date than any textbook
- articles on the history of analytical chemistry
- reports on meetings and book reviews

Trends in Analytical Chemistry comes in either the monthly **Person Edition** or the special **Library Edition** which includes the monthly issu plus a hardbound volume containing all the review articles published ov the year and indexed for easy retrieval.

Order Form

Special Introductory Offer for the Personal Edition valid until December 31, 1981

To **ELSEVIER Dept. TrAC**

P.O. Box 330
1000 AH Amsterdam
The Netherlands

52 Vanderbilt Avenue
New York, NY 10017

US residents may call (212) 867-9040 and charge their American Express, Master Charge or Visa/Bankamericard account.

Yes! Please enter my subscription now – Volume 1 – 1981/82

☐ Personal Edition ☐ Library Edition

I enclose my ☐ personal cheque ☐ bankcheque

Orders from individual subscribers must be prepaid.

☐ Please send me a free sample copy first.

Name: _____ Position: _____ Date: _____

Address: _____

_____

City: _____ State: _____ Postal Code _____

Analytica Chimica Acta, 133 (1981) 215—224
Computer Techniques and Optimization
Elsevier Scientific Publishing Company, Amsterdam — Printed in The Netherlands

POTENTIAL METHODS IN PATTERN RECOGNITION
Part 1. Classification Aspects of the Supervised Method ALLOC

D. COOMANS and D. L. MASSART*

Farmaceutisch Instituut, Vrije Universiteit Brussel, Laarbeeklaan 103, B-1090 Brussel (Belgium)

I. BROECKAERT

Dienst Gastro-Enterologie, Sint Pieter Hospitaal, Hoogstraat 322, B-1000 Brussel (Belgium)

A. TASSIN

Programmeringseenheid Humane Wetenschappen, Vrije Universiteit Brussel, Pleinlaan 2, B-1050 Brussel (Belgium)

(Received 21st January 1981)

SUMMARY

This paper on the application of potential functions in pattern recognition introduces the software package ALLOC to analytical chemistry, emphasizing the methodology of classifying objects. ALLOC is compared with other classification techniques on the basis of two data sets and is shown to perform very well.

Since pattern recognition techniques have been introduced in analytical chemistry, a growing number of successful applications has been found. Some of those techniques, such as the K-nearest neighbour rule (KNN), linear learning machine (LLM), statistical linear discriminant analysis (SLDA) and simple modelling of class analogy (SIMCA) have become more or less standard procedures. Some other supervised techniques such as density-type methods have not yet found application in analytical chemistry. The aim of the present paper is to introduce such a method for purposes of analytical chemistry and to illustrate its performance. The technique concerns a density method using potential functions, which was developed by Hermans and Habbema [1] and commercialized under the name ALLOC. Previously, it has been used mainly for medical diagnostic purposes, for example by Hermans and Habbema [1], Victor [2, 3] and Rioux and Nakache [4]. ALLOC comprises different facilities for supervised pattern recognition such as classification of samples, action-oriented classification and feature selection. In this paper, attention is focused on the first item; the other aspects will be considered in more detail in following papers.

THEORETICAL ASPECTS

The model

In ALLOC, an object of the learning set is considered as a point in the pattern space. Around this point there is a potential field. The highest potential is observed at the position of the object and the potential decreases with distance from the object.

The classification of an object from the test set into one of the learning classes is determined by means of the cumulative potential of the learning class in the position of the test object. The cumulative potential is obtained by adding up the individual potentials developed by the objects of the learning class in the position of the test object. The test object is then classified into the class which gives rise to the largest cumulative potential. The boundary between two classes is given by those positions where the cumulative potential caused by these two classes has the same value. The shape of the potential field depends on the choice of a potential function and a smoothing parameter. Many functions can be used for this purpose [5], but it is recommended for practical reasons, to select a simple one such as a discrete triangular function [2, 3] or a continuous gaussian function [1—4].

Figure 1 illustrates the discrete triangular and the continuous normal function for a learning class ω_p in a one-dimensional space. Together with potential functions arising from the individual points, the cumulative potential function $f(\vec{x}/\omega_p)$ is shown. The cumulative potential function is obtained by moving a test object along the x-axis and adding up the heights of the individual potential functions in each position. Figure 1 shows that the cumulative function constitutes a continuous line which is never zero within a class.

When the pattern space is extended to two dimensions, the cumulative function of each class constitutes a potential surface. For each position in the 2-dimensional pattern space, the degree of membership of a class is given by the height of the potential surface above the plane of the pattern space. Clearly, the model can be extended mathematically to higher dimensional pattern spaces, developing so-called potential hypersurfaces.

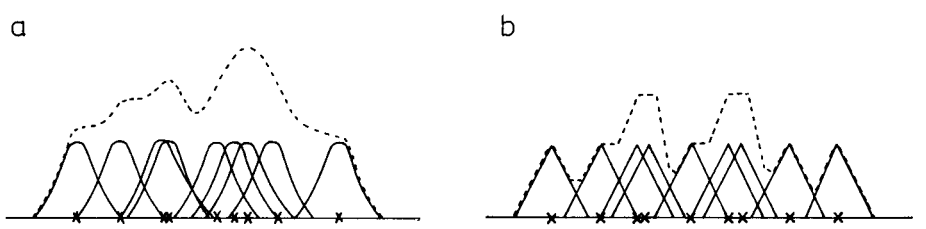

Fig. 1. Density estimation for a learning class ω_p using (a) normal and (b) triangular individual potential functions. The dotted line indicates the cumulative potential function $f(\vec{x}/\omega_p)$.

In ALLOC, the gaussian potential function is applied because experience has shown that continuous potential functions are always as good as discrete functions and often better [2]. A second parameter which has to be chosen is a smoothing parameter. This depends on the data set investigated. When the smoothing parameter is too small (Fig. 2a), most of the individual potential functions of a learning class do not overlap with each other and consequently the continuous potential surface of Fig. 1 is not obtained. In such a situation, a test object (x_i in Fig. 2a) which clearly belongs to a certain learning class, may seem to have a low degree of membership. But an excessive smoothing parameter gives rise to potential surfaces which are much too flat (Fig. 2b), so that discrimination between adjoining classes is difficult. The major task of the learning procedure in ALLOC is the selection of a suitable smoothing parameter.

The potential surface is defined above, for simplicity, by means of a cumulative potential function. In ALLOC, the potential surface is actually defined as the mean potential function instead of the cumulative function. Such a potential function assumes then a probabilistic character and may also be termed a probability function. Analogously to the cumulative function, the degree of membership of a test object with a class is given by the value of the probability function at that point. In this way, the potential method permits probabilistic classifications.

In probabilistic classifications it is also very important to obtain a consistent unbiased estimate of the probability density function $f(\vec{x}/\omega_p)$ of each

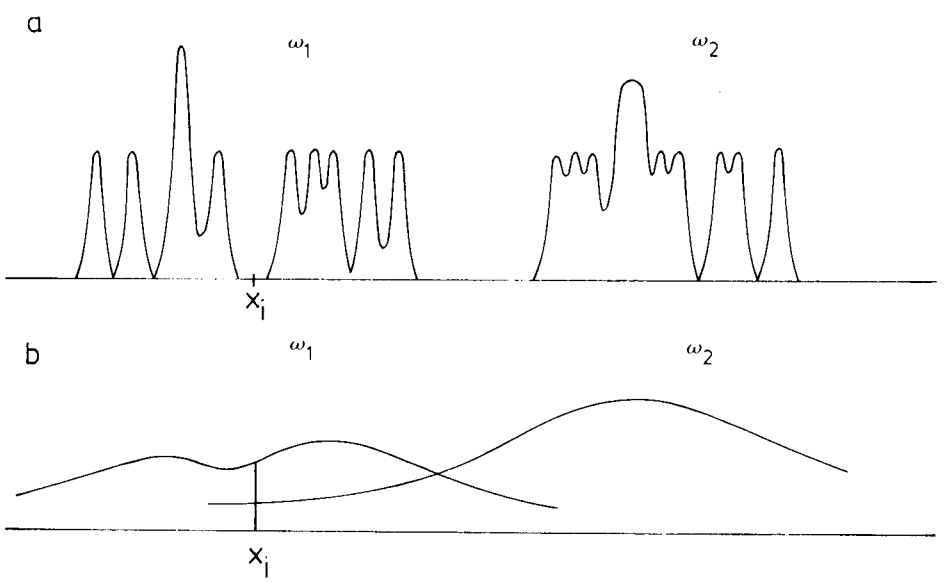

Fig. 2. The influence of the smoothing parameters of the potential function on the potential surfaces of two classes ω_1 and ω_2 and on the potential in the position x_i: (a) small smoothing value; (b) large smoothing value.

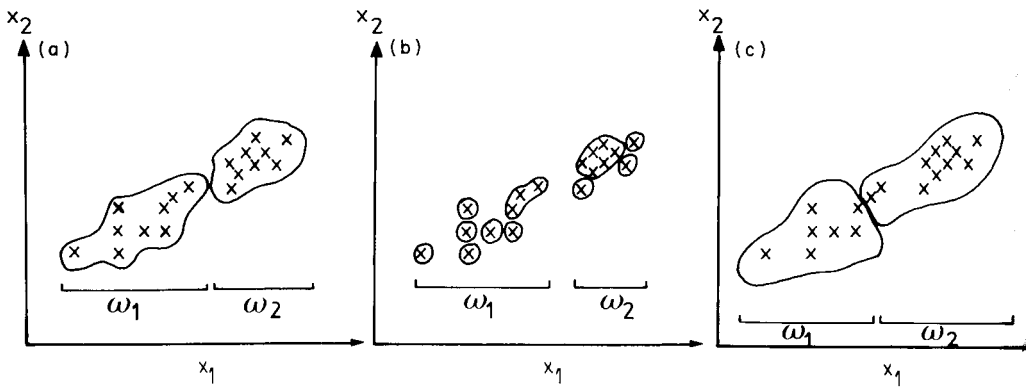

Fig. 3. The influence of the smoothness of the potential functions on the probability density surfaces and the position of the boundaries between two learning classes ω_1 and ω_2 is illustrated by contour diagrams with $P(\vec{x}/\omega_1) = P(\vec{x}/\omega_2)$ = constant. (a) Smoothing parameters are appropriate; (b) smoothing parameters are too small; (c) smoothing parameters are too large.

learning class ω_p. Figure 3 illustrates the influence of the smoothing parameter on the probability density surfaces of two learning classes in a two-dimensional pattern space on the basis of contour diagrams with $f(\vec{x}/\omega_1) = f(\vec{x}/\omega_2)$ = constant. When the smoothing parameters are too small (b), a sequence of peaks is obtained. But when the smoothing parameters are too large (c), an irrelevant distinction is obtained between the classes. A biased decision boundary occurs in Fig. 3(c). The boundary separates two objects of ω_1 from this class; objects from the more diffuse group are located in the more compact one. The optimal situation is illustrated in Fig. 3(a) Some criteria have been proposed for optimal estimation of the smoothing parameters [1, 4, 6].

Probabilistic decisions

A density estimation technique is designed to make decisions in a probabilistic way and may consequently be used in connection with the Bayes equation. This equation in a general form is written as follows:

$$P(\omega_p/\vec{x}_i) = P(\omega_p)\, P(\vec{x}_i/\omega_p) \Big/ \sum_{q=1}^{L} P(\omega_q)\, P(\vec{x}_i/\omega_q) \qquad (1)$$

where $P(\omega_p/\vec{x}_i)$ is the a posteriori probability that a test object i presenting a pattern vector $\vec{x}_i$ belongs to class ω_p; $P(\vec{x}_i/\omega_p)$ or $P(\vec{x}_i/\omega_q)$ is the probability density of class ω_p or ω_q (both belonging to the set of L classes of the classification problem) in the position x_i of the pattern space; and $P(\omega_p)$, $P(\omega_q)$ are the a priori probabilities of ω_p and ω_q, respectively.

In a classification problem using a probabilistic decision rule, object i is assigned to the class with the largest a posteriori probability.

Density estimation

Probabilistic pattern recognition techniques differ according to the way of estimating the probability densities for the classes $P(\vec{x}_i/\omega_p)$; $p = 1, \ldots, L$. The method presented here is a direct non-parametric technique.

A parametric technique assumes a known distribution function $f(\vec{x}/\omega_p)$ for each class, from which the probability that $\vec{x}_i$ belongs to a certain class may be derived by substituting the measurements of $\vec{x}_i$ in the equation of the function. This can be defined as indirect. In practical situations, the restrictions associated with parametric techniques are often not fulfilled. Therefore a non-parametric approach is of more interest in analytical chemistry. A well-known non-parametric estimation of $P(\vec{x}_i/\omega_p)$ $p = 1, \ldots, L$ is obtained by means of histograms. Such a method was implemented in the routine BAYES of the software package ARTHUR [7].

In univariate statistics, frequency histograms are frequently used to visualize the sample distribution of a variable. The same concept may be used and extended to divide the domain of a class in the pattern space in a number of subregions. The proportion of learning objects from the given class in such a subregion is an estimate of the probability density for that class in that subregion. In this way, $P(\vec{x}_i/\omega_p)$ is estimated indirectly, because $\vec{x}_i$ is related to a previously fixed subregion. The estimated probability densities of a class do not build up a continuous probability surface. Moreover, the probability value is independent of the position within the subregion. This is a disadvantage because the domain of a class is usually divided into subregions of equal size. This subdivision is artificial because in this way a possible heterogeneous distribution of the learning objects in a class is not considered. An illustration is given in Fig. 4, which shows that object i, which belongs to subregion V is in fact closer to some members of other subregions than to members of the subregion into which it is classified. A further division of the subregions may, at first sight, seem to be a good solu-

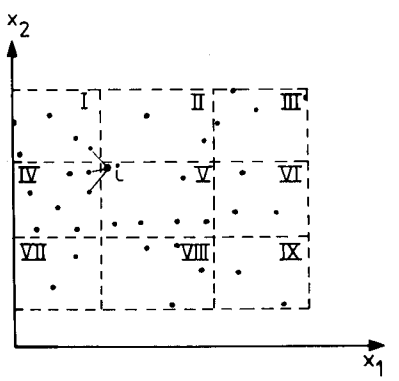

Fig. 4. An illustration of the shortcomings of the density estimation using multivariable histograms (here bivariate); all points belong to a class ω_1 which is divided in 9 subregions I–IX; the probability density in position i is required. It can be seen that i is more related to other subregions than the one in which it is classified.

tion, but it is necessary to beware of the decrease of relevance when the number of objects decreases in the subregions. A fixed subregion concept is therefore better replaced by a more flexible concept which determines the probability densities directly with regard to the position of $\vec{x}_i$. This may be done by means of a nonparametric direct-density estimation such as is offered by the ALLOC program.

Density estimation with potential functions

The probability density in $\vec{x}_i$ for a given learning class ω_p containing n_p samples is obtained by creating individual potential fields or kernels around each learning-sample point $\vec{x}_j^{(p)}$ and averaging the n_p different potential influences in the position $\vec{x}_i$. The influence of the potential field of $\vec{x}_j^{(p)}$ on $\vec{x}_i$, i.e., the contribution of $\vec{x}_j^{(p)}$ to the probability density $P(\vec{x}_i/\omega_p)$, is given by $\phi(\vec{x}_i, \vec{x}_j^{(p)})$, the potential function. Theoretically it is impossible to obtain a probability density in a point $\vec{x}_i$. Therefore the density is referred to an infinitesimally small hypercube with sides dx; the smallest angular point vector corresponds to $\vec{x}_i$ and the largest to $\vec{x}_i + d\vec{x}$. The probability density is then

$$P(\vec{x}_i/\omega_p) = f(\vec{x}_i/\omega_p)\, d\vec{x} \tag{2}$$

with

$$f(\vec{x}_i/\omega_p) = (1/n_p) \sum_{j=1}^{n_p} \phi(\vec{x}_i, \vec{x}_j^{(p)}) \tag{3}$$

The shape of the function may be any probability distribution function. It is however necessary that the function be symmetric and centered in $\vec{x}_j^{(p)}$ in order to avoid biased estimates. As mentioned earlier, ALLOC applies the normal function. The general equation of an R-variate gaussian potential function for a learning sample $\vec{x}_j^{(p)}$ is

$$\phi(\vec{x}, \vec{x}_j^{(p)}) = [(2\pi)^{R/2} |\sum_p|^{1/2}]^{-1} \exp\{-\tfrac{1}{2}(\vec{x} - \vec{x}_j^{(p)})' \sum_p^{-1} (\vec{x} - \vec{x}_j^{(p)})\} \tag{4}$$

where the prime (′) indicates the transpose of vector $\vec{x} - \vec{x}_j^{(p)}$ and $|\Sigma_p|$ is the determinant of matrix Σ_p.

For simplicity, the multivariate function does not take into account correlated coordinates and Σ_p consequently is a diagonal matrix. Although eqn. (4) resembles a statistical gaussian distribution, Σ_p is in fact a set of adjustable smoothing parameters. Once the shape of a function has been selected, suitable values for the smoothing parameters have to be chosen.

In ALLOC, the smoothing parameter matrix Σ_p for each class ω_p is given by

$$\Sigma_p = c_p^2 \cdot \begin{bmatrix} s_{p1}^2 \ldots & 0 & \ldots & 0 \\ \vdots & \vdots & & \vdots \\ 0 \ldots & s_{pk}^2 \ldots & & 0 \\ \vdots & \vdots & & \vdots \\ 0 \ldots & 0 & \ldots & s_{pR}^2 \end{bmatrix}$$

where s_{pk}^2 is the sample variance obtained from the objects of learning class ω_p for variable k. In this way the smoothing parameters are made proportional to the distribution of the variables; this is really a form of scaling of the data. One adjustable smoothing parameter c_p^2 for each learning class ω_p is estimated by a jack-knife maximum likelihood method [8]. A more detailed treatment of density estimation using potential functions may be found in the books by Meisel [6] and Duda and Hart [5].

Relation with other classification techniques

In ALLOC no assumptions are made about the distribution of the objects in the learning classes such as in SLDA [9, 10], or about the shape and the homogeneity of the learning classes such as in SIMCA [11]. No linear separability is required such as in LLM [6, 12]. In this respect, ALLOC is very similar to KNN [13]. In fact, KNN may be considered as a simplification of a direct-density estimation technique. When KNN is extended by taking the distance between $\vec{x}_i$ and the K'th neighbour into consideration, continuous probability surfaces related to those of ALLOC may be obtained. Extensions of KNN are for example the KnNN rule of Loftsgaarden and Quesenberry [14] and the KNN_3 rule of Patrick and Fisher [15].

DATA SETS AND COMPUTER PROGRAMS

ALLOC was applied to two data sets with continuous variables. No missing data were present. These data were chosen because classification results obtained by standard pattern recognition techniques are available.

The first set is concerned with the taxonomy of iris species (IRIS). Fisher's iris data [16] are often used as standard data for the comparison of classification models. The problem is to distinguish three classes of species of iris (each containing 50 samples) on the basis of four variables. To be comparable with the classification results of Sjöström and Kowalski [17] and Wold [11], the data were divided into a learning set and a test set as described by Wold [11].

The second set is related to the functional state of the thyroid gland (THYROID). This set comprises data from 215 patients from the same hospital [18]. For each patient 5 measurements were available (i.e., the laboratory tests RT3U, T4, T3RIA, TSH and ΔTSH). The individuals were divided into 3 diagnostic groups: (a) patients with normal thyroid function (EU: 150 cases); (b) patients suffering from a hyper-active gland (HYPER: 35 cases); (c) patients suffering from a hypo-active gland (HYPO: 30 cases). This three-fold classification problem was divided into two binary subproblems: the HYPO/EU and the HYPER/EU differentiation, for reasons mentioned earlier [18].

The software package ALLOC [1] is very attractive because it contains not only decision rules but also a feature-selection procedure. The package is written in Fortran IV and is designed for running on a IBM 370/158 com-

puter. However, implementation on a CDC CYBER 170/750 computer presented no difficulties.

For the data set THYROID, ALLOC was compared with the classification procedures BAYES, KNN and LLM available in the software package ARTHUR [6] and SLDA available in the software package SPSS [19].

RESULTS AND DISCUSSION

IRIS identification

In Table 1 the classification results obtained with ALLOC are given together with those published by Sjöström and Kowalski [17] for BAYES, KNN, SLDA, LLM and SIMCA. The results for the test set show that ALLOC performs as well as, or better than, the other techniques.

Another way to compare the techniques is to observe the misclassifications in the pattern space. To make visualization of the 4-dimensional space possible, the canonical variates determining the discriminant space obtained by SLDA are given. Although we were not interested in the first class (nos. 1—50) of the IRIS data set (no overlapping was observed with the other classes) the discriminant axes had to be calculated for the 3 classes to obtain a 2-dimensional display. On the SLDA diagram in Fig. 5, acceptable boundaries can be observed for SIMCA, ALLOC and of course SLDA. It is not possible to trace a boundary between the two classes for LLM, KNN and BAYES (autoscaled data) in the same way and the misclassifications for BAYES (orthogonal features) are really surprising: it differs very much from the other techniques. In that respect, ALLOC and SIMCA seem to be somewhat more related to SLDA than KNN and LLM.

THYROID identification

Table 2 summarizes the classification results of the HYPER/EU and HYPO/EU discrimination for six classification procedures. The pattern

TABLE 1

Comparison of the classification results (in %) for Fisher's IRIS data of ALLOC with other methods as reported by Sjöström and Kowalski [17]. The numbers between brackets identify the wrongly allocated objects.

Method	Learning set	Test set
ALLOC[a]	97 (71, 120)	96 (128, 134, 139)
BAYES (autoscaled data)	96 (73, 107, 120)	93 (78, 127, 134, 135, 139)
BAYES (orthogonal features)	100	91 (78, 88, 89, 134, 139, 147, 150)
KNN, $N = 3$	97 (107, 120)	93 (84, 134, 135, 139, 150)
SLDA	99 (71)	96 (84, 130, 134)
LLM	100	92 (42, 126, 130, 132, 134, 135)
SIMCA ($A = 2$)	97 (69, 71)	95 (84, 130, 132, 134)

[a] $c_1 = 0.8$, $c_2 = 0.6$, $c_3 = 0.7$.

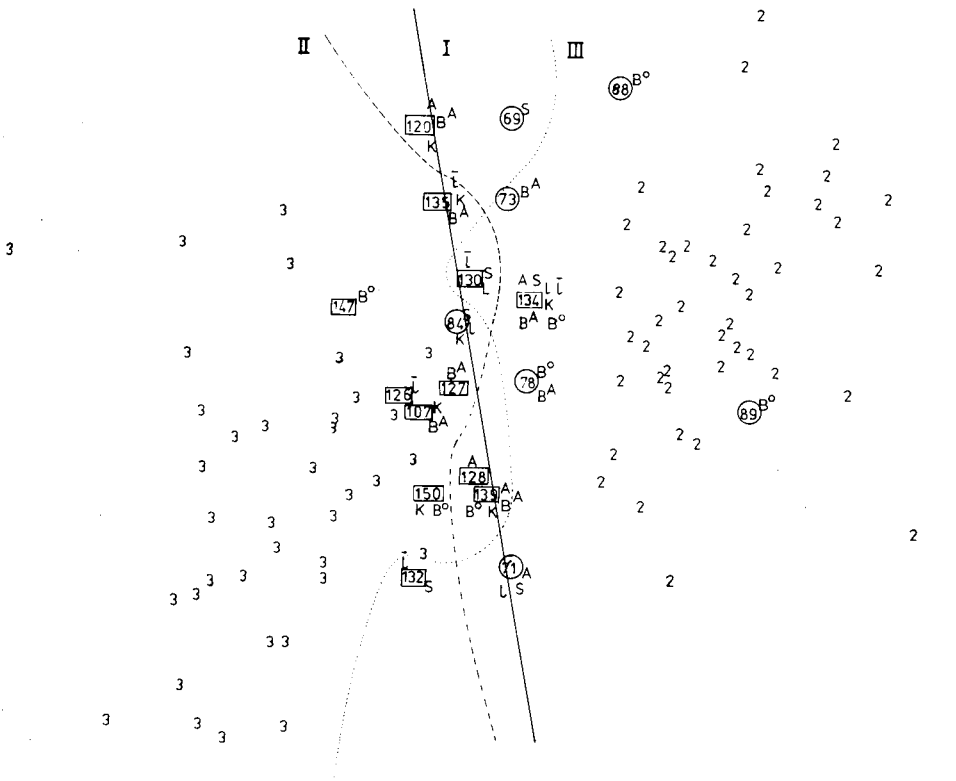

Fig. 5. SLDA map of class 2 (nos. 51—100) and 3 (nos. 101—150) of Fisher's IRIS data with indication of the boundaries for (I) SLDA, (II) ALLOC and (III) SIMCA, and indication of the members which were wrongly classified by various pattern recognition techniques: (A) ALLOC, (B^A) BAYES (autoscaled data), (B^0) BAYES (orthogonal data), (K) KNN, (L) SLDA, ($\bar{L}$) LLM and (S) SIMCA. Ringed numbers are wrongly classified members of class 2; boxed numbers are wrongly classified members of class 3.

recognition techniques were applied once on the entire data set and once after random separation into a learning set and a test set. Comparison with the other techniques shows that ALLOC yields a good separation in both problems HYPER/EU and HYPO/EU and that it performs at least as well as most other techniques.

Conclusions

A direct density method such as ALLOC has the advantage that probabilistic decisions can be made without there being any obligation to make assumptions about the structure of the learning classes. In conclusion, it can be stated that in level 1 sense of pattern recognition [20] ALLOC performs very well in comparison with other supervised pattern recognition techniques. It seems therefore of interest to evaluate ALLOC further on more data bases to decide whether it is only as good as or, as we think, better than other first level pattern recognition techniques.

TABLE 2

Classification results (in %) of THYROID data [18]

	Entire set			Learning set			Test set		
	EU	HYPER	MEAN	EU	HYPER	MEAN	EU	HYPER	MEAN
ALLOC	99	97	98	96	96	96	100	100	100
SLDA	100	91	95.5	100	92	96	100	90	95
BAYES (autoscaled data)	98	94	96	98	96	97	98	90	94
BAYES (5 orthogonal features)	98	91	94.5	98	92	95	98	80	89
KNN ($N = 1$)	99	94	96.5	99	92	95.5	100	90	95
LLM	100	100	100	100	100	100	100	100	100
	EU	HYPO	MEAN	EU	HYPO	MEAN	EU	HYPO	MEAN
ALLOC	99	87	93	99	80	89.5	98	100	99
SLDA	100	80	90	100	90	95	100	90	85
BAYES (autoscaled data)	100	80	90	100	75	87.5	100	80	90
BAYES (5 orthogonal features)	98	70	84	99	85	92	100	60	80
KNN ($N = 1$)	100	93	96.5	97	95	96	100	100	100
LLM	100	100	100	100	100	100	96	100	98

The authors appreciate technical help by M. Devreese, A. Van der Straeten and M. De Troyer.

REFERENCES

1 J. Hermans and J. D. F. Habbema, Manual for the ALLOC-discriminant analysis program. Department of Medical Statistics, University of Leiden, P.O. Box 2060 Leiden, The Netherlands, 1976.
2 N. Victor, Metamedicine, 1 (1980) 85.
3 N. Victor, Meth. Inform. Med., 17 (1978) 120.
4 P. Rioux and J. P. Nakache, Comp. Prog. Biomed., 10 (1974) 43.
5 R. O. Duda and P. E. Hart, Pattern Recognition and Scene Analysis, Wiley, Interscience, New York, 1973.
6 W. S. Meisel, Computer-oriented Approaches to Pattern Recognition, Academic Press, New York, 1972.
7 D. L. Duewer, J. R. Koskinen and B. R. Kowalski, ARTHUR (available from B. R. Kowalski).
8 G. T. Toussaint, IEEE Trans. Inf. Teor., II-20 (1974) 472.
9 D. Coomans, L. Kaufman and D. L. Massart, Anal. Chim. Acta, 112 (1979) 97.
10 H. E. Solberg, CRC Crit. Rev. Clin. Lab. Sci., (1978) 209.
11 S. Wold, Pattern Recognition, 8 (1976) 127.
12 N. J. Nilsson, Learning Machines, McGraw-Hill, New York, 1965.
13 B. R. Kowalski and C. F. Bender, Anal. Chem., 44 (1972) 1405.
14 D. O. Lofsgaarden and C. P. Quesenberry, Am. Math. Statist., 36 (1965) 1049.
15 E. A. Patrick and F. P. Fisher, Inf. Control, 16 (1970) 128.
16 R. A. Fisher, Ann. Eugenetics, 7 (1936) 179.
17 M. Sjöström and B. R. Kowalski, Anal. Chim. Acta, 112 (1979) 11.
18 D. Coomans, I. Broeckaert, M. Jonckheer, P. Blockx and D. L. Massart, Anal. Chim. Acta, 103 (1978) 409.
19 N. N. Nie, C. H. Hull, J. G. Jenkins, K. Steinbrenner and D. Bent, Statistical Package for the Social Sciences (SPSS), McGraw-Hill, New York, 1975.
20 C. Albano, W. Dunn, U. Edlund, E. Johansson, B. Norden, M. Sjöström and S. Wold, Anal. Chim. Acta, 103 (1978) 429.

Analytica Chimica Acta, 133 (1981) 225—239
Computer Techniques and Optimization
Elsevier Scientific Publishing Company, Amsterdam — Printed in The Netherlands

POTENTIAL METHODS IN PATTERN RECOGNITION
Part 2. CLUPOT — an Unsupervised Pattern Recognition Technique

D. COOMANS and D. L. MASSART*

Farmaceutisch Instituut, Vrije Universiteit Brussel, Laarbeeklaan 103, B-1090 Brussel (Belgium)

(Received 25th March 1981)

SUMMARY

The applicability of potential functions in unsupervised pattern recognition is demonstrated on the basis of a new clustering technique called CLUPOT. CLUPOT is a centrotype sorting technique which means that for each detected cluster of objects a representative object can be selected. CLUPOT uses a reliability curve which permits the detection of significant clusters. Applications to four data sets (Kowalski's archeological artefact data, Ruspini's fuzzy set data, Fisher's Iris data and a part of Esbensen's meteorite data) show that CLUPOT yields significant clusterings.

Although unsupervised pattern recognition is of special interest in some problems of data analysis there are not many applications in analytical chemistry. Unsupervised pattern recognition deals with the interpretation of the structure in a data matrix. The data matrix consists of many features (measurements) for many objects (samples, patients, analytical procedures...). The aim is to understand the relationship between either the objects or the features. This means that a priori division into classes such as in supervised pattern recognition is not assumed.

In the present paper, a new clustering procedure, CLUPOT, is described and considered for two types of application: (1) the detection of subsets or clusters of objects (or of features) which are clearly more related to each other than to the other objects of the data set; and (2) the selection of a small number of objects (or features) which represent the classes present in the data set as truly as possible.

THE MODEL AND ITS UNDERLYING PHILOSOPHY

In the same way as for the supervised learning technique ALLOC [1], a potential surface is constructed by averaging individual gaussian potential functions which are centered in the points of interest. If one is interested in the relationship between the objects of a data matrix, the points of interest are the objects positioned in a pattern space with the features as axes (object or measurement space). In contrast, if one is interested in the

relationship between features, the points of interest are the positions of the features in a pattern space with the objects as axes (feature space). Only the classification of objects will be considered here. However, features can be classified in exactly the same way. In contrast to ALLOC and because of the unsupervised character of CLUPOT, only one potential surface is constructed for the whole data set.

The basic clustering principle of CLUPOT is illustrated in Fig. 1 for a one-dimensional example. It can be formulated as follows. When the data set is heterogeneous and consequently the points in the pattern space are not homogeneously distributed but occur as clusters, the potential surface will take the form of a landscape with peaks, each of which defines a cluster. The objects situated within such a peak are the members of the cluster and the object presenting the largest average potential is called the cluster centrotype. In fact, CLUPOT does not describe the complete potential surface in order to find clusters because this would be uneconomic with respect to computer time. Moreover, the exact definition of the position in the space of the peaks by means of boundaries is seldom of interest. The object of CLUPOT is therefore only to decide which object belongs to which cluster centrotype, using its average potential to make this decision.

First, the average potential is computed for all the objects of the data set. Then the object presenting the largest average potential is selected as the cluster centrotype of a first cluster. The objects belonging to this cluster are found by moving from the cluster centrotype down the peak until objects are encountered that again present higher average potentials. This means that a new peak is then climbed. The objects belonging to the first cluster are those with decreasing average potential encountered when moving away from the centrotype. The objects of this first cluster are removed from the data set and one selects as the second cluster centrotype the object which represents the largest average potential of the remaining objects. The members of this second cluster are selected in the same way as those of the first cluster. The procedure proceeds until all the objects have been allocated to a cluster. The number of clusters (peaks) that are found depends not only on the structure of the data set but also on the selection of a smoothing parameter α, which determines the sharpness of the individual potential

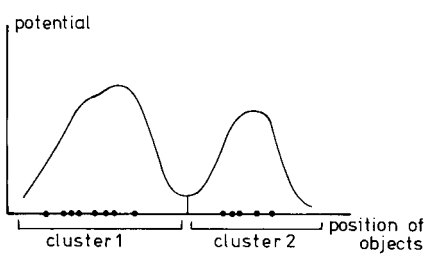

Fig. 1. Illustration of the basic clustering principle of CLUPOT for a one-dimensional example.

functions. Figure 2 shows the influence of α on the number of peaks on the potential surface for a two-dimensional pattern space. When α is very small (2a), all objects are found as individual clusters, i.e., there are as many peaks as objects, but when the α value is large enough (2d), the whole data set forms a single cluster. Between these two extreme α values intermediate solutions (2b and c) are obtained.

Significant clusters are then defined as clusters which are more or less resistant to some degree of variation of smoothing parameter α. Figure 3 shows how the number of significant clusters may be observed on a plot of the number of clusters versus the smoothing parameter α; this curve is called hereafter the reliability curve. Starting with a small α value (position A, in Fig. 3) where many clusters are present, a very fast decrease in the number of clusters occurs when the α value decreases. From a given α value (position B, Fig. 3) the number of clusters does not change over a certain interval of α. This indicates a significant number of clusters.

The concept of reliability curves in other clustering methods has been

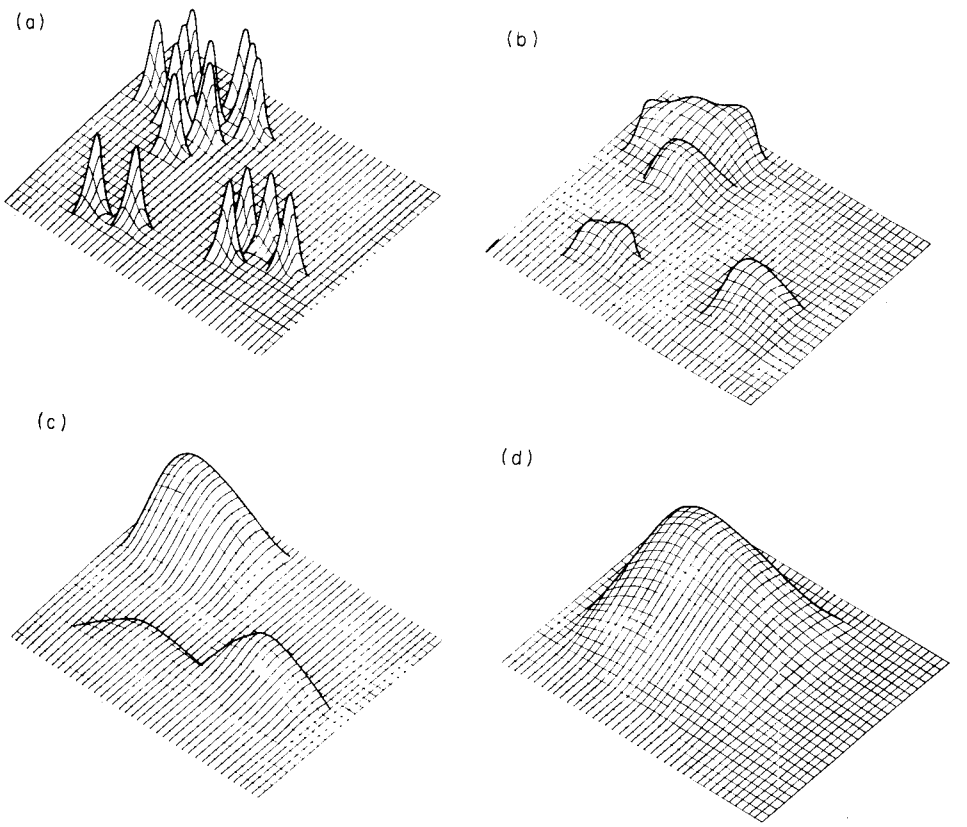

Fig. 2. Influence of the smoothing parameter α on the number of peaks in the potential surface for a two-dimensional pattern space. The value of α increases from a to d.

proposed and evaluated by Andrews [2], Thorndike [3] and Gower [4], for example. Applications in chemistry which use plots related to the reliability curve are for instance the selection of significant clusters in the classifications of glasses on the basis of their chemical constitution [5] and the classification of chemical substituents on the basis of physicochemical properties [6].

Figure 4 shows the difference between a reliable (a) and an unreliable (b) clustering.

DETAILED DESCRIPTION

Potential surface

N objects have to be clustered and K features are available for each object. First, the average potential ψ_i for each object is computed. ψ_i is the average of the potential influences of all objects on object i. The potential influence $\Phi_{i,j}$ of object j on i is the value of the potential function of j in the position of i.

The average potential ψ_i is then given by

$$\psi_i = N^{-1} \sum_{j=1}^{N} \Phi_{i,j} \tag{1}$$

with

$$\Phi_{i,j} = [(2\pi)^{K/2} \cdot \alpha^K]^{-1} \exp [-(2\alpha^2)^{-1} \sum_{k=1}^{K} (x'_{ki} - x'_{kj})^2] \tag{2}$$

where α is the smoothing parameter and x'_{ki} and x'_{kj} are the kth features for objects i and j, respectively. In CLUPOT x'_{ki} and x'_{kj} are usually standardized data but the raw data x_{ki} and x_{kj} may also be used. The standardization is obtained by

$$x'_{ki} = (x_{ki} - \bar{x}_k)/\sigma_k \tag{3}$$

where

$$\bar{x}_k = N^{-1} \sum_{i=1}^{N} x_{ki} \text{ and } \sigma_k = [\sum_{i=1}^{N} (x_{ki} - \bar{x}_k)^2 (N-1)]^{1/2}$$

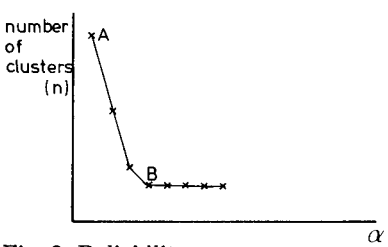

Fig. 3. Reliability curve.

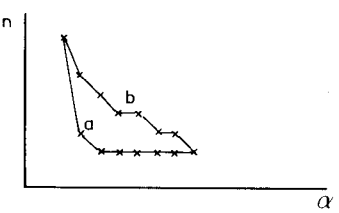

Fig. 4. Reliable (a) and unreliable (b) clustering.

The values of the potential influence $\Phi_{i,j}$ range from 0 to $[(2\pi)^{K/2} \cdot \alpha^K]^{-1}$. The first value is obtained when object j is infinitely distant from object i and the latter when object j is found in exactly the same place as i.

Clustering with fixed smoothing parameter α

One starts with a no-cluster ($\bar{n}$ Cl_0) situation. All the objects are in the set $\bar{n}$ Cl_0. In the first step the objects of $\bar{n}$ Cl_0 are classified either in cluster 1 (Cl_1) or not in cluster 1 ($\bar{n}$ Cl_1). In the second step the no-cluster situation $\bar{n}$ Cl_1 is divided into $\bar{n}$ Cl_2 and Cl_2. The procedure is continued until all objects belong to a cluster.

Each step of the clustering procedure starts with the selection of the centrotype of the cluster. For example, in step d, the object of $\bar{n}$ Cl_{d-1} with

$$\psi = \max \psi_i \ (i = 1,\ldots,N_{d-1}) \tag{4}$$

is the centrotype and is placed as the first one in Cl_d. The other members of $\bar{n}$ Cl_{d-1} are partitioned between $\bar{n}$ Cl_d and Cl_d. For this purpose three algorithms are used: the sequence algorithm, the selection algorithm and the classification algorithm.

Algorithms

Sequence algorithm. The objects of $\bar{n}$ Cl_{d-1} are subjected in a given sequence to the selection and classification algorithms. The objects are arranged according to decreasing potential influence of the centrotype c. In this way, the first object (assume it is s) with

$$\Phi_{s,c} = \max \Phi_{j,c} \ (j = 1,\ldots,N_{d-1} \text{ and } j \neq c) \tag{5}$$

is subjected first to the selection and classification algorithms.

Selection algorithm. In order to classify an object, it is compared with reference object p and classified accordingly. The selection algorithm is formulated as follows: the reference object p is an object already classified in either $\bar{n}$ Cl_d or Cl_d which corresponds to the largest influence:

$$\Phi_{s,p} = \max \Phi_{s,j} \ (j = 1,\ldots,N') \tag{6}$$

where N' is the total number of objects already present in $\bar{n}$ Cl_d and Cl_d.

Classification algorithm. Object s is classified in Cl_d if object p belongs to Cl_d and $\psi_{sp} \geqslant \psi_s$. It is classified in $\bar{n}$ Cl_d if object p belongs to $\bar{n}$ Cl_d or if it belongs to Cl_d but $\psi_{sp} < \psi_s$.

ψ_{sp} is the potential in a position sp between s and p, which is γ times closer to s than to p. ψ_{sp} is given by

$$\psi_{sp} = N^{-1} \sum_{j=1}^{N} \Phi_{sp,j} \tag{7}$$

where $\Phi_{sp,j}$ is given by eqn. (2) for $i = sp$ and

$$x'_{k,sp} = \gamma^{-1} x'_{k,p} + [(\gamma - 1)/\gamma] \ x'_{k,s} \tag{8}$$

For reliable clustering, γ lies in the range 10—1000 in most applications.

Figure 5 explains why the selection of *sp* is necessary. Suppose a potential surface in a one-dimensional pattern space for 11 objects (A—L). In order to classify object I, H is chosen as the reference object. One cannot simply compare ψ_I to ψ_H. Since $\psi_I < \psi_H$, the impression is given that the potential peak A—H extends to I although this is not the case. In reality, I is part of a separate potential peak with J, K and L.

The average potential ψ_I in I is compared with the average potential in a position between H and I but close enough to I (e.g., position HI in Fig. 5). Then, $\psi_{HI} < \psi_I$ indicates that a new peak is being ascended. The choice of the position HI (by mean of γ) is less critical than the choice of the smoothing parameter α, but it has to be large enough, e.g., $\gamma = 500$.

A SIMPLE EXAMPLE

Figure 6a shows 8 objects in a two-dimensional pattern space. First, the potential influence $\Phi_{i,j}$ (eqn. 2) and average potential ψ_i (eqn. 1) are com-

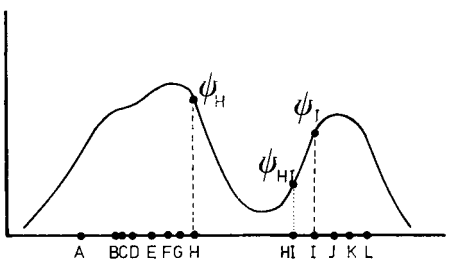

Fig. 5. Illustration of the classification algorithm of CLUPOT.

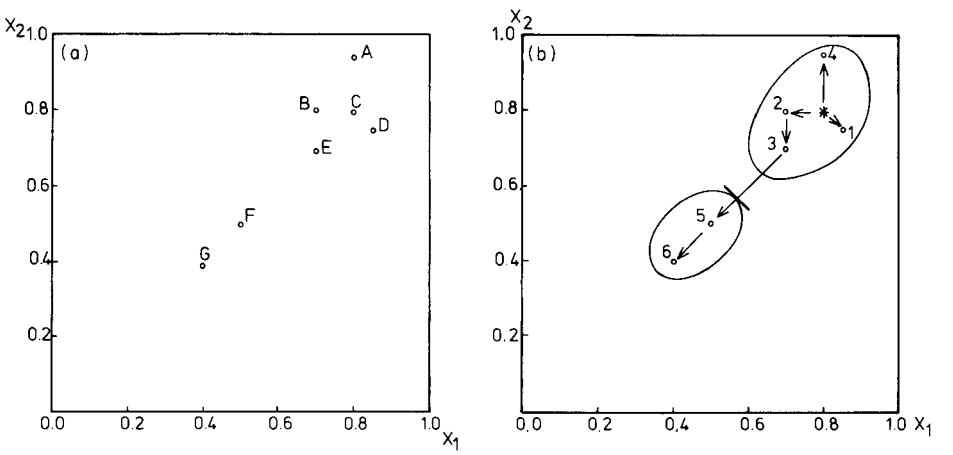

Fig. 6. Example of CLUPOT clustering: (a) two-dimensional data; (b) scheme of selection of the first cluster. The asterisk indicates the cluster centrotype; the numbers indicate the sequence of the procedure; the arrows are related to the selection algorithm.

puted (Table 1). Since $\Phi_{i,j} = \Phi_{j,i}$, the $\Phi_{i,j}$ matrix is symmetric in this example. The calculations were not performed on standardized data as proposed in eqns. 2 and 3, but immediately on the raw data.

The first cluster centrotype is then selected. Table 1 shows that this should be object C because this has the largest ψ value (4.004). The other objects are then arranged according to the sequence algorithm. In Fig. 6b, the centrotype is denoted with an asterisk and the sequence of the other objects is denoted with numbers. The first object (number 1) in the sequence is D. Object D must be compared with a reference object which is an object already present in $\bar{n}$ Cl_1 or Cl_1. Since $\bar{n}$ Cl_1 is empty and $Cl_1 = \{C\}$ one can only choose object C as reference. In Fig. 6b the decision is indicated by an arrow. Then, the potential ψ_{DC} is calculated according to eqns. (7) and (8); ψ_{DC} is the average potential in the position between C and D at $1/\gamma$ distance from D. For $\gamma = 10$ ψ_{DC} equals 3.564 (larger values of γ give the same result). According to the classification algorithm, D is classified in Cl_1 since $\psi_{DC} > \psi_D$ (see Table 1).

The new situation is thus $\bar{n}$ Cl_1 = empty and $Cl_1 = \{C,D\}$. In order to classify the next object (B), it is necessary to choose between two possible reference objects *nl.* C or D. According to the selection algorithm, the reference object is C because $\Phi_{CB} > \Phi_{DB}$ (see Table 1). Object B is classified in Cl_1 because ψ_{BC} (3.845) $> \psi_B$. In contrast with the preceding objects, the next object in the sequence (E) is not compared with the cluster centrotype C but with B, because $\Phi_{BE} > \Phi_{CE}$ and Φ_{DE}. Object E is also classified in Cl_1 since ψ_{EB} (3.517) $> \psi_B$. The fourth object in the sequence (A) is also classified in Cl_1 compared to reference object C because ψ_{AC} (2.905) $> \psi_A$.

The following object (F), however, is not considered as a member of Cl_1 because the reference object is E, and ψ_{FE} (1.913) is smaller than ψ_F. Object F is classified in $\bar{n}$ Cl_1. The last object (G) is also classified in $\bar{n}$ Cl_1, because its reference object F belongs to $\bar{n}$ Cl_1.

TABLE 1

Potential influences Φ_{ij} and average potentials ψ_i for the example of Fig. 6. The smoothness parameter α equals 0.15

Φ_{ij}	A	B	C	D	E	F	G
A	7.074						
B	3.425	7.074					
C	4.290	5.664	7.074				
D	2.751	4.059	6.330	7.074			
E	1.412	5.664	4.535	4.059	7.074		
F	0.011	0.394	0.130	0.116	1.196	7.074	
G	0.000	0.027	0.006	0.005	0.130	4.535	7.074
ψ_i	2.710	3.760	4.004	3.485	3.438	1.941	1.682

The situation at the end of the first step is

$Cl_1 = \{A, B, C, D, E\}$ and $\bar{n}\ Cl_1 = \{F, G\}$

The objects of Cl_1 are deleted from the data set and the clustering is carried out on {F G}. The cluster centrotype of Cl_2 is object F because $\psi_F > \psi_G$ (see Table 1). Object G belongs to Cl_2 because $\psi_{GF}(1.743) > \psi_G$.

COMPARISON WITH OTHER CLUSTERING TECHNIQUES

CLUPOT is a non-hierarchal clustering technique and is designed for the detection of natural densities, i.e., clusters which can be observed directly as distinct densities present in the pattern space. The philosophy of the method is closely related to the techniques of Butler [7], Schnell [8], and Gitman and Levine [9, 10] but the practical realization is quite different. These techniques have been reviewed by Bock [11].

Several non-hierarchal clustering techniques, such as ISODATA [12] and MASLOC [13, 14], have found application in analytical chemistry. In the same way as its supervised learning analogue ALLOC, the unsupervised method CLUPOT does not make assumptions about the structure of the data set; e.g., nothing is assumed about the shape of the clusters. ISODATA and MASLOC, however, are inclined to isolate more or less circular clusters.

ISODATA, MASLOC and CLUPOT are also designed to find the natural or significant number of clusters, in contrast with many other methods, such as FORGY, McQueens *k*-means, etc. In ISODATA, this is achieved by several user-defined parameters, which requires some a priori information of the user and includes a danger of subjectivity. MASLOC and CLUPOT do not require the user to enter values of splitting or joining parameters and therefore permit a more objective approach.

Both methods are able to find independently an optimal set of significant clusters by comparing situations with different numbers of clusters. This may be done by varying a single parameter. In MASLOC it is simply the number of clusters [13] and in CLUPOT it is the smoothness parameter α.

Since the selection of representative objects corresponds with sorting of centrotypes, only MASLOC and CLUPOT are recommended for this purpose. ISODATA is not a centrotype but a centroid-sorting technique.

APPLICATIONS

To illustrate the performance of CLUPOT, it was applied to some often used data bases: Kowalski's archeological artefacts data (ARCH), Ruspini's fuzzy set data (FUZZY) and Fisher's Iris data (IRIS) and to part of the data base of Esbensen concerning meteorite data (METEOR).

ARCH

CLUPOT was applied first to a 2-dimensional problem, namely a classification of archeological artefacts, described by Kowalski and Bender [15]. The original data base consisted of the concentration of ten trace elements in 45 samples. The origins of these samples were known and were divided in 4 categories. Kowalski and Bender reduced the 10-dimensional data to 2 dimensions (see Fig. 7a) using a non-linear mapping method. As data, the distance in mm from both axes was used here.

Since Fig. 7(a) shows 4 distinct clusters containing, respectively, the samples 1—9, 10—16, 17—37 + 45, 37—44, it would be expected that CLUPOT would divide the data set according to this, and indeed the reliability curve (Fig. 7b) shows that a large constant level of 4 clusters is obtained (from $\alpha = 0.35$). The 4 clusters correspond completely with expectations. A second largest level of 7 clusters is obtained between $\alpha = 0.21$ and 0.27 (see Fig. 7a); samples 15—16, 7—8 and 17—18—19 are separated from the large clusters and form 3 distinct clusters. Between the 7 cluster level and 4 cluster level some smaller levels are observed (in Fig. 7b) which correspond to a fusion of the 7 clusters to 4. An extension with 29 artefacts (46—74), is shown in Fig. 8a. Although here too 4 clusters are expected, this is less obvious. The reliability curve (Fig. 8b) shows that a first level is obtained with 7 clusters between $\alpha = 0.20$ and 0.25. A second level is obtained for 5 clusters for an α value equal to 0.26. The influence of the large and most dense cluster comprising the samples 15—16 + 47—49, is extended by absorption of more outlying samples, such as 73 and 50. A further increase of the smoothness gives rise to a further absorption of the cluster 15—16 + 47—49. Complete absorption is obtained with $\alpha = 0.3$ where a 4-cluster level is observed. Moreover, as in

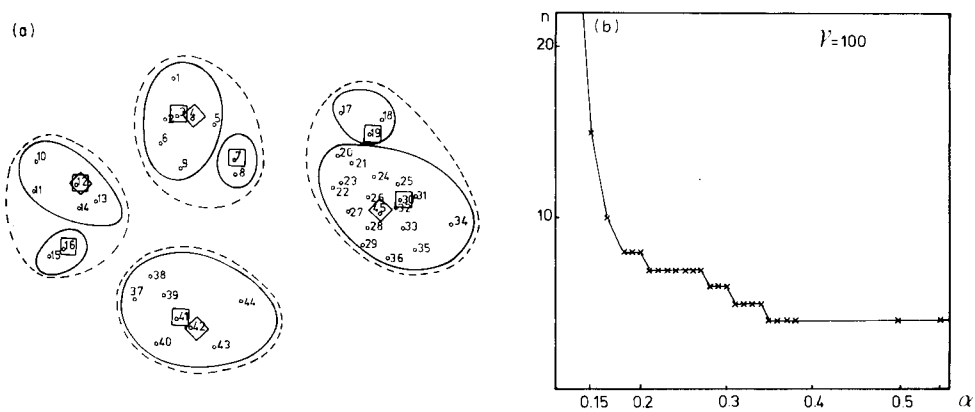

Fig. 7. (a) CLUPOT clusters for the ARCH data (45 samples): (—) and (□) indicate respectively the clusters and corresponding centrotypes for $\alpha = 0.23$; (---) and (◇) indicate respectively the clusters and corresponding centrotypes for $\alpha = 0.27$. (b) Reliability curve for the ARCH data (45 samples).

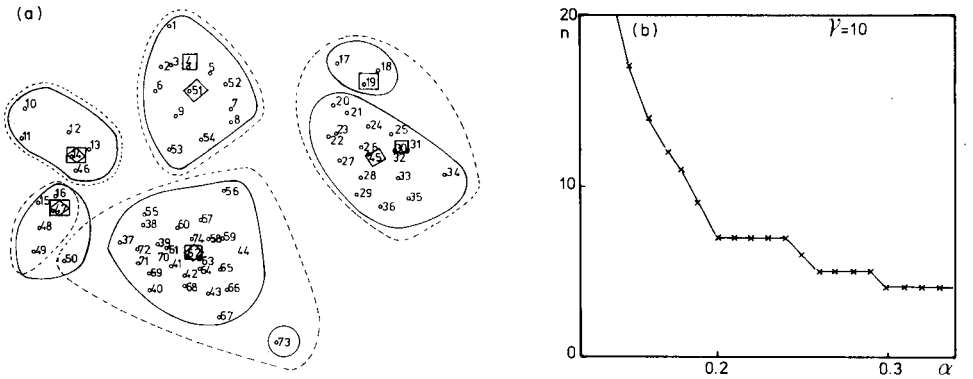

Fig. 8. (a) CLUPOT clusters for the ARCH data (74 samples): (—) and (□) indicate respectively the clusters and corresponding centrotypes for $\alpha = 0.20$; (---) and (◇) indicate respectively the clusters and corresponding centrotypes for $\alpha = 0.26$. (b) Reliability curve for the ARCH data (74 samples).

the 45-samples situation, the cluster 20—37 + 45 is found fused with the cluster 17—19 at the level $\alpha = 0.26$—0.29.

FUZZY

The data set of Ruspini [16] is an artificial one, consisting of 92 points in a two-dimensional space (Fig. 9a). It was used to work out the theory of fuzzy clustering. The reliability curve of CLUPOT is given in Fig. 9(b). A first level is obtained for 6 clusters. The constitution of these clusters is

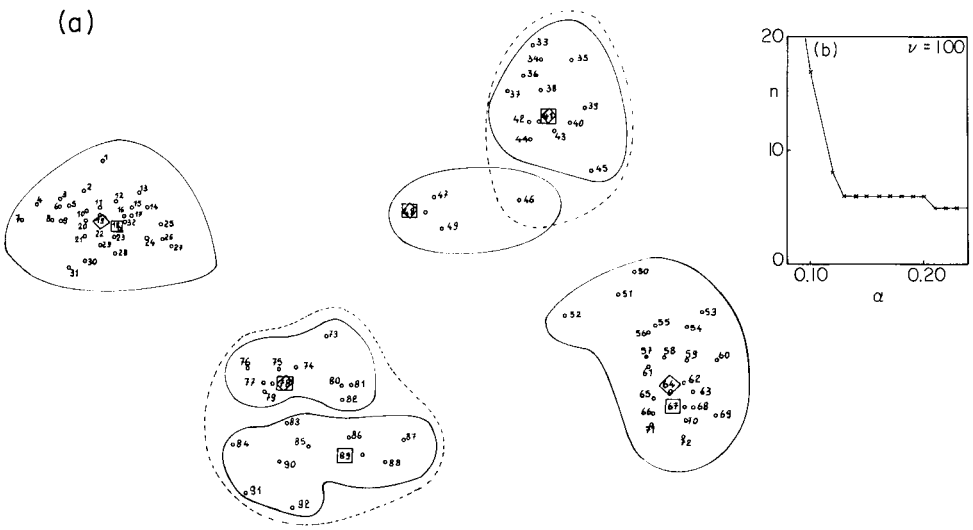

Fig. 9. (a) CLUPOT clusters for the FUZZY data: (—) and (□) indicate respectively the clusters and corresponding centrotypes for $\alpha = 0.14$; (---) and (◇) indicate respectively the clusters and corresponding centrotypes for $\alpha = 0.22$. (b) Reliability curve for the FUZZY data.

shown in Fig. 9(a). A second level consists of 5 clusters. One observes that by increasing the smoothness of the potential functions, the potential surface gives rise to a single peak for the set 73–92 instead of 2 peaks in the 6-cluster level. Furthermore, analogously to the ARCH example, it is shown in Fig. 9(a) that increasing the smoothness parameter results in an absorption of diffuse clusters or isolated points by more dense clusters. An example is the addition of 46 to the set 33—45.

IRIS

This data base of Fisher [17] is probably the most used multivariate data base. It consists of 150 Iris flowers on which 4 measurements were taken. The first 50 samples were from the species Iris setosa (class 1), the next 50 from the species Iris versicolor (class 2) and the last 50 from the species Iris virginica (class 3). Previous results have shown that the Iris versicolor and Iris virginica are very closely related to each other, but are easily distinguished from Iris setosa. The reliability curve for this data set is given in Fig. 10. A level of 6 clusters is obtained between $\alpha = 0.24$ and $\alpha = 0.30$.

In Table 2 it is shown that for the 6 cluster levels, Iris setosa forms a completely distinct cluster with sample 42 as outlier, which is not the case for the other two species. In this way, earlier results were confirmed. The other levels (4-cluster, 2-cluster) in Fig. 10 also coincide with the expectations.

METEOR

In this example, part of the data base of Esbensen and Buchwald [18, 19] concerning the chemical constitution of a selection of iron meteorites is used. Originally, the data base consists of 530 meteorites for which 13 chemical components were measured. Only two variables for which no data were absent, i.e., the concentrations of nickel and gallium were used in the present work. Only the meteorites with nickel concentrations between 5 and 12% and gallium concentrations between 38 and 120 ppm were in-

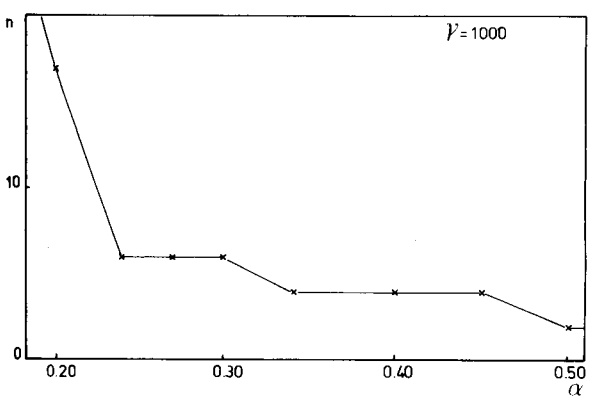

Fig. 10. Reliability curve for the IRIS data.

TABLE 2

The 6 clusters obtained with CLUPOT (α = 0.30) compared with the botanical classification of the objects for the IRIS data

Cluster Number	Setosa	Versicolor	Virginica
1	1—41, 43—50		
2		52, 55—57, 59—60, 62 64—68, 70—80, 83—85, 87, 89—93, 95—98, 100	102, 104, 109, 112 117, 122, 124, 134, 135, 139, 143, 143, 150
3			101, 103, 105, 111, 113—116, 121, 125, 129, 133, 137 140—142, 144—146, 148, 149
4		51, 52, 53, 58, 61, 63 69, 81, 82, 86, 88, 94, 99	107, 120
5			106, 108, 110, 118, 119, 123, 126, 130—132, 136
6	42		

vestigated here. The plot of these 185 meteorites is shown in Fig. 11(a). This example illustrates the performance of CLUPOT in detecting "natural" clusters, because the meteorites tend to form longitudinal groups [19] instead of the circular ones for which most clustering methods perform best. Figure 11(a) shows that at the 6-cluster level (α = 0.35) a clear longitudinal cluster is indeed obtained (cluster I). Also, cluster II is rather longitudinal but no fusion is obtained with cluster III. It can be concluded that the two subclusters in cluster I are more related than the clusters II and III are.

Figure 11(b) shows the reliability curve for this example. It can be seen that the 6, 8 and 9 cluster levels are relevant. The level from α = 0.51 defines two clusters which are fusions of the 6 clusters of level α = 0.35, i.e., II + III + IV + V and I + VI. As shown in Fig. 11(b), this fusion takes place in a sequence of short steps from α = 0.45 to α = 0.51.

Some practical relevance can be assigned to the clusters found by CLUPOT (Fig. 11b), when these clusters are compared with the meteorite groups defined by Esbensen and Buchwald. The meteorites in Fig. 12 belong to 12 classes, i.e., I A, I A-AN, I B, I C, I C-AN, II A, II B, II C, II D, II D-AN, III CD, III CD-AN. Moreover a number of outliers were labelled as "ungrouped" or UNGR. To obtain a sufficiently sharp separation between all the meteorite classes, at least 5 variables have to be considered. A correct classification cannot be expected with 2 variables. However, the clustering obtained is clearly far from meaningless and coincides rather well with the expected classification.

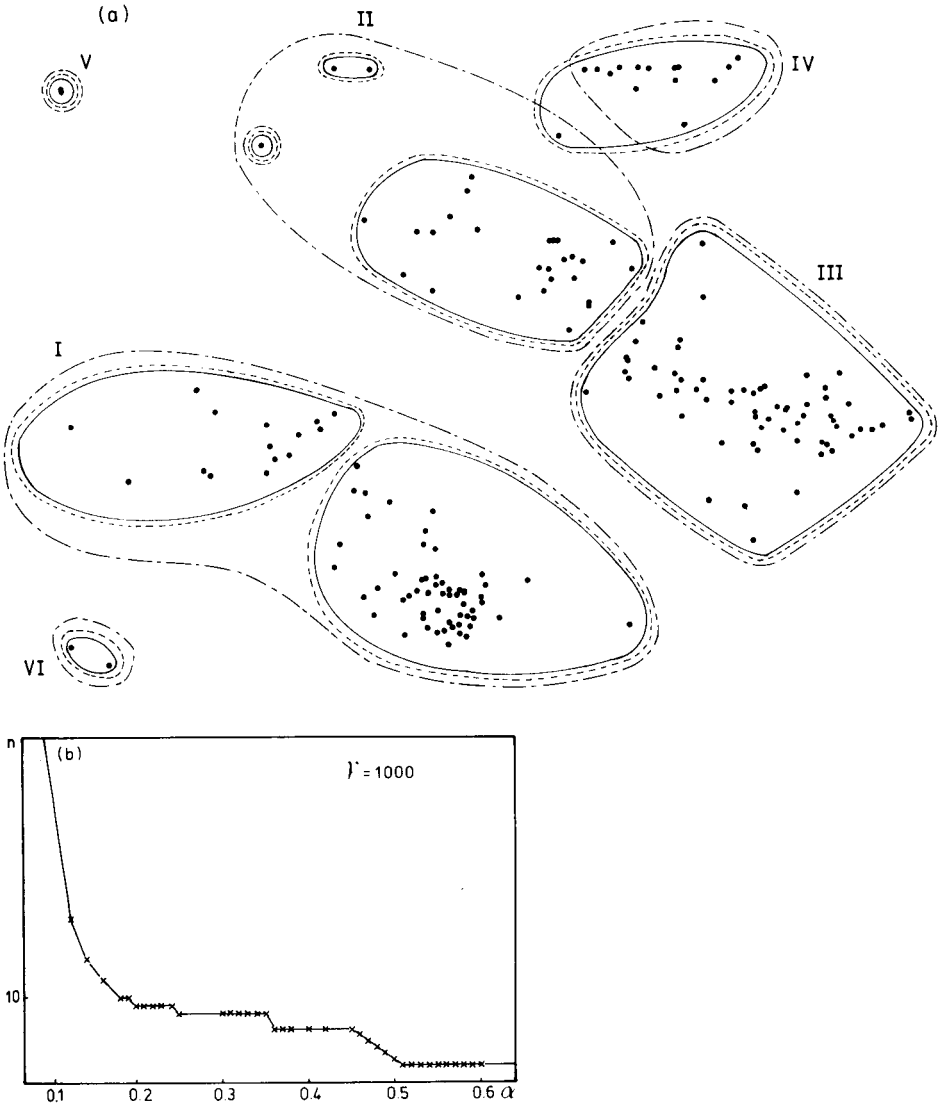

Fig. 11. (a) CLUPOT clusters for the METEOR data: (—) $\alpha = 0.20$; (---) $\alpha = 0.25$; (·····) $\alpha = 0.35$. (b) Reliability curve for the METEOR data.

Conclusion

The performance of CLUPOT in detecting significant clusters without prior knowledge of the data structure is successful. The examples show that expected clusters are found, and that the reliability curve is an essential tool for this purpose.

After each clustering step, the members of the previously selected cluster are removed from the analysis, and so the CLUPOT procedure may be con-

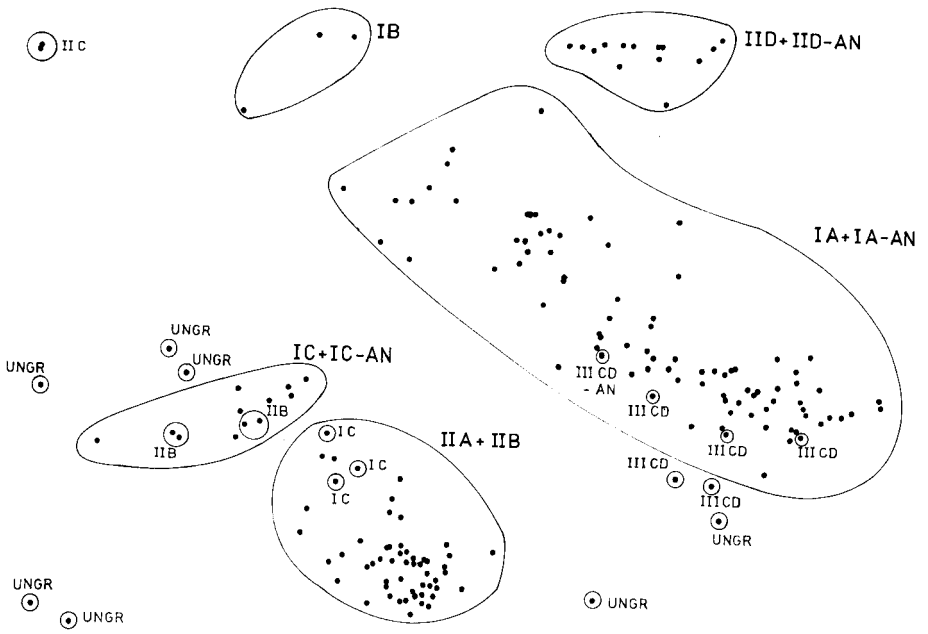

Fig. 12. Identification of the meteorites by Esbensen and Buchwald [18].

sidered economic in terms of computer time. Whether CLUPOT is as good as or better than other techniques such as ISODATA and MASLOC remains a matter for further investigation.

The authors thank A. Van der Straeten and L. Maes for technical help with the preparation of the manuscript, and FGWO for financial assistance.

REFERENCES

1 J. Hermans and J. D. F. Habbema, Manual for the ALLOC-discriminant analysis program, Department of Medical Statistics, University of Leiden, P.O. Box 2060, Leiden, The Netherlands, 1976.
2 H. C. Andrews, Introduction to Mathematical Techniques in Pattern Recognition, Wiley-Interscience, New York, 1972.
3 R. L. Thorndike, Psychometrica, 18 (1953) 267.
4 J. C. Gower, Goodness-of-fit criteria for classification and other patterned structures. In Proc. 8th International Conference on Numerical Taxonomy, W. H. Freeman, San Francisco, 1975, p. 38.
5 G. Nauer, E. Kny and T. E. Haevernick, Glastechn. Ber., 53 (1980) 29.
6 C. Hansch, S. H. Unger and A. B. Forsythe, J. Med. Chem., 16 (1973) 1217.
7 G. A. Butler, Pattern Recognition, 1 (1969) 291.
8 P. Schnell, Biometrika, 6 (1964) 47.
9 I. Gitman, Pattern Recognition, 4 (1972) 307.
10 I. Gitman and M. D. Levine, IEEE Trans. Comp., C-19 (1970) 583.
11 H. H. Bock, Automatische Klassifikation, Vandenbroeck und Ruprecht, Göttingen, 1974.

12 G. H. Ball and D. J. Hall, ISODATA, A novel method of Data Analysis and Pattern Classification, AD 699616, Stanford Res. Inst., Menlo Park, California, 1965.
13 D. L. Massart, L. Kaufman and D. Coomans, Anal. Chim. Acta, 122 (1980) 347.
14 D. L. Massart, A. Dijkstra and L. Kaufman, Evaluation and Optimization of Laboratory Methods and Analytica Procedures, Elsevier, Amsterdam, 1978.
15 B. R. Kowalski and C. F. Bender, Anal. Chem., 44 (1972) 1405.
16 E. H. Ruspini, A Theory of Mathematical Classification (1977) Dissertation, University of California.
17 R. A. Fisher, Ann. Engenetics, 7 (1936) 179.
18 K. H. Esbensen and V. F. Buchwald, Meteoritics, 14(4) (1979) 573.
19 D. L. Massart, L. Kaufman, D. Coomans and K. H. Esbensen, Bull. Soc. Chim. Belg. VZW, 90 (1981) 281.

Analytica Chimica Acta, 133 (1981) 241—250
Computer Techniques and Optimization
Elsevier Scientific Publishing Company, Amsterdam — Printed in The Netherlands

POTENTIAL METHODS IN PATTERN RECOGNITION
Part 3. Feature selection with ALLOC

D. COOMANS, M. DERDE and D. L. MASSART*

Farmaceutisch Instituut, Vrije Universiteit Brussel, Laarbeeklaan 103, B-1090 Brussel (Belgium)

I. BROECKAERT

Dienst Gastro-Enterologie, Sint-Pieter Hospitaal, Hoogstraat 322, B-1000 Brussel (Belgium)

(Received 7th May 1981)

SUMMARY

The feature selection procedure of ALLOC is compared with the SELECT procedure in the ARTHUR software package and with a procedure based on statistical tests in the SPSS software package. Since ALLOC classification is very sensitive to redundant variables, feature selection is necessary. This is not a disadvantage because detection of redundant variables is always desirable. The ALLOC selection procedure performs very well in the two applications considered here, i.e., differentiation of milk samples and characterization of thyroid function.

In Part 1 of this series [1] the supervised pattern recognition method ALLOC of Hermans and Habbema [2] was introduced for analytical applications and the methodology of classifying objects was discussed. ALLOC also includes a feature selection procedure based on the concept of potential functions. This paper discusses the performance of the feature selection procedure on two data bases compared with other feature selection methods.

THE METHOD

The feature selection procedure [2—5] is a forward one, which means that one starts with the selection of one variable; this is the variable which discriminates individually best between the learning classes. In a second step, a second variable is selected; this is the variable which in combination with the already selected variable, permits the best separation between the classes. The selection procedure continues in the same way with a third variable and so on, until all variables are selected or until the increase of the discrimination is less than a threshold value T. The discrimination power of each variable in the first step of the procedure and each combination of variables in the following steps is expressed in terms of probability of error. The probability

0378—4304/81/0000—0000/$02.50

of error is estimated by means of the leave-one-out classification of the members of the learning set and is given by the following expression:

$$P(\text{error}) = \sum_{q=1}^{K} P(\omega_q)\, n_q(\text{error})/n_q \qquad (1)$$

Here ω_q ($q = 1,\ldots K$) represents the K learning classes. $P(\omega_q)$ is the prior probability of ω_q, i.e., the probability that an object belongs to ω_q before the ALLOC classification is applied on that object. Usually there is no reason to assume a priori that an object belongs to one class rather than to another; in such a situation $P(\omega_1) = \ldots P(\omega_q) = \ldots P(\omega_K) = 1/K$. In eqn. (1), n_q (error) is the number of objects belonging to ω_q, misclassified on the basis of the leave-one-out procedure; and n_q is the total number of objects belonging to ω_q.

Discrimination increases with a decreasing P(error) value. The decrease in P(error) in each step must exceed T.

$$P(\text{error})_{\text{step } a} - P(\text{error})_{\text{step } a+1} > T \qquad (2)$$

Generally, the optimal subset of variables obtained during the selection procedure may be defined as the smallest subset corresponding with the smallest P(error) value or the largest correct classification rate. In order to obtain this subset, one may suppose that T should be taken equal to 0. Although in some applications the selection procedure of ALLOC with $T = 0$ gives rise to the optimal subset, this is not generally true. In the milk example (see Results and Discussion) it is shown that it is sometimes impossible to select the optimal subset with any T value.

In order to obtain the optimal subset, it is recommended that in the first instance more variables than necessary be selected by taking T negative enough (e.g., $T = -0.1$), and then that the optimal subset be determined (suppose it corresponds to step a) by

$$\text{step } a = \min\,(P(\text{error})_{\text{step } b}) \quad (b = 1 \ldots\ldots c) \qquad (3)$$

with step c the last step in the selection procedure of ALLOC taking $T = -0.1$.

COMPARISON WITH OTHER FEATURE SELECTION METHODS

A characteristic of the ALLOC selection procedure is the use of the classification rate as a selection criterion. This means that in each stage of the selection the discrimination is observed by means of an ALLOC classification. Of course, such a feature selection procedure can be used with each pattern recognition method. However, ALLOC is the only method, as far as we know, which actually proceeds in this way.

In the software packages SPSS [6] and BMDP [7], statistical linear discriminant analysis (SLDA) may be preceded by parametric forward stepwise selection procedures based on statistical tests, i.e., the F-test or the chi-square test.

In this study, an option available in SPSS where a generalized distance statistic called Rao's V is used in combination with the F-statistic, was chosen. Rao's V has a chi-square distribution if all the variables are normally distributed and the learning classes have a common variance—covariance matrix [8]. The first variable which is selected is the one which has the largest F-value. The other variables are added one by one until the addition of a new variable gives rise to an increase of Rao's V of which the chi-square value is below a given level of significance. The sequence in which the variables are brought in the selection procedure is based on the F-statistic (F-to-enter). This is possible only if the F-to-enter value for the entered variable is larger than a threshold value. Moreover, in a later step of the selection, a variable can be removed from the selected subset if the F-to-remove value is smaller than a threshold value.

The F-test and SLDA are very suitable for each other because they are based on identical statistical considerations. The F-test is designed for testing whether the centroids of the learning classes are significantly different or not, under the assumption of multivariate normality of the measurements of each class with equal variance—covariance matrices for the different classes. SLDA tries to define an optimal boundary between the centroids under the same assumptions as in the F-test. Therefore, it might be expected that the more distinct the centroids of the learning classes are from each other (i.e., the higher the F-value is), the better would be the separation of classes and the correct classification rate for SLDA. However, it has been shown by Habbema and Hermans [3] that a higher F-value implies a better classification rate of SLDA only in the special case of two learning classes satisfying the previous assumptions.

Clearly, the use of F-statistics is not an excellent choice, even in combination with parametric classification techniques such as SLDA. The chi-square statistic on the basis of Rao's V is also based on the same assumptions as the F-statistic and SLDA, but it is not difficult to imagine that if the assumptions are not fulfilled the methods are no longer adaptable to each other and the selection procedure may become unreliable.

In the ARTHUR software package [9] a forward stepwise feature selection procedure called SELECT [9—11] is available which is in itself very attractive. The SELECT procedure is based on the stepwise calculation of decorrelated weights for the variables. In this way the variables appear in a sequence according to decreasing weight; the variance or the Fisher weight may be used. Redundant variables are usually removed according to a threshold weight. However, SELECT cannot be considered completely adaptable to each of the classification techniques present in the package. Because the selection procedure is not based on the same assumptions as the classification procedures, the selection procedure cannot predict with certainty whether the selected subset of variables in a particular step will give rise to better or worse classification results than the selected subset in a following step. It is our opinion that selection procedures based directly on classification

rates should be used when possible. This is possible for classification techniques with a rapid learning phase such as KNN [9—11] and ALLOC. For other techniques such as SLDA and LLM [9—11], such a procedure is too time-consuming. For these techniques, one should use a selection procedure more related to the classification technique. For SLDA this is not necessarily the multivariate F-statistic or the Rao V statistic. It was found here that the ALLOC selection procedure may be suitable in connection with SLDA. A supplementary advantage of a classification rate criterion such as in ALLOC, is the possibility of formulating a valid stopping criterion for the selection of the optimal subset of variables. The statistical criteria as well as SELECT are rather abstract and it is difficult to define adequate threshold values for these selection procedures.

Data

Differentiation of pure milk from different species and mixtures (MILK). This data base has been investigated by Smeyers-Verbeke et al. [12] using SLDA. The variables are 15 gas-chromatographic measurements obtained from the fatty acid fraction of the milk samples. In addition, synthetic mixtures (20 samples for each mixture type) were prepared on the basis of the measurements of the pure samples. This enabled the detectability of adulterations to be established.

Functional state of the thyroid gland (THYROID). This data base was described in Part 1 [1].

RESULTS AND DISCUSSION

Milk

In the first instance, ALLOC was compared with SLDA and KNN on the basis of all 15 variables and for some learning sets used by Smeyers-Verbeke et al. [12]. Table 1 gives the classification results for two series of learning

TABLE 1

Differentiation between various milk samples

Classes	Correct classification (%)			Classes	Correct classification (%)			
	SLDA[a]	ALLOC[a]	ALLOC[b]		KNN[a]	ALLOC[a]	KNN[b]	ALLOC[b]
C S	100	100	100 (1)	C S G	98	100	100 (5)	100 (2)
S G	100	100	100 (1)	C S C9S1	63	78	88 (2)	95 (3)
C C9G1	93	68	100 (3)	C S C1S9	70	63	78 (5)	88 (3)
C C9S1	93	53	93 (3)	C G C1G9	68	77	85 (5)	93 (6)
G S1G9	73	53	80 (2)	C G C9G1	63	78	93 (2)	100 (3)
S C1S9	60	53	80 (3)	S G S1G9	65	58	87 (2)	87 (2)

[a]Applied to the complete set of 15 variables. [b]Applied to a reduced set of variables; numbers between parentheses indicate the number of selected variables.

sets consisting of 2 and 3 learning classes. In addition to differentiation of pure milk classes, the differentiation between binary mixtures (ratio 1/10) and related pure milk categories was investigated.

All the results of Table 1 were obtained by means of the leave-one-out procedure. Because the leave-one-out procedure applied to SLDA is very time-consuming, the application of SLDA was limited to the first series of learning sets. KNN was applied only to the second series. Table 1 reveals that a complete differentiation between the pure milk samples was obtained with SLDA and ALLOC. This is not surprising because Gattuso and Fazio [13] were able to do this with similar success on the basis of a ratio of two variables. However, it is surprising that ALLOC (and KNN) perform less well than SLDA for the learning sets containing mixed samples. The poor discrimination of ALLOC compared to SLDA is due to the presence of many redundant variables. KNN and ALLOC are very sensitive to noise because both techniques are based on geometrical measurements in which the variables are weighted equally, i.e., the euclidean distance in KNN and the potential influence [1—3] which is based on the euclidian distance in ALLOC. When all the variables are taken into account in the same way, noise is added to the euclidian distance and consequently to the potential influence when variables representing a small amount of information are included in the geometrical measurements. Other techniques such as SLDA are able to filter the noise more successfully by giving a different weight to the variables according to their importance.

For the milk example, Table 1 reveals much better classification results for ALLOC and KNN when a reduced set of optimally selected variables was used; "optimally" has to be considered in terms of classification rate (eqn. 1). For ALLOC, the typical ALLOC selection procedure was used to select the optimal set of variables. For KNN, the SELECT procedure of ARTHUR [9] based on the variance weight was applied. Table 1 shows that the pure and mixed milk samples can be identified with ALLOC after feature selection and KNN with at least as much success as with SLDA on 15 variables. It can also be seen that ALLOC classification after ALLOC feature selection performs systematically a little bit better than KNN after SELECT feature selection. Figures 1 and 2 show the relationship between the number of variables selected by the ALLOC selection procedure and the number of cases that were misclassified for the learning sets containing 2 and 3 classes, respectively. All the curves show a minimum misclassification rate [or minimum *P*-(error)] for a small subset of variables. When the number of variables decreases further, the differentiation becomes worse. An exception is the differentiation C/S/C1S9 where an optimal discrimination is obtained with only one variable. In all the differentiations between mixtures and related pure milk samples the superfluous variables disturb the differentiation process in a cumulative way, except for the pure milk problem C/S/G where the differentiation is so clear-cut that the superfluous variables do not interfere. It can be concluded that the ALLOC selection procedure

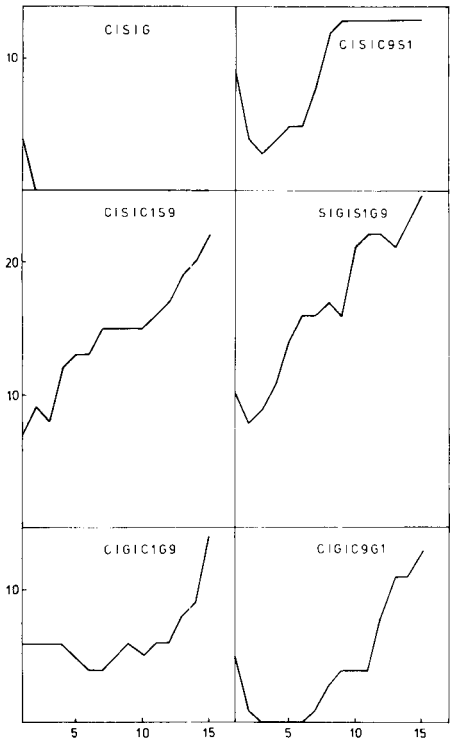

Fig. 1. Relationship between the number of selected variables (x-axis) and the number of misclassified samples (y-axis) for the ALLOC selection for milk (three classes).

gives a clear picture of the redundancy of the variables. The selection process can be visualized on a ΔP(error) versus number of selected variables diagram. In Fig. 3 such diagrams are shown for the differentiations C/G/C9G1 and C/G/C1G9. For the differentiation C/G/C9G1 a threshold value $T = 0$ [no decrease in P(error)] is adequate in order to obtain the optimal subset corresponding to the minimum P(error) in Fig. 1. In some situations such as for C/G/C1G9 (Fig. 3), the threshold value $T = 0$ leads to the selection of too few variables. In fact, it is impossible to find a threshold value T which gives rise to the selection of the optimal subset of variables corresponding to the minimum P(error) in Fig. 1. A threshold value $T = 0$ leads to the selection of only one variable (Fig. 3) whereas even with $T = -0.001$, as many as 7 variables are selected. It is therefore preferable to use the diagrams of Fig. 1 for the selection of the most suitable subset of variables. Moreover, information is then obtained about the degree of disturbance caused by redundant variables. In Table 2 the subsets of variables selected by three stepwise selection procedures are compared. For the SELECT procedure the variance-weight was used. The optimal number of variables was determined on the basis of the minimum P(error) for the KNN method. Table 2 shows that

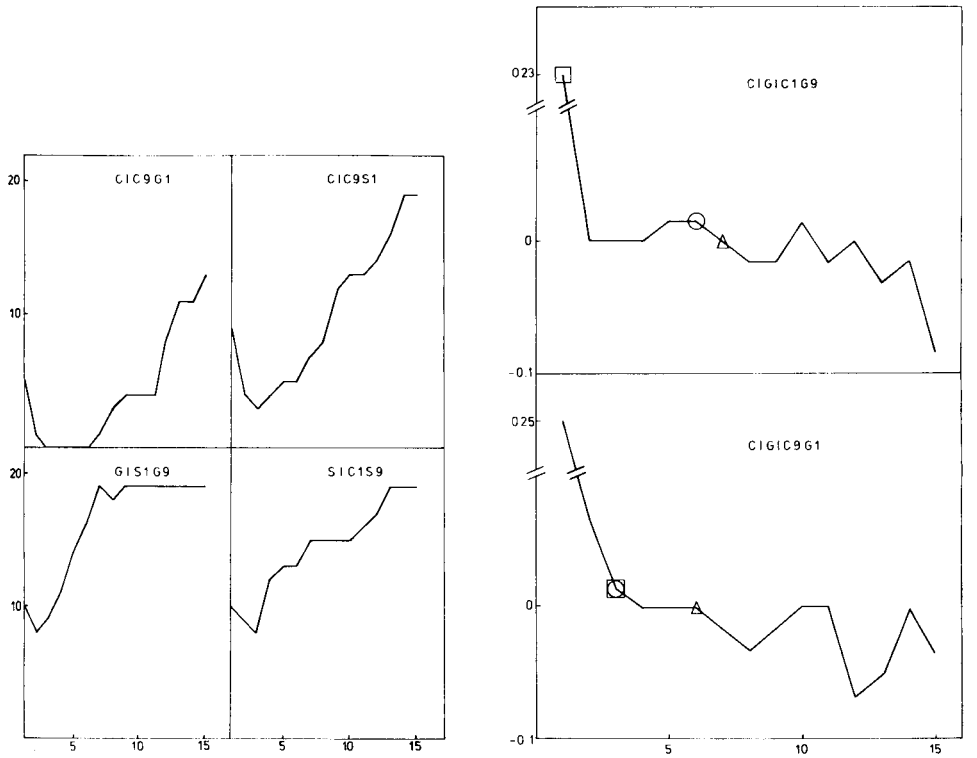

Fig. 2. Relationship between the number of selected variables (x-axis) and the number of misclassified samples (y-axis) for the ALLOC selection for milk (two classes).

Fig. 3. Relationship between the number of selected variables (x-axis) and the decrease of P(error) or ΔP(error) (y-axis) for C/G/C1G9 and C/G/C9G1. (□) Number of variables selected with threshold $T = 0$; (○) optimal number of variables according to minimum P(error) (see Fig. 1); (△) number of variables selected with threshold $T = -0.001$.

Rao's V procedure is not selective at all; at most one variable is deleted. In contrast, the ALLOC and SELECT procedures reduce considerably the number of variables. It can also be seen that the importance of the variables in the subsets differs considerably for the three selection procedures, although the first selected variable is often the same.

Thyroid data

Table 3 shows the results of the ALLOC selection for the differentiation between the HYPER and the EU classes starting from five laboratory tests (*RT3U*, *T4*, *T3*, *TSH* and ΔTSH). It can be seen that the optimal P(error) corresponds to the deletion of one variable: *TSH*. The number of cases of HYPER or EU class which are misclassified in each step of the selection of variables is indicated by n_{HYPER}(error) and n_{EU}(error). The total number of

TABLE 2

Milk differentiation: variables selected by three forward selection procedures

Classes	ALLOC	SELECT	RAO'S V[a]
C S G	1 3	4 1 3	4 5 1 15 2 (15)
C S C9S1	4 5 14	4 3	4 5 9 13 11 (15)
C S C1S9	15 5 14	4 3 15 9 2	9 15 4 5 11 (15)
C G C1G9	15 5 10 3 12 13	4 3 15 9 1	4 5 1 9 13 (15)
C G C9G1	4 5 1	4 3	4 5 1 3 15 (15)
S G S1G9	1 11	1 8	1 15 8 6 15 (15)
C S	3		3 15 2 9 5 (14)
S G	1		1 15 8 6 4 (15)
C C9S1	4 5 14		4 5 11 14 3 (15)
S C1S9	15 5 14		15 11 10 1 7 (14)
C C9G1	4 5 1		
G S1G9	1 11		1 8 13 2 10 (15)

[a]Only the first 5 selected variables are given; the total number of selected variables is indicated between parentheses.

TABLE 3

Stepwise ALLOC selection of variables for HYPER/EU differentiation

No.	Variables selected	n_{HYPER}(error)	n_{EU}(error)	P(error)	ΔP(error)
0				0.500	0
1	*T4*	3	8	0.070	0.430
2	*ΔTSH*	0	13	0.044	0.026
3	*T3RIA*	0	5	0.017	0.027
4	*RT3U*	0	3	0.010	0.007
5	*TSH*	1	1	0.024	−0.014

misclassified cases (EU + HYPER) does not coincide with P(error) because the latter takes into account the discrepancies between the number of cases in each class (35 HYPER and 150 EU). The redundancy of TSH coincides with the results published in an earlier paper [14] where two direct selection procedures indicated that the smallest contribution to the differentiation was due to *TSH* and no decrease of the classification rate was obtained with SLDA when *TSH* was removed from the set of 5 variables. Table 4 reveals that ALLOC gives rise systematically to somewhat better classification rates for the HYPER/EU discrimination during the selection procedure than SLDA does. Moreover, the ALLOC selection seems to select more appropriate subsets for SLDA than does the classical Rao's V selection method.

TABLE 4

Classification rates (in *YI%*) for subsets of variables for the HYPER/EU and the HYPO/EU discrimination

HYPER/EU				HYPO/EU		
No. of variables	ALLOC	SLDA 1[a]	SLDA 2[b]	No. of variables	ALLOC	SLDA
1	86			2	95	96
2	91	86	76	5	86	80
3	97	88	84			
4	98	91	89			
5	96	91	91			

[a]Using subsets selected by ALLOC. [b]Using subsets selected by Rao's *V*.

It should be noted here that the classification rates are expressed in Youden Index percent (*YI* %). For the HYPER/EU discrimination, for instance, this is given by: *YI* % = (% correct classified HYPER + % correct classified EU) − 100. In this way discrepancies between the number of patients (samples) in each type of thyroid function have been taken into account and the results are comparable with those published earlier [14]. For the differentiation between patients suffering from a HYPO dysfunction and EU patients, only two laboratory tests were selected by ALLOC. The tests are *T4* and ΔTSH. This result confirms the results of 5 other selection procedures including Rao's *V* stepwise selection method [14]. However, with these criteria it was possible to state only that *T4* and ΔTSH are the two most important variables; it was not possible to state that they were the only two important variables.

Conclusion

It is now clear that the ALLOC classification is very sensitive to redundant variables. Feature selection is therefore essential. This is no disadvantage because detection of redundant variables is always desirable and the ALLOC selection procedure performs very well. The use of the classification rate as the selection criterion may be considered an important advantage; in this way, feature selection is conceptually related to the classification procedure. The integration of the selection and classification process in ALLOC provides economic computer use; complete analysis of a data set may be done in one run.

The authors thank A. Tassin for efficient scientific help and FGWO for financial assistance.

REFERENCES

1 D. Coomans, I. Broeckaert, A. Tassin and D. L. Massart, Anal. Chim. Acta, 133 (1981) 215.
2 J. Hermans and J. D. F. Habbema, Manual for the ALLOC-discriminant analysis program. Department of Medical Statistics, University of Leiden. P.O. Box 2060, Leiden, The Netherlands, 1976.
3 J. D. F. Habbema and J. Hermans, Technometrics, 19 (1977) 487.
4 H. E. Solberg, CRC Crit. Rev. Clin. Lab. Sci., (1978) 209.
5 D. Coomans, L. Kaufman and D. L. Massart, Anal. Chim. Acta, 112 (1979) 97.
6 N. N. Nie, C. H. Hull, J. G. Jenkins, K. Steinbrenner and D. Bent, Statistical Package for the Social Sciences (SPSS), McGraw-Hill, New York, 1975.
7 W. J. Dixon, BMDP, Biomedical Computer Programs, University of California Press, Berkeley, 1975.
8 C. R. Rao, Advanced Statistical Methods in Biometric Research, J. Wiley, New York, 1952
9 D. L. Duewer, J. R. Koskinen and B. R. Kowalski, ARTHUR (available from B. R. Kowalski).
10 A. M. Harper, D. L. Duewer and B. R. Kowalski, in B. R. Kowalski (Ed.), Chemometrics, Theory and Practice, Am. Chem. Soc. Symp. Ser., No. 52, 1977.
11 B. R. Kowalski and C. F. Bender, Pattern Recognition, 8 (1976) 1.
12 J. Smeyers-Verbeke, D. L. Massart and D. Coomans, J. Ass. Offic. Anal. Chem., 60 (1977) 1382.
13 A. M. Gattuso and G. Fazio, Ind. Agrar., 12(4) (1974) 3.
14 D. Coomans, I. Broekaert, M. Jonckheer, P. Blockx and D. L. Massart, Anal. Chim. Acta, 103 (1978) 409.

Analytica Chimica Acta, 133 (1981) 251—259
Computer Techniques and Optimization
Elsevier Scientific Publishing Company, Amsterdam — Printed in The Netherlands

APPLICATION OF SIMCA MULTIVARIATE DATA ANALYSIS TO THE CLASSIFICATION OF GAS CHROMATOGRAPHIC PROFILES OF HUMAN BRAIN TISSUES

SVANTE WOLD* and ERIK JOHANSSON
Institute of Chemistry, Umeå University, Umeå (Sweden)
EGIL JELLUM and INGUNN BJØRNSON
Rikshospitalet, Oslo (Norway)
RAGNAR NESBAKKEN
Ullevål Hospital, Oslo (Norway)
(Received 15th April 1981)

SUMMARY

Sixteen samples of three types (classes) of brain tissue were characterized by capillary gas chromatography (g.c.). Each sample is thus characterized by the peak heights of 105 peaks in each g.c. profile. SIMCA pattern recognition is used to analyze the 16 × 105 data matrix in order to differentiate between the three classes on the basis of the g.c. data only. The SIMCA method is therefore applicable even when the number of variables (105) exceeds the number of objects (16). The results indicate that g.c. profiles are useful for the identification of brain tissue type.

Gas chromatography (g.c.), liquid chromatography (h.p.l.c.) and other separation techniques are widely used to characterize complex samples of biological, chemical and environmental origin [1—5]. Multicomponent analyses of this type frequently yield chemical profiles containing hundreds of constituents. Information retrieval from these patterns is often difficult, but combined with suitable computerized handling of the data, the profiles can be used to differentiate between related samples [4—7]. For instance, it is now possible to classify several bacteria and moulds based on characteristic differences of their g.c. profiles [4, 8].

The present paper is concerned with the possibility of using gas chromatography and pattern recognition methods to classify human cells. Different brain tumors were selected and their metabolic profiles (105 g.c. peaks) were determined followed by analysis of the data by the SIMCA pattern recognition method [9—11]. The latter allows the utilization of the information in multivariate data analysis regardless of the ratio between the number of variables (g.c. peaks) and the number of samples. Although several problems of both chemical and data analytical nature were encountered, the results demonstrate the feasibility of computer differentiation between normal

brain tissue and various brain tumors based solely on differences of their chemical (g.c.) profiles.

EXPERIMENTAL

Brain samples and g.c. separation

Brain samples (tumor and neighbouring normal tissue) were removed surgically. Parts of the samples were submitted to routine neuropathological examination, and parts were immediately submerged in liquid nitrogen and subsequently stored at −70°C until gas chromatography was applied. The frozen samples were then subjected to methanolysis (refluxing with anhydrous methanol saturated with hydrogen chloride) overnight. The solvent was removed by a stream of nitrogen and the residue was trimethylsilylated for 30 min at 80°C with bis(trimethylsilyl)trifluoroacetamide (BSTFA). The TMS derivatives were separated in a 50-m glass capillary g.c. column coated with SE-30. The temperature was kept at 50°C for 3 min after injection and then increased at a rate of 4°C/min to 240°C. A Carlo Erba Fractovap 2101 gas chromatograph was used.

Each chromatogram was translated into a quantitative data vector by measuring the height of 105 peaks which were present in the g.c. profiles of all the brain samples. The base line was arbitrarily chosen, but was the same in all cases. Since only relative differences in the data vectors were sought, the choice of the base line did not affect the results.

Three types of brain samples were included in this investigation: normal cerebral cortex (class 1, $n_1 = 6$), "brain tumor" (class 2, $n_2 = 3$) and pituitary tumor (class 3, $n_5 = 7$). Class 2 consisted of a meningeom and tumors caused by metastasis from lung and epithelium carcinoma. Class 3 can be subdivided into adenomas with production of growth hormone or prolactine or both. The small number of samples compared with the large number of variables is remarkable, and one of the main objects was to study whether any information at all could be obtained from this minimal data set.

Data preprocessing

In a situation like the present one, it is essential not to utilize the information about the class assignment of the samples to enhance the class separation at the data preprocessing stage. That would give a distinctly biased classification and would carry little information about the real value of multivariate analysis. Accordingly, the data were only normalized to a sum of 100 over all 105 peaks in each chromatogram. Thereafter, the logarithm was taken of each measurement to make the distribution of each variable (corresponding to each peak) less skewed.

Eigenvector projection

Each sample data vector can be considered as a point in a 105-dimensional space obtained by giving each variable one orthogonal coordinate axis (see

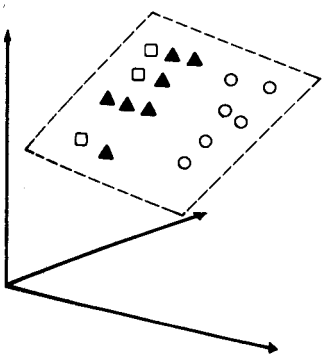

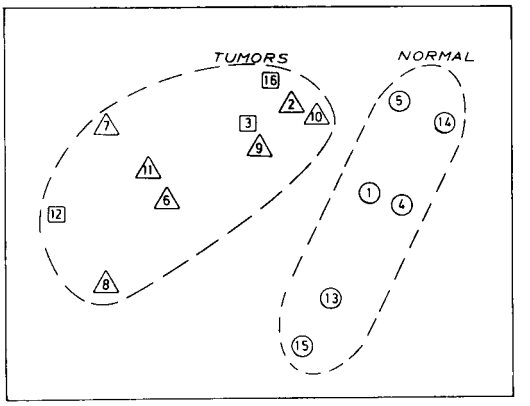

Fig. 1. Each sample data vector can be considered as a point in a 105-dimensional space, here modelled by a three-dimensional space. The plane corresponding to the first two eigenvectors is indicated. (○) Normal (class 1); (□) "brain tumors" (class 2); (▲) pituitary tumor (class 3).

Fig. 2. Eigenvector projection corresponding to the first two eigenvalues of the 16 samples. (○) Normal; (□) brain tissue tumor (class 2); (△) pituitary tumor (class 3).

Fig. 1). When the point swarm of the 16-sample data set is projected down on the plane conserving most of the variance, the so-called eigenvector projection corresponding to the first two eigenvalues of the data covariance matrix [12] is obtained (Fig. 2). The normal samples are clearly separated from the tumor samples and it is important to note that this projection is made without the use of information about the class assignment of the samples. The resulting separation is therefore a strong indication of a real difference between normal and tumor samples as reflected in their gas-chromatographic profiles.

SIMCA PATTERN RECOGNITION ANALYSIS

The SIMCA method has been described in detail elsewhere [4, 9, 10] and will therefore only be summarized. Data vectors are given for objects (here, samples) "known" to belong to a number of classes. These data vectors are collectively called the training set. In the present example, the training set consists of 16 objects divided into three classes.

The basic principle of the SIMCA method is to model the data of each class separately. With y_{ik}^{q} denoting the observed value of variable i for object k in class q the class models are principal component models

$$y_{ik}^{q} = \alpha_i^{q} + \sum_{a=1}^{A_q} \beta_{ia}^{q} \theta_{ak}^{q} + \epsilon_{ik}^{q} \qquad (1)$$

The parameters α_i^{q}, β_{ia}^{q} and θ_{ak}^{q} ($a = 1, 2, \ldots A_q$) are calculated so as to make the residuals ϵ_{ik}^{q} as small as possible over the class training set (least-squares

criterion). The principal component models range in complexity from a point with the coordinates $\alpha_i{}^q$ when $A_q = 0$ (the middle point of the class) to an A_q-dimensional hyperplane when $A_q > 0$. The complexity of each class model (i.e., the number of product terms A_q in eqn. 1) is estimated directly from the data using the technique of cross-validation [11]. This estimate provides the value of A_q with which the model best predicts the values of points temporarily kept out of the data set at the stage of parameter estimation.

A great advantage of SIMCA is that, in contrast to commonly used pattern recognition methods such as linear discriminant analysis (LDA) [13] and the very similar linear learning machine (LLM) [14] methods, it is not restricted in the number of variables (M) relative to the number of objects (N). Thus, the principal component models (eqn. 1) can be estimated regardless of the ratio between M and N. The only restriction is that the number of components, A_q, must be smaller than both M and N. In fact, the classification stability of SIMCA increases with the square root of M (for a given number of training set objects, N). In the present case with $N = 16$ objects, LLM and LDA would be restricted to a maximum number of variables of about 5 ($M < N/3$) which is far less than the present number of $M = 105$.

Graphically, the SIMCA method is simple to illustrate. Each class is approximated by a simple linear construction, a point ($A_q = 0$), a line ($A_q = 1$), and a plane ($A_q = 2$) or a hyperplane for higher values of A_q. These constructions are fitted to the points in the class training sets by non-linear least squares. In the present case, the cross-validation indicates that $A_q = 0$ for each class, i.e., the three classes are best approximated by their midpoints. This result is unusual. In Fig. 2 elongated structures are clearly seen for both classes 1 and (2 + 3). These structures are not present in sufficiently many variables, however, to give a significant first product term in the class models. This result is further discussed in the "problem" section below.

When a confidence interval is drawn around each class midpoint, each class is, in the present example, enclosed in a hypersphere in the 105-dimensional hyperspace, a situation analogous to the one of three dimensions in Fig. 3.

Classification

In the second phase of the data analysis, each object data vector is related to each of the obtained class models by a multiple linear regression. In the general case (for object k and class model q), the object parameters $t_{aq}{}^q$ are determined so as to minimize the residuals $\delta_{ik}{}^q$

$$(y_{ik} - \alpha_i{}^q) = \sum_{a=1}^{A_q} t_{ak}{}^q \beta_{ia}{}^q + \delta_{ik}{}^q \qquad (2)$$

In the present case with $A_q = 0$, the residuals are obtained directly

$$\delta_{ik}{}^q = y_{ik} - \alpha_i{}^q \qquad (3)$$

The distance between the object and the qth class model is directly measured by the residual standard deviation (RSD), $s_k{}^q$.

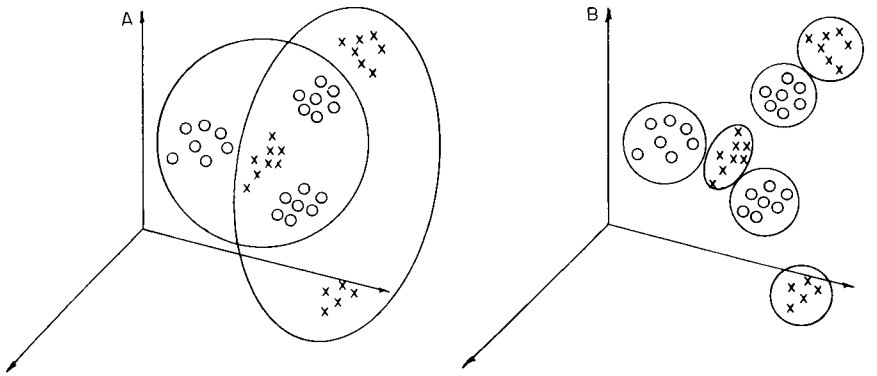

Fig. 3. A three-dimensional space with two classes (rings and crosses) which contain strong subgroups. (A) Models constructed without recognition of the subgrouping will overlap severely. (B) Models constructed with knowledge of the subgroups in the two classes give efficient class separation.

$$s_k^q = \left[\sum_{i=1}^{M} (\delta_{ik}^q)^2/(M - A_q) \right]^{1/2} \quad (4)$$

The object is then assigned to the class corresponding to the smallest RSD, provided that the RSD is not much larger than the "normal" RSD calculated from the residuals ϵ_{ik}^q in eqn. (1) when the object is classified as an "outlier". The RSD for each object and class model are listed in Table 1. It can be seen that each object is indeed closest to its "own" class model.

Class distances

Comparison of the pooled RSD obtained when the objects in the training sets of two classes are fitted to their "own" class models with the pooled RSD obtained when the same objects are fitted to the "other" class model, provides a measure of the relative distance between the two classes. Table 2 shows these relative distances for the present three classes. These distances (D_{rs}) can be tested for significance by an approximate F-test on $(D_{rs} + 1)^2$.

TABLE 1

Distances (RSD) between the 16 objects (tissue samples) and the three class models ($A_q = 0$) (eqn. 4)

Object	Class	RSD_1	RSD_2	RSD_3	Object	Class	RSD_1	RSD_2	RSD_3
1	1	0.15	0.42	0.40	2	3	0.49	0.51	0.26
4		0.25	0.59	0.55	6		0.46	0.39	0.17
5		0.24	0.49	0.49	7		0.53	0.40	0.23
13		0.26	0.61	0.55	8		0.58	0.53	0.30
14		0.29	0.57	0.62	9		0.45	0.43	0.22
15		0.27	0.62	0.59	10		0.50	0.52	0.27
3	2	0.49	0.21	0.46	11		0.50	0.44	0.20
12		0.55	0.24	0.45					
16		0.49	0.22	0.45					

TABLE 2

Symmetrized class distances, D_{rs} = [RSD(other)/RSD(own)] − 1, between classes 1—3 (eqn. 21 [10])

	1	2	3
1	0	0.96	0.96
2		0	0.72
3			0

According to this, the distances between classes 1 and 2 and between classes 1 and 3 are significant on the level $p < 0.01$ while the distance between the two tumor classes 2 and 3 is significant only at the level of $p < 0.05$.

Validation

The classification rate calculated from the fitting of the objects in the training set to the class models is overly optimistic. The reason is that the same objects are used both to define the class models and to test the classification agreement. An unbiased, but conservative [15] classification rate is obtained by a validation procedure where part of the training set is kept out of the model estimation and thereafter classified by the models obtained. This is done in 3 or 4 rounds so that each object in the training set is kept out only once.

In the present case the RSD's shown in Table 3 are then obtained. These are seen to give a rate of correct classification of 13/16, clearly less than the 100% obtained in the direct classification above. The lack of resolution of the tumor classes 2 and 3 is obvious. This result corresponds very well to the picture seen in Fig. 2 with class 1 rather well separated from classes 2 and 3 and objects 1 and 5 in class 1 being the "normal" objects being closest to a tumor class. An approximate ψ^2-test indicates, however, that 13/16 is significantly better than random ($p < 0.05$).

TABLE 3

Validation results obtained when each object was left out from the computation of its class model. Notation as Table 1

Object	RSD_1	RSD_2	RSD_3	Object	RSD_1	RSD_2	RSD_3
1	0.30	0.47	0.42	2	0.50	0.54	0.46
4	0.46	0.58	0.56	6	0.47	0.44	0.33
5	0.42	0.55	0.54	7	0.55	0.42	0.40
13	0.50	0.62	0.57	8	0.61	0.56	0.55
14	0.53	0.56	0.63	9	0.46	0.48	0.41
15	0.48	0.63	0.59	10	0.51	0.54	0.48
3	0.51	0.48	0.47	11	0.52	0.46	0.35
12	0.57	0.55	0.46				
16	0.51	0.50	0.47				

Relevance of variables

One of the advantages of SIMCA is that when $A_q > 0$, which usually happens, the method gives measures of relevance of each variable which is not directly related to the class separation. These measures can then form a basis for the selection of "good" variables, i.e., variables which participate in the class modelling, even in cases when $M > N$. In the present case, however, $A_q = 0$ for all classes and irrelevant variables cannot be deleted. This is one reason for the poor class separation, as discussed further below. Only the class discrimination power can be determined for each variable. This must not be used as the basis of variable selection when $M > N$ so that results will not be biased.

Chemical and data analytical problems

In the identification of biological samples, the greatest problem is usually the variability between samples (objects) of the same type, "the biological variability". This can be managed in the following ways.

Methods that can model part of the variability between samples of the same type. Principal component models have this ability and have recently been applied to g.c. data analysis [4, 16]. However, in the present case, the noise is too great in many of the variables, probably because of inadequate resolution and misidentification of several g.c. peaks. This "noise" obscures the systematic variation that probably exists in the data as seen in the elongated structure of classes 1 and 2 + 3 in Fig. 2. The result is that this type of "variability management" is not applicable in the present example.

The use of many variables (peaks) to characterize each sample. Even if each individual peak lacks sufficient reproducibility, functions based on the sum over all variables will be fairly stable. This is the philosophy behind numerical taxonomy; Sneath and Sokal [17] recommended the use of around 200 variables to achieve sufficient stability of classification. In the present case, the use of capillary g.c. gave sufficiently many variables, as about 160 g.c. peaks occurred. However, because retention times and "neighbouring peak pattern" were used to recognize these peaks, the identification was uncertain and only the 105 largest peaks could be retrieved from all 16 chromatograms with reasonable confidence. Secondly, the confidence is better in the identity of the larger peaks, and so the data were not scaled to the same variance of all peaks. This leads to a further loss of information; a few large peaks tend to dominate the patterns found in the data analysis. When the data were scaled, the separation between the classes was even less marked, confirming the uncertainty in the identity of peaks other than the largest ones. Hence, in order to improve the utility of capillary g.c. data, chemical identification of all peaks is desirable unless a better separation can be achieved.

Division of a class into homogeneous subgroups. Often the "biological variability" occurs because a "class" is not homogeneous but consists of several dissimilar subgroups. The latter is certainly the case in the present

material and probably explains the stretching of the "class models" over large areas in measurement space and the blurring of the classification (Fig. 3).

CONCLUSIONS

It has been shown that gas chromatographic data combined with pattern recognition can be used to differentiate between normal brain tissue and certain brain tumors. There are difficulties, however, in recognizing the subgroups known to occur among the brain samples investigated. Certain trends are nevertheless evident: for example, one class seems to be grouped in two subclasses, one consisting of a meningeom and metastasis from lung cancer and another subgroup represented by metastasis from epithelium carcinoma. Growth hormone producing pituitary tumors also have a tendency to be subgrouped together, but there were also overlaps between pituitary tumors and tumors owing to metastasis.

Improvement in the subclassification of the brain tumors might be brought about in several ways. First, absolute identification of all g.c. peaks of the chromatograms is desirable. This may be done by mass spectrometry, and if automatic quantification were also possible, as in the system of Sweeley and co-workers [18], much of the uncertainty in the chromatographic data would be eliminated. Secondly, in the present work the number of samples belonging to each subgroup was very small and needs to be increased. Thirdly, as the SIMCA program has been designed to operate with up to 1000 variables, it would be desirable also to include other information than gas chromatographic data. The inclusion of the pattern from high resolution two-dimensional electrophoresis [19, 20] of the brain specimens is a possibility that is currently being exploited.

The Norwegian Council for Science and the Humanities and the Swedish Natural Science Research Council are gratefully acknowledged for financial support of the project. This work was also supported by a NATO grant (RG.266.80).

REFERENCES

1 C. E. Dagliesh, E. C. Horning, M. G. Horning, K. C. Knox and E. Yarger, Biochem. J., 101 (1966) 792.
2 B. Halpern, Biomedical applications of gas chromatography—mass spectrometry, CRC Critical Reviews, (1980/81) in press.
3 E. Jellum, J. Chromatogr., 143 (1977) 427.
4 G. Blomquist, E. Johansson, B. Söderström and S. Wold, J. Chromatogr., 173 (1979) 19.
5 W. Kwan and B. R. Kowalski, Anal. Chim. Acta, 122 (1980) 215.
6 B. R. Kowalski, Anal. Chem., 52 (1980) 112 R.
7 M. C. McConnell, G. Rhodes, L. Watson and M. Novotny, J. Chromatogr., 162 (1979) 495.

8 B. M. Mitruka, Gas Chromatographic Applications in Microbiology and Medicine, Wiley, New York, 1975.
9 S. Wold, Pattern Recognition, 8 (1976) 127.
10 S. Wold and M. Sjöström in B. R. Kowalski (Ed.), Chemometrics, Theory And Application, ACS Symp. Ser. 52, 1977.
11 S. Wold, Technometrics, 20 (1978) 397.
12 B. R. Kowalski and C. F. Bender, J. Am. Chem. Soc., 95 (1973) 686.
13 P. A. Lachenbruch, Discriminant Analysis, Hafner Press, New York, 1975.
14 P. C. Jurs and T. L. Isenhour, Chemical Application of Pattern Recognition, Wiley, New York, 1975.
15 L. Kanal, IEEE Trans. Inf. Theory, 20 (1974) 697.
16 H. J. H. MacFie, C. S. Gutteridge and J. N. Norris, J. Gen. Microbiol., 104 (1978) 67.
17 P. H. A. Sneath and R. R. Sokal, Numerical Taxonomy, W. H. Freeman, San Fransisco, 1973.
18 S. C. Gates, M. J. Smisko, C. L. Ashendel, N. D. Young, J. F. Holland and C. C. Sweeley, Anal. Chem., 50 (1978) 433.
19 P. H. O'Farrel, J. Biol. Chem., 250 (1975) 4007.
20 N. L. Anderson and N. G. Anderson, Anal. Biochem., 85 (1978) 341.

Analytica Chimica Acta, 133 (1981) 261—270
Computer Techniques and Optimization
Elsevier Scientific Publishing Company, Amsterdam — Printed in The Netherlands

ORTHOGONAL TRANSFORMATIONS FOR FEATURE EXTRACTION IN CHEMICAL PATTERN RECOGNITION

L. DOMOKOS* and I. FRANK

Institute for General and Analytical Chemistry, Technical University of Budapest, Gellért-tér 4, H-1521 Budapest (Hungary)

(Received 23rd March 1981)

SUMMARY

A crucial point in pattern recognition methods is the extraction of features to determine the pattern vectors. Orthogonal transformations, e.g., Fourier, Walsh and Haar, are investigated as preprocessing methods for feature extraction. The theoretical considerations and conclusions are compared with computational results obtained by applying different pattern recognition methods to two different but similar collections of low-resolution mass spectra.

Pattern recognition has become quite widely used in multicomponent chemical data processing to classify and identify chemical objects (compounds) [1]. A chemical object is represented by a pattern vector, derived from the measured characteristics of the object. The determination of this pattern vector, referred to as feature extraction, is a crucial step in pattern recognition because of its great influence on the success of the classification. The aim is to obtain a low-dimensional but consistent pattern vector containing as much information as possible.

In geometric representation, a pattern vector is a point in a high-dimensional space, and classification involves separating these points by decision surfaces into subsets representing the classes. An important condition is that chemically similar objects have to be close to each other in the pattern space. Feature extraction aims to fulfil this condition as much as possible.

In this paper attention is focused on the utility of orthogonal transformations, especially the Fourier (FT), Walsh (WT), sometimes referred to as the Hadamard, and Haar (HT) transformations in chemical feature extraction.

Results on FT and WT have been published earlier [2—7], mainly with experimental backgrounds. The present paper offers some theoretical insight and explanations of the computational results.

THEORY

In general, orthogonal transformations can be defined in the abstract Hilbert spaces based on a complete orthogonal system of space. Later, the

n-dimensional Euclidean space, denoted by R^n, of n-dimensional vectors will be used. For practical reasons $n = 2^k$ (k is a positive integer) is assumed.

For example, if a spectrum of a chemical object S is measured, then the simplest way is to create a pattern vector s from the sampled intensity values of the spectrum, $\mathbf{s} = [s(1), s(2), \ldots, s(n)]'$, where $'$ denotes the transposition. The object S can be represented by its pattern vector s in the space R^n. The $s(1), s(2), \ldots, s(n)$ components are the coordinates of s in the coordinate system $\{\mathbf{e}_i\}$ of R^n, $\mathbf{e}_i = (0,0,\ldots, 1^i,\ldots, 0)'$, $i = 1, 2,\ldots, n$; which means that $\mathbf{s} = \sum_{i=1}^{n} s(i)\mathbf{e}_i$. A system of vectors $\mathbf{y}_i = (y_i(1), y_i(2), \ldots, y_i(n))'$, $i = 1, 2, \ldots, n$, is called a complete orthogonal system in R^n when

$$\mathbf{y}_i'\mathbf{y}_j = \sum_{k=1}^{n} y_i(k)y_j(k) \begin{cases} = 0 \text{ if } i \neq j \\ \neq 0 \text{ if } i = j \end{cases}$$

For example, the above $\{\mathbf{e}_i\}$ system of the unit vectors is orthogonal in R^n. An orthogonal system resembles the well known orthogonal (Cartesian) coordinate systems of the 2- or 3-dimensional (R^2, R^3) spaces. Each vector s, $\mathbf{s} \in R^n$ can be uniquely described in any (coordinate) system $\{\mathbf{y}_i\}$ by its coordinates $t(1), t(2), \ldots, t(n)$, which means that

$$\mathbf{s} = \sum_{i=1}^{n} t(i)\,\mathbf{y}_i \tag{1}$$

The coordinates $t(i)$, because of the orthogonality, are easily obtained as

$$t(i) = \mathbf{y}_i'\mathbf{s} = d^{-1} \sum_{k=1}^{n} y_i(k)\,s(k), \quad i = 1, 2, \ldots, n \tag{2}$$

or using matrix notation

$$\mathbf{t} = d^{-1}\, Y\mathbf{s} \tag{3}$$

where Y is the matrix of the row vectors $\mathbf{y}_i'$, $i = 1, 2, \ldots, n$; t is the vector of the coordinates $t(1), t(2), \ldots, t(n)$; and d is the length of each $\mathbf{y}_1, \mathbf{y}_2, \ldots, \mathbf{y}_n$ coordinate vector. Y is an orthogonal matrix which means that $YY' = dI$, where I is the identity matrix.

The operation for determining the coordinates $t(i)$ of object S in the system $\{\mathbf{y}_i\}$ from the original coordinates $s(i)$, described by eqns. (2) or (3), is called orthogonal transformation. The original pattern vector s of object S can be recovered using the inverse transformation (1), or equivalently

$$\mathbf{s} = Y'\mathbf{t} \tag{4}$$

It can be proved that the n-dimensional vectors of the equidistantly sampled first n functions of the Fourier, Walsh or Haar systems create orthogonal systems of R^n. The first eight functions and the corresponding Y matrices of the sampled values of these systems are depicted in Fig. 1.

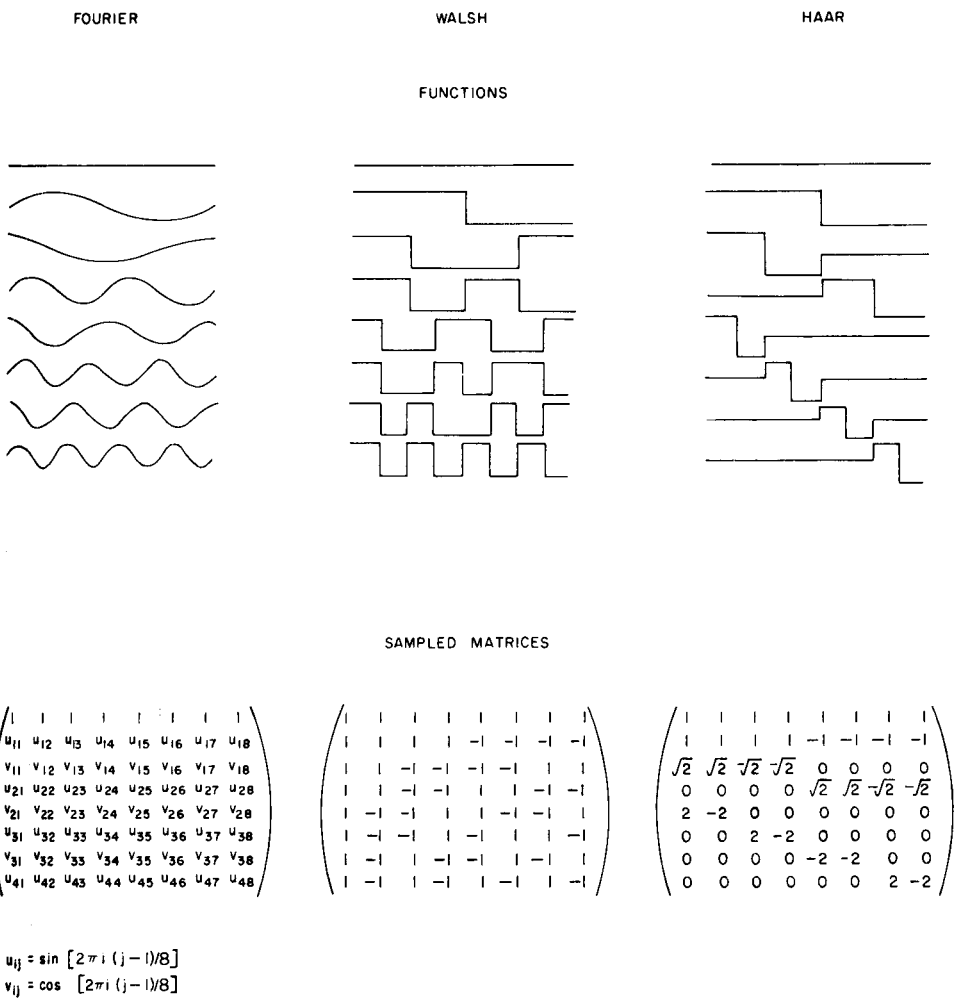

Fig. 1. The first eight functions of the Fourier, Walsh and Haar systems, and the matrices of their sampled values.

Further details about the Fourier (FT), Walsh (WT) and Haar (HT) systems and transformations are readily available [7—10].

Many other orthogonal systems are known in R^n, e.g. orthogonal polynomials or the systems of principal components which lead to the Karhunen Loève transformation [10] that is in some respects optimal. It is common to all orthogonal transformations that they describe how to alter the original coordinates $s(1), s(2), \ldots, s(n)$ of S, corresponding to the new orthogonal coordinate system which can be considered as a rotation and permutation of the original system $\{\mathbf{e}_i\}$. The main point is the fact that the position of the "point" S remains unchanged, although its coordinates change (Fig. 2).

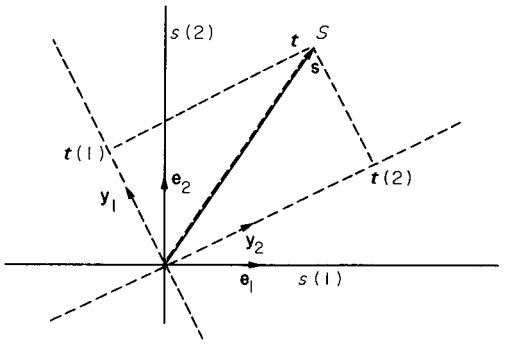

Fig. 2. The effect of changing the orthogonal (coordinate) system $\{e_1, e_2\}$ for $\{y_1, y_2\}$ on the coordinates of object S.

From this interpretation, it becomes clear immediately that the transformation does not change the geometric relationships, i.e. distances or angles between patterns $s_1, s_2, \ldots, s_M$ in R^n. All the Euclidean distances between them remain unchanged. Accordingly, this kind of transformation cannot be expected to produce any enhancement of the classification when the methods applied are based on Euclidean distance (e.g., KNN) or separating surfaces (e.g., binary linear classifier). However, slight changes in the result of classification might occur because of the imperfect convergence of the algorithms or of rounding errors in computation. Therefore, orthogonal transformation of the patterns is theoretically useless with algorithms based on Euclidean geometry of the pattern space. If another type of distance or algorithm is used, then a change in the result can be expected (e.g., city block distance).

From these considerations, it follows that the similarities, in the sense of the Euclidean distance, between free-induction-decay n.m.r. spectra are exactly the same as between the corresponding n.m.r. frequency spectra obtained by FT of the free-induction-decay data. The same is true for interferograms and frequency spectra in FT-I.R. or FT-I.C.R., etc.

Orthogonal transformations can, however, be used successfully together with feature reduction, particularly if the original data have some special properties relating to the orthogonal system of the transformation. For example, FT can be a very effective tool for data reduction of frequency-based signals and WT of sequency-based signals, respectively. Data reduction is done by discarding the non-significant components of the transformed vectors. One possibility is to use the minimum variance criterion when the components of the smallest variances are omitted. This method is optimal from the point of view of reconstruction of the original data. However, if the original pattern vectors $s_1, s_2, \ldots, s_M$ do not have a strict frequency or sequency property, as in the case of mass spectra, then not too much is to be gained by the transformation.

An advantage of using orthogonal transformations is their noise-reduction property. As the transformed values are weighted sums of the original values

(see eqn. 2), the expected statistical error of the pattern components is reduced by a factor of $n^{1/2}$. Therefore in the case of noisy data, this noise-reduction property can be utilized to attain more reliable results.

The applicability of the orthogonal transformations in common practice is due to the fast transformation algorithms, originated from Cooley and Tukey [11], which reduce the need of operations (multiplications and additions) from cn^2 to $cn\log n$ (c = constant). Furthermore, the fast WT and HT require only additions, and the HT merely needs $2(n-1)$ additions; in fact, HT is the fastest orthogonal transformation and needs only simple software. In addition to its speed, the HT has another remarkable property: in contrast to the FT and WT, several Haar-transformed components preserve better the local properties of the original pattern vector, because the Haar functions differ from zero over shorter intervals, see Fig. 1.

Several authors have reported on the feature-extracting properties of the FT and WT [2—7]. Their results can be well explained with the above theory. Jurs [2] underlined the error-resistance property of the transformed patterns. Brunner et al. [5] stated that classification of ^{13}C-n.m.r. spectra or the corresponding free-induction-decay data or the Walsh transform gave about the same result; this agrees perfectly with the distance-preserving property of orthogonal transformations described above. Jurs [2] and Kowalski and Bender [3] found FT and WT preprocessing advantageous in classification of low-resolution mass spectra by the binary linear classifier and KNN methods, respectively, in contrast to Brunner et al. [4] who found the WT patterns of ^{13}C-n.m.r. spectra less efficacious than the original patterns. Such differences in conclusions, also mentioned by Griffiths in his monograph [7], are due to the large uncertainty caused by investigating only one data base.

COMPUTATION

The computational experiments reported here were done to show that the performance of the different transformations varies with the applied data bases, algorithms and classification goals; therefore, none of these transformations can be declared decisively superior. Many earlier papers contain results obtained by using only one data set. It will be shown here that even when two different but fairly similar data collections are used, the results alter enough to change the validity of the assessment of the transformations.

Data and classifications

The data used here were taken from the mass spectral collections of ETH Zürich (OCETH), and of K. Varmuza, TU Vienna (WTH). In both cases, a data set consisting of 500 low-resolution mass spectra of simple organic compounds in the range C_{1-11} H_{1-22} O_{0-2} N_{0-2} was examined. The spectra had peaks up to m/z 151 with normalized peak intensities ranging from 0 to 100. The original 151 dimensions of pattern vectors were reduced to 128

(=2^7). The training set always consisted of 300 spectra, while the test set contained the remaining 200 spectra.

Supervised multicategory classification was made according to formula, i.e. to C, O, and N numbers. When the binary linear classifier was used, the training set was separated into structural classes as alkene or non-alkene, alcohol or non-alcohol, amine or non-amine compounds.

Classifying algorithms

Four different supervised classification methods were used to determine decision surfaces between the classes represented by the pattern vectors of the training set: binary linear classifier (BLC), multicategory linear classifier (MLC), potential function classifier (PFC) and the *K*-nearest neighbour classifier (KNN). The first three pertain to learning machine methods, and the training method applied was the error-correction feed-back [12]. BLC

TABLE 1

Percentages of recognition/prediction results on the OCETH mass spectra with various transformations

Classif. method	Chemical property	Preprocessing method					
		128-dimensional pattern vectors				65-dimensional pattern vectors	
		Orig.	FT	WT	HT	FSP	WSP
BLC	Alkene	94/84	95/85	93/86	95/85	90/82	89/83
BLC	Alcohol	90/87	89/88	90/87	88/86	85/82	84/80
BLC	Amine	91/86	89/83	92/86	90/86	86/81	87/81
MLC	O	84/72	82/73	85/72	82/72	73/69	75/70
MLC	N	90/85	91/85	90/86	89/86	82/80	86/81
PFC	C	45/40	43/39	43/40	45/39	39/37	41/38
PFC	O	71/63	73/64	70/65	71/61	66/60	63/59
PFC	N	81/78	80/75	83/80	82/80	80/75	81/73
KNN	C	46	46	46	46	41	42
KNN	O	75	75	75	75	71	69
		10-dimensional reduced pattern vectors					
BLC	Alkene	81/77	87/81	86/81	88/82	86/80	82/80
BLC	Alcohol	83/80	85/84	90/85	84/81	86/81	90/85
BLC	Amine	88/83	86/84	91/87	88/86	91/86	92/89
MLC	O	59/54	67/60	62/58	62/56	68/60	65/60
MLC	N	76/70	75/73	81/73	75/69	80/75	82/71
PFC	C	32/24	30/28	37/32	36/32	35/31	31/29
PFC	O	54/47	60/48	59/51	58/50	58/52	62/56
PFC	N	67/63	72/66	66/65	69/62	75/67	71/69
KNN	C	31	33	34	30	34	35
KNN	O	59	63	65	60	62	63

TABLE 2

Percentages of recognition/prediction results on WTH mass spectra with various transformations

Classif. method	Chemical property	Preprocessing method					
		128-dimensional pattern vectors				65-dimensional pattern vectors	
		Orig.	FT	WT	HT	FSP	WSP
BLC	Alkene	92/79	91/79	92/78	89/78	87/77	85/77
BLC	Alcohol	95/90	95/92	94/88	95/93	88/83	89/85
BLC	Amine	97/88	97/88	98/89	97/90	92/85	91/84
MLC	O	84/67	82/68	84/66	82/67	80/64	78/62
MLC	N	92/82	94/81	92/80	92/81	85/79	87/76
PFC	C	39/37	42/38	39/36	37/35	32/30	35/31
PFC	O	68/54	72/56	70/52	69/54	62/50	63/48
PFC	N	86/75	88/72	89/74	88/70	82/68	80/66
KNN	C	41	41	41	41	40	38
KNN	O	74	74	74	74	69	70
		10-dimensional reduced pattern vectors					
BLC	Alkene	83/77	87/80	86/77	86/80	87/77	81/76
BLC	Alcohol	84/84	85/86	89/86	85/80	88/82	87/83
BLC	Amine	84/84	85/84	87/86	87/86	89/83	89/84
MLC	O	60/52	65/56	63/54	64/55	66/63	69/63
MLC	N	78/72	76/70	83/73	78/72	81/76	84/71
PFC	C	30/29	32/28	34/29	35/29	34/30	33/30
PFC	O	56/53	63/50	64/50	62/52	55/50	63/58
PFC	N	75/70	73/71	68/67	71/69	78/70	75/68
KNN	C	34	34	35	31	36	35
KNN	O	59	64	66	62	64	66

trains only one linear decision function, in the form $g(\mathbf{x}) = \mathbf{w}'\mathbf{x}$, to separate two classes, where $\mathbf{x}$ denotes the pattern vector (in $n + 1$ dimensions) and $\mathbf{w}$ is the weight vector determined through the training. Decision between the two classes is made according to the sign of the function $g(\mathbf{x})$. MLC trains as many linear decision functions g_i as there are categories, and the classifying criterion is $\mathbf{x} \in$ category i, when $g_i(\mathbf{x}) > g_j(\mathbf{x})$ for all $i \neq j$. PFC involves linear regression, the classes being defined by the value of the inner product $\mathbf{w}\,\mathbf{x}$ of the pattern $\mathbf{x}$ and weight vector $\mathbf{w}$. KNN is a well-known classifying method in chemistry [1]; it was applied here with $K = 5$ and with Euclidean distance measure.

These classification methods were applied to the 128-dimensional original, to the pattern vectors obtained by FT, WT, HT, and to the 65-dimensional Fourier and Walsh power spectra obtainable from the transformed values [10]. Feature reduction was made for these data sets according to the minimum variance criterion [10]. The dimension of the reduced patterns was 10.

The necessary programs were written in FORTRAN. The results obtained using the 128- and 10-dimensional patterns are shown in Tables 1 and 2. The Tables contain the recognition and prediction abilities, i.e. percentages of correctly classified training and test vectors, respectively. The methods applied and the chemical properties are indicated in the first two columns. Table 3 contains the frequencies of the classes.

DISCUSSION

On the basis of the computational results (Tables 1 and 2), the following conclusions can be made. As expected from the distance-preserving property of the orthogonal transformations, the classifications of the 128-dimensional original and transformed pattern vectors resulted in about the same separation of classes. The 1—3% variations are due to the imperfect convergence of the algorithms; consequently, the uncertainty in the convergence of different methods can be estimated by the dispersion of the results within the rows of the 128-dimensional patterns. This uncertainty is equal to zero in the KNN method, which is obvious because KNN does not require iterative training of decision functions.

Because the transformed pattern components are linear combinations of the original measured intensities, it is usually expected that data reduction achieved by discarding several transformed components will cause less loss of information than reduction of the original pattern, where the information

TABLE 3

The percentages of the relative frequencies of classes in the selected OCETH and WTH data sets

Chemical property	OCETH data set		WTH data set	
	Training	Test	Training	Test
Alkene/ non-alkene	16/84	19/81	13/87	25/75
Alcohol/ non-alcohol	13/87	14/86	11/89	12/89
Amine/ non-amine	12/88	11/89	13/87	15/85
C-number 1—11	1 4 5 10 14 22 16 14 9 3 2	1 3 6 11 12 19 17 19 6 5 1	2 5 8 11 15 19 14 14 7 4 1	0 1 4 11 12 14 17 18 12 6 5
O-number 0—2	45 38 17	44 35 21	44 36 20	48 32 20
N-number 0—2	72 23 5	74 23 3	75 21 4	75 22 3

about omitted intensities is completely lost. This accounts also for the enhanced error resistance or stability of the reduced transformed patterns. In most cases, the intense data reduction from 128- or 65- to 10-dimensional patterns decreased the recognition/prediction performance somewhat less for the transformed patterns, especially for the power spectra, than for the original patterns, but this was not always so. The decreased performance with the reduced patterns was compensated by the greatly increased speed in computation and by easier data handling.

Comparison of the 10-dimensional tables of the OCETH and WTH data indicates that the differences in the final results can be considered as a pure stochastic variation. This is probably the reason why such different conclusions have been reported in the literature. It is clear that the investigation of only one data collection does not justify postulating the superiority of a certain method, even if the collection contains several hundreds or thousands of spectra. In fact, none of the transformations can be considered as decisively superior.

The variations in the goodness of classifications of the OCETH and WTH spectral data are remarkably less with the reduced FT, WT and HT vectors than with the original vector, which emphasizes the greater stability of the transformed pattern vectors. This seems to prove what was expected from the transformations.

In the case of the 128-dimensional pattern vectors, the WT was about 7 times faster, and the HT about 100 times faster than the FT. Otherwise, the HT does not seem to be better than the FT or WT.

From these results, it can be concluded that the application of orthogonal transformations, such as FT, WT or HT, has the advantage of some stability against the errors of the original data. Otherwise, it does not seem to be a universally applicable method unless the data have some frequency or sequency property suiting the applied orthogonal system. Feature extraction methods exploiting special chemical properties relating to the goal of classification, appear to be more promising. Because of the very great freedom in constructing orthogonal systems, it might be possible to build such a system, where the coordinate vectors relate to chemical properties. This is rather reminiscent of factor target rotation in factor analysis or principal component analysis.

We are grateful to Prof. Dr. E. Pungor for supporting this research and G. E. Veress for valuable discussion. We also thank J. T. Clerc (Bern), E. Pretsch (Zürich) and K. Varmuza (Vienna) for supplying the mass spectral data collections.

REFERENCES

1 P. C. Jurs and T. L. Isenhour, Chemical Applications of Pattern Recognition, Wiley-Interscience, New York, 1975.
2 P. C. Jurs, Anal. Chem., 43 (1971) 1812.
3 B. R. Kowalski and C. F. Bender, Anal. Chem., 45 (1973) 2234.

4 T. R. Brunner, R. C. Williams, C. L. Wilkins and P. J. McCombie, Anal. Chem., 46 (1974) 1799.
5 T. R. Brunner, C. L. Wilkins, R. C. Williams and P. J. McCombie, Anal. Chem., 47 (1975) 662.
6 C. L. Wilkins and T. L. Isenhour, Anal. Chem., 47 (1975) 1849.
7 P. R. Griffiths, Transform Techniques in Chemistry, Plenum Press, New York, 1978.
8 E. O. Brigham, The Fast Fourier Transform, Prentice-Hall, Englewood Cliffs, N.J., 1974.
9 K. G. Beauchamp, Walsh Functions and their Applications, Academic Press, London, 1975.
10 N. Ahmed and K. R. Rao, Orthogonal Transforms for Digital Signal Processing, Springer-Verlag, Berlin, 1975.
11 J. W. Cooley and J. W. Tukey, Math. Comp., 19 (1965) 297.
12 N. J. Nilsson, Learning Machines, McGraw-Hill, New York, 1965.

Analytica Chimica Acta, 133 (1981) 271—281
Computer Techniques and Optimization
Elsevier Scientific Publishing Company, Amsterdam — Printed in The Netherlands

RECONSTRUCTION OF MASS SPECTRA OF COMPONENTS OF UNKNOWN MIXTURES BASED ON FACTOR ANALYSIS

JIE-HSUNG CHEN and LIAN-PIN HWANG*

Union Industrial Research Laboratories, Industrial Technology Research Institute, Hsinchu (Taiwan)

(Received 30th May 1980)

SUMMARY

A method is described for the spectral resolution of combined gas chromatographic—mass spectrometric data. Factor analysis is applied to the identification of a second species in a single gas chromatographic peak. A plot can be constructed from the region of the non-negative values of spectral lines in the factor space. Feasible locations for the spectra of these constituents in the plot can be identified and give recognizable spectra of the separated constituents.

Much material has been published on the mathematical techniques and applications of factor analysis [1—5]. Lawton and Sylvestre [6] applied factor analysis to the resolution of a two-component u.v. system and demonstrated that the resolved spectrum could not be defined uniquely on the basis of non-negative values of spectral density and component concentration, but showed features analogous to those of the true spectra. Ohta [7] used the same method to resolve u.v. spectra of a three-component system and found that each possible component spectrum is distributed in the factor space. MacNaughton et al. [8], using similar assumptions, deconvoluted overlapped gas-chromatographic peaks to provide quantitative information.

A single chromatographic peak may contain one or more components. Several components are not easily distinguished because of the overlapping spectral lines of a mixture. Previous studies were limited to the application of factor analysis to data from combined gas chromatography—mass spectrometry (g.c.-m.s.) to determine the number of components in an unresolved gas-chromatographic peak [9—11]. A method of isolating the species present in mixtures would be extremely useful. In the work described here, the use of factor analysis in identifying a second species in a single peak was explored. Further, mass spectrometry was used to check whether the isolation of constituent spectra is feasible and to determine to what extent the method developed is applicable.

The advantage of invoking mass spectrometry is that the discrete m/z values in a mass spectrum are superior to optical spectrometry in studying

0378—4304/81/0000—0000/$02.50

the feasibility of spectral separation, partly because of the absence of baseline problems. To apply factor analysis to the separation of mixtures, mass spectra were obtained at fixed time intervals across a chromatographic peak and each mass spectrum was considered as a mixture. Since the true component spectra have no negative element at any spectral point, the technique described by previous authors was expanded, and a so-called θ—ϕ plot was employed in three-component systems to show where the constructed non-negative spectral density lies and then to locate the true spectra of the components. Unlike previous studies, the concentration of the non-negative component in the mixture is not utilized; but the condition of non-negative spectral density is retained here. The approach is illustrated by examples of the spectral resolution of mixtures and its validity is discussed.

DEVELOPMENT OF THE METHOD

The mathematical bases of factor analysis are well established [1, 2]. In this work, the m mixture spectra are considered as vectors with dimension p, the number of m/z points covered by the mass range studied. These spectra represent a set of vectors that is collected into a data matrix K with order $m \times p$ (usually $p \gg m$).

The column array in the data matrix K corresponds to different m/z values and the row array corresponds to the mixtures with different concentration ratios. After the factor analysis, the matrix is transformed into another matrix containing the same amount of information as the original data matrix. The new set of vectors, i.e. the eigenvectors, are also orthogonal. In the algorithm used, the vectors are output in descending order of the corresponding eigenvalues. From the distinct difference between successive eigenvalues, it becomes possible to determine the number of physically distinct components, n, in the mixtures, where n is presumably less than m. The n eigenvectors corresponding to the n largest eigenvalues form a matrix V with order $p \times n$ and form an n-dimensional eigenvector space. The rest of the eigenvectors, which are comparatively small, can be discarded without losing any significant feature because they contain the spectral noise.

In order to save computing memory and speed up processing, a modified computing method [5] based on the Cayley—Hamiltonian theorem was used. First, the covariance matrix $A \equiv K K^t$ was used; here A is a real symmetric matrix with order $m \times m$ and the superscript t represents the transpose of the matrix indicated. An orthogonal matrix Q to diagonalize matrix A can be found, so that $Q^{-1} AQ = \Lambda$; where Λ is a diagonal matrix and its diagonal elements, the eigenvalues, are the same as the m largest eigenvalues generated by the usual method [1, 2] which is used to diagonalize the matrix $K^t K$. From the distinction between successive eigenvalues, the number of components, n, can also be determined. In matrix Q, the n eigenvectors corresponding to the n largest eigenvalues form a matrix U with order $m \times n$. The matrix V can be obtained by

$$V \equiv K^t U \equiv (\mathbf{V}_1\ \mathbf{V}_2, \ldots, \mathbf{V}_n) \tag{1}$$

where the column matrices $\mathbf{V}_1, \mathbf{V}_2, \ldots, \mathbf{V}_n$ are n eigenvectors as obtained by the usual method of diagonalizing K^tK.

In the procedure leading to eqn. (1), since the order of the A matrix is much smaller than the order of K^tK, the time and memory spaces needed are dramatically reduced, yet the information obtained from the diagonalization of K^tK is the same. It is important for the small storage memory available in the Hewlett Packard 9825A to manipulate nine sets of mixture data simultaneously in the process of diagonalizing the covariance matrix. Since the spectrum of the component is a linear combination of $\mathbf{V}_i$ (i = 1, ·, n) [6], it will be shown how the pure component spectra can be generated approximately in terms of $\mathbf{V}_i$.

As an example, a two-component system is considered. It is assumed that the spectra of the components do not completely overlap and that the constructed spectra are properly normalized. Consequently, it needs only one variable to define a constructed spectrum from a linear combination of $\mathbf{V}_1$ and $\mathbf{V}_2$, which are the two eigenvectors corresponding to the two largest eigenvalues of the true factors arranged in order of descending magnitude. The constructed spectrum S (Fig. 1a) is then given by

$$S = \mathbf{V}_1 \cos\phi + \mathbf{V}_2 \sin\phi \tag{2}$$

where the element of S at every spectral point is non-negative and the values of ϕ are confined to the first (second) and fourth (third) quadrants as the elements of $\mathbf{V}_1$ are taken to be positive (negative). Therefore a non-negative region for S can be obtained on the $\mathbf{V}_1$—$\mathbf{V}_2$ plane by scanning the value of ϕ in the first and fourth quadrants. The non-negative region thus found is singly connected (see Fig. 6). Then the spectra of the components can be found on the two boundaries of this region respectively. This finding may be attributed to the fact that spectra found inside the non-negative region are hybrids of the component spectra while those found on the boundaries must have simpler structures because certain spectral lines vanish and tend to be

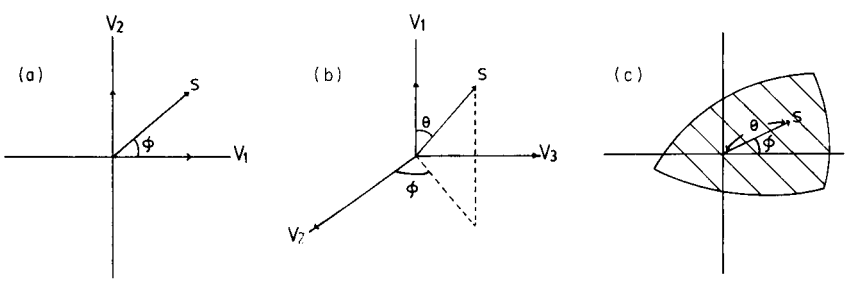

Fig. 1 (a). The relation of constructed spectrum S and eigenvectors ($\mathbf{V}_1$, $\mathbf{V}_2$) for a two-component system. (b) The relation of constructed spectrum S and eigenvectors ($\mathbf{V}_1$, $\mathbf{V}_2$, $\mathbf{V}_3$) for a three-component system. (c) The θ—ϕ plot of non-negative constructed spectra transformed from (b) for a three-component system.

negative, and therefore these two simpler and distinct spectra could be the component spectra.

For a three-component system, the relation of the constructed spectrum S and eigenvectors (V_1, V_2, V_3) of the three true factors (Fig. 1b) in this system is given by

$$S = V_1 \cos\theta + V_2 \sin\theta \cos\phi + V_3 \sin\theta \sin\phi \quad (3)$$

where the values of θ are not greater (less) than $\pi/2$ as long as the elements of the eigenvector V_1 are taken as positive (negative). Given the polar angles θ and ϕ, the spectrum S can easily be constructed from the eigenvectors. After factor analysis for the mixture spectra taken from the linear sums of these three components, three eigenvectors, V_1, V_2, and V_3, of the true factors are obtained. Thus by examining the relations of θ and ϕ for the boundaries of non-negative spectra generated from the linear combinations of V_1, V_2 and V_3, the θ—ϕ plot can be obtained. This is demonstrated in Fig. 1(c) where θ is taken as radial coordinate and plotted versus ϕ.

On the θ—ϕ plot, the values of (θ, ϕ) specified in the shaded area correspond to the non-negative spectra obtained from the linear sums of V_1, V_2 and V_3. By recognizing that the component spectra have simpler structures than the hybrid one, the location of a component spectrum in the factor space may be comparatively farther from V_1. In other words, the θ angle where the component spectrum is found may have a distinctly larger value. To obtain more definite information about the feasible region in which the component spectra lie, the component spectra and those resolved from the mixtures are compared. The three spectra shown in Fig. 2 are treated as the component spectra with the intensity values cited on each spectral line. For component 1 the range of m/z values is given from 1 to 10. For components

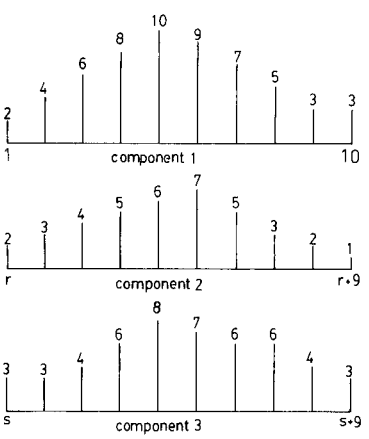

Fig. 2. Simulated component spectra used in the discussion of the θ—ϕ plot and overlapping effects. The values of r and s for components 2 and 3 are given in the text for three different cases.

TABLE 1

Combination coefficients for the simulated mixture spectra

Mixture	Combination coefficients $(a_1C_1 + a_2C_2 + a_3C_3)$[a]		
	a_1	a_2	a_3
1	0.12	0.64	0.24
2	0.13	0.63	0.24
3	0.27	0.52	0.21
4	0.28	0.41	0.31
5	0.36	0.47	0.17
6	0.35	0.56	0.09

[a] C_i indicates the spectrum of the ith component as shown in Fig. 2.

2 and 3, the range varies according to the three cases studied below. The combination coefficients of constituents in the six mixture spectra studied in the three cases are the same and are listed in Table 1. In case 1, the m/z ranges for components 2 and 3 are specified by $r = 11$ and $s = 21$, respectively, compared with $r = 6$ and $s = 21$ for case 2, and $r = 5$ and $s = 9$ for case 3.

In case 1, the three spectra of components are completely distinct from one another, while in case 2 there is partial distinction between them. The resulting θ—ϕ plots for cases 1 and 2 are shown in Fig. 3, and the resolved spectra of components can be found, at three vertices of the non-negative region on the θ—ϕ plot. For case 3, since the spectral range of component 2 is covered by components 1 and 3, the θ—ϕ plot reveals one additional obtuse vertex as shown in Fig. 3(c). The three components can still be found at the three vertices with sharper angles. The quality of the resolved spectra is not as good as that for the two-component system because of incomplete resolution. The contribution of the unwanted component in the resolved spectrum is about 2%. The resolution may be improved by taking a larger set of mixture spectra for factor analysis.

There are great differences in intensity among the spectral lines in any spectrum. A few percent of noise are commonly present in the spectra and its effect on spectral separation depends on its percentage contribution to the intensity. If the noise is of the same magnitude over the studied spectral range, the resulting percentage error for weak spectral lines is mainly affected. In factor analysis and subsequent spectral separation, noise may yield an extra spurious component and obscure the result. The situation may be improved by rejecting the insignificant spectral lines in the mixture spectra before proceeding with the factor analysis, i.e., the entire spectrum need not be used. The rejection of spectral lines with intensity less than 1% proved satisfactory here (see below). In conclusion, for noise-free and non-overlapping component spectra, only three sharp vertices account for the constituents, but for noisy and/or overlapping spectra, additional vertices may result and the feasibility of finding the component spectra depends on getting rid of the "spurious" vertices.

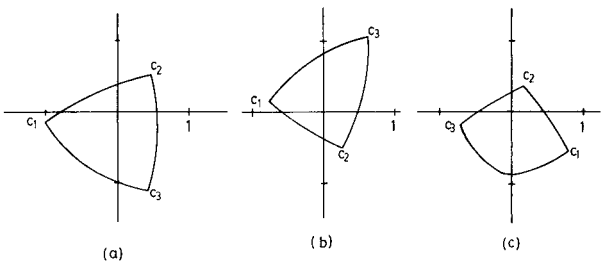

Fig. 3. (a), (b) and (c), are the θ—ϕ plots for cases 1, 2, and 3, respectively. The spectrum of component C_i (i = 1, 2, 3) corresponds to the system shown in Fig. 2.

EXPERIMENTAL

All experimental mass spectra were obtained on a Finnigan 4021 gas chromatograph—mass spectrometer equipped with a quadrupole analyzer and operated in the electron impact mode. The interface between the gas chromatograph and the mass spectrometer was an all-glass jet type enrichment device. The sensitivity and resolution of the spectrometer were carefully adjusted. The mass spectra of the g.c. effluents of various compositions across a g.c. peak suspected of being a mixture were recorded and acquired digitally with a Data General Nova 3/12 computer; the spectra and the intensity values were recorded with a Printronix 150 printer—plotter. The factor analysis and mathematical manipulations were then done by a Hewlett-Packard 9825A desk-top calculator. The Hewlett-Packard 9864A digitizer and 9862A plotter were also used.

With the experimental conditions listed in Table 2, unresolved gas-chromatographic peaks (Fig. 4) were obtained deliberately. A mass scan time of 0.1 s and a hold time of 0.9 s for each scan were set and the scan time for the desired mass range was kept as fast as possible so that the mass spectrum of each effluent could be treated as a mixture spectrum with good linearity in component concentration.

RESULTS AND DISCUSSION

In the gas chromatogram of the 1-pentanol and 2-(1-methylethoxy)-ethanol mixture (Fig. 4a), the ordinate represents the reconstructed ion current detected by the mass analyzer. It is clear that the mass spectra scanned at the overlapping portion of the g.c. peak must be the mixed spectra of 1-pentanol and 2-(1-methylethoxy)ethanol with different contributions to each mixed spectrum. The mixed spectra were selected and displayed in Fig. 5 with scan numbers 151, 157, 160, 171, 180, 199 and 208. For the factor analysis of the mixed spectra, spectral lines with intensity less than 1% of the most intense line are rejected and common significant spectral lines are selected. The choice of significant spectral lines is another

TABLE 2

Experimental conditions for obtaining mass spectra of mixtures with a Carbowax 20M column

Substances[a]	Temperatures (°C)			
	Column	Injection	Separator	Flow rate (ml min^{-1})
1-Pentanol, 2-(1-Methyl-ethoxy)ethanol	100—120 (2°C min^{-1})	150	120	12
1-Pentanol Toluene Butyl acetate	120	150	130	15

[a]All Merck GR grade.

feature of applying factor analysis to g.c.-m.s. systems. The pretreatment helps to avoid the effect of noise and to obtain more definite results in the determination of true eigenvalues and their corresponding eigenvectors. After spectral separation, the whole spectra of components can be regenerated by appropriate transformation using the relations of eigenvectors and resolved spectra (eqn. 2).

The eigenvalues corresponding to this system are listed in Table 3. The abrupt change in their magnitude indicates that there are two species in the system. The feasible region for component spectra is shown in Fig. 6 and the two species may be found at $\phi = 35°$ and $\phi = -30°$. The resolved and the real component spectra are displayed in Fig. 7. Indubitably, the method is satisfactory for a two-component system.

The gas chromatogram for the system containing 1-pentanol, toluene and butyl acetate is shown in Fig. 4(b). The mass spectra of those mixtures were obtained from the overlapping region of the g.c. effluent and the scan num-

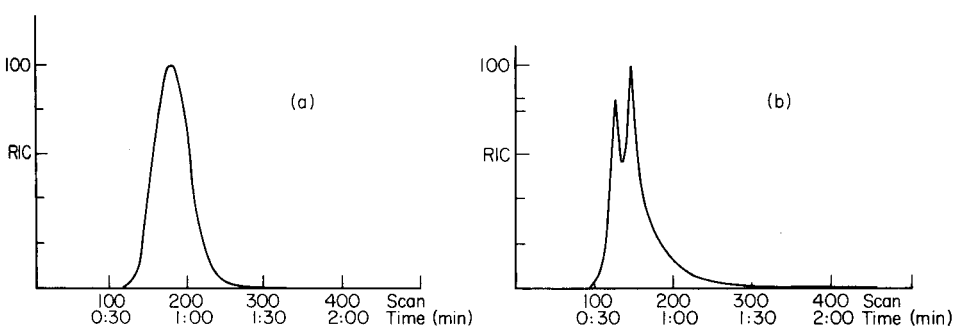

Fig. 4. Gas chromatograms of (a) 1-pentanol, 2-(1-methylethoxy)ethanol mixture; (b) 1-pentanol, toluene and butyl acetate mixture.

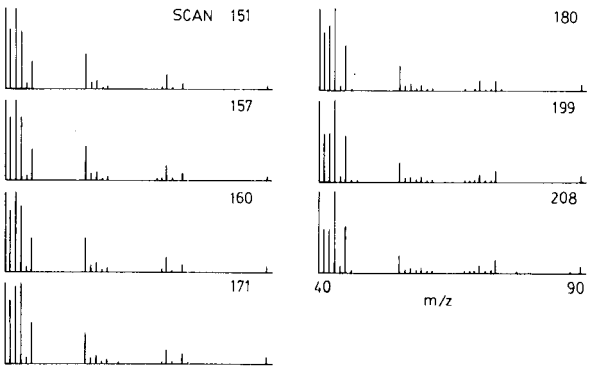

Fig. 5. Mass spectra of mixture obtained in Fig. 4(a) at scan number indicated.

bers are cited in Fig. 8. On factor analysis, the resulting eigenvalues indicate that there are three components in this system (Table 3). If the contributions in the factor analysis from whole spectra are considered without rejecting insignificant lines, definite information cannot be obtained about the locations of component spectra from the θ—ϕ plot of the non-negative region (Fig. 9(a)). However, Fig. 9(b) shows that when the insignificant spectral lines ($\leqslant 1\%$) are rejected, good results can be achieved. It can be seen that the spectra of toluene, 1-pentanol and butyl acetate can be found at the three vertices indicated. The resolved and the real component spectra are compared in Fig. 10; the resolved spectra closely resemble the experimental spectra of the pure component, except that extra spectral lines appear in the resolved spectrum of toluene. This may be due to incomplete resolution of the spectral lines which result from 1-pentanol and butyl acetate with large fractions. The reason for the absence of the $m/z = 44$ line in the spectrum of 1-pentanol is not clear and the appearance of an additional vertex at $\phi \approx 270^\circ$ may be attributed to the spectra of 1-pentanol and butyl acetate having many spectral lines in common. The analogous effect was discussed above in the third case in describing the method.

TABLE 3

Eigenvalues of experimental two- and three-component systems

Two component system		Three component system	
1.72×10^5	1.18	2.13×10^5	0.70
4.19×10^3	0.12	2.13×10^4	0.21
7.18	0.05	2.75×10^3	0.00
1.59		15.2	0.00
		2.41	

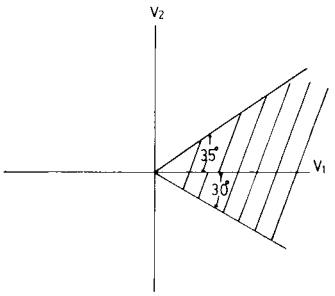

Fig. 6. Non-negative region, indicated by the shaded area, of the system in Fig. 5.

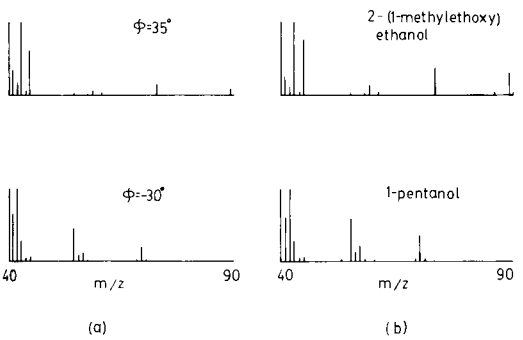

Fig. 7. Comparison of resolved (a) and real (b) component spectra.

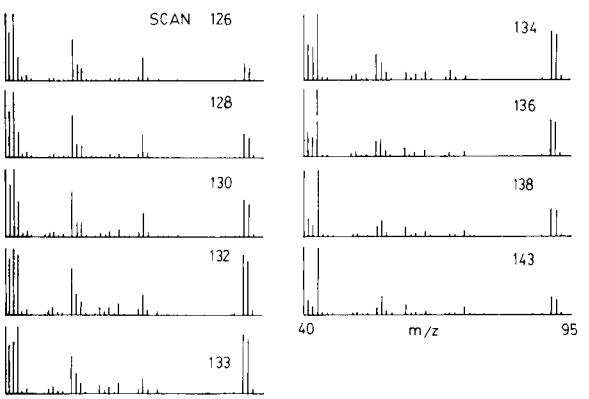

Fig. 8. Mass spectra obtained in Fig. 4(b) at scan numbers indicated.

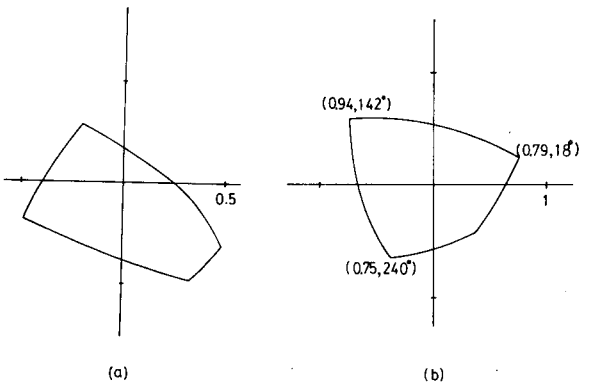

Fig. 9. The θ—ϕ plots of the non-negative region of the system in Fig. 8 obtained with (a) all spectral lines considered, and (b) only the spectral lines with intensity greater than 1% considered. The units for θ and ϕ given in (θ, ϕ) are radians and degrees, respectively.

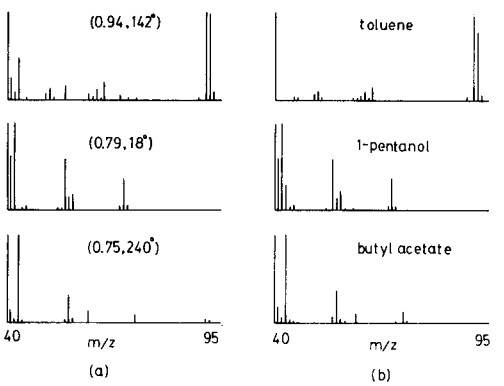

Fig. 10. Comparison of resolved (a) and real (b) component spectra of the system in Fig. 8.

CONCLUSION

Factor analysis is utilized to determine the possible spectra of constituents from the spectra of their mixtures. High signal/noise spectra are required for detecting second species in the mixtures. Data from intense spectral lines of the mass spectra can characterize component spectra better than data from the complete spectra. In such applications, however, deviation from the Dalton law must be eliminated with a small amount of sample injected. Applications of the method also require that the spectrum of one component does not overlap completely with the other, but the chance of this occurrence may be minimized by avoiding the use of small numbers of spectral lines. The excellent agreement of the identification of component spectra in a two-component system with the real spectra indicates that the

methodology is useful. The result for three-component system is less satisfactory although the resolved spectra are recognizable. Thus the approach reported may be helpful not only for detecting the presence of more than one species but also for recognizing their individual spectrum in a g.c. peak that appears to represent only one pure species. It has potential as a useful tool for the interpretation of combined chromatography—mass spectrometric data. With minor calculations, it can be extended to deconvoluting the chromatographic peak without prior knowledge of the peak shape of constituents.

REFERENCES

1 T. W. Anderson, Anal. Math. Statist., 34 (1963) 122.
2 T. W. Anderson, Introduction to Multivariate Analysis, Wiley, New York, 1958.
3 H. H. Harman, Modern Factor Analysis, University of Chicago Press, Chicago, 1967.
4 R. J. Rummel, Applied Factor Analysis, Northwest University Press, Evanston, 1970.
5 J. T. Bulmer and H. Shurvell, J. Phys. Chem., 77 (1973) 256.
6 W. H. Lawton and E. A. Sylvestre, Technometrics, 13 (1971) 617.
7 N. Ohta, Anal. Chem., 45 (1973) 553.
8 D. MacNaughton, Jr., L. B. Rogers and G. Wernimont, Anal. Chem., 44 (1972) 1421.
9 J. E. Davis, A. Shepard, N. Stanford and L. B. Rogers, Anal. Chem., 46 (1974) 821.
10 G. L. Ritter, S. R. Lowry, T. L. Isenhour and C. L. Wilkins, Anal. Chem., 48 (1976) 591.
11 E. R. Malinowski and M. McCue, Anal. Chem., 49 (1977) 284.

Analytica Chimica Acta, 133 (1981) 283—301
Computer Techniques and Optimization
Elsevier Scientific Publishing Company, Amsterdam — Printed in The Netherlands

A MICROPROCESSOR-BASED INSTRUMENT FOR CORRELATION CHROMATOGRAPHY AND DATA PROCESSING

H. C. SMIT*, R. P. J. DUURSMA and H. STEIGSTRA

Laboratory for Analytical Chemistry, University of Amsterdam, Nieuwe Achtergracht 166, 1018 WV Amsterdam (The Netherlands)

(Received 28th July 1980)

SUMMARY

A microprocessor-based instrument performing all actions necessary for correlation chromatography, a correlator, is described. This correlator is designed to make correlation chromatography as easily applicable as other types of chromatography. The instrument can also complete the data processing of the finished correlogram. Examples are the determination of the retention time, baseline drift corrections, the determination of the peak amplitudes and peak areas including the confidence levels. Design considerations and results are given. The systematic error defining the accuracy is typically 0.2%.

Correlation chromatography (c.c.) is a signal-enhancement technique based on general systems theory and statistical signal analysis. In the first practical description of the method, Izawa et al. [1] proposed the use of c.c. for continuous gas analysis, but applications in trace analysis were promising [2]. Because the method is still in the experimental phase and not yet generally used, a short explanation without a profound theoretical treatment will be given here. For more details the reader is referred to the literature [3—31].

Correlation chromatography requires rather comprehensive instrumentation and a good knowledge of correlation theory is indispensable in selecting the optimum conditions for each separation process. To make c.c. more generally accessible, an instrument called a correlator has been developed to perform all the actions necessary for c.c. This correlator was designed to be used by operators without particular skills in computer techniques and without detailed knowledge of the theoretical background.

Comparison of correlation and conventional chromatography shows that there are no differences concerning the columns and detectors. Experimental conditions (eluent composition, flow, temperature, etc.) are chosen according to the rules valid in normal chromatography. A difference is that the sample is not injected as a pulse in a very short time but is introduced according to a (pseudo)random pattern, a so-called pseudo-random binary sequence (PRBS).

In a random binary pattern only two signal values, e.g., 0 and 1, are

0378—4304/81/0000—0000/$02.50

possible; which of the two values will be present at any particular time is not predictable. However, a PRBS is a logical function combining the properties of a true (binary) random signal with those of a reproducible deterministic signal. After a certain time (a sequence) the pattern is repeated. If the value of the PRBS is 0, pure mobile phase flows into the column; if the value is 1, sample is injected. It may be necessary to reduce the duty cycle; sample is then introduced into the column only during part of a clockperiod with level 1.

At first sight, separation is out of the question, all peaks are confluent. However, if the cross-correlation function of the PRBS and the detector output are calculated, the result will be a correlogram, which is the same as a normal chromatogram obtained by a single injection [1, 2].

The main advantage of this rather complicated method of obtaining a chromatogram is that the noise of the system (detector noise, etc.) is not correlated with the PRBS and reduces to zero with increasing correlation time. Theoretically, any desired detection limit can be achieved if enough time and sample are available. Of course, in practice some limitations like the influence of non-stationarity exist [4].

An extension of the chromatographic system required to perform c.c. is a rather complicated injection system, for both g.c. and h.p.l.c. Some systems have been described [5, 12]. Moreover, a PRBS generator, a device with extensive data-processing capabilities, and power amplifiers for controlling the valves are required. These demands can be excellently fulfilled by a microcomputer at low cost. A very real obstacle to the wider introduction and application of c.c. is removed by this development of a cheap correlator.

The microprocessor can also perform more tasks than are strictly necessary in c.c. The data processing of the finished correlogram can be done very well: baseline corrections (offset and drift), peak amplitude, peak area and retention time, as well as the uncertainty of peak amplitude and peak area, can be determined. Two strategies for obtaining these data seemed possible. The first is the application of an optimal procedure for information extraction, i.e., the use of optimal filtering, peak finding procedures, baseline drift determinations, etc. Because the microprocessor is not the most appropriate computing device for these purposes, this possibility was abandoned. However, off-line application of such a procedure on the correlogram with a more suitable computer must be possible. The second strategy takes advantage of the judgement of the operator. In the displayed correlogram, points of the baseline can be selected by means of a cursor, indicating the peak limits for area determinations, peakless parts of the baseline for uncertainty determinations, etc. The operator is allowed to use his experience when controlling the displayed results. This, in general, will be sufficient in trace analysis.

INSTRUMENTATION FOR CORRELATION CHROMATOGRAPHY

Apart from the necessary modifications of the injection system [5], essential extensions to a chromatographic set-up to allow c.c. are (see Fig. 1): (a) the pattern generator which is necessary for generating either a single pulse (normal chromatography) or a PRBS (c.c.), and is used for stimulation of the column (valve switching) and for calculation of the CCVF (cross covariance function) from the detector output and the pattern; (b) the data sampler, which is used to sample the filtered electric detector signal and convert it to a digital value; (c) an arithmetic unit to calculate the CCVF; and (d) a display for the results.

Some extensions are not essential for c.c., but greatly improve its capabilities. Thus an interface to a data-storage medium like a digital cassette, paper tape or a minicomputer is useful. The output will be a copy of the sampled analog detector signal or the CCVF and can be used for theoretical calculations or compensating calculations if non-stationarities occur in the chromatographic system [4]. An interface to a hard copy unit, to a large computer or to the usual x—t recorder is valuable. Some facility for applying baseline corrections and for integrating (individual) peaks is desirable. In general, baseline drift correction with a number of straight lines is sufficient. Finally, the standard deviation of the baseline noise of the correlogram and the standard deviation of the integral should be determined.

THEORY

The CCVF, calculated by

$$\mathrm{CCVF}(\tau) = \lim_{T \to \infty} T^{-1} \int_0^T \mathrm{PRBS}(t)\, Y(t + \tau)\mathrm{d}t \qquad (1)$$

can be interpreted as the response of a chromatographic system, a chromatogram, if an appropriate PRBS signal is used to stimulate the system and $Y(t)$

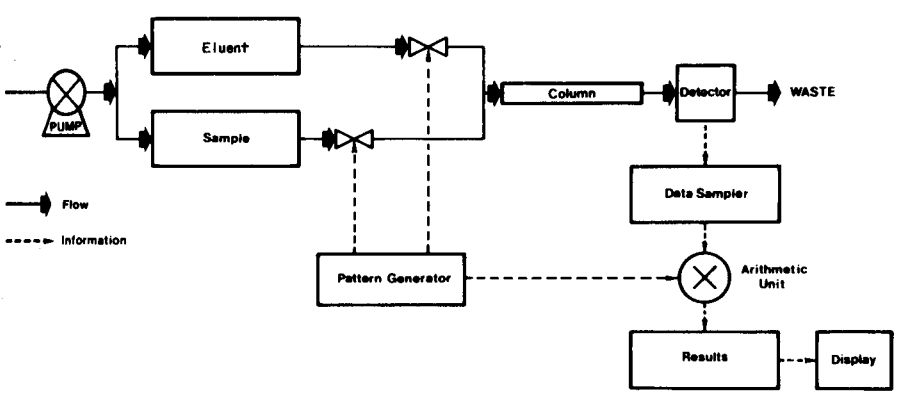

Fig. 1. Flow sheet for a correlation chromatography system.

is the response of the linear system to this stimulus. It can be shown that the CCVF has an average of zero if the PRBS used has an average of zero [4]. If the PRBS were purely random, +1 and −1 states would be expected equally. The length of a PRBS, however, is always an odd multiple of the clockperiod $\Delta\tau$ and is given by:

$$L_{\text{PRBS}} = N\Delta\tau = (2^n - 1)\Delta\tau \tag{2}$$

Therefore, the following corrections for a positive and a negative stimulus are used in the calculation of the CCVF:

$$C_{\text{P}} = 1 - (2^n - 1)^{-1} \tag{3}$$

$$C_{\text{N}} = 1 - (2^n + 1)^{-1} \tag{4}$$

The CCVF is given by:

$$\text{CCVF}(\tau) = \lim_{T\to\infty} T^{-1} \int_0^T X(t-\tau)Y(t)\text{d}t, \; X(t) = \text{PRBS}(t) \tag{5}$$

which is the time-shifted equivalent of eqn. (1). The response of a system, in general described by the pulse response $h(t)$, is calculated from the convolution integral

$$Y(t) = \int_0^\infty h(t')\,X(t-t')\text{d}t' \tag{6}$$

This implies that the CCVF is given by

$$\text{CCVF}(\tau) = \lim_{T\to\infty} T^{-1} \int_0^T \{X(t-\tau) \int_0^\infty h(t')\,X(t-t')\text{d}t'\}\,\text{d}t \tag{7}$$

$$= \int_0^\infty h(t') \{\lim_{T\to\infty} T^{-1} \int_0^T X(t-\tau)\,X(t-t')\text{d}t\}\text{d}t' \tag{8}$$

If an auto covariance function (ACVF) is introduced,

$$\text{ACVF}(\tau - t') = \lim_{T\to\infty} T^{-1} \int_0^T X(t-\tau)\,X(t-t')\text{d}t \tag{9}$$

then the CCVF is given by the convolution integral

$$\text{CCVF}(\tau) = \int_0^\infty h(t')\text{ACVF}(\tau - t')\text{d}t' \tag{10}$$

If the ACVF has a pulse-like shape, then the CCVF is not very different from the impulse response:

$$\text{CCVF}(\tau) = \int_0^\infty h(t')\delta(\tau - t')\text{d}t' \equiv h(\tau) \tag{11}$$

However, the ACVF of a PRBS is not a δ-Dirac function, but a triangle. If

this triangle has an area of unity, the consequence will be an increment of the second moment of the impulse response. This increment can be calculated by Fourier-transforming eqn. (10). The convolution integral (10) can be represented in the frequency domain by a simple multiplication of the Fourier-transforms of $h(t)$ and ACVF(t), if ergodicity of the system (Wiener–Khinchin) is assumed:

$$\int_0^\infty h(t')\mathrm{ACVF}(\tau - t')\mathrm{d}t' = \int_{-\infty}^{\infty} h(t')\mathrm{ACVF}(\tau - t')\mathrm{d}t' \tag{12}$$

$$\int_{-\infty}^{\infty} h(t)\mathrm{ACVF}(\tau - t')\mathrm{d}t' \equiv H(\omega)\,\mathrm{A}(\omega) \tag{13}$$

The second moment of the result, CCVF(τ), when $h(t)$ is a Gaussian function and ACVF(t) is a triangle or a rectangle, is given [14] (see Appendix) by

$$\mu_2 = (-j)^2\,\mathrm{d}^2 F(0)/\mathrm{d}\omega^2 \quad (j^2 = -1) \tag{14}$$

$$\mu_{2_\mathrm{T}} = (\Delta\tau^2/6) + \sigma^2 \text{ (triangular ACVF)} \tag{15}$$

$$\mu_{2_\mathrm{R}} = (\Delta\tau^2/12) + \sigma^2 \text{ (rectangular ACVF)} \tag{16}$$

Careful inspection of the ACVF of a PRBS, when corrections (3) and (4) are applied, reveals that the height H of the triangular ACVF is (see Appendix and Fig. 2):

$$H = 1 - (2^n - 1)^{-1} + (2^n - 1)^{-2} - (2^n - 1)^{-3} \tag{17}$$

Another correction term, k, originates from the injection into a column of samples with concentrations C and 0, instead of concentrations C and $-C$. The result is therefore decreased by $k = 2^{n-1}/(2^n - 1)^{-1}$. If the total correction factor k_T (for $n > 0$)

$$k_\mathrm{T} = k\,H = 2^{n-1}(2^n - 1)^{-1} - 2^{n-1}(2^n - 1)^{-2} + 2^{n-1}(2^n - 1)^{-3} - 2^{n-1}/(2^n - 1)^{-4} \tag{18}$$

is introduced, the pulse response is given by $h(t) = \mathrm{CCVF}(t)\,k_\mathrm{T}^{-1}$. If $n \geqslant 4$, the length of the PRBS is $(2^n - 1)\Delta\tau = 15\ \Delta\tau$. For this condition, k_T is approximated (with a maximal error of 0.5%) by

$$k'_\mathrm{T} = 2^{n-1}(2^n - 1)^{-1} - 2^{n-1}(2^n - 1)^{-2} \tag{19}$$

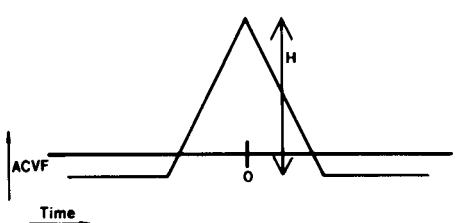

Fig. 2. General shape of the ACVF of a PRBS.

A second consequence of injections with concentrations C and O is that the average level of the injections is different from the level before any injection takes place. Therefore, a dummy sequence is necessary to allow the column to accommodate to the new level.

One of the parameters of the used PRBS, the clocktime $\Delta\tau$, is equal to the σ of the smallest peak. From eqn. (15) it follows that this increases the σ of the smallest peak by only 8%. The other parameter of the PRBS, n, is easily calculated

$$n = {}^2\log\,(L_{\mathrm{PRBS}}\,(\Delta\tau)^{-1} + 1) \tag{20}$$

The contribution of the quantization error (ϵ_q) to the CCVF is assumed to be the sum of mutually independent errors of this type. Further it is assumed that the PDF (probability density function) of the ϵ_q is constant between $-\Delta V/2$ and $+\Delta V/2$, where $\Delta V/2$ is the resolution of the A/D converter. For any point in the CCVF the mean square value of ϵ is [15]:

$$\epsilon_q^2 = \frac{1}{\Delta V}\int_{-\Delta V/2}^{\Delta V/2} \epsilon^2\,d\epsilon = \Delta V^2(12N)^{-1}\ (\text{where } N = 2^{n-1}) \tag{21}$$

Repetition (r = number of repetitions) of the estimation of the CCVF is equivalent to adding independent values

$$\epsilon_{q,r}^2 = \Delta V^2(12\,N\,r)^{-1} \tag{22}$$

Because the integral over the entire CCVF is zero (see Appendix), a baseline correction is essential. The user has to select points of the displayed results, which are representative of the baseline. If enough baseline points are selected, the baseline correction is applied by calculating straight lines between the points and subtracting these from the displayed result. The parameters of the corrections are saved to allow a reconstruction of the original correlogram. Peak areas can then be calculated by using the trapezium method.

An indication of the confidence interval is the standard deviation (σ_n) of a piece of the baseline selected by the operator. In case of determination of peak area by integration, the estimated value of σ_n is used to calculate the standard deviation σ_{I} of the integrated baseline noise. First-order, band-limited white noise is assumed to be representative of the baseline noise, although the spectrum of the noise of the most important detectors in chromatography is mainly of the $1/f$ type [16]. Nevertheless, the assumption is realistic because the correlation procedure acts as a high-pass filter [2] and remaining low-frequency components of the baseline are removed by the baseline drift correction procedure.

The value of σ_{I} is calculated [16] from $\sigma_{\mathrm{I}} = \sigma_n(2\,T_1\,T)^{1/2}$, where T is the integration time (related to the peak width) and T_1 is the time constant resulting from the assumed first-order character of the baseline noise. For

T_1 the value of the standard deviation of the smallest peak is chosen, because the adjustable cut-off frequencies of filters at the input are related to this minimal value.

A better procedure might be the integration of the ACVF of the baseline, but the reliable determination of this ACVF is prevented by the limited length of the baseline, and by the presence of peaks which divides the available information into pieces. Non-stationarity of the chromatographic system introduces noise, contributing to the lower part of the frequency spectrum [4] and thus necessitating the determination of the confidence from the correlogram itself and not from specifications of the detection noise.

To prevent aliasing of noise, it is necessary to include a tunable low-pass filter in the input. The filters used were of the minimal phase-shift type. The description of the applied second-order Bessel filter in the frequency domain is $H(\omega) = (1 + j\omega\tau_c)^{-2}$ where τ_c = time constant.

SOFTWARE

Pattern generator

The total number of points necessary for an adequate description of an entire chromatogram is calculated from the minimal number of points required to describe the first peak with minimal standard deviation and maximal time duration of the chromatogram. Limitations are the calculation time necessary to add/subtract the sample to/from the CCVF and the sample times realizable. The sample times are generated by a programmable timer which counts 10-ms pulses.

A routine is used to determine the most favourable sample time, clock frequency and sequence length. The clock frequency is a multiple of the sample frequency and allows the optimization of the response. Because the ACVF of the injected concentration pattern (equivalent to a PRBS) is a triangle [13] with a height determined by the concentration of the sample and a basewidth determined by the clock frequency, the amplitude of the CCVF is determined by the area of this triangle. Therefore, the minimal allowable clock frequency should be used. If this clock frequency is low or the sequence length is short, the sample frequency can be increased without surpassing the capabilities of the computer. The result is an optimization of the correlation method with respect to resolution and sensitivity.

The available memory of the microcomputer limits the maximum sequence length to 2048 samples. The minimal (practically usable) sequence length was set to 15 and consequently the number of bits used in the pattern generator has the limits $4 \leqslant n \leqslant 11$. The main results of the selection routine are displayed next to the values of the minimal sigma and maximal length, selected by the operator (see below). Other results of this routine are the correction (eqns. 3 and 4) and the mask used for the generation of the PRBS pattern. The mask is applied to n bits and the correlation level is calculated

with the modulo-2-addition of the selected bits [13]. The n bits are shifted one place and the vacant place is loaded with the correlation level. When the correlation is performed, a sample is always directly multiplied by the corrections (eqns. 3 and 4) and saved. These values are added to, or subtracted from, the already calculated part of the CCVF, depending on the correlation level. This allows the operator to monitor the growth of the CCVF during the correlation chromatographic experiment.

When single injection is used, only the addition of the response to the result remains. Both the calculation of the CCVF and the recording of a single injection can be repeated a number of times, which is equivalent to a signal-averaging procedure.

Data sampler

The electrical input of the system is amplified conventionally and fed to the inputs of second-order Bessel filters. The appropriate filter is selected by a software-controlled analog switch and the resulting signal is fed to a quad-slope integrating A/D converter. The conversion command is generated by the program, which is synchronized to a programmable timer by interrupts.

Arithmetic unit

A single injection results in an addition of the response to the previous result. The CCVF, however, is calculated from the formula

$$\mathrm{CCVF}(\tau) = T^{-1} \int_0^T \mathrm{PRBS}(t)\, Y(t + \tau)\mathrm{d}t$$

This is replaced for one sequence by

$$\mathrm{CCVF}(\tau) = (L_{\mathrm{PRBS}})^{-1} \int_0^{L_{\mathrm{PRBS}}} \mathrm{PRBS}(t)\, Y(t + \tau)\mathrm{d}t$$

which can be rewritten as

$$\mathrm{CCVF}(k\,\Delta\tau) = N^{-1} \sum_{i=1}^{N} \mathrm{PRBS}(i\,\Delta\tau)\, Y\{(i + k)\Delta\tau\}$$

or as

$$\mathrm{CCVF}(k\,\Delta\tau) = N^{-1} \sum_{i=1}^{N} \mathrm{PRBS}\{(i - k)\Delta\tau\}\, Y(i\,\Delta\tau)$$

This equation reveals that a sample $Y(i\ \Delta\tau)$ is added to or subtracted from the result. Because the value of $\mathrm{PRBS}\{(i - k)\Delta\tau\}$ can always be generated, only the sample $Y(i)$ multiplied by the correction factors (3) and (4), the intermediate results of the CCVF to be calculated, and the sum of the finished CCVF's need to be stored in memory. The remaining summations and subtractions are handled quickly enough by the Z80-instruction set to

preclude the use of hardware arithmetic units. Multiplications and divisions required elsewhere in the program are not time-critical and can be handled adequately by software.

Display

The display is usable for the visual inspection of the sampled detector signal, the intermediate results and the final result. The chosen graphical display is organised as a 256 × 256 dot matrix, which allows the use of a simple video monitor as a display. The authors used a simple, cheap television set, which was extended with a video input and proved to be adequate, although a cheap video monitor is also usable. The graphical matrix can be referenced through a cursor. The three possible signals, viz. the detector signal, the calculated CCVF and the final result, are copied, automatically scaled and stored in the graphical memory, and displayed on request. The graphical display is mixed with an alphanumeric display, used when the maximal length of the chromatogram and the minimal sigma of the peaks are selected and the resulting parameters are displayed. With the aid of a cursor it is possible to display the magnitude and the delay (retention) of a point. If the user is able to select enough points which are part of the baseline, a baseline correction is performed by subtraction of the constructed straight lines between the points. Selected points may also be used as integration limits for peak area determinations, as limits of a zoom function on the display (only 256 of the maximal 2047 points are displayed), or as limits of a piece of the baseline suitable for the confidence determination. In this way, the judgement of the user is combined sensibly with the computing capabilities of a microcomputer.

Interfaces to data storage and hard-copy peripherals

The interface to data storage is principally intended for simple 8-bit parallel interfacing and is without extensive control capabilities (Simplex operation). The interface to a hard-copy unit is organised as a first-in/first-out digital buffer and an 8-bit D/A converter for easy adaptation to different speeds of the copy unit. A copy of the display is produced.

Processing of the results

The possibilities of applying baseline corrections are described together with the used display.

HARDWARE

The hardware used is illustrated in Fig. 3. The design was organized around a standard microcomputer Z80-MCB (Zilog Inc.), containing a Z80-CPU, 16 kbytes of RAM, a serial controller for teletype/CRT interfacing, and programmable timers. The graphical display was obtained by an MTX 256**2 and MTX 1632 combination (Matrox, Canada). Other extensions

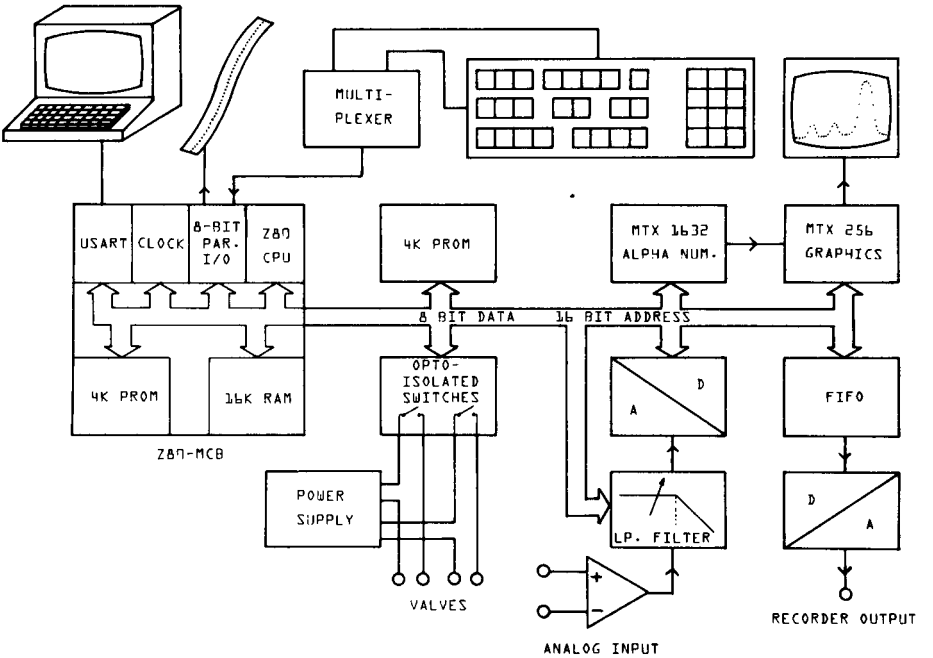

Fig. 3. Detailed overview of the microcomputer and the extensions used.

were separate power supplies for all logics, for the analog part and for the valve switching. The extensions were achieved on Euro-card PCB's connected to the Z80 memory bus: (a) a board with memory extensions (4 kbytes of PROM); (b) a board with instrumentation amplifier (AD 521, Analog Devices) and the second-order low-pass Bessel filters with cut-off frequencies (in Hz) of 0.269, 0.370, 0.51, 0.649, 0.962, 1.316, 1.786 and 2.5 Hz (one output is selected with an Analog Devices AD 7501 digital controllable analog switch); (c) a board with 13-bit A/D converter (AD 7550, Analog Devices) of the quad-slope integrating type with inherent hum rejection; (d) keyboard interface (a multiplex system); (e) an alphanumeric video display module (MTX 1632, Matrox); (f) a valve-switching board, optically isolated to prevent ground loops. A wide range of valves can be switched by adjustment of the power supplies.

The software has inherent development capabilities. If no teletype is present, the correlation program is automatically started. If it is present, the monitor (program) is started, allowing easy switch-over between development and implementation of the progam.

The program itself was developed with a macro cross-assembler which handles both the standard 8080- and Z80 mnemonics. The assembler runs on a Varian Data Machines V75 series minicomputer. The program has three distinct phases: (a) precorrelation consisting of selection of appropriate filters, interrupt times, sequence length, etc.; (b) the correlation or averaging

process, using the capabilities very efficiently (ca. 80% of the time is spent on calculating the CCVF); and (c) the post-correlation part, which includes baseline corrections, enlargement of small peaks, integration of peak areas, and estimation of confidence intervals.

RESULTS

For testing the correlator, a system with stable and predictable parameters (retention time, peak width, etc.) is required, and this is difficult to achieve with a real chromatographic system. Therefore, the operation and results of the correlator are illustrated with a simulated column (Fig. 4). This consisted of a microcomputer which was used to obtain two delayed injection patterns (with different delay times) and created most of the retention time, and 6—8 first-order low-pass filters in series which generated "chromatographic" curves from the injection patterns, and corresponds to the ideal mixer model. In this way, two peaks were obtained with different delays, different and predictable areas with a ratio of 1:1.5 (±0.5%) and different widths. The results, displayed on a video screen, were photographed as shown in Fig. 5.

When power is switched on, reset values of the parameters are selected (Fig. 5, 1). For the simulated system a maximal length of 100 s and a minimal sigma of the peaks of 1 s are sufficient (2). The number of repetitions was limited to 2. With these parameters it is possible to "inject" a single sample in the column (normal chromatography) or to perform correlation chromatography. A normal injection generates a conventional detector response (3) and result (4). The result is represented in the memory of the microcomputer as a series of numbers. Because the video screen accommodates a maximum of 256 dots in any direction, the result is compressed. In this example only 190 points are displayed, which is a compression of 1:2.

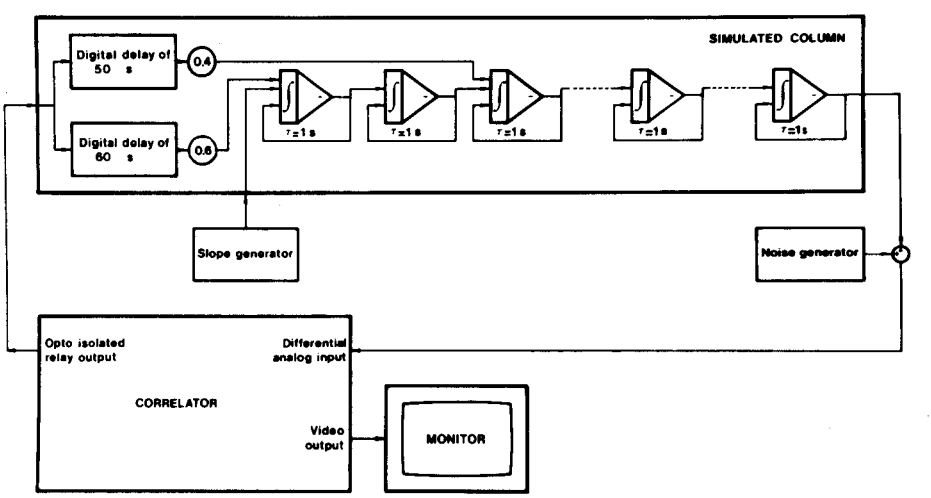

Fig. 4. Test system for the correlator.

1

2

3

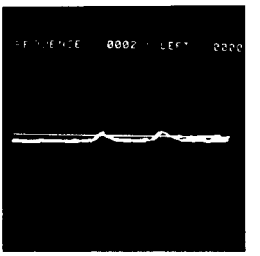

4

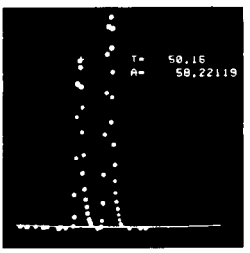

5

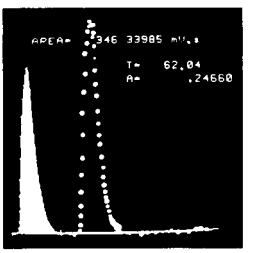

6

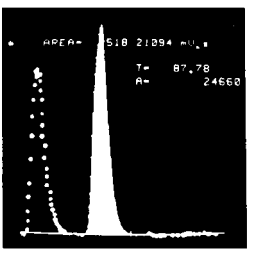

7

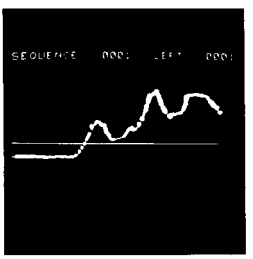

8

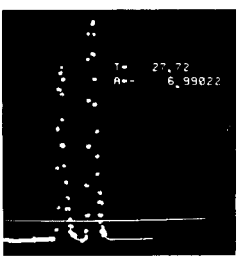

9

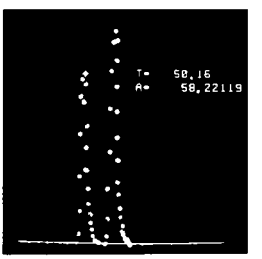

10

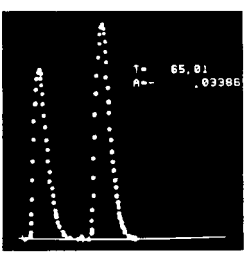

11

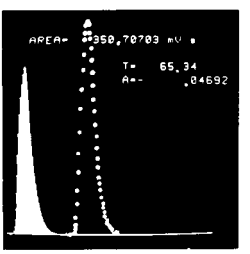

12

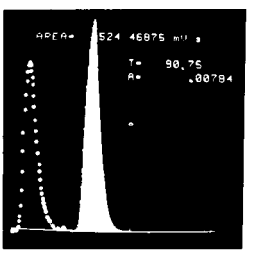

13

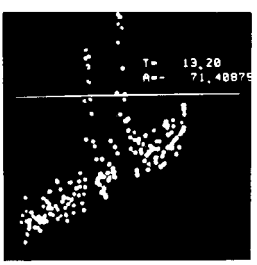

14

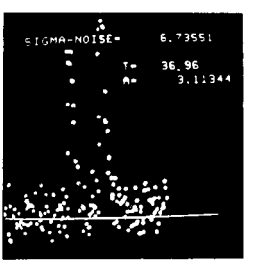

15

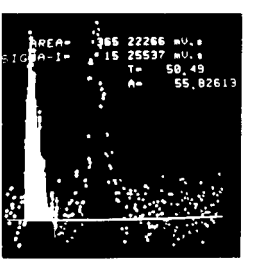

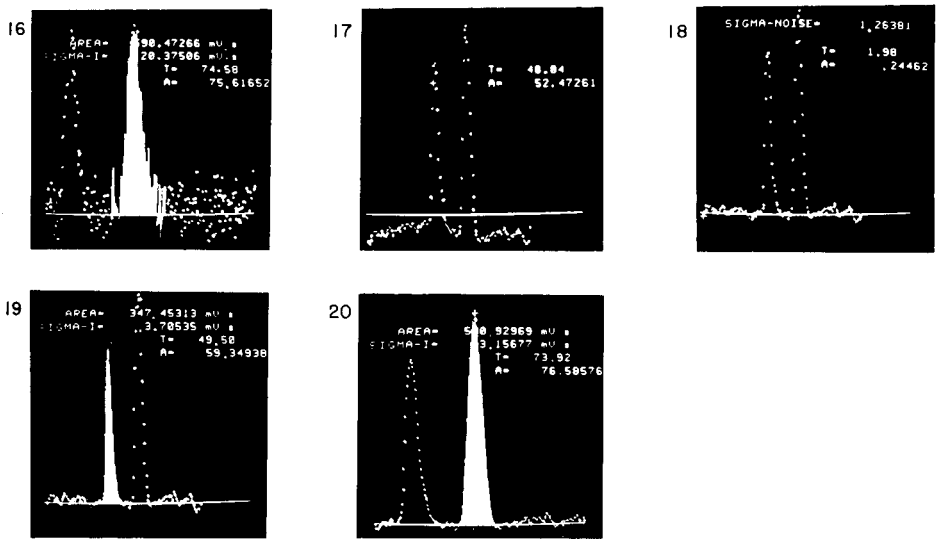

Fig. 5. Photographs of the results at various stages of performing correlation chromatography. For explanation, see text.

In the final stage of the program (processing of the results), the parts of interest can be enlarged (5). Integration of a peak gives a response proportional to the "injected amount" of sample, in this case $\sigma_{min}a$, where σ_{min} is the width of the injection and a is the attenuation of the analog computer. The values 344.2 mV s and 516.4 mV s for peaks 1 and 2 are calculated, while integration of the result gives 346.3 mV s and 518.2 mV s (5 and 6).

A correlation procedure stimulates the column with a PRBS; this gives a detector signal which cannot be interpreted (7). Because the integral over the entire result is zero, the baseline has to be shifted upwards (8). After selection of the proper integration limits (9), the areas of the peaks were calculated as 346.3 mV s and 518.2 mV s, respectively (10, 11).

The test was designed to compare the results of operation under theoretical conditions, and so the detector signal was disturbed by the introduction of theoretical noise and drift. The power spectrum of the added noise is given in Fig. 6 together with the power spectrum P_{out} of the signal at the end of the simulated column. The latter spectrum was obtained by multiplying the transfer function of the eight integrating networks by the Fourier-transform of the virtual injection of the CCVF

$$P_{out}(\omega) = |(1 + j\omega\tau)^{-8} \cdot (\omega^{-1} \sin \omega)|^2$$

The average of two normal injections is displayed in Fig. 5 (11). After drift corrections and selection of a piece of baseline, the function "confidence" gives the standard deviation of the noise, σ_n = 6.74 mV (13). Integration of the peaks gives the areas 365.2 mV s and 590.5 mV s, and the calculated standard deviations of the integrals 15.25 mV s and 20.37 mV s, respectively.

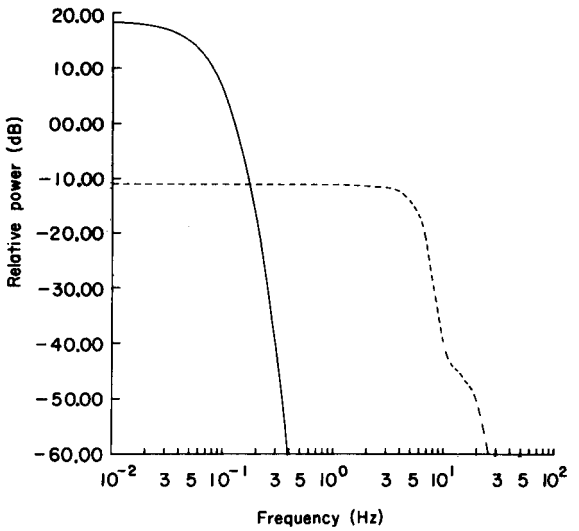

Fig. 6. Power spectrum of the output of the simulated column (solid line) and power spectrum of the added noise (dotted line); 0 dB is 1 V^2.

These standard deviations are calculated from $\sigma_I = \sigma_n(2T_1\ T)^{1/2}$; here T_1 is the assumed time constant of the noise and is set by the program to the value $\sigma_{min} = 0.99$ s [16].

When the results of the single injection method are compared with those of the correlation method, the inherent low-frequency correcting capabilities are manifest (Fig. 5, 11—16). The noise-suppressing capabilities of the correlation method can be derived from the value of σ_n: 1.26 mV (17), which shows a reduction of 1:5.34. Integration of the peaks gives a corresponding reduction in the uncertainty of the integrals (19 and 20).

An example of the performance of the system for real chromatographic problems is the separation of chlorinated phenols as reported earlier [5].

APPENDIX

Influence of the injection with a triangular/rectangular pulse on the second moment of a system response.

$$h(t) = \sigma\,(2\pi)^{-1/2}\ e^{-(t/\sigma)^2/2} \leftrightarrow H(\omega) = \sigma\ e^{-(\omega\sigma)^2/2}$$

$$x_T(t) = \begin{cases} 1 - \dfrac{|t|}{T}, & |t| < T \\ 0, & |t| > T \end{cases} \leftrightarrow g_T(\omega) = T\left(\frac{\sin\dfrac{\omega T}{2}}{\dfrac{\omega T}{2}}\right)^2$$

$$x_R(t) = \left.\begin{cases} 1 & , |t| < \dfrac{T}{2} \\ 0 & , |t| > \dfrac{T}{2} \end{cases}\right\} \leftrightarrow g_R(\omega) = T \frac{\sin \dfrac{\omega T}{2}}{\dfrac{\omega T}{2}}$$

(1) Stimulation of the system with a triangular pulse (normalized for area = 1)

$$H(\omega) g_T(\omega) = C(\omega) = \left(\frac{\sin \dfrac{\omega T}{2}}{\dfrac{\omega T}{2}} \right)^2 e^{-(\omega\sigma)^2/2} \qquad x = \frac{\omega T}{2}\,;\; y = \omega\sigma$$

$$C(\omega) = C(x, y) = \left(\frac{\sin x}{x}\right)^2 e^{-y^2/2}$$

$$= \left\{ \frac{x - \dfrac{x^3}{3!} + \dfrac{x^5}{5!} - \ldots}{x} \right\}^2 e^{-y^2/2} = \left(1 - \frac{x^2}{3!} + \frac{x^4}{5!} - \ldots\right)^2 e^{-y^2/2}$$

$$\frac{d}{d\omega} C(\omega) = \left[2\left(1 - \frac{x^2}{3!} + \frac{x^4}{5!} - \ldots\right)\left(-\frac{2x}{3!} + \frac{4x^3}{5!} - \ldots\right)\left(\frac{\tau}{2}\right) \right.$$

$$\left. + \left(1 - \frac{x^2}{3!} + \frac{x^4}{5!} - \ldots\right)^2 (-y\sigma) \right] e^{-y^2/2}$$

$$\frac{d^2}{d\omega^2} C(\omega) = \left[\left\{ \left(-\frac{2x}{3!} + \frac{4x^3}{5!} - \ldots\right)\left(-\frac{2x}{3!} + \frac{4x^3}{5!} - \ldots\right)(\tau) \right.\right.$$

$$\left. + \left(1 - \frac{x^2}{3!} + \frac{x^4}{5!} - \ldots\right)\left(-\frac{2}{3!} + \frac{12x^2}{5!} - \ldots\right)\tau \right\} \frac{\tau}{2} + \left(2 - \frac{2x^2}{3!} + \frac{2x^4}{5!} - \ldots\right)$$

$$\times \left(-\frac{2x}{3!} + \frac{4x^3}{5!} - \ldots\right)\left(\frac{\tau}{2}\right)(-y\sigma) + \left(1 - \frac{x^2}{3!} + \frac{x^4}{5!} - \ldots\right)^2 (-\sigma^2) \Big] e^{-y^2/2}$$

$$+ e^{-y^2/2} (-y\sigma) \left[2\left(1 - \frac{x^2}{3!} + \frac{x^4}{5!} - \ldots\right)\left(-\frac{2x}{3!} + \frac{4x^3}{5!} - \ldots\right)\left(\frac{\tau}{2}\right) \right.$$

$$\left. + \left(1 - \frac{x^2}{3!} + \frac{x^4}{5!} - \ldots\right)^2 (-y\sigma) \right]$$

$$\frac{d^2}{d\omega^2} C(0) = \left[\left\{ 0\tau + (1)\left(-\frac{2}{3!}\right)\tau \right\} \frac{\tau}{2} + \left(20\,\frac{\tau}{2}\right)(-y\sigma) + (-\sigma^2) \right] + 0[\ldots]$$

$$= -\frac{\tau^2}{6} - \sigma^2$$

$$\mu_2 = -\frac{d^2}{d\omega^2} C(0) = \frac{\tau^2}{6} + \sigma^2$$

(2) Stimulation of the system with a rectangular pulse: (normalized for area = 1)

$$H(\omega)g_R(\omega) = C(\omega) = \frac{\sin\frac{\omega T}{2}}{\frac{\omega T}{2}} e^{-(\omega\sigma)^2/2} \qquad x = \frac{\omega T}{2}\,;\; y = \omega\sigma$$

$$C(\omega) = C(x,y) = \frac{\sin x}{x} e^{-y^2/2} = \left\{\frac{\left(x - \frac{x^3}{3!} + \frac{x^5}{5!} - \ldots\right)}{x}\right\} e^{-y^2/2}$$

$$= \left(1 - \frac{x^2}{3!} + \frac{x^4}{5!} - \ldots\right) e^{-y^2/2}$$

$$\frac{d}{d\omega} C(\omega) = \left[\left(-\frac{2x}{3!} + \frac{4x^3}{5!} - \ldots\right)\frac{\tau}{2} + \left(1 - \frac{x^2}{3!} + \frac{x^4}{5!} - \ldots\right)(-y\sigma)\right] e^{-y^2/2}$$

$$\frac{d^2}{d\omega^2} C(\omega) = \left[\left\{\left(-\frac{2}{3!} + \frac{12x}{5!} - \ldots\right)\frac{\tau}{2} + \left(-\frac{2x}{3!} + \frac{4x^3}{5!} - \ldots\right)(-y\sigma)\right\}\frac{\tau}{2}\right.$$

$$\left. + \left(1 - \frac{x^2}{3!} + \frac{x^4}{5!} - \ldots\right)(-\sigma^2)\right] e^{-y^2/2} + e^{-y^2/2}\,(-y\sigma)\left[\left(-\frac{2x}{3!} + \frac{4x^3}{5!} - \ldots\right)\frac{\tau}{2}\right.$$

$$\left. + \left(1 - \frac{x^3}{3!} + \frac{x^4}{5!} - \ldots\right)(-y\sigma)\right]$$

$$\frac{d}{d\omega^2} C(0) = \left[\left\{\left(-\frac{2}{3!}\right)\frac{\tau}{2} + 0\right\}\frac{\tau}{2} + 1\,(-\sigma^2)\right] 1 + 0\,[\ldots] = -\frac{\tau^2}{12} - \sigma^2$$

$$\mu_2 = -\frac{d^2}{d\omega^2}(0) = \frac{\tau^2}{12} + \sigma^2$$

The properties of the ACVF of a PRBS

The following properties of a PRBS are assumed: (a) length of a PRBS (always odd) = $2^n - 1$ clock cycles; (b) positive levels = 2^{n-1} clock cycles; (c) negative levels = $2^{n-1} - 1$ clock cycles. To obtain an average level of zero, the positive and negative levels have the values $L_P = 1 - (2^n - 1)^{-1}$ and $L_N = 1 + (2^n - 1)^{-1}$. The shape of the ACVF of a PRBS is a triangle [6]. The values of the top and the base of this triangle are calculated separately (see Fig. 2).

For the calculation of the ACVF(τ), when $\Delta\tau \leqslant \tau \leqslant L_{PRBS} - \Delta\tau$, is assumed that the transitions between the levels are purely random. One sequence contains all statistical properties of a PRBS. Hence, when calculating the value

$$\mathrm{ACVF}_{PRBS}(\tau) = (L_{PRBS})^{-1} \int_0^{L_{PRBS}} x(t)\,x(t+\tau)\mathrm{d}t,\ \Delta\tau \leqslant \tau \leqslant L_{PRBS} - \Delta\tau$$

$$\mathrm{ACVF}(\tau) = (2^n - 1)^{-1} \sum_{i=1}^{2^n-1} x_i x_{i+\tau}$$

the next transitions occur in one sequence

$$L_P \to L_P : \frac{2^{n-1}}{2} \text{ times} \quad L_P \to L_N : \frac{2^{n-1}}{2} \text{ times}$$

$$L_N \to L_P : \frac{2^{n-1}}{2} \text{ times} \quad L_N \to L_N : \frac{2^{n-1}}{2} - 1 \text{ times}$$

Because the modulo 2 addition of zero's always yields a zero, there is 1 less transition $L_N \to L_N$, compared with the other transitions. The value of the ACVF is

$$\text{ACVF}_{\text{PRBS}}(\tau) = \frac{1}{2^n - 1}\left[\frac{2^{n-1}}{2}(L_P)^2 + \left(\frac{2^{n-1}}{2} - 1\right)(L_N)^2 \text{ (positive levels)}\right.$$

$$\left. -\left\{\frac{2^{n-1}}{2} L_N L_P + \left(\frac{2^{n-1}}{2} - 1\right) L_N L_P\right\}\right] \text{ (negative levels)}$$

$$\text{ACVF}_{\text{PRBS}}(\tau) = \frac{1}{2^n - 1}\left[\frac{2^{n-1}}{2}\left(1 - \frac{1}{2^n - 1}\right)^2 + \left(\frac{2^{n-1}}{2} - 1\right)\left(1 + \frac{1}{2^n - 1}\right)^2\right.$$

$$\left. -\left\{\frac{2^{n-1}}{2}\left(1 - \frac{1}{2^n - 1}\right)\left(1 + \frac{1}{2^n - 1}\right) + \left(\frac{2^{n-1}}{2}\right)\left(1 - \frac{1}{2^n - 1}\right)\left(1 + \frac{1}{2^n - 1}\right)\right\}\right]$$

$$\text{ACVF}_{\text{PRBS}}(\tau) = \frac{1}{2^n - 1}\left[\frac{2^{n-1}}{2}\left\{1 + \left(\frac{1}{2^n - 1}\right)^2\right\} - \left\{1 + \frac{2}{2^n - 1} + \left(\frac{1}{2^n - 1}\right)^2\right\}\right.$$

$$\left. - 2^{n-1}\left\{1 - \left(\frac{1}{2^n - 1}\right)^2\right\}\right]$$

$$\text{ACVF}_{\text{PRBS}}(\tau) = \frac{1}{2^n - 1}\left[-1 - \frac{2}{2^n - 1} + \left(\frac{1}{2^n - 1}\right)^2\right] = \frac{-\left(1 - \frac{1}{2^n - 1}\right)^2}{2^n - 1}$$

The value of $\text{ACVF}(\tau)$, $\tau = n\, L_{\text{PRBS}}$ and $|n| = 0, 1, 2, \ldots \infty$, is calculated from 2^{n-1} positive levels and $2^{n-1} - 1$ negative levels

$$\text{ACVF}_{\text{PRBS}}(0) = \frac{1}{2^n - 1}\left[2^{n-1}\left\{1 - \frac{1}{2^n - 1}\right\}^2 + (2^{n-1} - 1)\left\{1 + \frac{1}{2^n - 1}\right\}^2\right]$$

$$= \frac{2^{n-1}}{2^n - 1}\left\{1 + \left(\frac{1}{2^n - 1}\right)^2 - \frac{2}{2^n - 1}\right\} + \frac{(2^{n-1} - 1)}{2^n - 1}\left\{1 + \left(\frac{1}{2^n - 1}\right)^2 + \frac{2}{2^n - 1}\right\}$$

$$= \frac{2^n}{2^n - 1}\left\{1 + \left(\frac{1}{2^n - 1}\right)^2\right\} - \frac{1}{2^n - 1}\left\{1 + \left(\frac{1}{2^n - 1}\right)^2 + \frac{2}{2^n - 1}\right\}$$

$$= \frac{2^n - 1}{2^n - 1}\left\{1 + \left(\frac{1}{2^n - 1}\right)^2\right\} - \frac{2}{(2^n - 1)^2}$$

$$\text{ACVF}_{\text{PRBS}}(0) = 1 - \frac{1}{(2^n - 1)^2}$$

To calculate $\int_0^{L_{\text{PRBS}}} \text{ACVF}_{\text{PRBS}}(\tau)\text{d}\tau$, two points have to be noticed. First,

there are 2^{n-1} positive and $2^{n-1}-1$ negative levels in one sequence. Secondly, each level is multiplied by (a) 2^{n-1} positive levels, and (b) $2^{n-1}-1$ negative levels. Thus:

$$\int_0^{L_{PRBS}} \mathrm{ACVF}_{PRBS}(\tau)\mathrm{d}\tau = \frac{1}{2^n-1}\left[2^{n-1}\left(1-\frac{1}{2^n-1}\right)\left\{2^{n-1}\left(1-\frac{1}{2^n-1}\right)\right.\right.$$
$$\left.-(2^{n-1}-1)\left(1+\frac{1}{2^n-1}\right)\right\}-(2^{n-1}-1)\left(1+\frac{1}{2^n-1}\right)\left\{2^{n-1}\left(1-\frac{1}{2^n-1}\right)\right.$$
$$\left.\left.-(2^{n-1}-1)\left(1+\frac{1}{2^n-1}\right)\right\}\right]$$

$$\int_0^{L_{PRBS}} \mathrm{ACVF}_{PRBS}(\tau)\mathrm{d}\tau = \frac{1}{2^n-1}\left[\left\{2^{n-1}\left(1-\frac{1}{2^n-1}\right)\right\}^2-(2^{n-1}-1)(2^{n-1})\right.$$
$$\times\left(1-\frac{1}{2^n-1}\right)\left(1+\frac{1}{2^n-1}\right)+\left\{(2^{n-1}-1)\left(1+\frac{1}{2^n-1}\right)\right\}^2-(2^{n-1}-1)(2^{n-1})$$
$$\left.\times\left(1-\frac{1}{2^n-1}\right)\left(1+\frac{1}{2^n-1}\right)\right]$$

Assume $A = 2^{n-1}\left(1-\frac{1}{2^n-1}\right)$ and $B = (2^{n-1}-1)\left(1+\frac{1}{2^n-1}\right)$

then the integral can be rewritten as

$$\int_0^{L_{PRBS}} \mathrm{ACVF}_{PRBS}(\tau)\mathrm{d}\tau = \frac{1}{2^n-1}(A^2-2AB+B^2) = \frac{(A-B)^2}{2^n-1}$$

Because $(A-B)$ is

$$(A-B) = 2^{n-1}\left(1-\frac{1}{2^n-1}\right)-2^{n-1}\left(1+\frac{1}{2^n-1}\right)+\left(1+\frac{1}{2^n-1}\right)$$
$$= -2^{n-1}\left(\frac{2}{2^n-1}\right)+1+\frac{1}{2^n-1} = -\frac{-2^n}{2^n-1}+\frac{1}{2^n-1}+1 = 0$$

the integral is zero

$$\int_0^T \mathrm{ACVF}_{PRBS}(\tau)\mathrm{d}\tau = 0$$

Resuming, the height of the virtual triangle, used for injection has a height H

$$H = 1+\frac{1}{2^n-1}-\left(\frac{1}{2^n-1}\right)^2+\left(\frac{1}{2^n-1}\right)^3$$

REFERENCES

1 K. Izawa, K. Furuta, T. Fujiwara and N. Suyama, Ind. Chim. Belg., 32 (1967) 223.
2 H. C. Smit, Chromatographia, 3 (1970) 515.
3 T. T. Lub, H. C. Smit and H. Poppe, J. Chromatogr., 149 (1978) 721.
4 T. T. Lub and H. C. Smit, Anal. Chim. Acta, 112 (1979) 341.
5 H. C. Smit, T. T. Lub and W. J. Vloon, Anal. Chim. Acta, 122 (1980) 267.
6 G. C. Moss, P. J. Kipping and K. R. Godfrey, in S. G. Perry (Ed.), Proc. 9th Int. Symp. on Gas Chromatography, Montreux, 1972, Applied Science Publ., Barking, 1973, p. 187.
7 R. Annino and L. E. Bullock, in S. G. Perry (Ed.), Proc. 9th Int. Symp. on Gas Chromatography, Montreux, 1972, Applied Science Publ., Barking, 1973, p. 171.
8 R. Annino and L. E. Bullock, Anal. Chem., 45 (1973) 1221.
9 C. Largeau and B. Espiau, J. Chim. Phys., 71 (1974) 1143.
10 R. Annino and E. Grushka, J. Chromatogr. Sci., 14 (1976) 265.
11 M. Kaljurand and E. Küllik, in A. Zlatkis (Ed.), Proc. 14th Int. Symp. on Advances in Chromatography, Lausanne, 1979, Chrom. Symp., Dept. of Chem., Univ. of Houston, Texas, U.S.A., 1979, p. 173.
12 R. Annino, M. Gonnord and G. Guiochon, Anal. Chem., 51 (1979) 379.
13 W. D. T. Davies, Instrum. Pract., 22 (1968) 213.
14 A. Papoulis, The Fourier Integral and its Applications, McGraw-Hill, New York, 1962, Ch. 2.
15 F. R. Connor, Noise, Edward Arnold, London, 1972, p. 80.
16 H. C. Smit and H. L. Walg, Chromatographia, 8 (1975) 311.

Analytica Chimica Acta, 133 (1981) 303—318
Computer Techniques and Optimization
Elsevier Scientific Publishing Company, Amsterdam — Printed in The Netherlands

COMPUTER-AIDED STRUCTURAL ANALYSIS OF ORGANIC COMPOUNDS BY AN ARTIFICIAL INTELLIGENCE SYSTEM

B. DEBSKA, J. DULIBAN, B. GUZOWSKA-SWIDER and Z. HIPPE*
I. Łukasiewicz Technical University, 35-959 Rzeszów, P.O. Box 85 (Poland)
(Received 6th May 1980)

SUMMARY

The computer program SEAC is designed to elucidate the structure of organic compounds comprising C (up to 40 C atoms in a molecule), H, N, O, S, Cl, Br and/or I atoms. Artificial intelligence techniques are exploited for empirical interpretation of spectral-structural correlations obtained directly from i.r., ^{1}H-n.m.r. and u.v. spectra. SEAC works on five levels depending on the entropy of the information input on tested molecules. The computer prints out a set of alternative substructures (levels I—IV) or a set of complete structures which are consonant with the input data.

Organic structural analysis is important not only because of the fundamental knowledge obtained but because it can determine the further direction of experimentation. Mass spectrometry (m.s.), nuclear magnetic resonance (n.m.r.) and infrared spectroscopy (i.r.) are most frequently used for the determination of organic chemical structures, but the simultaneous application of several spectroscopic techniques gives better results, because the structural information obtained is often complementary, confirming or eliminating possible results. However, the amount of data that must then be processed is substantially greater than for a single technique, hence computers are almost essential for obtaining results in reasonable times.

Artificial intelligence [1, 2] applied to structure identification can be described as modelling of human intellectual processes during interpretation of spectra. The problems must be described formally, but it is extremely difficult to translate ideas into effective algorithms and then into suitable computer programs. Accordingly, known software systems for structure elucidation based on artificial intelligence are suitable only for limited sets of structures, and are usually restricted to a few component elements (e.g., C, H, O [3]), a certain range of carbons in the molecule (e.g., 15—20 [4]) or a particular type of compound. The extension of identifiable types of structure involves a tremendous increase in programming effort. However, identification systems based on artificial intelligence do not require spectra libraries, and the computer time for identification of a molecule depends only on the number of structural units in the molecule.

The work described here is concerned with the development of algorithms

for the interpretation of i.r., ^{1}H-n.m.r. and u.v. spectra. The principal goal of these investigations is to design a computer system for automatic identification of chemical structures far beyond the standards currently accepted in the field of artificial intelligence. This paper gives the first detailed description of the pilot system, called SEAC (Structure Elucidation Aided by Computer).

EXPERIMENTAL

Options of the system

The SEAC system is designed to elucidate the structure of organic substances built from carbon (up to 40 C atoms in a molecule), hydrogen, nitrogen, oxygen, chlorine, bromine and iodine atoms. Its scope includes the identification of saturated or unsaturated chain compounds, and ring structures comprising not only benzene or naphthalene rings but other saturated or unsaturated five- or six-membered carbocyclic rings, and compounds with one heteroatom. Structure identification is based on parameters calculated by means of the special computer programs IRMAT, NMRMAT, UVMAT [5] for mathematical treatment of the spectra; alternatively, the parameters may be read directly from the spectrum. The parameters used from infrared spectra are the band position (W, cm^{-1}), intensity (T, $\%T$), half-height width (D, cm^{-1}; this is used in the region 3600—2500 cm^{-1}, but for bands in other parts of the spectrum, O is used by convention); for n.m.r. spectra, the parameters are; location, (τ, ppm), intensity (H), multiplicity and coupling constant (input as a real number: multiplicity × coupling constant, Hz/100). The u.v. spectrum, specified by band position (X, nm) and intensity (A, $\%A$), is used only to check the results obtained. To increase the efficiency of identification, preliminary information on the qualitative composition or empirical formula of the compound is utilized. The system can operate on one of five levels; the level is initialized depending on the amount of information about the substance being tested (Table 1).

Structure of the system

The system is based on the principle of heuristic processing of spectrum—structure correlations; formally this runs in three successive stages. In the first stage, on the basis of spectral data and preliminary information (Table 1), substructures likely to be present in the compound are identified. In the second stage, correctness of identification is checked. In the third stage, a multielemental set of structural fragments is selected, and then the complete set of structures which are equally valid from the given information is generated. Another verification then takes place: the structures which are not in accordance with the input spectral data or which break some general rules (e.g., the valence rule) are rejected. The detailed description of these procedures is as follows.

Identification of substructures. This is achieved by artificial intelligence,

TABLE 1

Levels of the SEAC system

Level	Input data[a]					Results
	Qualitative composition	Empirical formula	I.r.	^{1}H-n.m.r.	U.v.	
I			•	○	○	List of groups detected
II	•		•		○	List of groups detected (reduced with higher probability)
III		•	•		○	Reduced list of groups and list of spectral inactive groups
IV	•		•	•	○	Full list of groups detected and information on environment
V		•	•	•	○	List of structural formulae

[a](•) Necessary information; (○) optional information.

with the help of two advanced computer programs with high logical interconnections. The programs were originally developed to interpret empirically i.r. and ^{1}H-n.m.r. spectra. Both programs consist of 11 subroutines, each of which is designed to analyse compounds with specified compositions which are statistically most frequently encountered (e.g., CHNO, CHO, etc.). The programs are intended to simulate human intellectual processes during interpretation of a spectrum. Usually, in the determination of a chemical structure, some bands that occur in relatively narrow ranges of wave number or chemical shift can be correlated with characteristic substructures regardless, to a first approximation, of their molecule environment. But detailed inspection of group frequencies in i.r. or chemical shift in ^{1}H-n.m.r. shows that the immediate molecular environment of a given substructure has a distinct influence on its spectral characteristics. This can be used, to a second approximation, for more precise recognition of a substructure or its chemical bonding to other parts of the molecule. However, the limits of resolution of i.r. or ^{1}H-n.m.r. spectroscopy cause some ambiguities, and so a single structure cannot usually be ascribed to a given portion of the spectrum; usually a set of substructures which are equally consonant with the spectral data is obtained. Those substructures are called alternative fragments here. The set of substructures accepted in SEAC (Table 2) contains 246 units altogether; 69 units can be detected by i.r. alone, 129 by ^{1}H-n.m.r., and 40 simultaneously by both techniques. Twelve possible fragments may be calculated if the empirical formula of the sample is known.

Each substructure is assigned to a unit of a two-dimensional matrix $G\,[I, J]$ (where $I = 1 \ldots 4$, and $J = 1 \ldots 70$) following the convention that monovalent substructures (e.g., CH_3—, —NO_2, —OH, —SH) are located in the first

TABLE 2

Storage of information on substructures in SEAC

No.		AS[a]	C1[b]	C2[c]	C3[d]	H1[e]	H2[f]	H3[g]
1	2	3	4	5	6	7	8	9
1	G(1, 1)	N=C=S	1010001	1	0			
2	G(1, 2)	S—C*N	1010001	1	0			
3	G(1, 3)	COO—	200001	1	0			
4	G(1, 4)	N=C=O	110001	1	0			
5	G(1, 5)	C*NO	110001	1	0			
6	G(1, 6)	C*N	10001	1	0			
7	G(1, 7)	N*C	10001	1	0			
8	G(1, 8)	CHO	100101	1	0			
9	G(1, 9)	COOH	200101	1	0			
10	G(1, 10)	O—CO—H	200101	1	0			
11	G(1, 11)	CS—NH2	1010201	1	0			
12	G(1, 12)	CO—NH2	110201	1	0			
13	G(1, 13)	CH3	301	1	0			
14	G(1, 14)	CH3(CH2)	301	1	1	—1		
15	G(1, 15)	CH3(CH)	301	1	1	—2		
16	G(1, 16)	CH3(C)	301	1	1	263		
17	G(1, 17)	CH3(C=)	301	1	1	—3		
18	G(1, 18)	CH3(C*)	301	1	1	—4		
19	G(1, 19)	CH3(S)	301	1	1	254		
20	G(1, 20)	CH3(O)	301	1	1	—5		
21	G(1, 21)	CH3(N)	301	1	1	—6		
22	G(1, 22)	CH3(CO)	301	1	1	—7		
23	G(1, 23)	CH3(AR)	301	1	1	—8		
24	G(1, 24)	NH—CS—NH2	1020301	1	0			
25	G(1, 25)	CS—NH—NH2	1020301	1	0			
26	G(1, 26)	NH—CS—NH—NH2	1030401	1	0			
27	G(1, 27)	C*CH	102	1	0			
28	G(1, 28)	CH=CH2	302	1	0			
29	G(1, 29)	THIOPH-2	1000304	1	0			
30	G(1, 30)	FUR-2	100304	1	0			
31	G(1, 31)	FUR-3	100304	1	0			
32	G(1, 32)	PYR-2	404	1	0			
33	G(1, 33)	PYR-3	10404	1	0			
34	G(1, 34)	TBU	904	1	0			
35	G(1, 35)	PYRI-2	10405	1	0			
36	G(1, 36)	PYRI-3	10405	1	0			
37	G(1, 37)	PYRI-4	10405	1	0			
40	G(1, 40)	PH-1	506	1	0			
45	G(1, 45)	NAPH-1	710	1	0			
46	G(1, 46)	NAPH-2	710	1	0			
47	G(1, 47)	SO—CL	11100000	1	0			
48	G(1, 48)	SO2—CL	11200000	1	0			
49	G(1, 49)	N=S=O	1110000	1	0			
50	G(1, 50)	N=O(O)	110000	1	1	—5		
51	G(1, 51)	N=O(N)	110000	1	1	—6		
52	G(1, 52)	N=O	110000	1	0			

TABLE 2 (continued)

No.		AS[a]	C1[b]	C2[c]	C3[d]	H1[e]	H2[f]	H3[g]
1	2	3	4	5	6	7	8	9
53	G(1, 53)	NO2	210000	1	0			
54	G(1, 54)	NO2(O)	210000	1	1	−5		
55	G(1, 55)	NO2(N)	210000	1	1	−6		
56	G(1, 56)	CL(AR)	10000000	1	1	−8		
57	G(1, 57)	N=N=N	30000	1	0			
58	G(1, 58)	SH	1000100	1	0			
59	G(1, 59)	SH(AR)	1000100	1	1	−8		
60	G(1, 60)	SO—OH	1200100	1	0			
61	G(1, 61)	SO3H	1300100	1	0			
62	G(1, 62)	OH	100100	1	0			
63	G(1, 63)	OH(AR)	100100	1	1	−8		
64	G(1, 64)	NH2	10200	1	0			
65	G(1, 65)	NH2(AR)	10200	1	1	−8		
66	G(1, 66)	CL	10000000	1	0			
67	G(1, 67)	BR	100000000	1	0			
68	G(1, 68)	I	1000000000	1	0			
69	G(1, 69)	CH(CO)	101	3	1	−7		
70	G(1, 70)	IPR	703	1	0			
71	G(2, 1)	CS	1000001	2	0			
72	G(2, 2)	CO	100001	2	0			
73	G(2, 3)	CO(X)	100001	2	1	−9		
74	G(2, 4)	CO—O	200001	2	0			
75	G(2, 5)	O—CO—O	300001	2	0			
76	G(2, 6)	C=N=N	20001	2	0			
77	G(2, 7)	N=C=N	20001	2	0			
78	G(2, 8)	CS—NH	1010101	2	0			
79	G(2, 9)	CO—NH	110101	2	0			
80	G(2, 10)	C=NH	10101	2	0			
81	G(2, 11)	CH2	201	2	0			
82	G(2, 12)	CH2(X)	201	2	1	−9		
83	G(2, 13)	CH2(S)	201	2	1	254		
84	G(2, 14)	CH2(O)	201	2	1	−5		
85	G(2, 15)	CH2(N)	201	2	1	−6		
86	G(2, 16)	CH2(C=)	201	2	1	−3		
87	G(2, 17)	CH2(C*)	201	2	1	−4		
88	G(2, 18)	CH2(CO)	201	2	1	−7		
89	G(2, 19)	CH2(C*N)	201	2	1	−10		
90	G(2, 20)	CH2(NO2)	201	2	1	53		
91	G(2, 21)	CH2(AR)	201	2	1	−8		
92	G(2, 22)	CH2(CH3, CH2)	201	2	2	13	−1	
93	G(2, 23)	CH2(CH3, CH)	201	2	2	13	−2	
94	G(2, 24)	CH2(CH2, CH2)	201	2	2	−1	−1	
95	G(2, 25)	CH2(CH3, C)	201	2	2	13	263	
96	G(2, 26)	CH2(CH2, CH)	201	2	2	−1	−2	
97	G(2, 27)	CH2(CH2, C)	201	2	2	−1	263	
98	G(2, 28)	CH2(CH, CH)	201	2	2	−2	−2	
99	G(2, 29)	CH2(CH, C)	201	2	2	−2	263	
100	G(2, 30)	CH2(C, C)	201	2	2	263	263	

TABLE 2 (continued)

No.		AS[a]	C1[b]	C2[c]	C3[d]	H1[e]	H2[f]	H3[g]
1	2	3	4	5	6	7	8	9
101	G(2, 31)	CH2(CH3, AR)	201	2	2	13	−8	
102	G(2, 32)	CH2(CH2, AR)	201	2	2	−1	−8	
103	G(2, 33)	CH2(CH, AR)	201	2	2	−2	−8	
104	G(2, 34)	CH2(C, AR)	201	2	2	263	−8	
105	G(2, 35)	CH2(AR, AR)	201	2	2	−8	−8	
107	G(2, 37)	CH2(CH2, X)	201	2	2	−1	−9	
108	G(2, 38)	CH2(CH, X)	201	2	2	−2	−9	
109	G(2, 39)	CH2(C, X)	201	2	2	263	−9	
110	G(2, 40)	CH2(AR, X)	201	2	2	−8	−9	
112	G(2, 42)	CH2(CH3, S)	201	2	2	13	254	
113	G(2, 43)	CH2(CH2, SH)	201	2	2	−1	58	
114	G(2, 44)	CH2(CH2, S)	201	2	2	−1	254	
115	G(2, 45)	CH2(CH, SH)	201	2	2	−2	58	
116	G(2, 46)	CH2(CH, S)	201	2	2	−2	254	
117	G(2, 47)	CH2(C, SH)	201	2	2	263	58	
118	G(2, 48)	CH2(C, S)	201	2	2	263	254	
119	G(2, 49)	CH2(AR, SH)	201	2	2	−8	58	
120	G(2, 50)	CH2(AR, S)	201	2	2	−8	254	
121	G(2, 51)	CH2(CH3, O)	201	2	2	13	−5	
122	G(2, 52)	CH2(CH2, O)	201	2	2	−1	−5	
123	G(2, 53)	CH2(CH, O)	201	2	2	−2	−5	
124	G(2, 54)	CH2(C, O)	201	2	2	263	−5	
125	G(2, 55)	CH2(AR, O)	201	2	2	−8	−5	
126	G(2, 56)	CH2(O, O)	201	2	2	−5	−5	
127	G(2, 57)	CH2(CH3, CO)	201	2	2	13	−7	
128	G(2, 58)	CH2(CH2, CO)	201	2	2	−1	−7	
129	G(2, 59)	CH2(CH, CO)	201	2	2	−2	−7	
130	G(2, 60)	CH2 (C, CO)	201	2	2	263	−7	
131	G(2, 61)	CH2(CH3, N)	201	2	2	13	−6	
132	G(2, 62)	CH2(CH2, N)	201	2	2	−1	−6	
133	G(2, 63)	CH2(CH, N)	201	2	2	−2	−6	
134	G(2, 64)	CH2(C, N)	201	2	2	263	−6	
135	G(2, 65)	CH2(AR, N)	201	2	2	−8	−6	
136	G(2, 66)	CH2(C, C=)	201	2	2	263	−3	
137	G(2, 67)	CH2(C, C*)	201	2	2	263	−4	
138	G(2, 68)	CH2(C=, C=)	201	2	2	−3	−3	
139	G(2, 69)	CH2(C=, C*)	201	2	2	−3	−4	
140	G(2, 70)	CH2(C*, C*)	201	2	2	−4	−4	
141	G(3, 1)	CS—N	1010001	3	0			
142	G(3, 2)	C=N	10001	3	0			
143	G(3, 3)	CH	101	3	0			
144	G(3, 4)	CH(CH3, CH3, C)	101	3	3	13	13	263
145	G(3, 5)	CH(CH3, CH2, C)	101	3	3	13	−1	263
146	G(3, 6)	CH(CH3, CH, C)	101	3	3	13	−2	263
147	G(3, 7)	CH(CH2, CH2, C)	101	3	3	−1	−1	263
148	G(3, 8)	CH(CH3, C, C)	101	3	3	13	263	263
149	G(3, 9)	CH(CH2, C, C)	101	3	3	−1	263	263
150	G(3, 10)	CH(CH, C, C)	101	3	3	−2	263	263

TABLE 2 (continued)

No.		AS[a]	C1[b]	C2[c]	C3[d]	H1[e]	H2[f]	H3[g]
1	2	3	4	5	6	7	8	9
151	G(3, 11)	CH(C, C, C)	101	3	3	263	263	263
153	G(3, 13)	CH(CH3, CH2, X)	101	3	3	13	−1	−9
154	G(3, 14)	CH(CH3, CH, X)	101	3	3	13	−2	−9
155	G(3, 15)	CH(CH2, CH2, X)	101	3	3	−1	−1	−9
156	G(3, 16)	CH(CH3, C, X)	101	3	3	13	263	−9
157	G(3, 17)	CH(CH2, C, X)	101	3	3	−1	263	−9
158	G(3, 18)	CH(CH, C, X)	101	3	3	−2	263	−9
159	G(3, 19)	CH(C, C, X)	101	3	3	263	263	−9
161	G(3, 21)	CH(CH3, CH3, S)	101	3	3	13	13	254
162	G(3, 22)	CH(CH3, CH2, SH)	101	3	3	13	−1	58
163	G(3, 23)	CH(CH3, CH2, S)	101	3	3	13	−1	254
164	G(3, 24)	CH(CH2, CH2, SH)	101	3	3	−1	−1	58
165	G(3, 25)	CH(CH3, C, SH)	101	3	3	13	263	58
166	G(3, 26)	CH(CH3, CH, S)	101	3	3	13	−2	254
167	G(3, 27)	CH(CH2, CH2, S)	101	3	3	−1	−1	254
168	G(3, 28)	CH(CH3, C, S)	101	3	3	13	263	254
169	G(3, 29)	CH(CH2, C, SH)	101	3	3	−1	263	58
170	G(3, 30)	CH(CH2, C, S)	101	3	3	−1	263	254
171	G(3, 31)	CH(CH, C, SH)	101	3	3	−2	263	58
172	G(3, 32)	CH(CH, C, S)	101	3	3	−2	263	254
173	G(3, 33)	CH(C, C, SH)	101	3	3	263	263	58
174	G(3, 34)	CH(C, C, S)	101	3	3	263	263	254
175	G(3, 35)	CH(CH3, CH3, O)	101	3	3	13	13	−5
176	G(3, 36)	CH(CH3, CH2, O)	101	3	3	13	−1	−5
177	G(3, 37)	CH(CH3, CH, O)	101	3	3	13	−2	−5
178	G(3, 38)	CH(CH2, CH2, O)	101	3	3	−2	−2	−5
179	G(3, 39)	CH(CH3, C, O)	101	3	3	13	263	−5
180	G(3, 40)	CH(CH2, C, O)	101	3	3	−1	263	−5
181	G(3, 41)	CH(CH, C, O)	101	3	3	−2	263	−5
182	G(3, 42)	CH(C, C, O)	101	3	3	263	263	−5
183	G(3, 43)	CH(CH3, O, O)	101	3	3	13	−5	−5
184	G(3, 44)	CH(CH2, O, O)	101	3	3	−1	−5	−5
185	G(3, 45)	CH(CH, O, O)	101	3	3	−2	−5	−5
186	G(3, 46)	CH(C, O, O)	101	3	3	263	−5	−5
187	G(3, 47)	CH(CH3, CH3, CO)	101	3	3	13	13	−7
188	G(3, 48)	CH(CH3, CH2, CO)	101	3	3	13	−1	−7
189	G(3, 49)	CH(CH3, CH, CO)	101	3	3	13	−2	−7
190	G(3, 50)	CH(CH2, CH2, CO)	101	3	3	−1	−1	−7
191	G(3, 51)	CH(CH3, C, CO)	101	3	3	13	263	−7
192	G(3, 52)	CH(CH2, C, CO)	101	3	3	−1	263	−7
193	G(3, 53)	CH(CH, C, CO)	101	3	3	−2	263	−7
194	G(3, 54)	CH(C, C, CO)	101	3	3	263	263	−7
195	G(3, 55)	CH(CH3, CH3, N)	101	3	3	13	13	−6
196	G(3, 56)	CH(CH3, CH2, N)	101	3	3	13	−1	−6
197	G(3, 57)	CH(CH3, CH, N)	101	3	3	13	−2	−6
198	G(3, 58)	CH(CH2, CH2, N)	101	3	3	−1	−1	−6
199	G(3, 59)	CH(CH3, C, N)	101	3	3	13	263	−6
200	G(3, 60)	CH(CH2, C, N)	101	3	3	−1	263	−6

TABLE 2 (continued)

No.		AS[a]	C1[b]	C2[c]	C3[d]	H1[e]	H2[f]	H3[g]
1	2	3	4	5	6	7	8	9
201	G(3, 61)	CH(CH, C, N)	101	3	3	−2	263	−6
202	G(3, 62)	CH(C, C, N)	101	3	3	263	263	−6
203	G(3, 63)	C=C=N	10002	3	0			
204	G(3, 64)	C=CH	102	3	0			
205	G(3, 65)	PH-124	306	3	0			
206	G(3, 66)	PH-123	306	3	0			
207	G(3, 67)	PH-135	306	3	0			
210	G(3, 70)	N	10000	3	0			
211	G(4, 1)	CH2(C=, X)	201	2	2	−3	-	
212	G(4, 2)	CH2(C*, X)	201	2	2	−4	−9	
213	G(4, 3)	CH2(C=, S)	201	2	2	−3	254	
214	G(4, 4)	CH2(C=, O)	201	2	2	−3	−5	
215	G(4, 5)	CH2(C*, O)	201	2	2	−4	−5	
216	G(4, 6)	CH2(C=, N)	201	2	2	−3	−6	
217	G(4, 7)	CH2(C*, N)	201	2	2	−4	−6	
218	G(4, 8)	CH2(C, N=)	201	2	2	263	−11	
219	G(4, 9)	C*C	2	2	0			
220	G(4, 10)	C=C=O	100002	2	0			
221	G(4, 11)	CO—O—CO	300002	2	0			
222	G(4, 12)	ECH=CH	202	2	0			
223	G(4, 13)	ZCH=CH	202	2	0			
224	G(4, 14)	C=CH2	202	2	0			
225	G(4, 15)	CH3—C—CH3	603	2	0			
226	G(4, 16)	THIOPH-25	1000204	2	0			
230	G(4, 20)	PH-12	406	2	0			
231	G(4, 21)	PH-13	406	2	0			
232	G(4, 22)	PH-14	406	2	0			
239	G(4, 29)	SO	1100000	2	0			
241	G(4, 31)	SO—O	1200000	2	0			
242	G(4, 32)	SO2	1200000	2	0			
243	G(4, 33)	SO2(N)	1200000	2	1	−6		
244	G(4, 34)	O—SO2	1300000	2	0			
245	G(4, 35)	O—SO—O	1300000	2	0			
246	G(4, 36)	O—SO2—O	1400000	2	0			
247	G(4, 37)	O	100000	2	0			
248	G(4, 38)	O(AR)	100000	2	1	−8		
249	G(4, 39)	O(C=)	100000	2	1	−3		
250	G(4, 40)	NO	110000	2	0			
251	G(4, 41)	N=NO	120000	2	0			
252	G(4, 42)	NH	10100	2	0			
253	G(4, 43)	NH(AR)	10100	2	1	−8		
254	G(4, 44)	S	1000000	2	0			
255	G(4, 45)	N=N	20000	2	0			
256	G(4, 46)	C=C	2	4	0			
257	G(4, 47)	C=C=C	3	4	0			
258	G(4, 48)	PH-1234	206	4	0			
259	G(4, 49)	PH-1245	206	4	0			
260	G(4, 50)	PH-1235	206	4	0			

TABLE 2 (continued)

No.		AS[a]	C1[b]	C2[c]	C3[d]	H1[e]	H2[f]	H3[g]
1	2	3	4	5	6	7	8	9
261	G(4, 51)	PH-12345	106	5	0			
262	G(4, 52)	PH-123456	6	6	0			
263	G(4, 53)	C	1	4	0			
264	G(4, 54)	CH2(N=)	201	2	1	−11		
265	G(4, 55)	NH—CS—NH	1020201	2	0			
266	G(4, 56)	CH(N)	101	3	1	−6		
267	G(4, 57)	CH(O)	101	3	1	−5		
268	G(4, 58)	CH(S)	101	3	1	254		
269	G(4, 59)	CH(X)	101	3	1	−9		
270	G(4, 60)	CH(O, O)	101	3	2	−5	−5	

[a]Name of substructure. [b]Empirical formula of substructure. [c]Valence of substructure. [d]Number of substituents which are indicated in the molecular environment of the substructure. [e]Variable which describes substructures with a particular molecular environment (e.g. CH3(CH2), CH_3 group connected with CH_2). [f]Variable which describes substructures which have two kinds of molecular environment (identical or different). [g]Variable which describes substructures with three kinds (identical or different) of molecular environment.

row, bivalent substructures in the second row, etc. During the SEAC procedure, matrix G is initialized by assigning the value of zero to each structural unit. Identification of a given substructure changes the value of the appropriate effect of the matrix to a specified extent connected with a particular identification probability. This identification probability of a substructure is a complex function of the diagnostic usefulness of the spectral signal selected for a particular substructure and the number of other substructures that can be represented by the same signal. For example, the identification of an absorption band ($T < 36\%$) at 1830—1720 cm^{-1} in an i.r. spectrum, when the test substance contains more than two oxygen atoms in the molecule, suggests the presence (with equal probability) of —C(=O)—O— or —O—C(=O)—O—

Checking the correctness of identification. This is done by means of the i.r. or ^{1}H-n.m.r. spectral features which are different from those used for identification; the u.v. spectra are also utilized. Generally, confirmation of the presence of a given substructure increases its probability (i.e., the absolute value of a particular unit in matrix G is increased). But if the substructure is not confirmed by the checking algorithm, the probability of its presence is decreased or even nullified. Another checking mechanism is based on cross-correlations between structural fragments detected by both i.r. and ^{1}H-n.m.r.; the molecular environment detected in the n.m.r. spectrum is checked against the substructures identified by i.r.

Structure generation. After these operations of identification and checking, the set of substructures obtained with highest probability is processed in the structure generation step. The action of this step is very flexible: at the first, second and fourth levels, a list of substructures detected and their respective probabilities is output; at the third level the list printed out is completed by the sets of spectrally inactive groups (e.g., $-\overset{|}{\underset{|}{C}}-$, $-\underset{|}{N}-$) which supplement the empirical formula. At the fifth level, the general standard connectivity matrix of the structure analysed is created.

The efficient action of the structure generator requires storage of the following data for each substructure: its number, code, empirical formula, valence, number of substituents which can be connected with the substructure, and, for fragments with specified molecular environments, information about the allowed substituents; an example of the information on structural fragments is given in Table 2. The second, even more essential requirement was to devise a mechanism which would indicate whether or not a substructure detected could really be included in the structure examined; the system would then estimate the repetition factor (e.g., the number of CH_2 groups that might be included in the structure if one such group is identified), and would finally indicate whether or not the empirical formula is consistent with the sum of the formulae of all substructures with respect to any element and/or degree of unsaturation.

These very sophisticated functions of the algorithm generating the chemical structures, were simplified to a large extent by application of a novel mathematical operation, called vector division.

If vectors $\mathbf{X} = (x_1, x_2, \ldots, x_n)$ and non-zero $\mathbf{Y} = (y_1, y_2, \ldots, y_n)$ are given such that $x_i y_i \geqslant 0$ for $i = 1, 2, \ldots, n$, then the quotient of vectors $\mathbf{X}/\mathbf{Y}$ is $\mathbf{X}/\mathbf{Y} = \min (x_i/y_i)$ for $y_i \neq 0$ and $i = 1, 2, \ldots, n$.

For the operation defined, it is easy to demonstrate the dependences successfully used in the algorithm:

$$(a\mathbf{X})/\mathbf{Y} = a(\mathbf{X}/\mathbf{Y}) \text{ and } \mathbf{X}/(a\mathbf{Y}) = (\mathbf{X}/\mathbf{Y})/a$$

(for $a > 0 \wedge a \in \mathrm{R}$, where $a\mathbf{X}$ and $a\mathbf{Y}$ are the products of the vector and a number), and

$$\mathbf{X}/(\mathbf{Y}1 + \mathbf{Y}2 + \ldots + \mathbf{Y}(N-1)) \geqslant \mathbf{X}/(\mathbf{Y}1 + \mathbf{Y}2 + \ldots + \mathbf{Y}(N-1) + \mathbf{Y}N)$$

(where $\mathbf{Y}1 + \mathbf{Y}2 + \ldots + \mathbf{Y}N$ is the operation of addition of vectors)

The algorithm for structure generation relies, inter alia, on the following input information:

(1) vector $\mathbf{B} = (B_1, B_2, \ldots, B_9)$ in which the coordinates $B_1, B_2 \ldots, B_8$ indicate the number of atoms C, H, N, O, S, Cl, Br, I in the investigated molecule, and B_9 the number of unsaturated linkages;
(2) set z_0 (with numerical force Q) of detected substructures;
(3) matrix S [1:9, 1:Q] in which each column vector $\mathbf{s}_i = s_{1,i}, s_{2,i}, \ldots, s_{9,i}$ is assigned to substructure i. Numbers $s_{1,i}, s_{2,i}, \ldots, s_{8,i}$ indicate how many

C, H, N, O, S, Cl, Br, I atoms are included in the structural fragment i; s_9, i describes the unsaturation of the fragment.

During structure generation the number of members of set z_0 has to be reduced. In this respect the operation of vector division is extremely successful. The general algorithm for solving this problem is summarized as follows. First, structural fragments for which the inequality $B/s_i < 1$ for $i = 1, 2, \ldots, Q$ is satisfied (which means that substructures exceeding the empirical formula of the molecule with regard to any element and/or unit of unsaturation) are rejected. Then these members of set z_0 are selected, starting with the most probable, for which following inequalities are satisfied:

$$B/\left(\sum_{i=1}^{Q_0} s_i\right) \geqslant 1 \text{ and } B/\left(\sum_{i=1}^{Q_0+1} s_i\right) < 1$$

(where Q_0 is the number of structural fragments selected of the set z_0, $Q_0 \leqslant Q$). In this way, a set with less numerical force is obtained; this is very important for the generation of all linear combinations which fulfil the input empirical formula.

Application of the vector division operation make it possible to unify the checking of chemical structure generation at each stage of the process, owing to the development of a single common procedure. This in turn considerably reduces the program and the computer time required.

In order to generate the correct structure, the computer forms set z_1 in the following manner: set z_0 is completed by 12 (level III, Table 3) or 11 (level V, Table 3) fragments which are spectrally inactive. Thus $Q_1 = Q_0 + 12$ for level III and $Q_1 = Q_0 + 11$ for level V, where Q_1 is the number of members of set z_1. Then, for the members of set z_1, the computer generates all linear combinations of elements which fulfil the equation

$$B = \sum_{i=1}^{Q_1} N_i S_i$$

TABLE 3

Substructures calculated from empirical formula

No.		Name of group	No.		Name of group
1	G[1, 66]	Cl	7	G[4, 9]	C*C
2	G[1, 67]	Br	8	G[4, 44]	S
3	G[1, 68]	I	9	G[4, 45]	N=N
4	G[3, 2]	C=N	10	G[4, 46]	C=C
5	G[3, 3]	CH[a]	11	G[4, 53]	C
6	G[3, 70]	N	12	G[4, 52]	PH-123456

[a]Substructure calculated in level III onlv.

TABLE 4

Some results of structure elucidation of selected organic compounds by the SEAC system

No.	Substance analysed	Structure generated
1	$CH_3COCH_2CH_3$	$CH_3COCH_2CH_3$
2	$CH_3(CH_2)_3CH_2COCH_3$	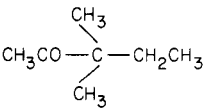 and $CH_3(CH_2)_3CH_2COCH_3$
3	$CH_3CH_2CH_2CH_2CHO$	$CH_3CH_2\,CH_2CH_2CHO$
4	$CH_3CO-OCH_2CH_2CH_3$	$CH_3\,CO-OCH_2CH_2CH_3$
5	$CH_3COCH_2CO-OCH_2CH_3$	$CH_3COCH_2\,CO-OCH_2CH_3$
6	$H-CO-OCH_2CH_2CH_3$	$H-CO-OCH_2CH_2CH_3$
7	$(CH_3)_2CHCH_2OH$	$(CH_3)_2CHCH_2OH$
8	$(CH_3)_2CHCOOH$	$(CH_3)_2CHCOOH$
9	$CH_2=CHCH_2COOH$	$CH_2=CHCH_2COOH$
10	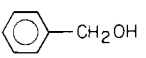	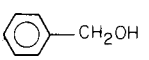
11	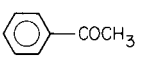	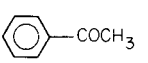
12	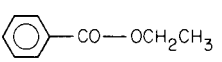	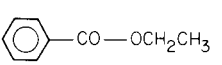
13	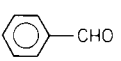	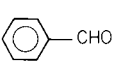
14	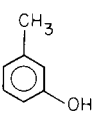	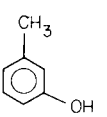
15	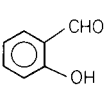	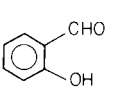

TABLE 4 (continued)

No.	Substance analysed	Structure generated
16	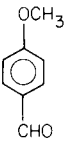	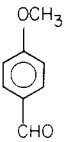
17	$CH_3(CH_2)_7CH_2OH$	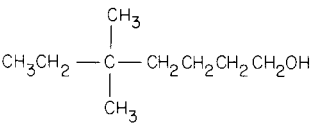 and $CH_3CH_2CH_2CH_2CH_2CH_2CH_2CH_2CH_2OH$
18	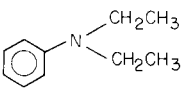	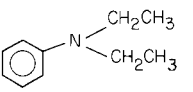
19	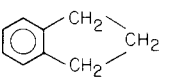	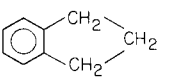

where S_i is the column vector of matrix S, assigned to structural fragment i, and N_i is the product of fragment i. $N_i = 0, 1, 2, \ldots, L_i$; the maximum product L_i of structural fragment i is calculated from the equation: $L_1 = \text{INT}(B/S_i)$ (for $i = 1, 2, \ldots, Q_1$).

For the linear combination of structural fragments which fulfil the above requirements, the computer produces the connection matrix K, applying sequentially the following data: the molecular environment of a given substructure, the connections between multifunctional groups, and the connections of monofunctional groups with polyfunctional fragments (valence > 1). The structural formula is printed as a table which contains the column vectors of connection matrix K.

RESULTS AND DISCUSSION

SEAC was tested with the use of model structures selected to check the correctness of almost all blocks of the system. It was of interest to see first how the computer printout changes for a given structure, throughout the different levels I—V of the system.

The information printed out about the test compound depends on the information of entropy of the input data. At level I, the set of substructures detected contains all the elements which are included in the molecule, but it

TABLE 5

Input data and results for levels I—V

LEVEL I

INPUT DATA

QUALITATIVE COMPOSITION: UNKNOWN

IR SPECTRUM

W(1/CM)	T(%)	D(1/CM)
3086	50	40
3030	39	40
2959	16	50
1600	75	0
1488	30	0
1462	37	0
1433	51	0
1316	71	0
1266	74	0
1220	76	0
1163	78	0
1081	74	0
1042	77	0
1026	67	0
924	78	0
749	7	0
738	12	0

STRUCTURAL GROUPS FOUND (IR)

GROUP	PROBABILITY, %
PH-12	90
CH2	72
PYRI-2	54
CH2(AR)	36

LEVEL II

INPUT DATA

QUALITATIVE COMPOSITION: CH

IR SPECTRUM (AS FOR LEVEL I)

STRUCTURAL GROUPS FOUND (IR)

GROUP	PROBABILITY, %
PH-12	90
CH2	72
CH2(AR)	36

LEVEL III

INPUT DATA

CHEMICAL FORMULA: C9H10

DEGREE OF UNSATURATION = 5

IR SPECTRUM (AS FOR LEVEL I)

STRUCTURAL GROUPS FOUND (IR)

GROUP	PROBABILITY, %
PH-12	90
CH2	72
CH2(AR)	36

GROUPS COMPLETING CHEMICAL FORMULA

NUMBER	SET
1	2 CH2

LEVEL IV

INPUT DATA

QUALITATIVE COMPOSITION: CH

IR SPECTRUM (AS FOR LEVEL I)

NMR SPECTRUM:

TAU (PPM)	INT. (Hz)	MULT./C. CONST.
2.85	4	1.00
7.97	2	5.08
7.09	4	3.08

STRUCTURAL GROUPS FOUND (IR + NMR)

GROUP	PROBABILITY, %
CH2	90
CH2(CH2, AR)	72
PH-12	58
CH2(CH2, CH2)	35
CH3(CH3, CH)	35
PH-14	18
PH-13	18
CH2(AR)	16

LEVEL V

INPUT DATA

CHEMICAL FORMULA: C9H10

DEGREE OF UNSATURATION = 5

IR SPECTRUM: (AS FOR LEVEL I)

NMR SPECTRUM: (AS FOR LEVEL IV)

STRUCTURAL GROUPS FOUND (IR + NMR)

GROUP	PROBABILITY, %
CH2	90
CH2(CH2, AR)	72
PH-12	58
CH2(CH2, CH2)	35
CH3(CH3, CH)	35
CH2(AR)	16

CHEMICAL FORMULA

CONNECTION MATRIX NR 1

NR	1	2	3	4	GROUP
1	0	1	1	0	PH-12
2	1	0	0	1	CH2
3	1	0	0	1	CH2
4	0	1	1	0	CH2

OR ALLOWED ISOMERS

also contains groups with atoms which are not present in the compound; e.g., for indane, the substructure

(PYRI-2) is printed out. It should be emphasized that its identification probability is smaller than those for substructures that are really present in the molecule. When information about qualitative composition is used (level II), any substructures containing elements that are not present in the test substance are rejected. At level III, apart from the detected structural fragments, the computer prints sets of substructures which supplement the empirical formula. Identification by i.r. and ^{1}H-n.m.r., when the qualitative composition is known (level IV), increases the identification probability for groups detected by i.r. spectroscopy and supplements the set by substructures with specified molecular environments. At level V, the computer creates the connectivity matrix of the substructure examined; e.g., for indane a single, correct structure is generated. The results (level V only) are summarized in Tables 4 and 5. The results in Table 4 show that for each compound the correct structure was generated, and in most cases the answer was unambiguous. Only for compounds 2 and 17 were two isomeric structures generated.

Further improvements in the SEAC system will be concerned with inclusion of other spectroscopic techniques and the interactive change of the value of units in matrix G. This is easy because of the concept of storing information on detected substructures in matrix G. During the computer run, the user can, in advance, reject some structural fragments from set z_0 or can input known macrofragment(s), based on prior information about the test compound. This approach will certainly reduce the number of generated structures and the computer time for identification of molecules.

REFERENCES

1 N. A. B. Gray, Anal. Chem., 47 (1975) 2426.
2 L. A. Gribov and M. E. Elyashberg, Zh. Anal. Chim., 32 (1977) 2025.
3 S. Sasaki, H. Abe, Y. Hirota, Y. Ishida, Y. Kudo, S. Ochiai, K. Szito and T. Yamasaki, Sci. Rep. Tohoku Univ., Ser. I, 60 (1978) 153.
4 S. Sasaki, Y. Kudo and S. Ochiai, Jpn. Anal., 22 (1973) 25.
5 B. Dębska, J. Duliban and B. Guzowska-Swider, Ph.D. theses, Technical University, Łódź, 1980.

Analytica Chimica Acta, 133 (1981) 319—327
Computer Techniques and Optimization
Elsevier Scientific Publishing Company, Amsterdam — Printed in The Netherlands

EFFECTS OF SOLUTE—SOLVENT INTERACTIONS ON ELECTRONIC SPECTRA: A PREDICTIVE ANALYSIS

LISA J. HILLIARD, D. STEVEN FOULK and HARVEY S. GOLD*
Department of Chemistry, University of Delaware, Newark, DE 19711 (U.S.A.)
CARL E. RECHSTEINER
Arthur D. Little, Inc., Acorn Park, Cambridge, MA 02140 (U.S.A.)
(Received 25th June 1980)

SUMMARY

Ultraviolet-visible and fluorescence spectra have long been utilized for qualitative and quantitative purposes despite numerous complicating factors. In this study, anthracene, 1-naphthol, and 9-acetylanthracene are used as model systems to distinguish solvent-induced effects via multiple regression techniques. The ability to predict changes in spectral peak locations and quantum efficiencies arising from solute—solvent interactions is critical to the development of a versatile computer-searchable library of electronic spectra.

In recent years, several studies have been directed towards utilization of electronic spectra for identification of species. At present, two complementary numerical methods exist for such identification. One utilizes a video-fluorimeter to obtain an "emission-excitation matrix" [1] while the other uses conventional ultraviolet-visible or fluorescence spectroscopy followed by spectral decomposition [2—4]. A recent paper has shown that principal component analysis and decomposition analysis can be used synergically to determine how many species are present, and their identity [5]. However, none of these methods has been able to deal with major changes in spectral features caused by solvent changes.

The role of the solvent on various colligative properties of solutions is of course fundamental; drastic changes in peak locations and/or quantum efficiencies with change of solvent are not rare. This feature of electronic spectra has thwarted development of a computer-based spectral library. A major step in that direction would be the attainment of a predictive ability for changes in spectral appearance as a function of solvent character. To that end, one must look to physical models of solvent behavior.

While molecular fluorescence is viewed theoretically as a process involving individual sample molecules, experimentally a large ensemble of molecules whose bulk properties are influenced by the medium is examined. Although certain generalizations can be made regarding solvent effects, relatively little

is known of the origin of such features as bathochromic shifts, and still less is known of the effect of solvent identity on fluorescence intensity [6]. These effects are fundamental in the utilization of molecular spectroscopy since most investigations are carried out in solution, wherein the emitting or absorbing entity is necessarily under the direct influence of neighboring molecules. The experimentally observed spectra will therefore contain information not only of the sample molecule per se, but also of the system composed of the molecule plus solvent.

These phenomena do not seem to have been described in a general form, although workers drawing on concepts of the molecular structure of liquids have made some progress [7—11]. In order to predict spectral changes, it is necessary to find a set of physical parameters of the solvent—solute system that can be utilized in a predictive manner.

Among the mechanisms proposed for interaction of solvent and solute molecules are hydrogen bonding [12], electromagnetic interaction between the dipole moments of solute and polar solvent [13], and solvent reorientation [14]. In general, modern theory [15] holds that molecular interactions in solution can be divided into two distinct primary types: (a) universal interactions associated with the influence of the aggregate (colligative) properties of the surrounding solvent molecules, and (b) specific interactions between the solute molecule (taken individually) and one or more of the surrounding particles in the solvent sphere. While a given system may not exhibit any specific interactions, all systems experience colligative interactions differing only in degree of effect. A complete description of a real system can be achieved by considering both the colligative (macroscopic) and the specific (microscopic) effect of solvent molecules on the spectrum of the solute molecule. Since specific interactions will exist to some degree in most real systems, the key to successful interpretation would appear to be consideration of the solute molecule, now linked via a specific interaction to one or more solvent molecules, as a new center of absorption that is acted upon by the colligative properties of the solvent.

Clearly, colligative interactions form a backdrop against which specific interactions must be viewed. Therefore, the first step must be an investigation of the colligative aspects of the problem and definition of their contribution. This requires adoption of a predictive model to represent the combined solvent—solute system. Since the current primary goal is to adjust a spectrum for solvent effects, the sole reliable criterion for applicability must be agreement between this model and the experimental data.

Investigations of the influence of solvent on absorption spectra have utilized the Onsager model to represent the solute—solvent system [8—11]. In this model, the solute is represented as the dipolar sum of the permanent and (electromagnetically) induced dipole moments present in a dielectric medium and subject to internal fields of the solvent. Kutsyna and Ogurtsova [15] showed that many molecules have a dipole moment in their first excited singlet state that exceeds that of their ground state; it is the size of

this difference that determines the positions of energy levels. The degree to which solvent identity affects the positions of these levels determines the degree of spectral shifts.

Using the Onsager model, Bakhshiev [16] developed an expression for shifts in spectral bands relative to gas phase spectra of the form

$$\Delta\nu = \nu_{sol} - \nu_{vap} = \frac{1}{r^3}\left[C_1\left(\frac{2\epsilon - 2}{2\epsilon + 2}\right) + (C_2 + fC_3)\left(\frac{2n^2 - 2}{2n^2 + 1}\right)\right] \quad (1)$$

where r is the Onsager radius (effectively the molecular radius), ν_{sol} is the observed band frequency in cm^{-1}, ν_{vap} is the band frequency observed for gas phase spectra, ϵ and n are the dielectric constants and refractive indices, respectively, of the pure solvent, f is the oscillator strength of the particular electronic transition, C_1 and C_2 are constants representing functions of the permanent dipole of the solute in the lower and upper electronic states, and C_3 is a constant which depends on the frequency of the purely electronic transition. This equation adequately treats all cases of spectral shifts from the case of dipolar molecules in a polar solvent through non-dipolar species in nonpolar solvents. A general discussion of solvent effects has been published [17].

For the present purpose, terms in eqn. (1) can be combined and rearranged to yield

$$\nu_{sol} = \nu_{vap} + K_1\,(2\epsilon - 2)/(2\epsilon + 1) + K_2\,(2n^2 - 2)/(2n^2 + 1) \quad (2)$$

where $K_1 = C_1/r^3$ and $K_2 = (C_2 + fC_3)/r^3$

Equation (2) is the two-parameter form of the general equation

$$y = \alpha + \beta_1 \chi_1 + \beta_2 \chi_2 + \cdots \beta_n \chi_n \quad (3)$$

as such, it is amenable to solution for intercept, α, and coefficients, β_i, by multiple regression techniques. The goal is then to obtain estimates of ν_{vap}, K_1, and K_2 (corresponding to α, β_1, and β_2) and ultimately to utilize these data for prediction of spectra in a solvent outside the data base, but of known dielectric constant and refractive index.

EXPERIMENTAL

Instrumentation and reagents

A Hitachi MPF-2A fluorescence spectrometer was used in the direct mode to obtain emission spectra of the sample solutions; 5-nm emission and 5-nm excitation slits were used for anthracene and 1-naphthol; 10-nm emission and 10-nm excitation slits were used for 9-acetylanthracene. Data obtained from chart recordings were converted to cm^{-1} before further processing.

The solvents used were spectroquality carbon tetrachloride, benzene, acetone, chloroform, methanol, pentane, cyclohexane (all Fisher), pyridine, n-butanol (both Aldrich); A.C.S. certified hexanes, toluene, dioxane, chloro-

benzene, acetic anhydride, xylenes, methyl acetate (all Fisher); reagent-grade ether, cyclohexanol (both Fisher); n-octanol, n-heptanol, n-hexanol, amyl alcohol (all Aldrich), ethyl acetate, glycerol (both Baker); benzyl alcohol, mesitylene (both Aldrich Gold Label); absolute ethanol; acetic acid (Eastman); and ethylene glycol (Fluka). Refractive indices were obtained using an Abbé refractometer and compared with literature values as an indication of purity.

Anthracene (Aldrich Gold Label), 9-acetylanthracene, and 1-naphthol (both Aldrich) were the solutes.

Data analysis

The data were processed by Data General ECLIPSE and Digital Equipment Corporation DEC-10 computers using a least-squares fit to the multilinear equations. The program utilizes a Gauss-Elimination method to solve sets of equations; the program operation is briefly summarized below.

For a multilinear equation of the form shown in eqn. (3), the least-squares criterion requires that the square of the sum of the errors be minimized. In this case, the residual error, S, is

$$S = \sum_{i=1}^{m} (y_i - \alpha - \beta_1 \chi_{1i} - \beta_2 \chi_{2i} - \cdots \beta_n \chi_{ni})^2 \tag{4}$$

This can be solved by differentiation of the coefficients with respect to α and β_i coefficients giving

$$\partial s/\partial\alpha = \sum 2(y_i - \alpha - \beta_1 \chi_{1i} - \beta_2 \chi_{2i} - \cdots \beta_n\chi_{ni})\,(-1) = 0$$

$$\partial s/\partial\beta_1 = \sum 2(y_i - \alpha - \beta_1 \chi_{1i} - \beta_2 \chi_{2i} - \cdots \beta_1 \chi_{ni})\,(-\chi_{1i}) = 0$$

$$\partial s/\partial\beta_n = \sum 2(y_i - \alpha - \beta_1 \chi_{1i} - \beta_2 \chi_{2i} - \cdots \beta_n \chi_{ni})\,(-\chi_{ni}) = 0$$

Rearrangement gives

$$\sum y_i = \alpha \cdot m + \beta_1 \sum \chi_{1i} + \beta_2 \sum \chi_{2i} + \cdots \beta_n \sum \chi_{ni} \tag{5a}$$

$$\sum \chi_{1i} y_i = \alpha \sum \chi_{1i} + \beta_1 \sum \chi_{1i}^2 + \beta_2 \sum \chi_{1i} \chi_{2i} + \cdots \beta_n \sum \chi_{1i} \chi_{ni} \tag{5b}$$

$$\sum \chi_{ni} y_i = \alpha \sum \chi_{ni} + \beta_1 \sum \chi_{1i} \chi_{ni} + \beta_2 \sum \chi_{2i} \chi_{ni} + \cdots \beta_n \sum \chi_{ni}^2 \tag{5c}$$

This system of equations can be solved by use of standard matrix methods; a Gauss—Jordan elimination [18, 19] was utilized here. As implemented, the current program processes sets of equations containing up to nine independent parameters and returns the coefficients α, β_1, β_2, $\cdots$ β_8. The program recognizes systems that are likely to produce singular matrices and identifies these to the user.

RESULTS AND DISCUSSION

Figure 1 illustrates the effect of various solvents upon the fluorescent spectrum of 2-acetylanthracene. The range of shifts in peak positions is dramatic, as is the overall shape of the spectral envelope. The spectra of this

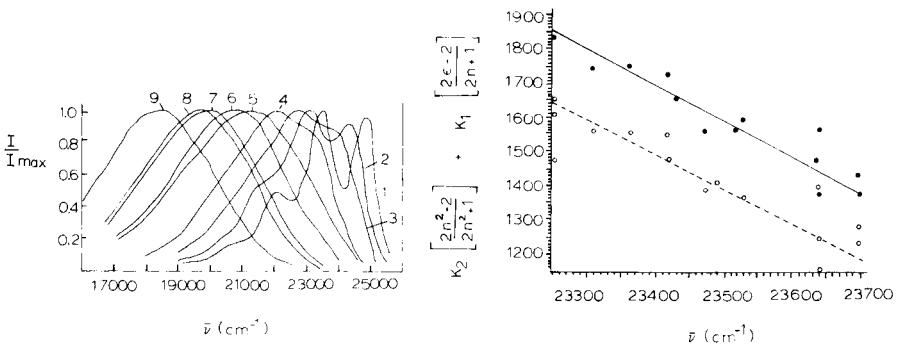

Fig. 1. Fluorescence spectra of 2-acetylanthracene in various solvents: (1) hexane; (2) diethyl ether; (3) benzene; (4) pyridine; (5) acetic anhydride; (6) octanol; (7) methanol; (8) benzyl alcohol; (9) water.

Fig. 2. Results of regression analysis of fluorescence spectra for anthracene in the solvents shown in Table 1. The experimental points are given as a function of: (•) n_D and ϵ; and (○) n_D only.

compound are extreme examples of solvent-induced shifts. While less dramatic, other species undergo similar shifts. Anthracene, 9-acetylanthracene, and 1-naphthol are representative of non-polar, weakly polar, and highly polar species, respectively. Fluorescence spectra were obtained for each in a variety of solvents with markedly different physical properties. Table 1 shows the solvents utilized in each case, arranged in order of increasing dielectric constant, ϵ. The refractive indexes, n_D, are also given.

The spectra of each sample in various solvents were acquired and the peak locations visually determined. Anthracene and 9-acetylanthracene both have three easily discernible peaks in most solvents (25974, 25125, and 23696 cm^{-1} in hexane for anthracene and 26738, 25000, and 23809 cm^{-1} in hexane in the case of 9-acetylanthracene), while 1-naphthol has two peaks (30628 and 29586 cm^{-1} in hexane).

Coefficients K_1 and K_2 and intercept ν_{vap} were calculated for each peak by using the procedure described above. In each case, fits were obtained as a function of ϵ alone, n_D alone, and both ϵ and n_D. As an indication of the fit, the sum of the squared residuals was calculated for each. Since anthracene is non-polar, the peak shifts should depend primarily upon n_D. Similarly, the fit for 1-naphthol (a polar species) should include a strong ϵ term in addition to the n_D term and 9-acetylanthracene should be intermediate. The 23696 cm^{-1} (hexane) peak of anthracene is illustrative of this. As a function of n_D only, the error is 7.52×10^4, as a function of ϵ only it is 1.09×10^7, and as a function of both it is 6.40×10^4. The experimental data are thus consistent with the expectation of dependence on n_D only since the residual error is least in this case. Corresponding results were obtained for the other peaks and species.

TABLE 1

Solvents utilized for each sample. Literature dielectric constants and refractive indices are listed

Solvent	ϵ^{20}	n_D^{20}	1-Naphthol	Anthracene	9-Acetyl-anthracene
Pentane	1.844	1.3575	X		
Hexane	1.885	1.3758	X	X	
Cyclohexane	2.023	1.42662	X	X	
Dioxane	2.217	1.4224		X	X
Carbon tetrachloride	2.238	1.4601		X	
Mesitylene	2.27	1.4994	X	X	
Xylene	2.270	1.4961		X	
Benzene	2.284	1.5011	X	X	X
Toluene	2.39	1.4961	X	X	X
Chloroform	4.806	1.4459			X
Chlorobenzene	5.708	1.5241		X	X
Ethyl acetate	6.095	1.3723	X		X
Acetic acid	6.15	1.3716			X
Methyl acetate	6.79	1.3593	X		
n-Octanol	10.3	1.4295			X
Benzyl alcohol	13.1	1.5396			X
n-Hexanol	13.85	1.4178			X
Amyl alcohol	14.27	1.4101		X	
Acetic anhydride	20.7	1.3901			X
Ethanol	25.0	1.3611		X	
Methanol	33.62	1.3275		X	X
Ethylene glycol	38.68	1.4318			X

To a first approximation, K_1 and K_2 should be constant for each species regardless of the peak chosen. Table 2 summarizes the results for all three species. While there is some variation in values among peaks, these are well within the experimental ability to determine the original peak locations. The ability to predict peak positions is best judged from Figs. 2 and 3.

Figure 2 shows the best fit to data for anthracene. Fits as a function of n_D only and of both n_D and ϵ are plotted. As discussed above, the fit to n_D only results in less total error. While there is considerable scatter of points around the line, the deviations are within experimental error. Furthermore, the difference between calculated and experimental peak positions is less than 1 nm in all instances. Corresponding agreement between experimental and calculated data was obtained for 9-acetylanthracene and 1-naphthol (Fig. 3). These spectra are plotted as a function of both n_D and ϵ. While the residual error does not decrease significantly for non-polar anthracene, neither does it increase. It is thus reasonable to state that curve-fitting for non-polar molecules requires incorporation of only the refractive index, while polar molecules require that dielectric constant be utilized in addition to refractive index.

The significance of these results is that peak positions can be predicted

TABLE 2

Calculated least-squares parameters for peaks of each species

Calculated parameters		Species		
Peak	Term	Anthracene[a]	9-Acetylanthracene[b]	1-Naphthol[b]
1	ν_{vap}	27125	27537	31586
	K_1	0	162.93	−856.78
	K_2	−3268.2	−3015.2	−1729.3
1	ν_{vap}	26272	26134	30550
	K_1	0	−56.7	−563.92
	K_2	−3446.1	−3258.3	−2051.47
3	ν_{vap}	24898	25216	
	K_1	0	−268.61	
	K_2	−3444.7	−3775.8	

[a]Plotted as a function of n_D. [b]Plotted as a function of n_D and ϵ.

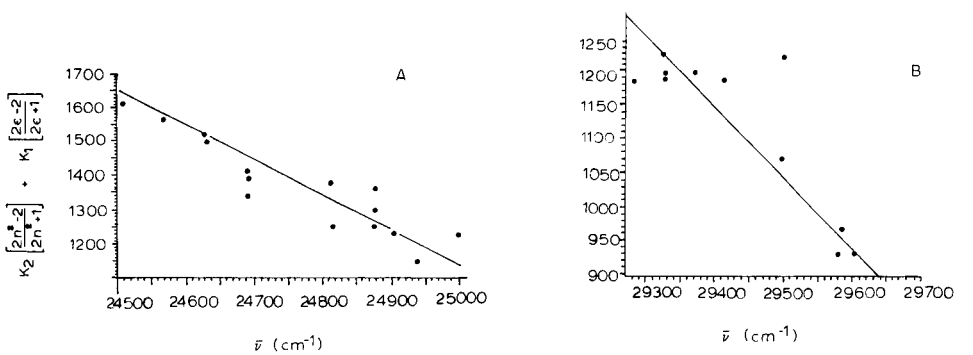

Fig. 3. Results of regression analysis of fluorescence spectra of (A) 9-acetylanthracene and (B) 1-naphthol for the solvents shown in Table 1. The experimental points are given as a function of n_D and ϵ.

regardless of solvent-induced changes. Not only do peak maxima shift, but the entire envelope moves. In an ideal case, this can be envisioned as a predictable and uniform shift across the entire spectral range. In reality, individual component peaks within a single spectral envelope may be shifted to varying degrees. This can be appreciated by recalling that $\pi \rightarrow \pi^*$ transitions are red-shifted and $n \rightarrow \pi^*$ transitions blue-shifted in going from nonpolar to polar solvents [6]. This non-equivalence of transition interactions with the solvent can result in variable overlap of peaks, an effect visible in Fig. 1.

While this is an unfortunate aspect of fluorescence, it helps explain the variation in calculated peak parameters described above. Furthermore, this effect can be utilized to great advantage if the positions of individual transi-

tions (peaks) are accurately known. This process of spectral decomposition has been described previously [2—5]. The long-term goal of implementing a computer-searchable data base of electronic spectra is now close at hand. Used in conjunction with spectral decomposition, the predictive ability demonstrated above should require that only a minimal number of spectra be acquired and stored, because knowledge of physical parameters of solvents permits adjustment of the reference spectrum. The accuracy of the identification can be further enhanced by adjusting individual component peaks and then generating a composite spectral envelope if needed.

Perhaps the most interesting application involves correction of spectra and intensities obtained from fluorescent probe molecules in biological media. A persistent problem in bioanalysis has been the inability to adjust for intensity (and thus concentration) variations that necessarily arise when the probe molecule goes from solution into a micelle or cell membrane. While modern biophysics is able to predict or model both refractive index and dielectric constant gradients as a function of penetration into micelles, it has until now not been possible to utilize this information to adjust spectral parameters. By combining these biophysical models with the results of the present paper, correction of fluorescent probe data for changes in fluorescence yield and peak positions becomes feasible. Preliminary work in this area has already begun in this laboratory.

Source listings in FORTRAN of the regression and residual error computer programs are available from the author.

This work was presented in part at the 14th Middle Atlantic Regional Meeting of the American Chemical Society, Valley Forge, PA, April, 1980. Partial support by the University of Delaware Research Foundation and the American Cancer Society (under Grant IN-139) is gratefully acknowledged.

REFERENCES

1 I. M. Warner, G. D. Christian, E. R. Davidson, and J. B. Callis, Anal. Chem., 49 (1977) 564.
2 H. S. Gold, C. E. Rechsteiner, and R. P. Buck, Anal. Chim. Acta, 103 (1978) 51.
3 C. E. Rechsteiner, H. S. Gold, and R. P. Buck, Anal. Chim. Acta, 95 (1977) 51.
4 H. S. Gold, C. E. Rechsteiner, and R. P. Buck, Anal. Chem., 48 (1976) 1540.
5 H. S. Gold, G. T. Rasmussen, J. A. Smith, D. G. Whitten, and R. P. Buck, Anal. Chim. Acta, 122 (1980) 171.
6 C. A. Parker, Photoluminescence of Solutions, Elsevier, Amsterdam, 1968, pp. 373—378.
7 N. S. Baglis and E. G. McRae, J. Phys. Chem., 58 (1954) 1002.
8 Y. Ooshika, J. Phys. Soc., Jpn., 9 (1954) 594.
9 N. Mataga, Y. Kaifu, and M. Koizumi, Bull. Chem. Soc., Jpn., 28 (1955) 690; 29 (1956) 465.
10 E. G. McRae, J. Phys. Chem., 61 (1957) 562.
11 E. Lippert, Z. Electrochem., 61 (1957) 962.
12 N. Mataga and S. Tsuno, Bull. Chem. Soc. Jpn., 30 (1957) 368.
13 N. Mataga, Y. Torihashi, and K. Ezumi, Theor. Chim. Acta, 2 (1964) 158.

14 J. Eisinger and G. Navon, J. Chem. Phys., 50 (1969) 2069.
15 L. M. Kutsyna and L. A. Ogurtsova, Bull. Acad. Sci. (USSR) Phys. Ser., 27 (1963) 738.
16 N. G. Bakhshiev, Bull. Acad. Sci. (USSR) Phys. Ser., 24 (1960) 593.
17 I. B. Berlman, Handbook of Fluorescence Spectra of Aromatic Molecules, Academic Press, New York, 1971, pp. 52—54.
18 P. R. Bevington, Data Reduction and Error Analysis, McGraw Hill, New York, 1969, pp. 293—303.
19 C. R. Wylie, Jr., Advanced Engineering Mathematics, 3rd edn., McGraw Hill, New York, 1966, pp. 447—459.

Analytica Chimica Acta, 133 (1981) 329—338
Computer Techniques and Optimization
Elsevier Scientific Publishing Company, Amsterdam — Printed in The Netherlands

AUTOMATIC ANALYSIS OF MIXED SPECTRA
Generalised Spectral Subtraction Applied to Electron Spin Resonance Spectroscopy

J. C. EVANS* and P. H. MORGAN
Chemistry Department, University College, P.O. Box 78, Cardiff CF1 1XL (Great Britain)
(Received 10th November, 1980)

SUMMARY

A new technique is described for estimating the pure component spectra from a set of linearly independent spectra. The process is one of generalised spectral subtraction in which an iterative combination of multivariate linear least-squares analysis and matrix transformation is applied to the input data to give estimates of the number of independent components in the original mixed spectra. This technique is applicable to bipolar data (e.g. from e.p.r. spectra) as well as absorption spectra determined by any spectroscopic technique, provided that the spectra may be reasonably assumed to be an additive mixture of unknown pure components. Numerical model examples are given together with an experimental application to electron spin resonance.

In spectroscopy, spectra which are additive mixtures of basic components are frequently found [1]. This arises in cases where spectra are taken from systems of non-interacting species. It is often important to be able to estimate the spectra of the pure components by subtracting the spectra from each other until the result is judged to be representative of a pure spectrum. It is, of course, better practice to change the experimental conditions to obtain the pure spectrum directly, but this is not always possible.

Implicit in the idea of spectral subtraction is the notion of a simple spectrum. The simplest spectrum is defined here as that which approaches zero most often in the interval of interest. Figure 1 shows two hypothetical spectra $A(t)$ and $B(t)$ together with the schematic results for the subtraction of $B(t)$ from $A(t)$; β is a multiplication factor. Without this, or some other notion of simplicity, acting as a constraint upon the subtraction, it is impossible to appreciate when the subtraction is successful. It is, of course, generally impossible to perform a successful subtraction unless one of the pure components has a significantly large number of points which approach zero where the other pure spectrum is finite. In the event that the points of overlap are such that the one spectrum is completely overlapped by the other, then only the former spectrum can be completely recovered whereas the latter will only be recoverable outside the region occupied by the former.

In practice, equidistantly sampled values are often considered rather than

0378—4304/81/0000—0000/$02.50

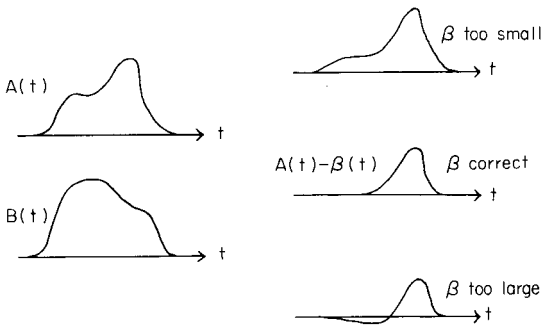

Fig. 1. A schematic diagram showing spectra subtraction.

the original spectra. This is certainly true if spectral data must be processed. It is often convenient to think of such spectral data values as being the components of a vector in a space of n dimensions (for n data values). The problem of subtraction then becomes one of vector subtraction where the aim is to make as many as possible of the resultant vector components simultaneously zero. However, experimentally, spectra always contain added noise and do not always conveniently die away to zero at some region of the experimentally accessible region. It is necessary therefore to weight the experimental points in order of decreasing importance as their absolute value increases. One simple way of doing this is to institute a threshold value below which the values are effectively considered to be zero. The subtraction is now no longer exact, and so the pure components are now estimated rather than obtained accurately. Even if the overlap between the pure components is apparently complete, then a linear transformation may improve the situation. In Fig. 2 the use of such a linear transformation is shown.

Linear transformations such as the Fourier cosine transform are such that the sum of the transforms is the transform of the sum and therefore subtraction may be carried out in the transform domain before inverse transformation to visualize the subtraction in terms of the original variable t.

If again the data are viewed as a set of vectors, then these linear transformations can be interpreted as matrix transformations of these vectors.

THEORY

A practical method for dissecting spectra into their pure components is now considered. The method is best introduced by referring to a simple hypothetical example involving two spectra. In Fig. 3 two spectra A(t) and B(t) are plotted against each other using t as a parameter. The region between the dashed lines is the region of overlap of the two underlying pure components. The regions where there is no overlap manifest themselves in the parametric plot as straight lines passing through origin. The process of dissecting A(t) and B(t) into their pure components C(t) and D(t) consists in

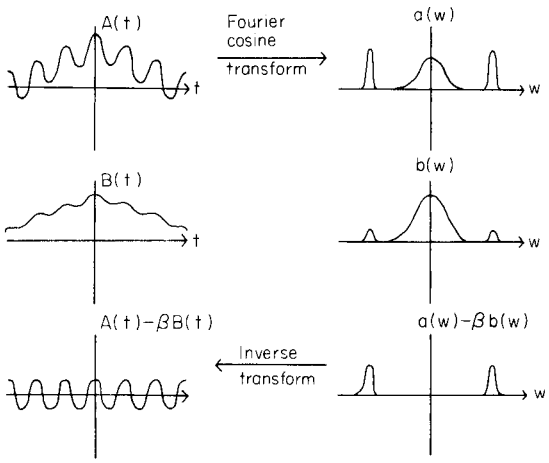

Fig. 2. The use of a linear transformation for preprocessing prior to spectral subtraction. A(t) and B(t) are even functions of t for simplicity of illustration; a(w) and b(w) are the transforms of A(t) and B(t).

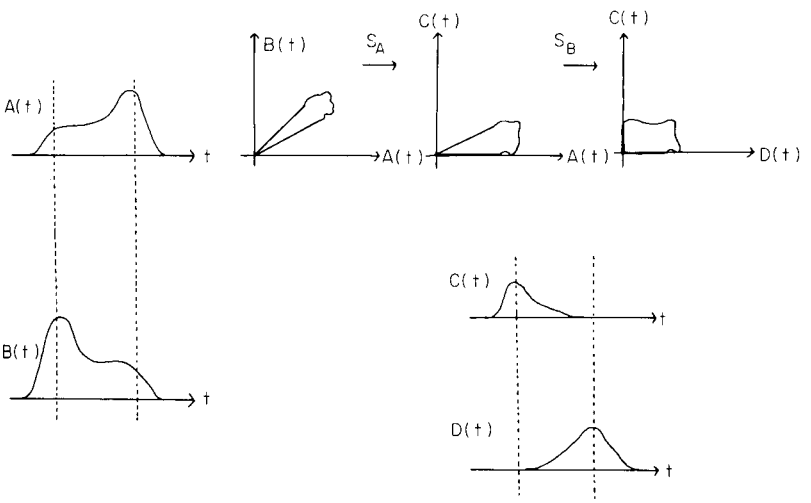

Fig. 3. The relationship between spectral subtraction and the parametric plot of one spectrum against another.

identifying these straight-line portions and using them to contrive two consecutive shear operations S_A and S_B which bring these straight-line portions into coincidence with the axes. These operations correspond to subtraction of spectrum A(t) from B(t) followed by subtraction of the resultant from spectrum A(t). If the spectra are sampled at values t_1, t_2, etc., then the operations above correspond to the identification of clusters of points lying on straight lines through the origin.

One method of identifying these linear clusters is to proceed as follows.

(1) (B.A)/(A.A) is calculated; this is the slope α_A of the straight line passing through the origin which minimizes the sum of squared differences between the components values B and those predicted by the straight line which is

$$[B - A(B.A)/(A.A)].[B - A(B.A)/(A.A)]$$

or more concisely $(B - \alpha_A A).(B - \alpha_A A)$. Here the spectra are represented as vectors A and B and the sums of squares, etc., are represented as scalar products.

(2) The next step is to remove those points having an absolute deviation from the calculated line greater than a specified number of standard deviations from the line. If this fails to remove any points, the restriction is narrowed until at least one point is removed.

(3) The straight line is then recomputed as in (1) using only the points remaining from stage (2). The process is repeated from (2) until all remaining points lie within a specified deviation from the straight line.

The choice of the factor to multiply by the standard deviation should be such that a sufficient proportion of the points are removed at each stage to render the convergence of the process sufficiently rapid and not so restrictive so as to risk false convergence. The limit at which the process is stopped corresponds to the threshold value mentioned above. It is the estimated value at which the signal "disappears" into the experimental noise. One must also start with the assumption that, in this two-dimensional case, the two clusters sought are those with the greatest number of points associated with them.

(4) When the final value of α_A has been established, the vector B is replaced by $(B - \alpha_A A)$ and the process is repeated by computing a similar sequence of lines based upon $\alpha_B = (A.B)/(B.B)$.

Assuming that a correct subtraction has been performed as $(B - \alpha_A A)$, then the points along the first line which have been sheared to the A axis by the transformation S_A contribute nothing to the computation of the second line since $A_i B_i = 0$ for these points.

For the case of n spectra, an exactly similar process is followed in which hyperplanes are fitted to hyperplanar clusters of maximum density. The first vector A_1 is taken and the normal equations are

$$\alpha_2 A_2.A_2 + \alpha_3 A_2.A_3 + \ldots\ldots + \alpha_n A_2.A_n = A_2.A_1$$

$$\alpha_2 A_3.A_2 + \alpha_3 A_3.A_3 + \ldots\ldots + \alpha_n A_3.A_n = A_3.A_1$$

$$\alpha_2 A_n.A_2 + \alpha_3 A_n.A_3 + \ldots\ldots + \alpha_n A_n.A_n = A_n.A_1$$

since $A_i.A_k = A_k.A_i$, only $0.5\, n(n + 1) - 1$ of n^2 possible scalar products need be evaluated. α_i is the slope of the hyperplane in the case of the ith spectrum. It should be noted that A_i is the ith spectrum, not to be confused with A_i the ith component of the spectrum A.

The solution of these simultaneous equations gives the α_i values which

characterize the hyperplane through the origin which minimizes the sum of the squared deviations of the components A_1 from that hyperplane.

As, in practice, the spectra have added experimental noise, it is necessary to iterate the process described above. The sequence of hyperplanes tends in general toward the hyperplane lying within a hyperplanar cluster and minimizing the sum of squared deviations from the points in that cluster. En route to this limiting hyperplane, some points which could have contributed to its formation are often lost in the earlier stages of the process because of the influence of points which are distant from the limiting hyperplane but contribute greatly to the scalar products computed in these initial stages. A necessary safety measure therefore computes a limiting hyperplane and uses the resulting α_i as starting values to recommence the procedure with all the points. This is repeated until the α_i values change only by less than some specified amount.

The tolerances in the α_i values which determine the point at which the iteration is stopped may be directly related to the "size" of the corresponding vectors A_i. Since the $A_i.A_i$ are calculated in the process of solving the normal equations it makes sense to use $(A_i.A_i)^{1/2}$ as a measure of the size of A_i though there is no reason why some other norm should not be used.

In theory, with completely noise-free data, the normal equations may become singular if the number of independent components is less than the number of spectra. In practice, the equation set only becomes near-singular and this causes little problem. The hyperplanar clusters associated with a non-overlapped component degenerate to pairs of linear clusters but this causes no singularity problems.

When the α_i corresponding to A_1 have been determined, A_1 is replaced by $(A_1 - \alpha_2 A_2 \ldots - \alpha_n A_n)$. If S_1 is a shear matrix of the type given below then S_1 acts on each point of the parametric plot in n dimensions forming the new A_1 as a linear combination of the A_i. The process is then repeated for A_2 to A_n.

The proportions of the final vectors which have to be added together to give the mixtures is found as follows. If $S_1, S_2, \ldots$ are the successive shear matrices along the 1, 2, ... directions, then the total shear matrix is their product $S_n\ S_{n-1} \ldots S_2 S_1 = S$. S^{-1} is the matrix giving the original mixtures in terms of the pure components whereas S gives the pure components in terms of the original mixtures.

for $n = 4$

$$S_3 = \begin{bmatrix} 1 & 0 & 0 & 0 \\ 0 & 1 & 0 & 0 \\ -\alpha_1 & -\alpha_2 & 1 & -\alpha_4 \\ 0 & 0 & 0 & 1 \end{bmatrix} \quad \text{and } S_3^{-1} \begin{bmatrix} 1 & 0 & 0 & 0 \\ 0 & 1 & 0 & 0 \\ \alpha_1 & \alpha_2 & 1 & \alpha_4 \\ 0 & 0 & 0 & 1 \end{bmatrix}$$

Using the familiar matrix result that $(M_1 M_2)^{-1} = M_2^{-1}\ M_1^{-1}$, $S^{-1} = S_1^{-1}\ S_2^{-1} \ldots S_{n-1}^{-1}\ S_n^{-1}$ so that S^{-1} may be accumulated by successive multiplication on the right by the inverses of S_1, etc. Naturally the elements of S^{-1} can only be

interpreted physically in absolute terms if the relationship between the species concentration and the corresponding spectral intensity is known. The ith column of S^{-1} gives the relative proportions of the ith component in the original spectra.

The number of components in the original spectra is given by the number of output vectors from the algorithm which have a magnitude greater than that of some upper limit derived from experimental considerations. Thus the algorithm functions, incidentally, in the same way as methods which determine the number of components, using effective matrix rank determination [2].

Other workers [2, 3] have tackled the problem of determining the number of independent components in a set of mixed spectra. The method presented in this paper approaches the problem of analysing mixed spectra from the point of view of determining the forms of pure components. The number of independent components is estimated, as a by-product of the algorithm used. If the spectra are not base-line corrected, then this base line must be treated as an extra component. Hence in this case the ideal situation for k spectral components including base line, is to have $k + 1$ spectra input to the algorithm. If there are indeed only k components, then the $(k + 1)$th array will be blank upon output. However, what counts as a blank spectral array will have to be decided by a statistical test in borderline cases, and this aspect of the problem is not tackled here.

RESULTS

Several model problems were used to test the algorithm above. In the first, four 64-point arrays were computed as sums of differing mixtures of Gaussian functions having different peak width and position. The resulting values were truncated to give an absolute error of 0.01 (ca. 1% relative error). The algorithm above was coded in FORTRAN IV and implemented on the ICL 470 system at University College, Cardiff. The input and resulting output are shown in Fig. 4 as output through a line-printer plotting subroutine employing symmetrical rounding of values before plotting. Each plot is scaled to its largest absolute value. The threshold values below which the values are considered negligible were taken as 0.01 for each synthetic spectrum. This value was chosen as the minimum reasonable one consistent with an absolute error of 0.01. Reference to Fig. 4 shows that a very reasonable component separation is obtained.

If the input spectra are almost linearly dependent, this should cause difficulties because the algorithm is working with a near-singular case. Figure 5 shows the input and results from a model problem designed to explore such a difficulty. Again, four 64-point arrays were generated as the sum of Gaussian peaks with a truncation error of 0.001%. The ratios of the three component peaks in the four arrays were $1:\frac{1}{2}:\frac{1}{3}$, $\frac{1}{2}:\frac{1}{3}:\frac{1}{4}$, $\frac{1}{3}:\frac{1}{4}:\frac{1}{5}$ and $\frac{1}{4}:\frac{1}{5}:\frac{1}{6}$ which are notoriously close to being linearly dependent, cf. the solution of a

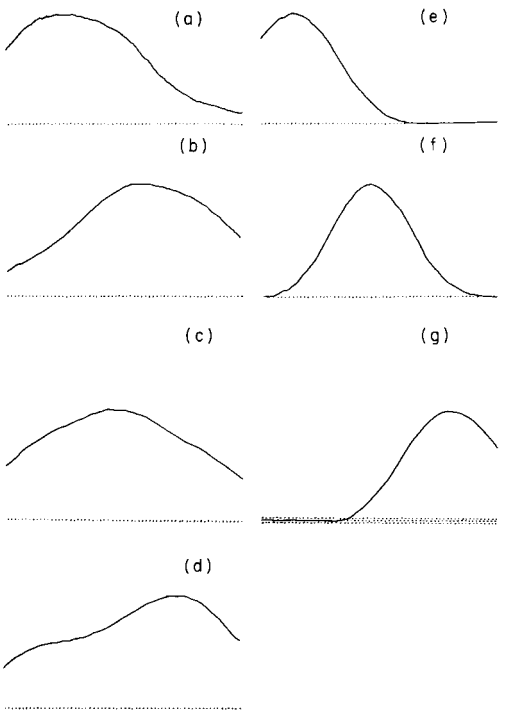

Fig. 4. (a—d) Plots of synthetic spectra input to the algorithm. (e—g) Output plots giving the three non-zero pure components present in (a—d). Peak position and width are exactly those expected.

set of simultaneous equations which are derived from the Hilbert matrix [4].

As described above, when the component spectra entirely overlap, it will be impossible to perform a subtraction. The spectra, however, may be processed with a linear transformation to "separate" the pure components before the algorithm is used. To test this method, four 64-point arrays were computed from the expression

$$a_1 \sin \frac{2\pi}{4}(t-1) + a_2 \sin \frac{2\pi}{32}(t-1) + a_3 \exp -\frac{(t-40)^2}{15}$$

for $t = 1 \rightarrow 64$ with varying values of the amplitude constants $a_{1,2,3}$. The relative truncation error was about 1% and the absolute error 0.01. The Fast Walsh Transform [5] was applied to the resulting model data. This transformation tends to separate components of different spatial frequency and, though not as efficient in this respect for continuous data as the Fast Fourier Transform, it is computationally a much faster operation. It is a unitary transformation and can be thought of as a multidimensional rotation of the data vectors. Further work on optimising the method of transformation is in hand and will be reported in a future communication. Figure 6

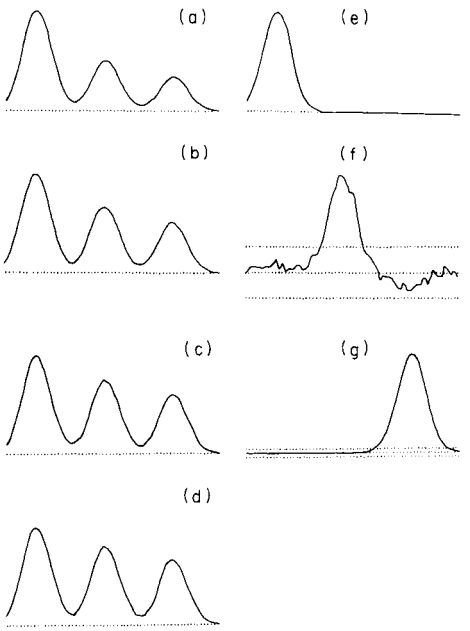

Fig. 5. (a—d) An almost linearly dependent set of synthetic input spectra. (e—g) The output non-zero components present in the four mixtures. S^{-1} gives the proportions of e, f, g in the mixtures a, b, c, d. S^{-1} exp. gives the actual values used in calculating a, b, c, d. The values were as follows:

	e	f	g	
	1.000	0.500	0.333	a
S^{-1} =	0.496	0.332	0.246	b
	0.331	0.249	0.194	c
	0.247	0.199	0.161	d
	1.000	0.500	0.333	a
S^{-1}_{exp} =	0.500	0.333	0.250	b
	0.333	0.250	0.200	c
	0.250	0.200	0.167	d

shows the data before transformation and, though the presence of some periodicity is obvious, it is by no means obvious that a gaussian peak is present in all of the mixed synthetic spectra. After processing followed by inverse transformation the resolution of the mixtures into two sine components and a gaussian component is clearly seen. The two sine components (Fig. 6, e, f) are completely resolved and have the same periods as those used to make the synthetic mixed spectra. The slight ripple remaining on the gaussian peak (Fig. 6, g) is due to the inefficiency of the Fast Walsh Transform in separating this peak from the short-period sine wave. However the mean peak position and width are very close to the values used in preparing the synthetic mixed spectra. The fourth array is "blank" upon output, showing that only three independent components are present in the mixture. This array is not included.

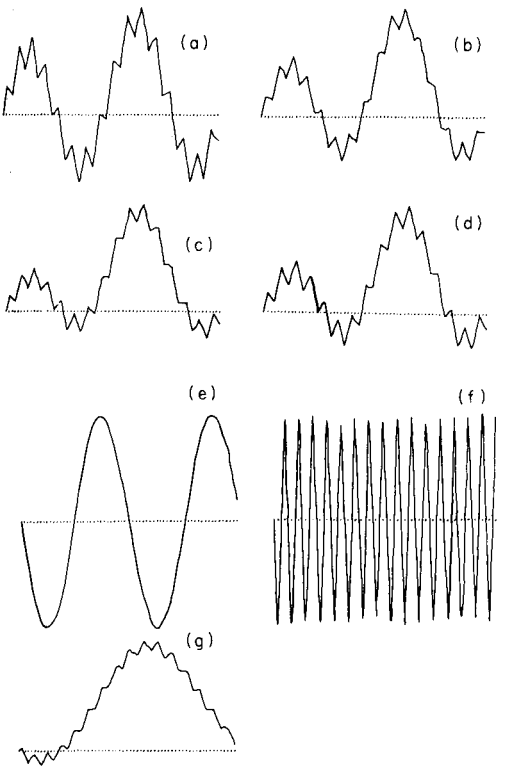

Fig. 6. (a—d) Synthetic spectra composed of sine and Gaussian components. (e—g) Reconstructed pure components using the algorithm.

Figure 7 contains an example in which six e.p.r. spectra, each obtained by passing hydrogen sulphide for 1 h over a sulphided Akzo 153E catalyst containing 15% MoO_3 and 3% NiO supported on η-alumina at various temperatures between 250 and 500°C. After heating to the desired temperature the system was allowed to cool and the e.p.r. spectra measured at room temperature. The experimental e.p.r. spectra (Fig. 7) were digitised by hand to create the input data. After processing, three independent spectra were obtained showing the presence of four and only four species. These are shown in Fig. 8 as joined-up line-printer plots. Figure 8(a) contains two species which are chemically distinct and the fact that they occur together in the same output plot implies their linear dependence; this was subsequently found experimentally [6]. These species were shown to be a sulphur radical (species 1) and a molybdenum(V) component (species 2) which is isotropic from its symmetrical shape, suggesting that the species is in an octahedral environment in the bulk of the solid catalyst. The g values obtained by this procedure were identical with those of published data [7]. Figure 8(b) (species 3) shows another species with three g value components which is at

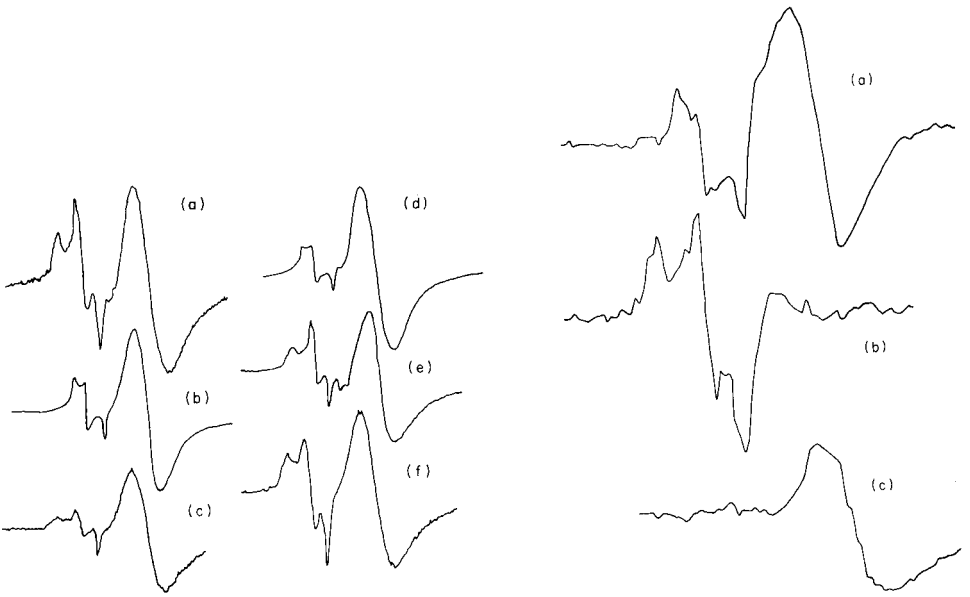

Fig. 7. (a—f) Experimental e.p.r. spectra obtained from a sample of sulphided Akzo 153E catalyst (see text) obtained under anaerobic conditions.

Fig. 8. Computer output of non-zero components from spectra in Fig. 7. (a) Species 1, sulphur radical, g values = 2.051, 2.030, 1.998; species 2, molybdenum(V), g value = 1.923. (b) Species 3, g values = 2.071, 2.032, 2.001. (c) Species 4, molybdenum(V), g value = 1.939.

maximum intensity at 450°C. This is the temperature for maximum efficiency of the catalyst for hydrodesulphurisation. Figure 8(c) (species 4) is another molybdenum(V) species which from its anisotropic character suggests a low-symmetry surface site. This peak was not previously resolved in the e.p.r. input spectra. Much of this information could not have been obtained but for the use of this analytical program.

We thank Mr. T. Horlick Jones for helpful discussion. One of us (PHM) thanks the SRC for financial support.

REFERENCES

1 B. E. Barker and M. E. Fox, Chem. Soc. Rev., 9 (2) (1980) 143.
2 C. Burgess, UV Spectroscopy Group Bulletin No. 7 (1979) 25.
3 J. E. Davies, A. Sheperd, N. Stanford and L. B. Rogers, Anal. Chem., 46 (1974) 821.
4 B. W. Arden and K. N. Astill, Numerical Algorithms: Origins and Applications, Addison-Wesley, U.S.A., 1970.
5 K. G. Beauchamp, Walsh Functions and their Applications, Academic Press, London, 1975.
6 J. C. Evans, J. Mortimer and J. D. Rule, unpublished data.
7 A. K. Kolosov, V. A. Shuets, N. D. Chuvylkin and V. B. Kazansky, J. Catal., 47 (1977) 190.

Analytica Chimica Acta, 133 (1981) 339—347
Computer Techniques and Optimization
Elsevier Scientific Publishing Company, Amsterdam — Printed in The Netherlands

COMPUTERIZED DETECTION AND EVALUATION OF PEAKS IN SURVEY SPECTRA FROM PHOTOELECTRON SPECTROSCOPY

E. BRUNINX* and A. van EENBERGEN
Philips Research Laboratories, Eindhoven (The Netherlands)
(Received 10th November 1980)

SUMMARY

The computer program described is written in Algol-60 and allows a fast data analysis of photoelectron peaks in survey spectra (0—1500 eV). Additional peak parameters such as area, background and peak width are also determined. The assumptions about peak shape are kept to a minimum. In spectra with good counting statistics, it is possible to detect peaks with peak/background ratio down to 0.01.

In photoelectron spectroscopy, the spectra normally required are of two types. For samples whose composition is unknown, a preliminary wide-energy scan (survey spectrum) is usually required to identify elements present in a sample. In such a measurement an accurate determination of the binding energy is not a prime requisite, and high resolution is also of secondary importance. For more advanced studies, however, detailed spectra taken over a narrow energy interval are preferred. These allow a more accurate determination of the binding energy and various other peak parameters. Such spectra are usually measured with a better resolution than for survey spectra. In addition, featureless regions containing no information can be omitted, thus allowing a more efficient use of spectrometer time.

The program described in this paper is used to detect and evaluate peaks in a survey spectrum. The method is based on well known peak-search methods, which have long been employed in γ-ray spectrometry [1]. It should be emphasized that no manual intervention or selection is required for this peak-detection procedure.

METHODS

The survey spectra (0—1500 eV) were measured with a Leybold-Hereaus LHS-10 electron spectrometer [2] and stored in a Canberra multichannel analyzer, (2048-channels, 0.73 eV/channel). The spectra were recorded with a retardation factor of 3 and a sweep time of 20 s.

For peak detection the method of Mariscotti [3] was used; this assumes that the peak can be approximated over a limited energy range by a Gaussian

0378—4304/81/0000—0000/$02.50

curve superimposed on a linear background. In photoelectron spectroscopy the assumption of a Gaussian peak shape may not always be correct. Experience has shown, however, that this condition is sufficiently accurate for the present purpose.

The program is based on the fact that the second derivative (sd_i) passes through a well defined minimum at the position of the peak maximum; the value of sd_i is given by

$$sd_i = y_{i-1} - 2y_i + y_{i+1} \tag{1}$$

where y_i is the channel content of channel i. Mariscotti has shown that in order to detect the weakest peaks in a spectrum, this second derivative should be replaced by the average, $sd_i(w)$, of the sd_i values over $w = 2m + 1$ channels centered around i (m is the number of channels to the left and to the right of i):

$$sd_i(w) = \sum_{j=i-m}^{i+m} sd_j \tag{2}$$

In order to reduce even more the statistical scatter the process of calculating $sd_i(w)$ can be repeated a number of times (z)

$$sd_i(w, z) = \sum_{j=i-m}^{i+m} sd_j(w, z-1) \tag{3}$$

The method of calculating the second derivative is illustrated in Table 1 for $w = 1$, $z = 1$; the complete set of coefficients for $w = 3$, $z = 1$—5 is given in Table 2.

Calculation of the second derivative over a window w channels wide and repeating the process z times results ultimately in a reduction of the relative standard deviation of the second derivative as compared to the relative standard deviation of the simple second derivative (eqn. 1). The reader is referred to the original literature for more details.

The choice of the parameter w is the most important one and Mariscotti gives as an estimate $w \approx 0.6\ FWHM$, where $FWHM$ is the full width at half

TABLE 1

Computation of second derivative for $w = 3$, $z = 1$

Channel	$i-2$	$i-1$	i	$i+1$	$i+2$
		1	−2	1	
	1	−2	1		
			1	−2	1
$sd_i = y_{i-2} - y_{i-1} - y_{i+1} + y_{i+2}$	1	−1	0	−1	1

TABLE 2

Coefficients for $w = 3$ and $z = 0$—5

Channel	—6	—5	—4	—3	—2	—1	0	1	2	3	4	5	6
$z = 0$						1	—2	1					
$z = 1$					1	—1	0	—1	1				
$z = 2$				1	0	0	—2	0	0	1			
$z = 3$			1	1	1	—2	—2	—2	1	1	1		
$z = 4$		1	2	3	0	—3	—6	—3	0	3	2	1	
$z = 5$	1	3	6	5	0	—9	—12	—9	0	5	6	3	1

maximum intensity. With the measuring conditions used here, the *FWHM* lies around 3 eV, thus $w \approx 1.8$ eV ≈ 3 channels. The number of averaging steps (z) in the program was taken as 5; fewer averaging steps result in a larger standard deviation of the second derivative.

Table 2 gives the coefficients for $w = 3$ and $z = 0, 1, 2, 3, 4, 5$ for calculating the second derivative. This means that for $w = 3$ and $z = 5$, the channel contents are multiplied by the coefficients given in the last line of Table 2, and summed to obtain the value of $sd_i(w, z)$ with $w = 3$ and $z = 5$. Fixing these two parameters means inevitably that the broader Auger peaks or the plasmon-broadened peaks are not so efficiently detected as the photoelectron peaks. In view of the qualitative character of the survey spectra, this possible loss of information is not important because elemental identification is almost uniquely based on well defined photoelectric peaks and to a lesser extent on a few sharp Auger lines.

Description of the program

Smoothing. The original spectrum is smoothed twice by the five-point smoothing procedure described by Savitzky and Golay [4].

$$ys_i = (-3y_{i-2} + 12y_{i-1} + 17y_i + 12y_{i+1} - 3y_{i+2})/35 \qquad (4)$$

where y is the measured channel content and ys is the smoothed channel content. Smoothing with more points results in a marked distortion of the peaks. The efficiency of the smoothing procedure is somewhat difficult to assess. For spectra with very good counting statistics, the influence of smoothing is minimal. For spectra with less good counting statistics, it appears that smoothed spectra show fewer false peaks. In the remaining part of the paper ys will always be the smoothed channel content.

Computation of second derivative and standard deviation. The second derivative sd_i is calculated by means of

$$sd_i = ys_{i-6} + 3ys_{i-5} + 6ys_{i-4} + 5ys_{i-3} - 9ys_{i-1} - 12ys_i + ys_{i+6} + 3ys_{i+5} + 6ys_{i+4} + 5ys_{i+3} - 9ys_{i+1} \qquad (5)$$

The coefficients are taken from Table 2 ($w = 3$, $z = 5$). The standard devia-

tion (SD) of sd_i for a given point is calculated from $SD = 21.166\ (ys_i)^{1/2}$. The coefficient 21.166 is taken from the original table in Mariscotti's paper, where it is shown that the value of the coefficient used in calculating the standard deviation is equal to $(\Sigma c_i^2)^{1/2}$; c_i represents the coefficients (from Table 2) used in calculating sd_i ($w = 3, z = 5$).

A peak is detected whenever $sd_i > 2.5\ SD$, and $sd_{i+1} < 0$ and $sd_{i-1} < 0$, and $sd_{i-1} \geqslant sd_i \leqslant sd_{i+1}$. Decreasing the ratio sd_i/SD to a value of 1.5, for example, results in the detection of more false peaks. Normalization constants are not necessary because the second derivative is compared to its standard deviation.

Peak position. Once the channel with the smallest value of the second derivative has been found, it is necessary to check whether this channel k corresponds also to the channel (p) with the largest number of pulses. This is necessary since some peaks can have an asymmetric shape. The channel position of the peak (npk) is then calculated by fitting a parabola through the three top-channel contents [1]

$$npk = p + (ys_{p+1} - ys_{p-1})/2(2ys_p - ys_{p+1} - ys_{p-1}) \tag{6}$$

where p is the channel with the highest number of pulses in the smoothed spectrum.

For some ill-defined peaks with considerable statistical scatter, it can happen that this calculation yields a value of npk such that $|npk - k| > 4$, while a visual inspection of the peaks does not warrant such a conclusion. In such a situation npk is calculated by means of the centre of gravity method

$$npk = \sum_{j=p-2}^{p+2} (ys_j\, ch_j/ys_j) \tag{7}$$

where ch_j is the channel number.

If $|npk - k|$ is still >3 then the peak is definitely rejected, i.e., the position of the minimum in the second derivative and the peak maximum must be within 3 channels. The choice of the values of 4 and 3 is based upon experience.

Overlapping peaks. It may happen that a second peak overlaps partially with the peak detected. Therefore the peak detection process described above (computation of sd_i and SD, and npk) is repeated between the channels $p + 3$ and $p + 7$. If a second peak is found, the process is repeated once more until no peak is found within 3 to 7 channels following the last detected peak. Usually one cycle is sufficient. Sometimes a triplet is found: in nearly all cases, it is due to a broad, ill-defined peak. The overlapping peaks are not further decomposed in single constituents by this program.

Limits of peak integration. The low-energy ($n1$) and high-energy limit ($n2$) for peak area integration are found [5] by testing at what value of n the following equations are no longer valid.

$$\text{for } n1\text{: } ys_{n-4} < ys_n - xb\ (ys_n)^{1/2} \tag{8}$$

for $n2$: $ys_{n+4} < ys_n - x\ bg(ys_n)^{1/2}$ (9)

A step size of 4 is used, because it was observed that for ill-defined photoelectric peaks with considerable scatter, or for peaks showing a small shoulder, the descent stopped too early. Practically, the value of the coefficient $x\ bg$ is set at 0.7. A peak is discarded whenever $n2 - n1 \leqslant 3$.

Calculation of net peak area and background area. Once $n2$ and $n1$ are known, the background area (bg) is calculated using three channels on each side and averaging.

$$bg = \left[\left(\sum_{i=n1}^{n1-2} ys_i + \sum_{i=n2}^{n2+2} ys_i\right)\Big/6\right](n2 - n1 - 1) \tag{10}$$

The background is thus subtracted by drawing a straight line between the limits of peak integration. This may not be the best method, but in view of earlier-mentioned limitations, this approximation is sufficiently accurate.

The total area (tot) between $n1$ and $n2$ is given by $tot = \Sigma_{i=n1+1}^{n2-1} ys_i$. The net peak area ($ar$) is simply obtained by subtracting the background area from the total number of pulses (tot) collected between $n1$ and $n2$: $ar = tot - bg$.

Calculation of standard deviation. The standard deviation of area (SD_{ar}) and background (SD_{bg}) are calculated [1] from

$$SD_{ar} = [tot + (n2 - n1 - 1)\ bg/6]^{1/2} \tag{11}$$

$$SD_{bg} = [(n2 - n1 - 1)\ bg/6]^{1/2} \tag{12}$$

A peak is discarded whenever $SD_{ar} > 0.6\ ar$. It must be emphasized that the uncertainty calculated in this way does not make any allowance for systematic uncertainties.

Computation of peak width. The full width at half maximum (*FWHM*) is found by descending from peak maximum to bottom and testing (e.g., on the low energy side of the peak) if $ys_i > ihm > ys_{i-1}$; ys is the smoothed channel content corrected for background and ihm is the maximum intensity/2 (corrected for background). As soon as this condition is fulfilled, the channel position (l) corresponding to ihm is calculated by simply interpolating between n_i and n_{i-1}.

A similar procedure is used for the high-energy side, yielding h. Finally $FWHM = h - l$ where l and h are non-integer numbers. When $FWHM < 3$ channels, the peak is rejected. Background subtraction is necessary because a peak may be superimposed on a steeply sloping background.

With a similar procedure, the full width at 1/5th maximum intensity (*FWFM*) is calculated. Whenever a small peak is located close to the main peak, the *FWFM* will vary more rapidly than the *FWHM* and is therefore a somewhat better indicator of possible small, unresolved doublets.

The peak identification procedure is shown schematically in Fig. 1; the detailed program listing, written in Algol 60, is described elsewhere [6].

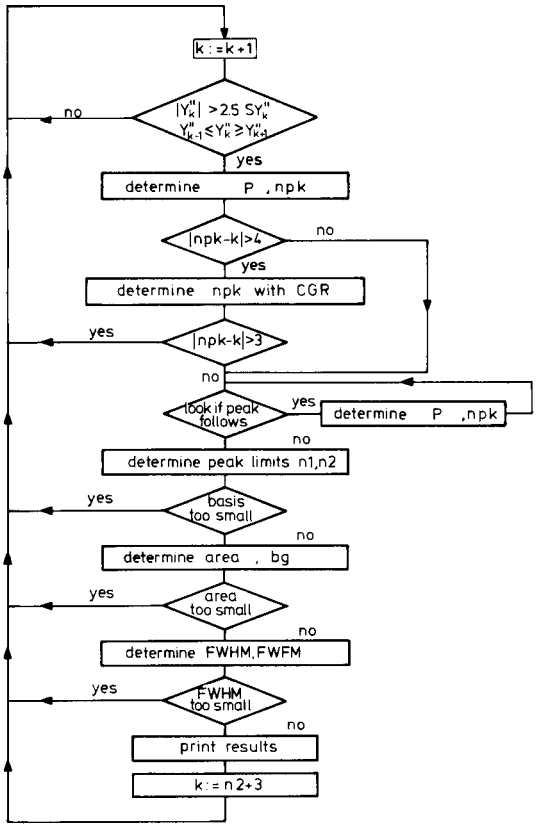

Fig. 1. Flow sheet of the peak identification procedure. For reasons of space the following abbreviations have been used: y'' and sy'' are the second derivative (eqn. 5) and its standard deviation SD, respectively; p is the channel with highest number of pulses; npk is the exact peak position (eqn. 6); CGR is the centre of gravity method (eqn. 7).

RESULTS AND DISCUSSION

Figure 2 shows a gold spectrum obtained after 1 and 5000 sweeps. The single-sweep spectrum shows one false peak (labelled *f* at 510 eV) the 4*p* 3/2 and the 5*p* peaks are not found. The maximum channel content in the 4*f* peaks is around 400 pulses, resulting in a large scatter in the measured data. In the 5000-sweep spectrum, peaks labelled P and S are, respectively, plasmon and satellite peaks. The peak at 70 eV is due to low-energy electrons originating in the residual gas analyser. Most of the peaks between 200 and 400 eV could be ascribed to gold Auger lines [7, 8]. No attempt was made to identify definitely the peaks around 780, 1220 and 1260 eV: they could also be weak high-energy gold Auger lines. The peak/background ratio for these Auger lines is near 0.01. Such weak lines are only detected with a large number of sweeps (good counting statistics). In normal practice, a

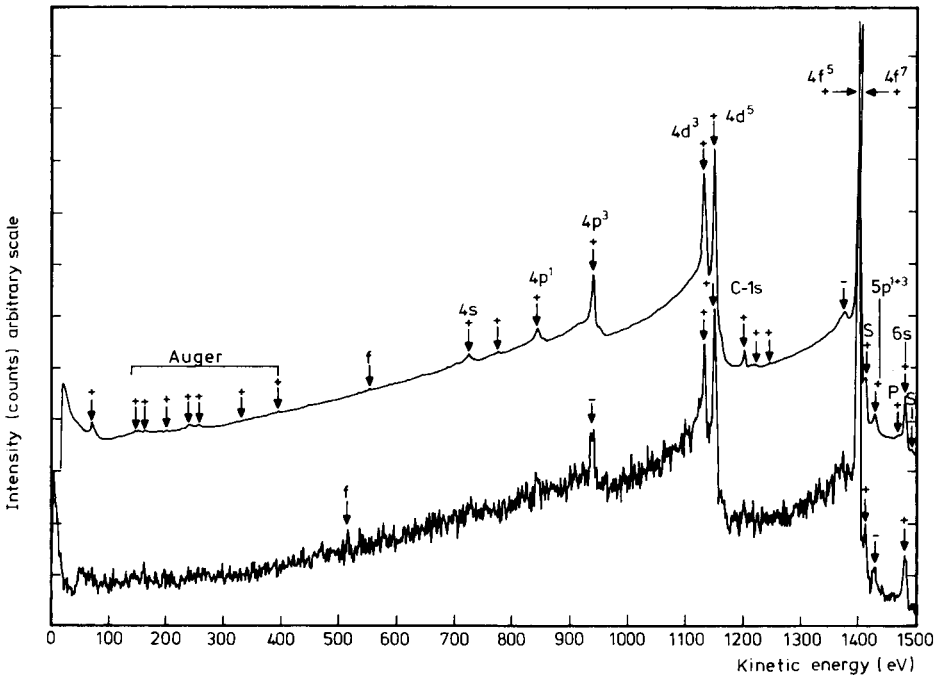

Fig. 2. Gold spectra after 1 and 5000 sweeps, respectively. Spectra are shifted vertically by an arbitrary amount. (+) Peak detected by peak-search procedure; (—) peak not detected; (*f*) false peak detected; (*P*, *S*) plasmon and satellite peaks.

smaller number of sweeps is used and consequently most peaks detected will have a higher peak/background ratio.

The 4*f* plasmon peak, although quite well defined, is not detected. This is due to the rather flat top which results in turn in a top channel content differing only very little from its neighbours. In practice this means that peak area integration stops too early, yielding a too small area and rejection of the peak. This is one of the drawbacks of this method: in such a situation the window w ($w \approx 0.6$ *FWHM*) should be made larger and the step size (eqns. 8 and 9) adapted to such a broad peak. Figure 3 shows, enlarged, the 130—180 and 1380—1430-eV regions taken from the 5000-sweep spectrum. Above the spectra are plotted the values of *sd/SD* (eqns. 5). Whenever this value becomes sufficiently negative, the presence of a peak is indicated. In the first region, the three observed minima correspond clearly to the three maxima in the spectrum (gold Auger lines). Although much broader than the photoelectron lines, they are still detected, because of the very good counting statistics.

The second region shows that the detection of quite small peaks (satellites at 1412 eV) is possible in the presence of the much larger 4*f* 7/2 line. The satellite peak shows a double structure, but this is no longer resolved by the

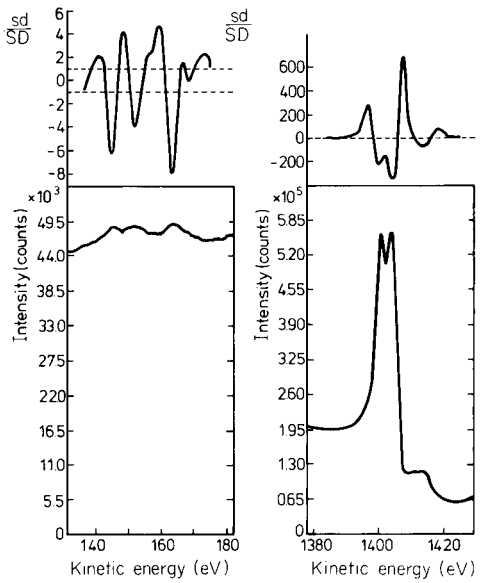

Fig. 3. Enlarged regions from 5000-sweep spectrum. In the upper part *sd/SD* are plotted. Dotted lines (left) indicate ±1 standard deviation. On the right, the thickness of the dotted line indicates roughly ±1 standard deviation.

program. Peaks observed in photoelectron spectra do not have a unique form. Photoelectric peaks are more or less Gaussian; Auger and plasmon peaks can be quite asymmetric. Notwithstanding these differences in shape, it appears that the program is able to identify 90—100% of the peaks occurring in a spectrum. This was confirmed in the analysis of some 1000 survey spectra. The number of unaccounted peaks is around 3—4 per spectrum.

The calculated binding energies are within ±1 eV of the binding energies determined with a high resolution in a narrow energy-range scan. This inaccuracy is quite sufficient for identification purposes.

Preliminary calculations on relative cross-sections derived from the computed peak area indicate that the agreement between experimental and theoretical values is fair. Further work on this topic is still in progress.

Conclusion

The advantage of this program lies in the automated analysis of the survey spectra, which requires no intervention at all. The binding energies obtained are sufficiently accurate for identification of elements in unknown samples. A disadvantage is that broader peaks, such as plasmon and Auger lines, are less efficiently detected.

REFERENCES

1 M. Verheijke, J. Radioanal. Chem., 10 (1972) 299.
2 H. G. Nöller, H. D. Polaschegg and H. Schillalies, J. Electron Spectrosc. Relat. Phenom., 5 (1974) 705.
3 M. Mariscotti, Nucl. Instrum. Methods, 50 (1967) 309.
4 A. Savitzky and M. Golay, Anal. Chem., 36 (1964) 1627.
5 G. Guzzi, J. Pauly, F. Ginardi and B. Dorpema, EUR 3469e, 1967.
6 E. Bruninx and A. van Eenbergen, unpublished report, 1980.
7 W. Coghlan and R. Clausing, A catalog of calculated Auger transitions for the elements ORNL-TM-3576, 1971.
8 J. Mathew, F. Netzer and E. Bertel, J. Electron Spectrosc. Relat. Phenom., 20 (1980) 1.

Analytica Chimica Acta, 133 (1981) 349—358
Computer Techniques and Optimization
Elsevier Scientific Publishing Company, Amsterdam — Printed in The Netherlands

RESOLUTION ENHANCEMENT OF A.C. POLAROGRAPHIC PEAKS BY DECONVOLUTION USING THE FAST FOURIER TRANSFORM

B. S. GRABARIC,[a] R. J. O'HALLORAN,[b] and D. E. SMITH*
Department of Chemistry, Northwestern University, Evanston, IL 60201 (U.S.A.)
(Received 12th December 1980)

SUMMARY

A method for resolution enhancement of a.c. polarograms (voltammograms) is presented. The method is based on deconvolution using fast Fourier transforms. Overlapped a.c. polarograms are mathematically narrowed and sharpened, retaining the peak position and linear proportionality of the sharpened peak height with concentration. The advantages and limitations of the method are demonstrated on simulated and experimental a.c. polarograms. The same approach is applicable to related techniques such as differential pulse and square-wave polarography.

The resolution in polarographic and voltammetric electrochemical techniques is governed mainly by the differences in half-wave potentials of two or more electroactive species present in the analyzed solution, their concentration ratio and the shape of the current—potential curve obtained by using a particular technique.

In d.c. and normal pulse polarography the sigmoidal polarograms do not offer a particularly advantageous response with respect to resolution. The most common approach to improve resolution has been to change the medium in order to complex or mask one electroactive species present in the solution and therefore to shift the half-wave potentials further apart. Alternatively, numerical methods [1, 2] can be employed which are especially convenient when computerized electrochemical instrumentation is used.

Responses obtained in a.c. polarography, differential pulse polarography, square-wave polarography, and related techniques offer much better resolution because peaks are formed, but serious overlapping occurs when the difference in half-wave potentials of two species is less than $100/n$ mV (n being the number of electrons involved in electrochemical reduction or oxidation), especially when the concentration ratio of the species is greater than 3:1.

---

[a]Present address: Department of General and Inorganic Chemistry, Faculty of Technology, University of Zagreb, POB 179, Zagreb, Yugoslavia.
[b]Present address: Materials Research Laboratories, P.O. Box 50, Ascot Vale, Victoria 3032, Australia.

For overlapping waves of two species with up to $100/n$-fold excess of one species, a simple approach was proposed [3] using only sampling, storing, and subtracting routines of a microprocessor-controlled polarograph. A determination of lead(II) and thallium(I) ions at the 10^{-7} M level, having peak potentials at approximately −0.37 V and −0.43 V, respectively, vs. an Ag/AgCl electrode, was possible using differential pulse anodic stripping voltammetry at a hanging mercury drop electrode in $100/n$-fold excess of one species. Such extreme overlapping situations will be very difficult, if not impossible, to handle by any numerical method. However, the method requires several estimated concentrations of one of the overlapping components to be recorded and stored in the computer memory for subsequent subtraction from the resultant overlapping response.

In a recent paper [4], quantitative resolution of overlapped peaks in programmed potential-step voltammetry was achieved by using multilinear least-squares regression analysis. It was shown that a quantitative resolution of thallium(I) and cadmium(II) ions at the 10^{-5} M level with concentration ratio 17.6:1, respectively, was possible with half-wave potential difference, $\Delta E_{1/2} = 102$ mV.

One alternative approach to improving the resolution of two or more overlapping peaks in electrochemistry is by deconvolution using fast Fourier transforms (FFT). This method has been applied to enhance resolution in chromatography [5] and spectroscopy [6].

Some of the applications of computerized on-line FFT electrochemistry [7] clearly show all the advantages and versatility of the FFT approach in both experiment performance and data processing. As far as data processing is concerned, the simplicity of using the FFT lies in the fact that many very complex mathematical data treatments in time domain can be done with a much simpler algorithm by transforming data to the Fourier or frequency domain. For example, a.c. polarographic and other electrochemical experimental data [8] can be smoothed simply by multiplying the frequency spectrum by a smoothing function, i.e., setting high-frequency components contributing to the noise to zero, and applying an inverse FFT. The same applies to the time domain interpolation of electrochemical data [9] which again is done simply by forward FFT followed by zero filling of the high-frequency part of the Fourier spectrum, which does not contribute to the shape of time domain data. After an inverse FFT, the time domain data have the same shape, but they are defined with more points, i.e., they are interpolated. This interpolation using the FFT enables shorter experimental time and easier evaluation of electrochemical parameters.

The convolution and deconvolution procedures in time domain are usually complex from a numerical point of view, but using the FFT simplifies the algorithm. The convolution in time domain is equivalent to (complex number) multiplication in frequency domain, while deconvolution in time domain is equivalent to (complex number) division in frequency domain.

On-line broadband faradaic admittance measurements developed in this laboratory have been used to investigate and apply two types of deconvolution viz., deconvolution of nonideal high-frequency response of the analog circuitry [10] and deconvolution of heterogeneous charge-transfer kinetic effects [11]. The deconvolution of nonideal high-frequency response of the analog circuits is performed by dividing the theoretical admittance spectrum of the known dummy cell by the observed admittance spectrum of the same dummy cell in order to obtain the deconvolution function which is then used to extract deconvoluted distortion-free admittance data. The second application is where one uses the FFT for deconvolution of heterogeneous charge-transfer kinetic effects ("kinetic deconvolution"). This is done by dividing the observed admittance frequency profile with the measured $G(\omega)$ frequency profile (see eqn. 1), thus extracting reversible admittance for thermodynamic and analytical measurements. However, this deconvolution procedure was not applied to multicomponent systems, although it should work in this context.

The simplification of deconvolution by using forward FFT, division in Fourier domain and inverse FFT was used in the present paper to enhance the resolution (i.e., to sharpen the peak response) in a.c. polarography. The same approach can be used in related techniques, e.g. differential pulse polarography, square-wave polarography, etc.

EXPERIMENTAL

All chemicals used were of analytical-grade purity. Solutions were thermostated at 23 ± 1°C and degassed with argon for a minimum of 15 min prior to recording a.c. polarograms.

All a.c. polarograms were obtained with a conventional three-electrode system. The reference electrode was Ag/AgCl (saturated aqueous NaCl) for aqueous solutions and Ag/AgI (0.1 M tetrabutylammonium iodide in dimethylformamide) for nonaqueous solution measurements.

The electrochemical instrumentation consisted of a home-made potentiostat interfaced to a Raytheon RDS-500 minicomputer via a synchronous data generator and sampler (SYDAGES) which performs broadband FFT electrochemical relaxation measurements. SYDAGES consists of a D/A converter, two A/D converters, three 1024-word shift register memories, and control circuitry. Signal generation and signal data acquisition are synchronized up to data rates of 500 kHz [10]. A.c. admittance polarograms were recorded in multifrequency mode [10]. The examples used in this paper are in-phase components of a.c. admittance selected at 146.5 Hz.

RESULTS AND DISCUSSION

For the simple electrode reaction $O + ne \rightleftharpoons R$, where rate is controlled by diffusion and/or heterogeneous charge-transfer kinetics, the fundamental

harmonic current response to an a.c. potential—time perturbation in a.c. polarography (voltammetry) is given by the well-known equation

$$I(\omega t) = I(\omega t)_{rev} F(t) G(\omega) \sin(\omega t + \phi) \quad (1)$$

$$\text{where } I(\omega t)_{rev} = (nF)^2 A C_0^* (\omega D_0)^{1/2} \Delta E \, [4RT \cosh^2(nx)]^{-1} \quad (2)$$

$$\text{and } x = F(2RT)^{-1} (E_{DC} - E_{1/2}^r) \quad (3)$$

The rest of the notation is the same as that used earlier [11]. In the limit of diffusion-controlled behavior, $G(\omega) = 1$ and $F(t)$ is a slowly changing function of potential which has negligible influence on a.c. polarographic wave shape [12]. If slow heterogeneous charge-transfer kinetics cause $G(\omega)$ to differ significantly from unity, the "kinetic deconvolution" procedure mentioned above can be applied to eliminate or minimize this effect. Thus, the obvious choice for the deconvolution function is

$$f(x) = k/\cosh^2(n_d x) \quad (4)$$

where k is an arbitrary constant. The n_d value can be viewed as the electron number of the deconvolution function, but it need not be restricted to an integer.

The deconvolution procedure using the FFT consists in obtaining the Fourier spectra of the function to be deconvoluted and the deconvolution function defined by eqn. (4). The next step in the deconvolution procedure is to divide the Fourier spectrum of the function to be deconvoluted by the Fourier spectrum of the deconvolution function and to perform an inverse FFT on the result of the division.

An illustration of deconvolution using the FFT of the simulated function to be deconvoluted with an identical deconvolution function, having the shape according to eqn. (1), is given in Fig. 1. The result of discrete, numerical deconvolution in this example is one point corresponding to the magnitude of the function to be deconvoluted at the peak potential.

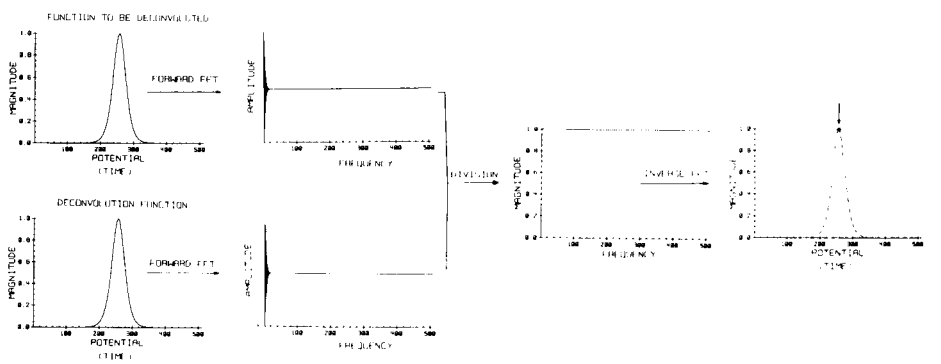

Fig. 1. Deconvolution procedure representation where the function to be deconvoluted and deconvolution functions are identical (simulated data). $n = n_d = 2$.

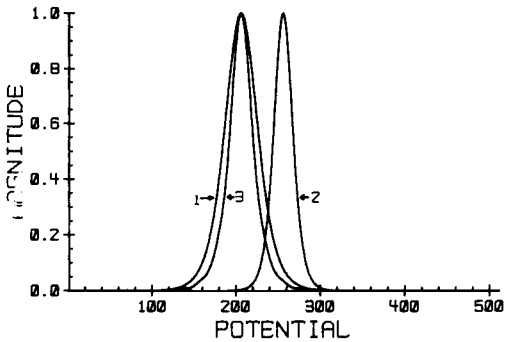

Fig. 2. Narrowing the simulated a.c. polarographic peak. (1) Peak to be deconvoluted $n = 2$; (2) deconvolution function $n_d = 3.5$; (3) deconvoluted peak.

In practical situations, however, the shape of the function to be deconvoluted is not precisely known nor is the data noise-free as it was in Fig. 1. Using the deconvolution function (eqn. 4), with different n_d values makes it possible to obtain intermediate results, i.e., narrowing of the peak will be obtained as shown in Fig. 2. This narrowing of the peak-shaped a.c. polarograms obtained by deconvolution using an FFT is a key factor for resolution enhancement in this and related techniques.

The deconvolution of two overlapped a.c. peaks using the FFT, obtained with simulated data for different half-wave potential separations, $\Delta E_{1/2}$, different concentration ratios, C_1/C_2, and different n values are shown in Figs. 3—7.

The degree of sharpness of the deconvoluted a.c. polarograms depends on the half-width of the deconvolution function (i.e., on the n_d value in eqn. 4). If the half-width of the deconvolution function is close to the half-width of the narrower component in overlapped a.c. polarograms which are going to be deconvoluted, oversharpened peaks are obtained with small side peaks (Figs. 4C and 6B). The same effect was reported for sharpening chromatographic peaks [5]. This effect of oversharpening does not influence the peak

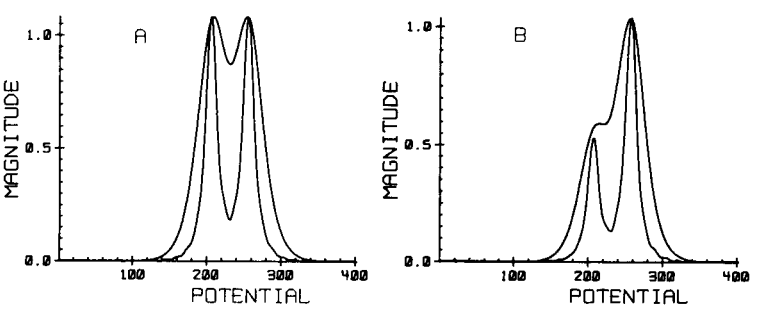

Fig. 3. Sharpening of two simulated overlapped a.c. polarographic peaks. ($\Delta E_{1/2} = 50$ mV, $n_1 = n_2 = 2$ and $n_d = 4.5$): (A) $C_1/C_2 = 1$; (B) $C_1/C_2 = 2$.

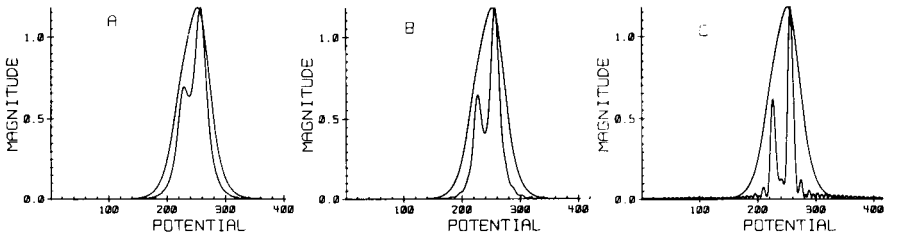

Fig. 4. Different degrees of sharpening of simulated a.c. polarographic peaks ($\Delta E_{1/2}$ = 30 mV, C_1/C_2 = 2 and $n_1 = n_2$ = 2): (A) n_d = 5.5; (B) n_d = 4.5; (C) n_d = 3.2.

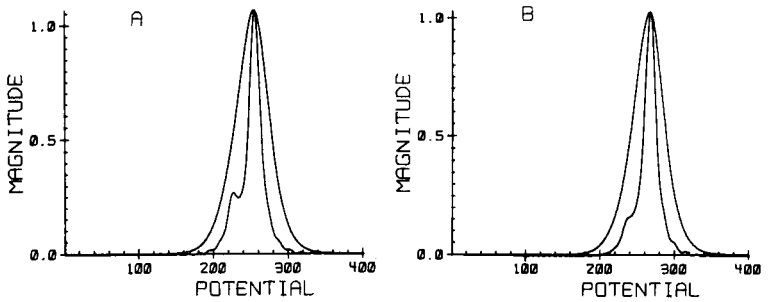

Fig. 5. Sharpening of simulated a.c. polarographic peaks with different C_1/C_2 ratio ($\Delta E_{1/2}$ = 30 mV, $n_1 = n_2$ = 2, and n_d = 4.0): (A) C_1/C_2 = 5; (B) C_1/C_2 = 10.

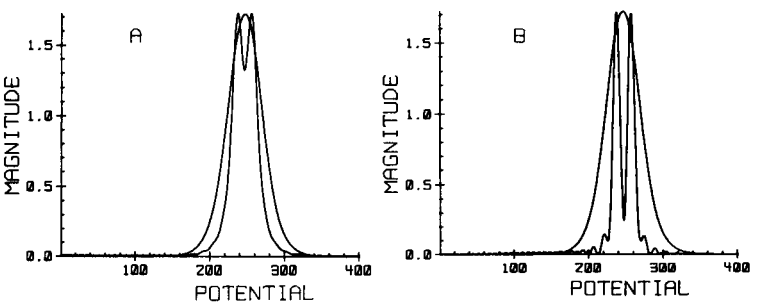

Fig. 6. Sharpening of two overlapped symmetrical simulated a.c. polarographic peaks using deconvolution function of different half-width ($\Delta E_{1/2}$ = 20 mV, C_1/C_2 = 1, $n_1 = n_2$ = 2): (A) sharpened, n_d = 4.0; (B) oversharpened, n_d = 2.8.

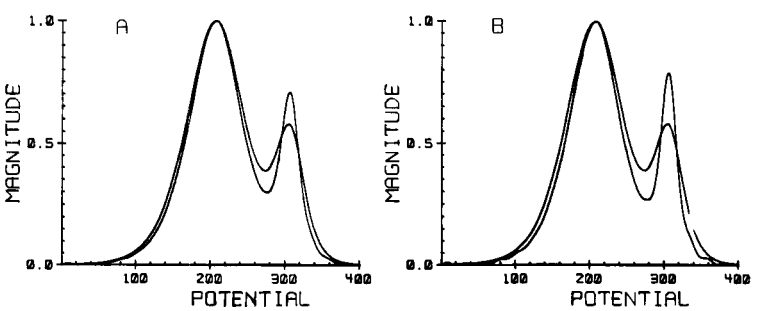

Fig. 7. Sharpening of two overlapped simulated a.c. polarographic peaks with different n-values ($\Delta E_{1/2}$ = 100 mV, C_1/C_2 = 4, n_1 = 1, n_2 = 2): (A) n_d = 4.0; (B) n_d = 3.0.

position, unless oversharpening occurs to such an extent that the result of the deconvolution will be an oscillating function over the entire potential region. Nevertheless, moderate oversharpening can lead to ambiguity in the determination of the number of actual peaks in an unknown sample. Various degrees of sharpening the same simulated overlapped a.c. polarogram are shown in Fig. 4. The degree of resolution depends only on the n_d value of the deconvolution function. The optimal n_d value should be determined by inspecting the deconvoluted peaks. With the exception of Figs. 4C and 6B, all other narrowed peaks illustrated were sharpened to the point of initial onset of ripples near the extremities of the peak.

By this method it is possible to deconvolute one symmetrical a.c. polarographic peak which is the result of overlapping two peaks with the same height ($C_1/C_2 = 1$) and number of electrons ($n_1 = n_2 = 2$) separated by 20 mV. After the FFT deconvolution procedure has been used, two peaks are revealed (Fig. 6).

The limitation of the method can be estimated from the results shown in Fig. 5, where $\Delta E_{1/2} = 60/n$. When the concentration ratio is $C_1/C_2 = 10$ (Fig. 5B) only the shoulder appears after deconvolution, which is at least an indication of the existence of a second peak within the response. Without deconvolution, only one peak is observed.

Figure 7 clearly indicates that the deconvolution procedure is much less effective when the overlapping peaks are characterized by different n-values, an observation which is not surprising.

In any case, some care must be exerted in using the deconvolution to prevent erroneous conclusions regarding the number of peaks, especially when the number of electroactive species is unknown.

The application of the proposed method for a.c. polarographic peak sharpening of actual experimental data requires a slightly modified approach. With the computerized electrochemical instrumentation, the experimental a.c. polarographic response is sampled and stored in the computer memory. Therefore, because of the digital format recording, one is dealing with a finite number of data points. Moreover, the total measurement time in a.c. polarography depends on drop time and scan rate which are related to the number of points required to obtain appropriate resolution. These factors require optimization between resolution and total measurement time. Also, when experimental data are considered, noise from various sources is always present in the recorded response. When, however, the FFT subroutine is available as a part of the software support in the computerized electrochemical system, the same FFT subroutine can be used for simultaneous smoothing and interpolation [8, 9], as well as for subsequent deconvolution.

In practical cases, the a.c. admittance vs. d.c. potential response may be sampled at 40—50 potentials (data points). The forward FFT is then applied to the admittance polarogram, giving frequency components characterizing the data domain response. Usually 12—15 frequency components are sufficient to define an a.c. polarographic admittance peak. Higher-frequency

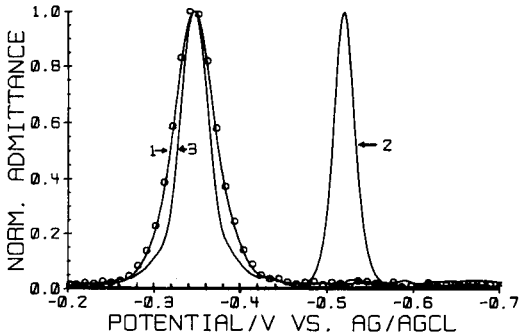

Fig. 8. Narrowing the experimental normalized a.c. polarogram of 5×10^{-5} M Pb(II) in 0.5 M KNO_3 at pH 2.5 (E_p = 369 mV): (○) experimental data points; (1) smoothed and interpolated data; (2) deconvolution function, n_d = 3.2; (3) deconvolution (narrowed) a.c. response.

components represent the noise contribution. Therefore, by setting higher frequency components to zero and zero filling 2^N (N = integer) points, it is possible after inverse FFT simultaneously to smooth and describe (interpolate) the original 40—50 points with 256 or 512 points. Such smoothed and interpolated a.c. admittance data are subsequently deconvoluted.

The result of smoothing, interpolation, and deconvolution using the FFT of the normalized a.c. polarogram of 5×10^{-5} M lead(II) solution in 0.5 M KNO_3 at pH 2.5 is shown in Fig. 8. It can be seen that the a.c. polarogram after deconvolution is narrower than the original one. Sharpening of the overlapped a.c. polarographic peaks of lead(II) and thallium(I) in 0.5 M KNO_3 at pH 2.5 having $\Delta E_{1/2}$ = 60 mV and C_1/C_2 = 1 and 3.5 is shown in Figs. 9A and 9B, C, respectively. Sharpening a three-component overlapping system containing Pb(II), Tl(I), and Cd(II) ions in the solution is shown in Fig. 10. In all of the examples, sharper peaks were obtained and the peak location was reproducible within ±1 mV, even in the case where in the original data set only a shoulder was present. Peak height of the deconvoluted peaks was always proportional to the concentration using the same n_d value of the deconvolution function described by eqn. (4).

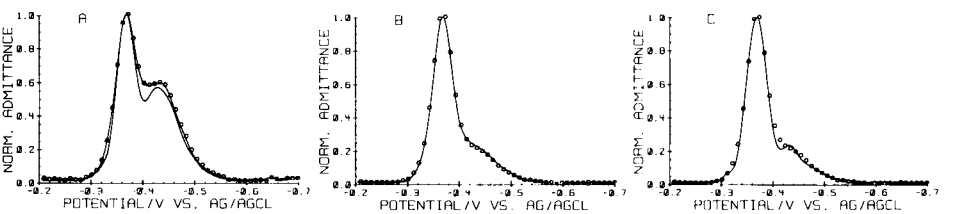

Fig. 9. Sharpening of the experimental overlapped a.c. admittance peaks of Pb(II) and Tl(I) in 0.5 M KNO_3 at pH 2.5 (E_p = −429 mV for Tl(I) and E_p = −369 mV for Pb(II); n_d = 6.0): (A) 5×10^{-5} M Pb(II) and Tl(I); (B) 5×10^{-5} M Pb(II) and 1.4×10^{-5} M Tl(I) smoothed and interpolated a.c. response; (C) same as (B) after deconvolution.

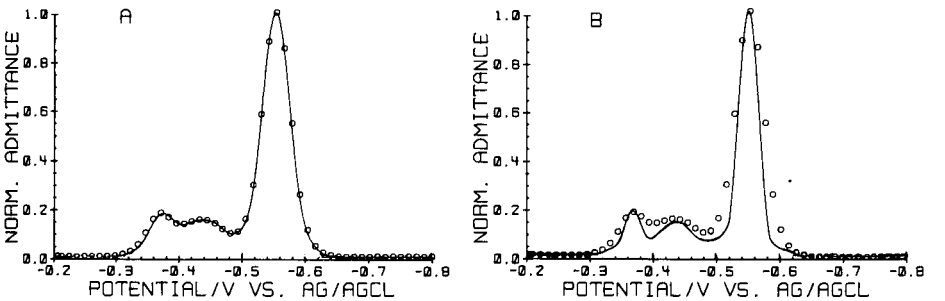

Fig. 10. Sharpening of the experimental three-component system containing Pb(II), Tl(I), and Cd(II) ions in 0.5 M KNO_3 at pH 2.5 (n_d = 5.5; E_p = —547 mV for Cd(II), C = 2.5 × 10^{-4} M; E_p = —430 mV for Tl(I), C = 9 × 10^{-5} M; E_p = —369 mV for Pb(II), C = 5 × 10^{-5} M: (A) smoothed and interpolated data; (B) same as A after deconvolution.

Organic electroactive species having $E_{1/2}$ potentials within overlapping range are even more abundant than inorganic ones. The proposed method can be successfully applied in pharmaceutical and biochemical analysis of different organic electroactive species and in various solvents.

An example of FFT deconvolution resolution enhancement of two overlapped a.c. admittance polarograms of 2-nitroaniline and 4-nitrotoluene in 0.1 M tetra-n-butylammonium iodide (TBAI)/dimethylformamide (DMF) solution is shown in Fig. 11. Both compounds undergo one-electron reduction forming radical anions in DMF solutions, as shown in a kinetic study of a series of nitro compounds in DMF [13]. Their $E_{1/2}$ separation is 98 mV. Applying the FFT deconvolution procedure to the overlapped a.c. admittance peaks provides a significant sharpening for different C_1/C_2 ratios (Fig. 11).

The analytical application of the method was confirmed by the calibration data presented in Table 1. A straight-line calibration plot was obtained for 4-nitrotoluene in mixtures with a constant concentration of 2-nitroaniline in 0.1 M TBAI/DMF solutions. Peak heights and peak potentials were evaluated by using quadratic curve fitting of the peak itself and the baseline [14] after denormalization of the deconvoluted peaks. Peak potentials were reproducible to ±1 mV, while the reproducibility of the peak heights was ±2% for the system and experimental parameters used. A linear calibration plot for 4-nitrotoluene was obtained within the limit of resolution of the

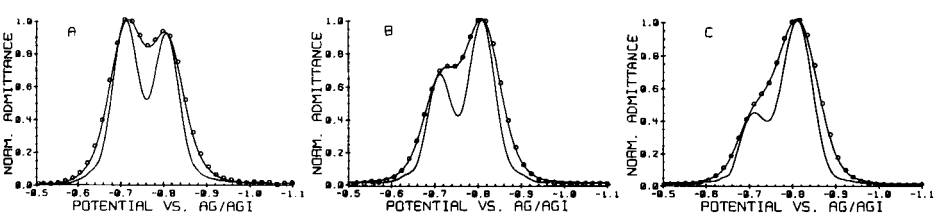

Fig. 11. Sharpening of the overlapped a.c. admittance peaks of 2-nitroaniline (2NA), E_p = —810 mV, and 4-nitrotoluene (4NT), E_p = —712 mV, in 0.1 M TBAI/DMF solutions (n = 1; C_{4NT} = 2.19 × 10^{-4} M, n_d = 3.5): (A) C_{2NA} = 2.05 × 10^{-4} M; (B) C_{2NA} = 4.10 × 10^{-4} M; (C) C_{2NA} = 9.23 × 10^{-4} M.

TABLE 1

Calibration curve data for 4NT—2NA mixtures

4-Nitrotoluene			2-Nitroaniline		
Conc. ($\times 10^{-4}$ M)	I_p^a	$-E_p$ (mV)	Conc. ($\times 10^{-4}$ M)	I_p^a	$-E_p$ (mV)
4.10	77.2	712.2	2.19	51.0	810.1
2.34	46.5	711.6	2.19	49.5	810.5
1.17	24.4	712.4	2.19	50.2	811.3
0.52	11.3	712.3	2.19	51.3	810.2

[a]Arbitrary units.

deconvolution method, while the peak height of the 2-nitroaniline was constant within the limit of experimental error for all concentrations of 4-nitrotoluene.

Conclusions

The presented method of peak sharpening is very simple and is especially valuable when an on-line computerized FFT electrochemical system is used because the same FFT routine can be used for multiple purposes, e.g., a.c. multiple frequency signal generation, deconvolution of the broadband frequency a.c. admittance response distorted by nonideal analog circuitry behavior at high frequencies, smoothing, interpolation, and deconvolution in order to enhance the resolution. The method can be used in combination with other known peak-sharpening methods [3, 4] and it can be applied to related electrochemical techniques. At the same time the peak-sharpening method must be used with appropriate caution so that false peaks arising from oversharpening do not confuse interpretation of the peak data.

The authors are indebted to the National Science Foundation (Grant No. CHE77-15462) for support of this work.

REFERENCES

1 I. Ruzic and M. Branica, J. Electroanal. Chem., 22 (1969) 243, 422.
2 I. Ruzic, J. Electroanal. Chem., 25 (1970) 144; 29 (1971) 440.
3 A. M. Bond and B. S. Grabaric, Anal. Chem., 48 (1976) 1624.
4 P. A. Boudreau and S. P. Perone, Anal. Chem., 51 (1979) 811.
5 D. W. Kirmse and A. W. Westerberger, Anal. Chem., 43 (1971) 1035.
6 G. Horlick, Anal. Chem., 44 (1972) 943.
7 D. E. Smith, Anal. Chem., 48 (1976) 221A; 517A.
8 J. W. Hayes, D. E. Glover, D. E. Smith and M. W. Overton, Anal. Chem., 45 (1973) 277.
9 R. J. O'Halloran and D. E. Smith, Anal. Chem., 50 (1978) 1391.
10 R. J. Schwall, A. M. Bond, R. J. Loyd, J. G. Larsen and D. E. Smith, Anal. Chem., 49 (1977) 1797.
11 R. J. Schwall, A. M. Bond and D. E. Smith, Anal. Chem., 49 (1977) 1805; J. Electroanal. Chem., 85 (1977) 217.
12 J. R. Delmastro and D. E. Smith, Anal. Chem., 38 (1966) 169.
13 M. E. Peover and J. S. Powell, J. Electroanal. Chem., 20 (1969) 427.
14 A. M. Bond and B. S. Grabaric, Anal. Chem., 51 (1979) 337.

Analytica Chimica Acta, 133 (1981) 359—367
Computer Techniques and Optimization
Elsevier Scientific Publishing Company, Amsterdam — Printed in The Netherlands

A FACTOR ANALYSIS STUDY OF PHOSPHATE BENEFICIATION BY CALCINATION

DAVID ISSAHARY

Negev Phosphates Ltd., Oron; and Department of Chemistry, Ben Gurion University of the Negev, Beer Sheva (Israel)

ITHAMAR PELLY*

Department of Geology and Mineralogy, Ben Gurion University of the Negev, Beer Sheva (Israel)

(Received 6th February 1981)

SUMMARY

Mineralogical changes during beneficiation of phosphate ore by calcination and washing were studied by factor analysis with oblique rotation, and by using factors of factors (obtained with a factor—factor correlation matrix as input). Several minerals and reactions are indicated, including the possibility of distinguishing between different contributions to the CO_2 variance. From the point of view of using the results as a guide for multiregression analysis and building a linear model for the process, the most important results are as follows. The parameters of the product grade (P_2O_5 and chloride) are influenced by factors measured by x-ray fluorescence (Al_2O_3, SiO_2, SO_3 and MgO). Factors measured by thermogravimetry (water of hydration, portlandite and carbonate) have only a small influence. Most of the variance for halite is determined by elements derived from clay, whereas most of the variance for CO_2 is correlated with MgO. Magnesium replacing calcium in the francolite indicates the CO_2 level and thus the decrease in P_2O_5 content. The MgO content in the francolite can be used to indicate the maximum P_2O_5 content in the product.

Calcined phosphate is a raw material for the manufacture of phosphoric acid and fertilizers. One method of beneficiation of the ore is by calcination and washing. The essence of the calcination process is crushing, sieving, washing (to lower clay and chloride content), classification, calcination at about 900°C, hydration and separation of the lime formed, and finally another washing and drying. The raw phosphorite contains francolite, gypsum, halite, quartz, clays and calcite (dolomite). Several papers [1—6] have described the reactions and mineralogical changes during phosphate calcination. There are several contradictions and the detailed mechanism and products are not exactly known, partly because not all product minerals and elemental sites in the minerals can be identified by x-ray diffraction, infrared or microscopic methods. Most studies of the calcination process are based on simulation runs. A distinction must be made between laboratory experimental results, usually obtained with a static electric furnace

and results obtained with a rotary kiln, which are different [6]. The major product is fluorapatite with a CaO/P_2O_5 ratio lower than in the raw francolite.

Some of the problems are as follows. The fate of the calcium oxide produced during the calcination is uncertain: it may combine with tricalcium phosphate to form some more basic product or it may form a calcium silicate. The minerals in the product identifiable by x-ray diffraction (x.r.d.) or microscopy cannot explain the factors governing the grade of the product; there is a diluent heavier than silica which binds the calcium oxide (during calcination) [6]. Other doubtful features are possible segregation of fluoride during calcination, and a realistic explanation for the evaluation of P_2O_5 in the francolite on the basis of the amount of magnesium replacing calcium (P_2O_5/MgO is about 10). Further, a major cause of decreasing the P_2O_5 in the product is the clay fraction, and there is a difference in the grade of the product depending on whether the raw material is of high or low sulphate grade. Another problem, not discussed in the literature, is that of the chloride which appears as halite. The product left after the final 2-h washing and separation of the water (containing about 1500 ppm chloride) contains 18% water. Logic dictates that all the original halite should have been dissolved and its content in the product should be $1500 \times 0.18 = 270$ ppm. The final product contains about 800 ppm. This means that the chloride was transformed to a much less soluble form.

Detailed descriptions of the theory, equations and computational procedures of factor analysis are readily available [7, 8]. Only aspects relevant to this study will be described here. Factor analysis can help to determine the degree to which one or more variables are part of a common phenomenon. Input may be raw data, a correlation matrix or a factor matrix. A matrix is obtained, which includes the number of factors, the variables loading each factor, the loading (or contribution) of each variable on the factor and the variance of dispersion of each variable among the different factors. After extraction of the initial factors, iteration is performed. The procedure can be controlled by specifying the number of factors to be extracted or the minimum value of an eigenvalue for which a factor will be extracted. After factor extraction, rotation can be done. Among the various rotation types are the orthogonal varimax and the direct oblimin method of oblique rotation. The exact configuration of the factor structure is not unique and one factor solution can be transformed into another by rotation. There is no unique and generally accepted best solution, yet not all the types of factor solutions are equally meaningful. Each tells us something different about the structure of the data. It is necessary to choose the best rotational method to arrive at the solution that satisfies the needs of the research problem. Orthogonal (independent) factors are mathematically simpler to handle (but the division to different factors is not always clear enough). Rotation will have the effect of shifting the values in each group to the limits, close to one or to zero, so as to obtain a clearer picture. The oblique factors are empirically more realistic.

There is no reason to favor one method over another and the choice should be made on the basis of the particular needs of a given research problem.

Some of the implications for chemical mineralogical systems are as follows. If chemical elements are the variables, clear correlations (if they exist) may be found even in a system of a large number of variables even if the same element appears in different factors. These factors may represent minerals or may be just correlations (e.g., several trace elements on a clay). If SiO_2 and Al_2O_3 are taken as an example, it may be found not only that there is a correlation (obtainable from a Pearson correlation matrix with perhaps no clear reason for the correlation) but that there is a high correlation (high loading) of these elements on two factors. There are no theoretical answers to questions about whether or not the SiO_2 and Al_2O_3 appear in two minerals (e.g., orthoclase and a clay); or if these factors can be used as input for factor analysis (contrary to Davis' view [9]); or if the new factors will be indicators for mineral associations (i.e. a clay with sodium chloride); or of which rotation is best suited to show mineralogical correlations in a set of elemental analyses; or if only negative correlations can be expected to arise from dilution in a closed system (i.e., the more clay present, the less apatite). In the absence of theoretical decisions, it is necessary to estimate if the obtained factor solutions and their interpretations make sense compared with what is known about the elements, minerals, the possibility of reactions among them, etc.

The aim of this study was to find the best method of explaining, by statistical treatment of chemical analytical data the nature of multi-elemental systems of raw materials and products of the process of beneficiation of phosphates by calcination. This will show the correlations caused by chemical bonding and by interactions or reactions of minerals, and will provide a guide for a multiregression analysis [10] to find which are the independent factors and which factors can be described as linear combinations of the others. This enables, by routine on-line elemental determinations, both the optimal product from a given raw material (mining control) and the efficiency of the calcination plant to be established. All this will be done by routine on-line analysis and not by laboratory simulations.

EXPERIMENTAL

As an example, a set of 31 product samples, to which on-line x-ray fluorescence spectrometry (x.r.f.) and thermogravimetry had been applied routinely was chosen. These were calcination products of a high sulphate ore and were of relatively low P_2O_5 grade.

A simultaneous multi-element (8) analysis was done, using an A.R.L. 74000 analyzer. Instrumental parameters, sample preparation, measurements, calibration and statistical treatment are described elsewhere [11]. The results are presented in Table 1. For the thermogravimetry, a Stanton TG model 750 was used. Three peaks were observed: (1) 100—300°C corresponding to loss

TABLE 1

Mean concentrations and standard deviations

Species	MgO	Na_2O	Al_2O_3	SiO_2	P_2O_5	SO_3	Cl	CaO	H_2O	$Ca(OH)_2$
Mean conc. (%)	0.35	0.81	0.36	0.65	33.18	2.65	0.076	55.54	0.48	0.51
S.d.	0.057	0.11	0.18	0.40	0.80	0.29	0.017	0.83	0.26	0.51

of hydration water, (2) 400—500°C corresponding to loss of $Ca(OH)_2$ constitutional water, and (3) 650—1000°C, corresponding to loss of CO_2. Six runs with samples of the same powder were used to determine the analytical error variance of the method. The relative standard deviations found were 3.5% for CO_2, 11.8% for $Ca(OH)_2$ and 14.0% for H_2O (corresponding σ are 0.063, 0.136 and 0.055 respectively). Means and standard deviations for the 31 samples used for this study are given in Table 1. Because of the large amount of analytical data, only means are given in Table 1.

For calculations, standardized concentrations were used (i.e., $Ci/\sigma i$) so that the variance of each element is unity and the total variance is equal to the number of elements in the system. Calculations were done using SPSS procedures [8]. Specific solutions used will be described in the discussion.

RESULTS AND DISCUSSION

In contrast to the procedure in social sciences, where common variance is desired, here reliable specific variability (i.e., without the error component) also is a meaningful result. If SiO_2 does not have any correlation, this is an indication that silica appears as an independent mineral.

The method depends on the precision and accuracy of the chemical analysis. If the errors of the measurements are relatively large, they will be included in the statistical treatment and correlations and factors caused by these errors may be obtained. The total variance consists of the communality of the element and the component of the variance contributed by the analytical error (e_i^2). If this error variance is subtracted from the total variance, a new criterion for the number of significant factors is obtained, i.e., the number of factors that explain only the variance caused by "real" concentrations, which is the only variance for which explanation is needed. Mathematically, this was done by estimating the precision of the analytical method and calculating

$$\sum_{i=1}^{11} \frac{e_i^2}{\sigma_i} = \sum_{i=1}^{11} \frac{\text{analytical error variance of element } i}{\text{total variance of element } i} = 0.425$$

The percentage of standardized error variance of the system out of the total variance is 100(0.425/11) = 3.9%. Accordingly, it is necessary to seek a number of factors (eigenvectors) whose sum of eigenvalues will be about

96% of the system variance. The aim is not to get a minimal number of factors needed to describe the system (as in social studies) but to obtain a solution with minimum loadings with opposite signs on the same factor and in which all factors have significant loadings. Correlations will be able to disperse among maximum factors so that if correlations among elements remain on the same factor, it will not be because of lack of space, but because they have a real correlation.

The usual way of presenting the interactions is the varimax rotated factors matrix (VRFM). The data are presented in Table 2. Though some correlations are seen in this table, a much clearer picture of the correlations can be obtained by using the method studied and discussed here (Tables 3—5).

The solution chosen here is the direct oblimin in which the factors are not independent [7] (oblique factors). This method was chosen because of intuition (it cannot be proven) that factors in this method are devoid of dilution effects among elements. Trial and error showed that when δ is chosen in such a way that the direct oblimin criterion is close to zero (positive), there are few meaningful loadings on each factor but these have a high value (i.e., intermediate values become zero). This selection of the iteration criterion has to be based on intuition and mineralogical knowledge because there is no other realistic criterion. A satisfying solution was found where n (number of factors) is 7, $\delta = 0.21$ and the iteration criterion is 0.069.

The matrix presented (Table 3) is the factor pattern matrix (FPM) which

TABLE 2

OVRFM: Orthogonal varimax rotated factor matrix (after rotation with Kaiser normalization)

	Factor 1	Factor 2	Factor 3	Factor 4	Factor 5	Communality
MgO	0.97429	—0.11702	0.13003	0.15317	—0.01927	1.00
Na_2O	0.06174	0.34848	0.87281	0.09027	—0.13234	0.91
Al_2O_3	0.64524	—0.05678	0.34206	0.53199	0.18918	0.86
SiO_2	0.61651	—0.18062	0.32328	0.69107	0.05328	1.00
P_2O_5	—0.84162	—0.02809	—0.21812	—0.27238	—0.00105	0.83
SO_3	—0.25592	0.48174	0.09511	—0.66779	—0.00578	0.75
Cl	0.52340	—0.10656	0.65565	0.06562	0.12485	0.74
CaO	—0.00127	0.95340	0.09014	—0.23139	—0.11201	0.98
H_2O	0.7018	—0.08859	—0.02288	0.02178	0.83595	0.71
$(OH)^-$	—0.46908	0.47089	—0.64406	—0.02260	—0.11675	0.87
CO_2	0.75952	—0.05224	0.13897	0.18931	0.47258	0.86
% Explanation of the system variance	57.6	19.0	9.7	8.7	4.9	

TABLE 3

FPM: Factor pattern matrix (oblique)

	Factor 1	Factor 2	Factor 3	Factor 4	Factor 5	Factor 6	Factor 7	Communality
MgO	0.12631	0.03401	−0.17155	0.01145	−0.25390	0.86614	−0.05206	1.00
Na_2O	0.04348	0.07115	−0.08540	−0.01879	0.19955	−0.19191	0.90862	0.89
Al_2O_3	1.16043	0.07564	0.03330	−0.02923	−0.03726	−0.12507	−0.07602	0.93
SiO_2	0.68431	−0.26870	−0.12318	−0.04770	0.17238	0.18371	−0.02461	0.99
P_2O_5	0.06475	0.05174	0.16109	−0.04083	−0.05357	−0.98732	−0.03219	0.86
SO_3	−0.02490	0.98743	0.00730	−0.13425	−0.05347	−0.02527	−0.07242	0.86
Cl	−0.09447	−0.13855	0.16161	0.08827	−0.23675	0.11888	0.86537	0.86
CaO	0.02727	0.55988	−0.04279	−0.57270	0.07063	0.21192	0.18407	0.92
H_2O	0.04127	−0.00720	0.84726	−0.04502	0.00977	−0.02422	0.05091	0.70
$Ca(OH)_2$	−0.13274	−0.13735	0.05950	−0.75197	−0.02336	−0.18056	−0.25581	0.92
CO_2	−0.03778	0.05954	0.31572	0.05525	0.11269	0.91294	−0.08984	0.88
% Explanation of the variance	56.2	18.4	9.4	8.6	4.9	1.9	0.7	

TABLE 4

FPC: Factor pattern correlations

	Clay	Gypsum	Carbonization	Portlandite		Apatite	Halite
	Factor 1	Factor 2	Factor 3	Factor 4	Factor 5	Factor 6	Factor 7
Factor 1	1.00000	−0.50712	0.18020	0.38289	0.01086	0.87563	0.60906
Factor 2	−0.50712	1.00000	−0.15577	−0.47805	0.24404	−0.37996	0.08800
Factor 3	0.18020	−0.15577	1.00000	0.27963	−0.08294	−0.21585	−0.10506
Factor 4	0.38289	−0.47805	0.27963	1.00000	−0.24820	−0.32488	0.21780
Factor 5	0.01086	0.24404	−0.08294	−0.24820	1.00000	−0.22934	0.15860
Factor 6	0.87563	−0.37996	0.21585	0.32488	−0.22934	1.00000	0.53265
Factor 7	0.60906	0.08800	−0.10506	0.21780	0.15860	0.53265	1.00000

TABLE 5

FFC: Factors of factor correlations. Varimax rotated factor matrix (after rotation with Kaiser normalization)

	Factor 1	Factor 2	Factor 3	Factor 4	Communality
F1 Clay	−0.77009	−0.42469	0.58515	0.02324	1.12
F2 $CaSO_4$	0.25045	0.64108	−0.06550	0.31085	0.57
F3 Carbonization	−0.15146	−0.33903	−0.10714	−0.00485	0.15
F4 Portlandite	0.13106	0.77137	0.00063	−0.24051	0.67
F5	0.08961	−0.02433	0.08606	0.58185	0.35
F6 Apatite	0.99041	0.05812	0.22523	0.25722	1.10
F7 Halite	0.08441	0.13203	0.87339	0.12684	0.80
% Explanation of the system variance	45.0	26.7	20.9	7.4	

shows correlations among elements loading the factor. If all loadings on the same factor had the same sign, the factor was treated as representing variance of elements in the same mineral.

The first factor consists of a high loading of alumina and a medium loading of silica. This can be explained in terms of the residual clay not washed out from the products. Silica loading is not so high, as it has other interactions with other factors. The second factor has a high loading of sulphate and a medium loading of calcium oxide and represents a calcium sulphate phase. The negative loading of silica may point to a reaction between silica and the sulphate phase, which lowers the silica content.

The third factor contains a high loading of water of hydration (evolved up to 300°C) and a medium one of CO_2. This factor may indicate a recarbonization reaction of the remaining portlandite in the drying furnace. This implies the assumption that the water evolved in the reaction does not evaporate and remains bound to the product during the final drying at 80°C. The fourth factor has negative polarities of hydroxide and calcium oxide and represents portlandite. The fifth factor does not show meaningful correlations with elements. This factor cannot be dropped by lowering the dimension of the solution because there are meaningful factors following it, with a lower variance. This phenomenon also appeared in other product systems that were checked.

The sixth factor has a high negative loading of P_2O_5 and high positive loadings of MgO and CO_2. The following conclusions can be drawn. First, most of the variance of CO_2 has a correlation with MgO. This resembles what Lehr et al. [2] found for uncalcined francolite, i.e., that the magnesium replacing calcium in the francolite is indicative of the CO_2 level in the francolite and thus to the decrease in P_2O_5 content. The MgO content in the francolite can be used to calculate the maximum P_2O_5 content in the product [10]. Secondly, since most of the CO_2 is the result of recarbonization in the drying process (as indicated by CO_2 measurements at different stages of the process), it is bound to calcium oxide which was free before drying, hence free calcium oxide was mainly in the apatite. This calcium oxide was not extracted from the apatite during the 1-h immersion in hot water before drying. Thirdly, the amount of MgO in the product is indicative of the CaO that cannot be separated, as well as of the substituted CO_2 in raw francolites [2].

The seventh factor has a high loading of sodium and chloride which shows that most of the chloride remains in the product as halite, but does not explain why this halite does not dissolve.

Another matrix obtained with FPM is the factor pattern correlations matrix, FPC (Table 4). At this stage each factor is treated as a mineral or a mineralogical reaction, except for the case of a one-element loading which is treated as an oxide. This matrix shows the correlations among the factors. Factor—factor correlations can be used in this case, because the meaning of the factor correlations is known, i.e., correlations among minerals and not

some superfactor [9]. As the FPC is a symmetric square matrix, it can be simplified by factor analysis in which the correlations are the input data.

It should be noted that the determinant of the matrix is zero. This shows that one of the factors (the sixth, apatite, as noted in the program printout) is a linear combination of all the others, which is a very important conclusion. This shows the difference between elemental correlation matrix (not presented here), whose determinant was 0.5×10^{-5}, and FPC in which the variables (factors) are linear combination of the elements. In the process of lowering the dimension of the system, the noise variance was filtered out causing the determinant to be zero. It should also be noted that one of the eigenvalues (one of those rejected, explaining variance from analytical error) is zero. This may be due to the method of estimating the communality rather than to any physical or chemical cause.

The factor solution used this time is the varimax method [7] which gives independent factors and loads most of the variance on the first factors. The aim is to obtain an explanation for a high percentage of the variance but to obtain meaningful factors, i.e., not too many which have only one loading. This factors of factors correlations matrix, FFC (Table 5) simplifies the picture seen in the FPC matrix.

There is no meaning to communalities higher than one. It seems that the first factor is exaggerated. If the variance of clay and apatite is lowered so that the apatite communality will be 1, then the results obtained are: F1 clay 0.72929, communality 1.06 and F6 apatite 0.93794, communality 1.00; this means (factor 1) that 88% of the apatite variance is determined by a clay correlation.

In the third factor it can be seen that about 76% of the variance of the halite (composed of the variance of chloride and the variance of sodium) is determined by elements derived from clay. It is known that calcination products of clays take up chloride (cement studies [12, 13, 14]) but it has not been shown for the phosphate calcination process. The second factor has no loading on the variance of apatite and halite. This factor shows a positive correlation of portlandite and recarbonization (recarbonization has a negative polarity in Table 3) and correlations with derivatives of gypsum and clay. Portlandite and carbonate increase with sulphate and with decrease of clay. The fourth factor shows a correlation between $CaSO_4$ and the unexplained factor 5 of Table 3.

A major point which emerges from this analysis is that the parameters of the product grade (P_2O_5 and chloride) are influenced by factors which can be measured by x.r.f. spectrometry (Al_2O_3, SiO_2, SO_3, MgO). Factors measured by thermogravimetry (water of hydration, portlandite and carbonate) have only a small influence on the grade parameters. This is a very important conclusion for building a linear model and for everyday understanding and control of plant operation.

It must be stressed that the mineralogical correlations shown here hold for the set of analyzed samples given here as an example. Other product

systems studied, using raw material with a different composition, show other correlations (such as calcium aluminates, etc.).

It is intended to use the method and results described here as a guide for multiregression analysis [10] and to construct a linear model for the process of beneficiation of phosphate by calcination and washing.

REFERENCES

1 G. G. Memminger, W. H. Waggaman and W. T. Whitney, Ind. Eng. Chem., 22 (1930) 443.
2 J. R. Lehr, G. H. McClellan, J. P. Smith and A. W. Frazer. Tennessee Valley Authority, Coll. Inter. Sur. les Phosphates et Mineraux Solides, 2 (1967) 29.
3 A. Talmi, E. R. Herman and D. Kellerman, Bull. Res. Counc. Isr., Sect. C, 10 (1962) 144.
4 H. Feilchenfeld and C. Eden, Appl. J. Chem., 8 (1959) 358.
5 Ish-Shalom, Oron Phosphate Rock, Project 995/LTP/0300, Israel Ceramic and Silicate Institute, Haifa (1968) (In Hebrew).
6 S. Axelrod, Project 404/MTA/0667, Israel Ceramic and Silicate Institute, Haifa (1968); Projects 5-1215 (1970), 5-1264 (1971) and 5-1524 (1975) Chemicals and Phosphates Ltd., Haifa (In Hebrew).
7 H. H. Harman, Modern Factor Analysis, The University of Chicago Press, 3rd edn., 1976.
8 H. N. Nie, (Ed.), Statistical Package for the Social Sciences, McGraw-Hill, New York, 2nd. edn., 1975.
9 J. C. Davis, Statistics and Data Analysis in Geology, Ch. 7, Wiley, New York, 1973, p. 517.
10 D. Issahary and I. Pelly, Anal. Chim. Acta, 133 (1981) 000.
11 D. Issahary and I. Pelly, X-ray Spectrom., 00 (1981) 00.
12 I. Odler and J. Skalny, J. Am. Ceram. Soc., 54 (1971) 362.
13 G. V. Liberman and V. A. Kireev, J. Appl. Chem. U.S.S.R., 37 (1964) 194.
14 V. S. Ramachandran, Mater. Struct. 19 (1971).

Analytica Chimica Acta, 133 (1981) 369—378
Computer Techniques and Optimization
Elsevier Scientific Publishing Company, Amsterdam — Printed in The Netherlands

A REGRESSION ANALYSIS STUDY OF PHOSPHATE BENEFICIATION BY CALCINATION

DAVID ISSAHARY

Negev Phosphates Ltd., Oron; and Department of Chemistry, Ben Gurion University of the Negev, Beer Sheva (Israel)

ITHAMAR PELLY*

Department of Geology and Mineralogy, Ben Gurion University of the Negev, Beer Sheva (Israel)

(Received 23rd March 1981)

SUMMARY

A method is presented for expressing P_2O_5 as a linear combination of other components in the product of the process of beneficiation of phosphate by calcination and washing. Factor analysis is used to understand the correlations obtained by regression calculations. Partial regression coefficients are used to determine the independent variables and to find quantitative molar correlations among impurities. Regression equations were obtained for P_2O_5 in the product obtained from high-sulphate, medium-sulphate and low-sulphate raw materials.

Calcined phosphate is an important raw material but many problems are encountered in describing the reactions and mineralogical changes during phosphate calcination [1]. The aim of the present study was to establish a mineralogical description of the process and to build a model that would predict the grade of the product from the composition of the raw material. This requires the determination of the parameters needed for such a model, which must then be tested in the calcination plant. Such a model is very important from two aspects. First, mining control advance planning by calculating the optimal product from a given raw material. Secondly, control of the calcination plant operation could be improved by comparing the actual product grade to the optimal grade that can be expected from the raw material. This has to be done by on-line measurements and not by using static laboratory simulations.

The first step was the development of on-line simultaneous multi-element determinations by x-ray fluorescence spectrometry (x.r.f.) [2]. Several factor analysis techniques (using results from the on-line measurements) were then tested, to explain the nature of the multi-elemental systems of raw materials and products of the process of calcination. As an example, elemental and mineralogical associations in product samples obtained from a high-sulphate raw material were described.

0378—4304/81/0000—0000/$02.50

From the point of view of using the results as a guide for regression analysis and building a linear model for the process, there were four important results. First, the parameters of the product grade (P_2O_5 and Cl^-) are influenced by factors measured by x.r.f. (Al_2O_3, SiO_2, SO_3 and MgO), whereas factors measured by thermogravimetry have little influence. Secondly, most of the variance of halite in the product is determined by elements derived from clay. Thirdly, most of the variance of CO_2 in the product has a correlation with MgO. Magnesium replacing calcium in the apatite is indicative of the CO_2 level and thus of decreased P_2O_5 content. Magnesium oxide in the product can be used to indicate the maximum P_2O_5 content in the product. Fourthly, one of the factors (apatite) can be described as a linear combination of the other factors.

Factor analysis helps in choosing the influencing factors in the description of P_2O_5 as a linear combination of the other components and in understanding the reasons therefore. Regression analysis shows the exact quantitative relations and (using regression coefficients) helps to determine which are the influencing factors, but does not provide the reasons therefore. Regression analysis has been well described in the literature; the book of Draper and Smith [3] was used as a guide here.

The present paper describes an attempt to determine the quantitative relations among the components of the calcined phosphate system and to evaluate their statistical significance, and to build a linear model to describe the P_2O_5 content in the product using the results of on-line measurements in the calcination plant.

EXPERIMENTAL

The thermogravimetric and x-ray fluorescence spectrometric procedures were as described previously [1, 2]. Because of the large amount of analytical data, only means and standard deviations are presented in the relevant Tables.

The factor analysis techniques used for different purposes have been described [1]. For factor analysis, using SPSS procedures [4], standardized concentrations were used (i.e., $Ci/\sigma i$) so that the variance of each element is unity and the total variance is equal to the number of elements in the system.

Multiregression calculations were done using SPSS procedures [4], which also present partial regression coefficients, F test, the significance of regression coefficients in the partial equations, F test for the regression equations and their significance, etc. The F test criteria were taken from Draper and Smith [3]. The following rules were used: if $F \geqslant F(p-1, n-p, 0.01)$, the model will be considered as predictive; and if $F(p-1, n-p, 0.05) < F < F(p-1, n-p, 0.01)$ the model will be considered as explanatory only. Here $F(r_1; r_2; \alpha)$ is the critical value for F distribution for r_1 and r_2 degrees of freedom and significance α; n is the number of samples and P is the number of variables.

RESULTS AND DISCUSSION

In addition to building a linear model, regression analysis is used to estimate quantitative relations among the variables, aimed at obtaining stoichiometric relations. A problem arises for which regression analysis (and factor analysis) does not have an answer: in the case of a highly significant correlation, which is the influencing parameter and which is the influenced parameter cannot be established.

Let us assume that among N variables there are two, j and i, having a meaningful correlation. The regression equation of j against the other measured parameters in the system will yield $B_{j;i}$, which is the partial regression coefficient between j (dependent) and i (independent). But the regression equation of i against the other measured parameters will yield $B_{i;j}$, which is the partial regression coefficient between i (dependent) and j (independent). The F value will be the same in both cases and a choice cannot be based on statistical considerations. In order to determine which is the independent variable, the following rule was used in this study: i is a function of j if $|(B_{j;i})^{-1}| > |B_{i;j}|$.

A mixture containing small amounts of a clay and quartz diluted with a large amount of a mineral devoid of silica and alumina (such as calcite) will be used as an example. A change in the alumina content will cause a change in the silica content, according to the clay stoichiometry, and a partial regression coefficient $B_{SiO_2;\ Al_2O_3}$ will be obtained. But changes in the quartz content will cause only a small change in the alumina content (by dilution) and $B_{Al_2O_3;\ SiO_2}$, a very small number in absolute terms, will be obtained. In order to compare numbers of the same dimension ($|SiO_2|/|Al_2O_3|$ in this case) the reciprocal of $B_{Al_2O_2;SiO_2}$ will be used and so $|(B_{Al_2O_3;\ SiO_2})^{-1}| > |B_{SiO_2;\ Al_2O_3}|$. Accordingly, SiO_2 will be treated as a function of alumina, i.e., SiO_2 is influenced (dependent) by the influencing (independent) mineral Al_2O_3.

The regression analysis was studied in order to obtain a linear model for the P_2O_5 content of the product as a function of the amount of impurities in the product. It can also be used to find quantitative weight correlations between the binding species and the bound species, e.g., if the impurity is due to MgO; then the units of impurity bound to an MgO unit can be estimated. It is assumed for calculation purposes that the impure apatite in the product consists of pure apatite and external adventitious minerals as impurities, i.e., internal impurities (such as CO_2 and MgO) will be treated as if they were external impurities for the sake of calculations. The following relation holds: $Ap + \Sigma\ G_{im} = 100$, where Ap is the concentration of pure apatite (% w/w) and $\Sigma\ G_{im}$ is the sum of the impurity minerals (3% w/w). If the weight ratios P_2O_5/P_2O_5, CaO/P_2O_5 and F/P_2O_5 are considered, it is found that each P_2O_5 unit (in % w/w) contributes the following to the weight of the apatite: 1.00 P_2O_5 unit, 0.07 F units (0.115 from which equivalent oxygen, calculated in CaO, has to be subtracted [5]) and 1.33 CaO units (in natural pure apatites) [5]. Thus each P_2O_5 unit contributes 2.40 units

to the weight of the apatite in the product; McConnell [6] used 2.37 for apatites. The value for fluoride [5] was taken from products calcined for different times under different conditions. Hence, the value obtained is $P_2O_5 = (100 - \Sigma\ G_{im})/2.40$.

If additional units, M_j, are bound (e.g., Ca) to a unit of a contaminator j which influences P_2O_5 (such as MgO, SiO_2 or SO_3), then $[G_j] = (1 + M_j)[X_j]$, where $[X_j]$ is the concentration of j (% w/w). From this the regression coefficient is obtained:

$$d\ P_2O_5/d\ X_j = \{100 - \Sigma\ (1 + M_{im})[X_{im}]/2.40\}/d\ X_j = -(1 + M_j)/2.40 = B_{P_2O_5;j}$$

The weight of the material bound to 1% of the contaminator will be

$$M_j = 2.40\ (-B_{P_2O_5;j}) - 1 \qquad (1)$$

It is logical to assume that in the case of the contaminators SO_3 and SiO_2 the bound material is CaO, and for the contaminator MgO the equivalent bound material is $CaCO_3$ (see Issahary and Pelly [2] for the product and Lehr et al. [7] for raw francolite).

System 1. High-sulphate raw material

A detailed factor analysis of 31 samples of product formed from a high-sulphate raw material has been reported [1]. To obtain a complete picture, in terms of meaningful regression coefficients, the relevant regression data (statistically significant regression coefficients and statistical tests) are presented in Table 1. The regression coefficients obtained were used to calculate the weights of bound impurities by eqn. (1) (Table 2). No further treatment and no attempt to obtain a model for this system were tried, because of the relatively small number of samples.

Another product system, also obtained from a high-sulphate raw material and consisting of 204 samples, was used to obtain a model for a high-sulphate system. Mean concentrations of species and standard deviations are presented in Table 3. Thermogravimetry was not applied to samples in this system.

TABLE 1

Regression data for 31 samples of product from a high-sulphate raw material

Influencing variable j	Influenced variable i	$B_{i;j}$	F test for $B_{i;j}$	α significance	Molar ratio $B_{i;j}[M_j][M_i]^{-1}$
MgO	P_2O_5	−8.16	15.0	0.001	
	CO_2	10.2	7.4	0.011	9.27
Al_2O_3	SiO_2	0.91	5.8	0.025	1.54
SiO_2	P_2O_5	−0.77	5.0	0.037	
	SO_3	−0.57	5.5	0.029	−0.43
SO_3	P_2O_5	−0.47	4.1	0.053	
	CaO	1.096	4.1	0.053	1.57
Cl	$Ca(OH)_2$	−16.8	5.8	0.026	−10.6
$Ca(OH)_2$	CaO	0.51	3.6	0.067	0.5

TABLE 2

Molar relationships of bound impurities for the high-sulphate system (31 samples)

Binding variable	Weight bound to 1% binding variable	Bound variable	Molar ratio Bound variable/ Binding variable
MgO	18%	$CaCO_3$	7.2
SO_3	~0		
SiO_2	0.84	CaO	0.90

Factor analysis showed [1] that parameters measured by thermogravimetry (CO_2, water of hydration, portlandite) have only a small influence on P_2O_5 variance. These factors were also measured for system 2 (medium-sulphate) and the same result was obtained. Multiregression analysis of system 2 also showed that these parameters do not influence the variance of P_2O_5.

A detailed factor analysis can be found elsewhere [8]. The relevant major conclusions are: (1) the clay factor has higher SiO_2 and Al_2O_3 loadings (i.e., a better correlation); (2) the sulphate factor has no loading of CaO (which means that gypsum has a negligible effect on CaO variance; (3) there is a contribution of sodium to the substitutions in the apatite of the product (as was found for raw francolite [7]). In this system the factor including MgO and Na_2O is separated from the P_2O_5 factor (unlike the 31-sample system) and there is a negative correlation between them.

The significant regression data for the 204-sample system (statistically significant regression coefficient and statistical tests) are presented in Table 4. To exemplify the criterion for determining which is the independent (influencing) variable $B_{P_2O_5;X}$ from Table 4 is compared with $B_{X;P_2O_5}$ taken from the proper partial regression equations.

X	$B_{P_2O_5;X}$	$B_{X;P_2O_5}$	$[B_{X;P_2O_5}]^{-1}$
MgO	−4.45	−0.0148	−74.8
SiO_2	−1.008	−0.1811	−5.52
SO_3	1.005	−0.037	−27.0

It is seen from the identical $B_{i;j}$ and $B_{j;i}$ for Cl-Na_2O (Table 4) that it is impossible to determine which is the independent variable.

TABLE 3

Mean concentrations and standard deviations for a high-sulphate system (204 samples)

Species	MgO	Na_2O	Al_2O_3	SiO_2	P_2O_5	SO_3	Cl	CaO
Mean concentration (%)	0.34	0.79	0.27	0.45	33.50	2.73	0.077	55.73
Standard deviation	0.038	0.09	0.11	0.25	0.60	0.29	0.061	0.75

TABLE 4

Regression data for the high-sulphate system (204 samples)

Influencing variable j	Influenced variable i	$B_{i;j}$	F test for $B_{i;j}$	α significance	Molar ratio $B_{i;j}[M_j][M_i]^{-1}$
MgO	CaO	10.2	21.8	<0.001	7.29
	P_2O_5	−4.45	11.2	0.001	
Na_2O	Cl	0.3151	12.9	<0.001	0.55
	SO_3	−0.5043	4.8	0.031	−0.39
	CaO	−2.44	9.6	0.002	−2.70
	Al_2O_3	0.9811	14.9	<0.001	0.63
Al_2O_3	CaO	6.70	24.7	<0.001	12.2
	SiO_2	1.722	279.0	≪0.001	2.93
SiO_2	P_2O_5	−1.008	18.4	<0.001	
	CaO	−2.187	9.9	0.002	−2.34
	SO_3	−0.5954	8.9	0.004	0.89
SO_3	P_2O_5	1.005	29.9	<0.001	
Cl	SO_3	0.4948	4.6	0.034	0.23
	Na_2O	0.315	12.8	0.001	0.35
	CaO	1.875	5.5	0.021	1.14

As explained above, the independent variables that describe P_2O_5 variance are MgO, SO_3 and Al_2O or SiO_2 (as the last two represent the same factor). The contribution of the other variables was statistically insignificant. By a stepwise regression the following model is obtained.

$$[P_2O_5] = 38.22 - 4.451\,[MgO] - 1.005\,[SO_3] - 1.008\,[SiO_2]$$

(coefficient of correlation $r = 0.5802$, standard error = 0.42% P_2O_5, F value = 20.34 and $\alpha < 0.001$, i.e., the model can be accepted with a 99.9 confidence level).

In the discussion above it was found that

$$P_2O_5 = (100 - \sum G_{im})/2.40 = 41.73 - 0.417 \sum G_{im}$$

It is logical to assume that a model explaining all the dilution will have a constant of 41.73 while a model which does not explain the dilution will have a constant equal to the mean P_2O_5 content (33.50 in the 204-sample system). In the model for the 204-sample system the constant was 38.22, thus

$$\text{percentage of explained dilution} = \frac{\text{explained dilution}}{\text{total dilution}} = \frac{38.22 - 33.50}{41.73 - 33.50} = 0.58$$

0.58 is identical with r, the correlation coefficient found for this model by statistical methods (0.5802).

System 2. Medium-sulphate raw material

This system included only 35 product samples obtained from "medium-sulphate" (less than 2%) raw material, because they were scarce at that time.

Analysis included elements determined by x.r.f. and thermogravimetry, except for sodium (as that channel was not operative at the time). Mean concentrations of species and standard deviations are presented in Table 5.

Here again a factor analysis [1] was used as a guide to understand the results obtained mathematically by multiregression analysis. A detailed analysis is available elsewhere [8]. The relevant major conclusions were as follows. First, a factor with loadings of P_2O_5 and MgO exists; in contrast to the high-sulphate systems, there is no CO_2 loading (which may show that the recarbonization takes place out of the apatite). Secondly, 80% of the apatite variance is determined by dilution caused mainly by silica and to a small degree by calcium aluminate. Thirdly, there is a factor with loadings of Al_2O_3 and CaO. This was not seen in the high-sulphate systems and together with a very low Al_2O_3—SiO_2 correlation may indicate that sulphate (gypsum) prevents the decomposition of clays to aluminates and silicates by preventing them from being bound to CaO. Fourthly, the determinant of the factor pattern correlation matrix is not equal to zero (0.003) which indicates that not all the "noise" was filtered out in this system. It should be noted that only in the 31-sample high-sulphate system was the determinant exactly equal to zero, so that P_2O_5 in the other systems is not strictly a linear combination of the other elements. Further, a factor correlating carbonization and calcium aluminate helps to explain part of the chloride variance (probably by adsorption). Here again, it was found that parameters measured by thermogravimetry have almost no influence in explaining the P_2O_5 variance. As a guide line for regression analysis, factor analysis shows that the factors influencing P_2O_5 variance are MgO and Al_2O_3 or SiO_2.

The relevant regression data for system 2 are presented in Table 6.

According to eqn. (1), the amount of impurity bound by 1% of MgO is 21.7% and by Al_2O_3 is 8.12%. These high values can be explained as follows. For MgO, if (as in system 1) the regression between MgO and CaO is accepted as describing the $CaCO_3$ in the francolite (though factor analysis for system 2 does not show it), the amount of $CaCO_3$ will be (from Table 6) $12.32 \times 100/56 = 22\%$, which is close enough to the 21.7% found above. In order to attempt to explain the value obtained for Al_2O_3, it is necessary to assume the correlation between SiO_2 and Al_2O_3 (though not significant). Thus CaO bound to Al_2O_3 is 7.27% (Table 6) and to silica is 1.41%, giving a total of 8.68% bound to 1% Al_2O_3, compared with the 8.12% mentioned above.

TABLE 5

Mean concentrations and standard deviations for the medium-sulphate system

Species	MgO	Al_2O_3	SiO_2	P_2O_5	SO_3	Cl	CaO	H_2O	$(OH)^-$	CO_2
Mean concentration (%)	0.35	0.205	0.826	33.96	1.82	0.072	54.43	0.33	1.25	1.9
Standard deviation	0.030	0.053	0.29	0.58	0.16	0.011	0.85	0.12	0.52	0.38

TABLE 6

Regression data for the medium-sulphate system

Influencing variable j	Influenced variable i	$B_{i;j}$	F test for $B_{i;j}$	α Significance	Molar ratio $B_{i;j}[M_j][M_i]^{-1}$	Inverse regression coefficient $B_{j;i}$
MgO	P_2O_5	−9.45	12.1	0.002		0.0345
	CaO	12.32	4.4	0.046	8.8	0.0122
Al_2O_3	P_2O_5	−3.8	8.2	0.008		0.008
	SiO_2	1.415	1.5	0.229[a]	2.604	0.041
	CaO	7.27	8.1	0.009	13.2	0.009
P_2O_5	CaO	1.138	13.5	0.001	2.89	0.308
	$Ca(OH)_2$	−0.645	9.8	0.004	1.64	−0.436
SO_3	SiO_2	0.779	5.77	0.024	−1.04	−0.241
	CaO	−1.08	1.55	0.224	1.54	−0.054
	CO_2	1.03	4.54	0.043	1.87	0.149
Cl	MgO	0.729	5.69	0.025	0.65	0.163
$Ca(OH)_2$	CaO	0.309	12.1	0.002	0.90	0.362
H_2O	CO_2	1.30	6.15	0.020	0.44	0.152

[a]This is not statistically significant. It is presented here with the assumption that this resulted from the clay origin of the silica, not clear because of the existence of calcium aluminate.

A linear model was built for system 2 despite the small number of samples. The independent factors influencing P_2O_5 are Al_2O_3 and MgO. A regression analysis using these parameters gives

$$[P_2O_5] = 38.60 - 11.18\,[MgO] - 3.34\,[Al_2O_3]$$

(correlation coefficient $r = 0.571$, F value = 21.26 and $\alpha < 0.001$ or 99.9 confidence level).

$$\text{Percentage of explained dilution} = \frac{\text{explained dilution}}{\text{total dilution}} = \frac{38.60 - 33.96}{41.73 - 33.96} = 0.597$$

which corresponds well with r, the correlation coefficient found for system 2 by statistical methods (0.571).

The information in Table 6 shows that chloride influences part of the MgO variance but not vice versa; factor analysis cannot determine this issue.

System 3: Low-sulphate raw material

This system included 214 product samples obtained from low-sulphate raw material. Mean concentrations of species, except for magnesium (as that channel was not operative at the time) and standard deviations are presented in Table 7.

Here again, factor analysis [1] served [8] as a guide to understand the results obtained mathematically by the regression analysis. The relevant major features were: (1) a factor with high positive loadings of P_2O_5 and CaO

TABLE 7

Mean concentrations and standard deviations for the low-sulphate system

Species	Na_2O	Al_2O_3	SiO_2	P_2O_5	SO_3	Cl	CaO
Mean concentration (%)	0.42	0.226	1.05	34.02	1.54	0.054	55.47
Standard deviation	0.11	0.06	0.24	0.58	0.19	0.017	0.34

(apatite), also seen (weakly) in system 2 (medium sulphate) but not at all in system 1 (high sulphate); (2) a factor with loadings of Al_2O_3 and most of the chloride variance, a factor with Al_2O_3 and SiO_2 (caused by their common source, clay in the raw material), a factor with Al_2O_3 and sulphate, and a factor with high loadings of Al_2O_3—Cl factor and Al_2O_3—sulphate factor (these are associations known from the cement industry and concrete mineralogy); and (3) the more Al_2O_3—sulphate phase formed, the higher the apatite concentration. The relevant regression data are presented in Table 8.

A full linear combination obtained is

$$[P_2O_5] = -0.131 + 0.6779\,[CaO] - 0.0158\,[Na_2O] - 1.984\,[Al_2O_3] - 17.6\,[Cl] - 0.436\,[SiO_2] - 1.062\,[SO_3]$$

In order to obtain an applicable linear model (leaving only elements with a simple correlation between product and raw material), instead of the terms

TABLE 8

Regression data for the low-sulphate system

Influencing variable j	Influenced variable i	$B_{i;j}$	F test for $B_{i;j}$	α significance	Molar ratio $B_{i;j}[M_j][M_i]^{-1}$	Inverse regression coefficient $B_{j;i}$
Na_2O	SO_3	0.3578	13.0	<0.001	−0.28	0.165
Al_2O_3	Na_2O	−0.5605	11.2	0.001	−0.92	0.092
	SiO_2	2.606	78.5	<0.001	4.5	0.106
	SO_3	0.5449	4.7	0.031	0.69	0.041
	CaO	2.74	5.1	0.026	5.0	0.087
	P_2O_5	−1.984	5.5	0.020		−0.013
SiO_2	P_2O_5	−0.4361	6.6	0.011		−0.070
Cl	Na_2O	1.712	10.7	0.001	1.05	0.029
	Al_2O_3	1.035	25.4	<0.001	0.36	0.274
	SiO_2	−3.242	9.4	0.002	−1.9	0.013
	P_2O_5	−17.6	53.9	<0.001	4.4	−0.012
	CaO	2.405	47.8	<0.001	1.52	0.078
CaO	P_2O_5	0.6779	35.43	0	0.267	0.1394
	SiO_2	0.6292	10.9	0.001	0.587	0.080
SO_3	P_2O_5	−1.062	22.4	<0.001	—	−0.092

for chloride, Na_2O and CaO, their regression coefficients multiplied by their mean concentration (Table 7) were used, yielding

$$[P_2O_5] = 36.52 - 1.984\ [Al_2O_3] - 0.436\ [SiO_2] - 1.062\ [SO_3]$$

While the low α for each coefficient in the first equation can be calculated, there is no statistical test for the abbreviated equation. But, if the significance of the elements that remained in the equation is understood, it seems justified.

To summarize, it was shown that P_2O_5 concentration in the product can be described as a linear function of other independent variables in the product. For the high-sulphate system 1, the model is

$$[P_2O_5] = 38.22 - 4.451\ [MgO] - 1.008\ [SiO_2] - 1.005\ [SO_3]$$

For the medium-sulphate system 2, the model is

$$[P_2O_5] = 38.60 - 11.18\ [MgO] - 3.338\ [Al_2O_3]$$

For the low-sulphate system 3, the model is

$$[P_2O_5] = 36.52 - 1.984\ [Al_2O_3] - 0.436\ [SiO_2] - 1.062\ [SO_3]$$

If the P_2O_5 concentrations predicted by the models are compared with the measured mean P_2O_5 of each system, the fit is good

	1	2	3
1 model	33.51	34.00	34.06
2 model	33.90	34.00	33.93
3 model	32.90	33.82	33.98
measured system mean (%)	33.50	33.96	34.02

A linear model for P_2O_5 concentration in the product, a linear model predicting the P_2O_5 grade in the product as a function of the composition of the raw material, and the fit to on-line tests in the calcination plant will be discussed in a later paper.

REFERENCES

1 D. Issahary and I. Pelly, Anal. Chim. Acta, 133 (1981) 359.
2 D. Issahary and I. Pelly, X-ray Spectrom., (1981) in press.
3 N. R. Draper and H. Smith, Applied Regression Analysis, Wiley, New York, 1966.
4 H. N. Nie (Ed.), Statistical Package for the Social Sciences, 2nd edn., McGraw-Hill, New York, 1975.
5 S. Axelrod, Report 5-1524, Chemicals and Phosphates Ltd., Haifa, Israel, 1975 (in Hebrew).
6 D. McConnell, Apatite, Springer-Verlag, Berlin, 1973.
7 J. R. Lehr, G. H. McLellan, J. P. Smith and A. W. Frazier. Tennessee Valley Authority, Coll. Inter. sur les Phosphates et Mineraux Solides, Vol. 2, 1967, p. 29.
8 D. Issahary, M.Sc. thesis, Ben Gurion University of the Negev, Beer Sheva, 1979 (in Hebrew).

Analytica Chimica Acta, 133 (1981) 379—392
Computer Techniques and Optimization
Elsevier Scientific Publishing Company, Amsterdam — Printed in The Netherlands

AUTOMATED INDUCTIVELY-COUPLED PLASMA OPTICAL EMISSION SPECTROMETRY BASED ON A SEQUENTIAL READING MONOCHROMATOR†

JAN-OLA BURMAN*, BÖRJE JOHANSSON[a], BERTIL MOREFÄLT[b] and KJELL-HÅKAN NÅRFELDT[c]

Department of Economic Geology, University of Luleå, S-951 87 Luleå (Sweden)

LENNART OLSSON

Division of Applied Electronics, University of Luleå, S-951 87 Luleå (Sweden)

[a—c]Present addresses:

(a) *Primdata AB, Fack, S-951 88 Luleå, Sweden.*
(b) *MEFOS, Metallurgical Research Plant, Box 812, S-951 28 Luleå, Sweden.*
(c) *Microcomputer Centre, University of Luleå, S-951 87 Luleå, Sweden.*

(Received 4th February 1981)

SUMMARY

An automated computer-controlled sequential reading monochromator system for optical emission spectrometry with an inductively-coupled plasma as source is described. The system selects the set of emission lines which are best suited for each type of sample. Multi-element analysis of major and trace elements is done automatically, including sample changing, calibration, background correction and presentation of results.

Inductively-coupled plasmas (i.c.p.) have been commercially available for some years as excitation sources for optical emission spectrometry [1—4]. Analytically, these plasmas are superior to flames in atomic absorption spectrometry [5, 6] even if source characteristics are not optimized for each element. Many of the i.c.p. systems in use today are direct reading polychromators for simultaneous determination of 20—40 elements. Direct reading polychromators are advantageous for large series of samples of similar type, e.g., geological samples; such systems permit 200—300 multi-element analyses each 8-h shift. However, many laboratories cannot use direct readers economically because of small sample series (often of different origins). The loss of analytical output of polychromators is probably acceptable to many laboratories if they gain the flexibility of a computerized scanning monochromator [7, 8]. Scanning monochromators are useful alternatives for applications where not too many elements ($\leqslant 10$) have to be determined in each run.

†Presented at the Pittburgh Conference of Analytical Chemistry and Applied Spectroscopy, March, 1980.

0378—4304/81/0000—0000/$02.50

Approximately 70 elements in the periodic table can be determined by i.c.p.e.s. [9]. All these elements can be determined with a scanning monochromator; the same element can be measured at several emission lines, and identical results at these lines indicate satisfactory performance of the instrument. This is of special value when suitable standard samples are unavailable.

Several computer-controlled monochromators have been described [10—13] and discussed by Boumans et al. [14]. Floyd et al. [15] have outlined a clever user-oriented system. The design of the present system is based on the experience gained during three years of method development which in turn has been much influenced by routine work with i.c.p.e.s. spectrometers [16—22]. The units are mounted on the same optical axis around a joint i.c.p. source [18]. One unit is a sequential reading polychromator ARL 33000, and the other is a monochromator ARL 35000, which originally was largely manually operated. Wavelength selection, profiling, PM voltage, integration time, read-out and sample changing were performed or controlled manually.

The following instrumental parameters are computer-controlled in the new system (Fig. 1): (1) sequential reading of emission lines by a miniscanning procedure; (2) number of steps and the steplength in the miniscanning; (3) background measurements; (4) integration time; (5) photomultiplier voltage; (6) observation height in the plasma tail. Points (2—6) can all be set individually for each emission line. None of the published [10—15] computerized monochromators offer all these features. Furthermore, some safety systems, autosampler, rinsing and data handling are also controlled by the computer

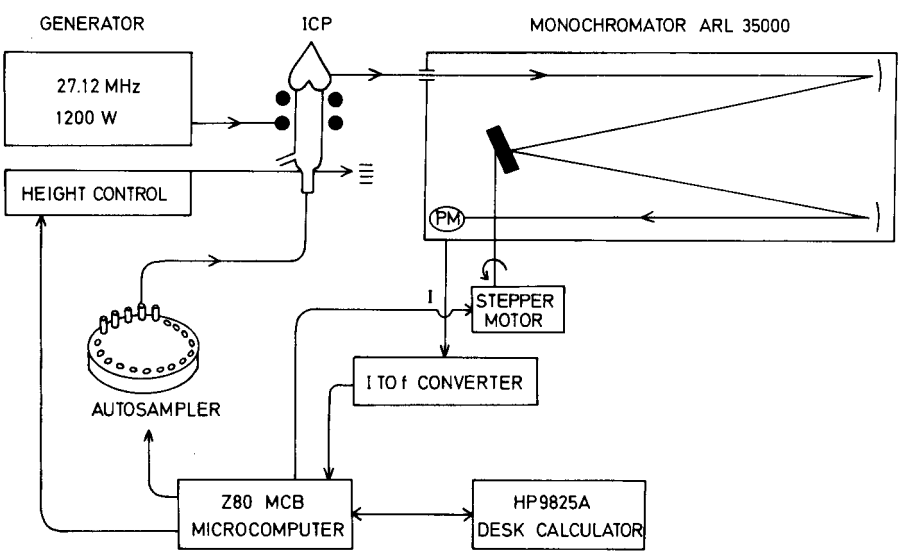

Fig. 1. Block diagram of the computer-controlled sequential reading monochromator with an inductively-coupled plasma as excitation source.

system. These basic instrumental control facilities are assembled in two software packages, one being used for method development and the other for routine determinations. The knowledge obtained during method development is then used to define routine analytical programs, which are stored on tape. The operator activates a complete automatic analytical sequence by giving only two commands. This system makes it easy to achieve maximum spectroscopic information by tailoring routine programs optimally suited for each sample type, i.e., the best set of emission lines can be selected for any given sample.

EXPERIMENTAL

Computer configuration

The computer system comprises a desktop calculator, a Hewlett-Packard 9825A, and a microcomputer, Zilog Z-80A, which compute at two levels. The control functions and measurements were most easily solved with an unsophisticated language which permits manipulation on bit-level, whereas the data handling and all estimations are best performed with a versatile high-level language like Hewlett-Packard-Language (HPL). The HP 9825A could have been used alone for control of the spectrometer system if suitable interface electronics had been constructed, but a drawback with this is the difficulty of making changes in specially tailored interfacing units. Furthermore, the number of logic circuits in such a system would be large, requiring excessive development work to become operable.

These difficulties are avoided with a microcomputer, because it is easier to adapt to the spectrometer system; the microcomputer can be regarded as a programmable part of the interface between the HP 9825A and the spectrometer (see Fig.2 and Table 1).

Tasks for Z-80A. The Z-80A handles communication with the HP 9825 via a HP-IB. It also controls the stepper motor. All measurements are made as miniscans over the emission line; single-point measurements are impossible because of lack of mechanical reproducibility. Step lengths and number of steps in the miniscans are programmable (Fig. 3). The smallest step length is 1/1000 revolution of the stepper motor axis, equalling 2.7 pm with the 2160 line/mm grating, i.e., all step lengths are multiples of 2.7 pm. The

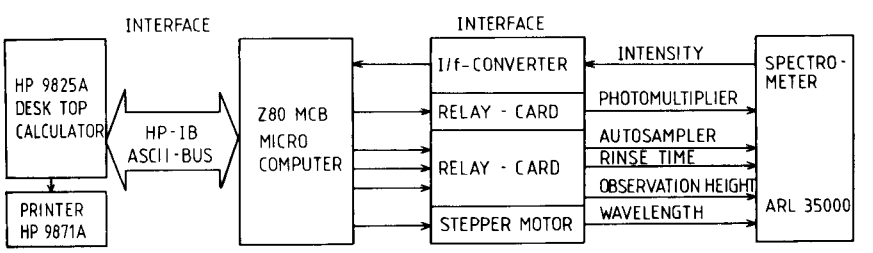

Fig. 2. Block diagram of the hardware components in the automated spectrometer system.

TABLE 1

System components and operating conditions

Spectrometer	Applied Research Laboratories (ARL) 35000; Czerny-Turner 1-m focal length
Grating	2160 line/mm
Slits	Entrance 20 μm; exit 60 μm
Stepper motor	Superior Electric Company Slo-Syn MO62-FD09 with power supply MPS 3000X
Stepper-motorlogic	Superior Electric Company: Slo-Syn translator module type STM 103
Computer	Microcomputer Zilog Z80-MCB, 4K bytes memory and desktop calculator Hewlett-Packard HP 9825A, 24K bytes memory
Printer	Hewlett-Packard HP 9871A
Interfaces	Hewlett-Packard HP-IB 98034A, the ASCII-bus and relay cards [23]
A/D converter	Analog Technology Corp. Model 151 current to frequency converter
RF-generator	Henry Generator Model 3000 PGC/27, 3000W. Operated at 1200W, reflected power <5W.
Ar flow rates	Cooling gas flow 12 l min^{-1}, plasma gas flow 0.8 l min^{-1}; central gas flow 1 l min^{-1}; pressure 3 atm.
Nebulizer	Concentric glass nebulizer, J. E. Meinhart type T-200-A4.
Solution uptake	0.8 ml min^{-1}; peristaltic pump.

stepper motor and the spectrometer grating are coupled by a transmission which divides the rotation of the stepper motor axis four times and also minimizes the distinct jerk typical of the stepper motor. Acceleration and retardation during start and stop of the motor are program-controlled, producing a smooth change in speed in five intervals, which decreases mechanical wear, increases reproducibility and prevents the stepper motor from skipping a step.

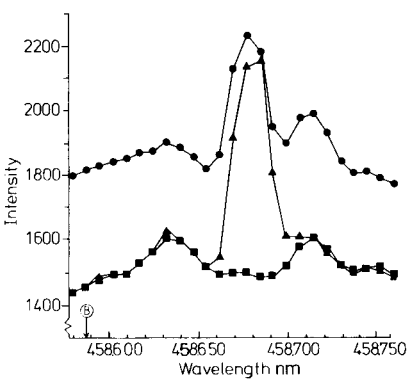

Fig. 3. A copy of an original plot showing (■) blank, (●) calibration solution and (▲) unknown sample. Point B is chosen for background correction in measuring the net intensity. The sample was rock dissolved in $HF/HClO_4$ and the calibration solution contained 100 mg La l^{-1} corresponding to 10 ppm in the rock. This miniscan was done in 24 steps with a step length equal to three times the least possible step length for the stepper motor, 3 × 2.7 pm. The resolution is improved by a software-controlled coordinate transformation. The intensity axis begins at the background level.

The Z-80A controls the PM voltage, integration time and observation height. The gain is regulated in 256 steps in the range 690—845 V. The voltage can be set individually during each miniscan, which is advantageous for samples with large differences in the elemental concentrations. The integration time can be varied between 0.1 s and 14 min, which is program-controlled by the microcomputer clock. The system offers alternative heights 14, 18, 22 and 26 mm above the induction coil. The height can be changed between each emission line to obtain the optimal signal-to-background or signal-to-noise ratio. The microcomputer controls the height by simulating the appropriate signals via the logic rack of the polychromator (ARL 33000) which has a height regulator.

The current from the PM tube normally varies between 10^{-10} and 10^{-5} A. To take advantage of the large dynamic measuring range of an i.c.p., the system uses a current-to-frequency converter and a 32-bit binary counter. The output frequency is integrated by the counter, which is controlled and read by the microcomputer; all intensities are transferred to the HP 9825.

A 24-position turntable autosampler is controlled by the microcomputer in a similar way as the height control. A safety system is constructed to eliminate the risk of damage to the grating mechanism during abnormal or other uncontrolled conditions. Microswitches break the pulse train to the stepper motor if the λ_{max} (or λ_{min}) limits are passed. Special precautions must be taken to reactivate the spectrometer system if the safety system has shut it down.

Tasks for HP 9825A. The HP 9825A communicates with the operator. All questions to the operator are presented on an LED display and answered via the keyboard. All parameters for each emission line are defined as a row in a matrix. This matrix is stored in the HP 9825A and each row is fed into the microcomputer, one for each emission line during the analytical sequence.

The tape cartridge of the HP 9825A handles the recording of intensity, including administration, sorting and storage of the information. Finally, the results are calculated, including background corrections, and presented. Miniscan profiles, calibration curves and tabulated results are presented on the HP 9871A printer. The tape cartridge of the HP 9825A is also used as a library for analytical programs which have been defined by the operator in order to run routine analyses.

Software configuration

Only a simplified description of the software configuration is given; details of the programs have been described [23] and are available from the authors on request, along with structured diagrams using the top-down method [24]. The HP 9825A directs the Z-80A and makes all computations. Communication programs and system subroutines have been developed to accomplish these functions.

Microcomputer software. The programs in the microcomputer communicate with the desktop calculator and execute commands which are given via

the desktop calculator. The microcomputer works in four interrupt levels, which steer the following activities.

Level 1 is an alarm routine which stops the stepper motor when the wavelength limits for the grating mechanics have been exceeded; all dangerous combinations of power supply failure to the systems also stop the stepper motor. Level 2 is the clock for control of integration time and pulse generator for the stepper motor; this clock can be used for both functions because change of wavelength and intensity measurements are never done simultaneously. At level 3, the clock controls the time delays needed for different spectrometer functions. At level 4 communication routines are activated.

Level 1 has the highest priority. The microcomputer is part of a real-time system which executes different software modules depending on other activities. This interaction between different routines is most easily described with state diagrams (Fig. 4). The circles represent various states (routines) for the microcomputer and the arrows show allowed transitions. The condition for the transitions is indicated beside the arrow. For example, the following conditions are required for a transition between RECEIVE and BREAK: the microcomputer must have received its listener address (MLA), the routine RECEIVE must have been completely executed, and the command B (BREAK) must have been found by the command decoder.

When the power is turned on or a RESET is performed, the microcomputer goes through an initiating routine (INIT) and reaches the state MAIN. In order to start a communication cycle, the control line ATN of the desktop

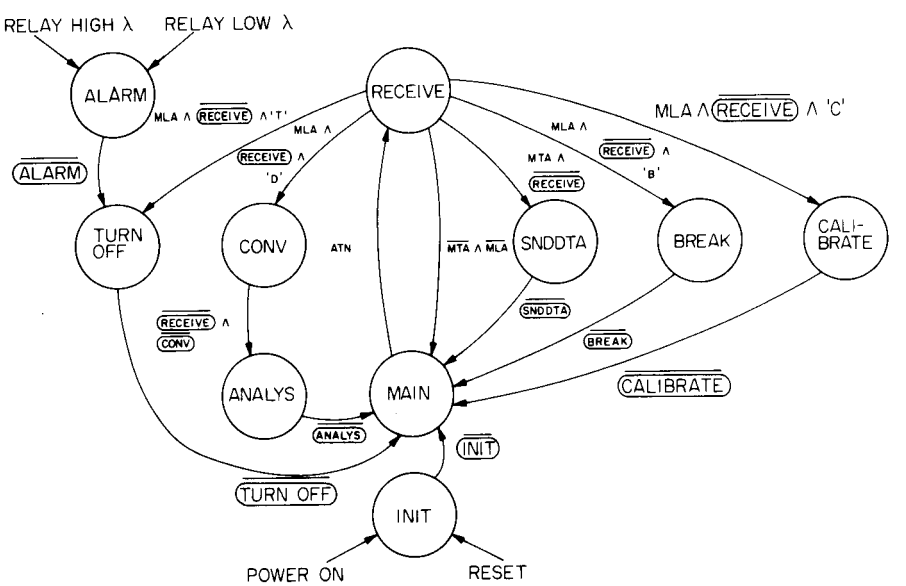

Fig. 4. State diagram for the different software modules of the microcomputer system. The conditions to get a transition between two states are indicated beside the arrows showing all possible transitions. ∧ stands for the logic operation AND; MTA = My talk address; MLA = My listen address.

calculator is lowered and the RECEIVE routine is activated. The microcomputer returns to MAIN if no listener address or talker address is obtained. If the listener address is received during execution of RECEIVE, a transition takes place to either (CONV) + ANALYSE, CALIBRATE, BREAK or TURN OFF depending on the command from the desktop calculator; but if the talker address is received then the routine send data (SNDDATA) becomes activated. Every transition from the microcomputer to the desktop calculator is activated by the microcomputer which lowers the control line SRQ. All data are transmitted as ASCII characters. The numerical values are on base 8 during communication.

Desktop calculator software. The software comprises different program modules representing various functions. The conditions for transitions between the modules are described in Fig. 5. The desk calculator has four interrupt levels, only two being used, one for the keyboard and another for the HP-IB. The interrupt request from the microcomputer goes via the Service Request (SRQ) line on the HP-IB. The interrupt decoding of HP—IB

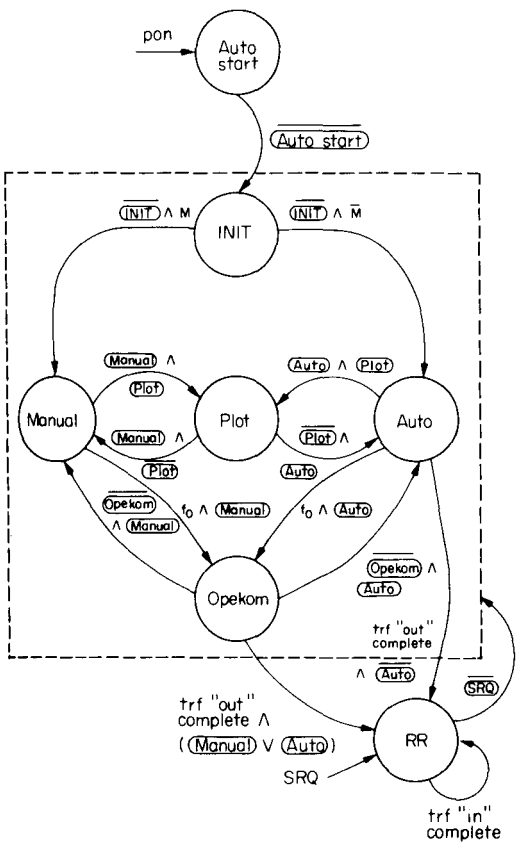

Fig. 5. State diagram for the different program modules of the desktop calculator. ∧ stands for the logic operation AND.

can be done by serial or parallel poll. Serial poll is used to maximize the information transfer via the interrupt decoding. The operator communication is initiated by the keyboard interrupt, which has higher priority than the HP-IB. This gives the operator full control over the system.

The AUTOSTART and INIT (initiation) routines load programs for initiation of the calculator and operator communication, and programs for service request interrupts from the HP-IB interface. AUTOSTART is automatically activated when the power is turned on, provided that the data cartridge is positioned in the magnetic tape station. MANUAL and AUTO are two subroutines used in combination with subroutine OPECOM either for method development (MANUAL) or for routine analysis (AUTO). In the RR (receive routine), activation of the control line SRQ on HP-IB by the microcomputer implies that the microcomputer has information for the calculator; RR is activated by an interrupt.

The subroutine operator communication (OPECOM) gives the operator control of the system by a series of commands: C (calibrate) is used for optical and mechanical calibration of grating versus stepper-motor position; D (data input) is used when defining a run during the MANUAL mode; A (automatic run) provides a complete analytical program filed on tape; S (save) is used for defining a complete analytical routine scheme stored on tape.

When the HP calculator is interrupted by the microcomputer it also receives the reason for the interrupt request. This acknowledgement is used to control the sequence of commands given by the operator. The operator must therefore start every reading with command "C" (optical/mechanical calibration).

The PLOT subroutine is used to present the results on the HP 9871A printer/plotter.

Optical calibration

The spectrometer is optically tuned before each series of measurements, involving calibration of the stepper motor versus the position of the grating by scanning over the total reflexion at 0 nm (see Fig. 6). The scanning starts

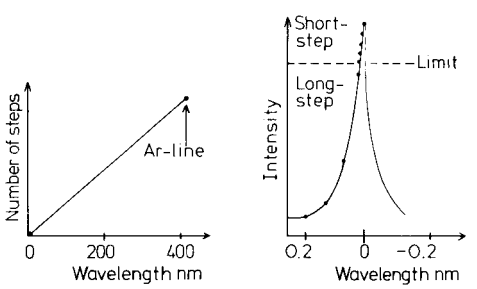

Fig. 6. The distance between the Ar line 394.898 nm and 0 nm is used to calculate once for all the relation between the number of steps and wavelength. An optical/mechanical single-point calibration is performed, before each series of measurements by localizing the total reflexion obtained at 0 nm.

at approximately 0.2 nm with a step length of 0.01 nm until a given intensity limit is reached, whereafter the shortest step length is used to locate the intensity maximum accurately; the distance in steps between total reflexion and the argon line 407.201-nm line yields a straight-line relation between wavelength and number of steps. All measurements are terminated by a return to approximately 0.2 nm to facilitate adjustment for subsequent use.

Program package for method development

The basic principle is illustrated in Fig. 7. The miniscan facility gives important information about the vicinity of the emission line, revealing possible spectral overlaps and background shifts caused by stray light or line broadening [25] (Fig. 3). The spectral window examined can be varied both by the length of each step (2.7—270 pm) and the number of steps (at most 30). This flexibility permits the selection of the optimal emission line and if needed the corresponding position for background correction; up to 10 emission lines in 24 different samples can be investigated in each run. All results obtained during the use of this routine are presented as profiles on the printer/plotter. Scaling of both the wavelength and intensity axes is done by software. The minimum intensity measured during the miniscan is subtracted from all intensity readings in order to obtain better resolution in the plot. The intensity/wavelength coordinates for each sample are indicated by a symbol in the plot and a straight line is drawn between each coordinate. The original plot is 30 × 30 cm; Fig. 3 shows a copy redrawn for clarity. At most eight profiles are presented in the same plot to obtain legible results. This means that the results obtained for one emission line with maximum sample load, 24, are presented on three plots with eight samples or profiles on each.

Contamination from reagents or sample containers can be detected if a blank solution gives a peak during the miniscanning. The profile discloses such contaminations, whereas the fixed-slit systems commonly found in polychromators makes it harder to detect a small increase in the background.

This way of presenting spectral information has proved to be very valuable during method development. In addition, it is also possible to have all parameters but the observation height fixed so that the profile indicates the signal-to-background ratio as a function of height. Ion lines are generally best read in the low region and atom lines high up in the plasma.

Program package for routine analyses

The same principle as in Fig. 7 is used for routine analyses, but the evaluation of data differs. In method development, miniscans are usually needed over a wide range to decide whether or not background correction is needed. In routine analyses, the number of readings in every miniscan must be minimized to enlarge the analytical output.

In the peak-seeking routine, the three highest intensities in the window defined by the miniscan are used to estimate the intensity maximum (Fig. 8);

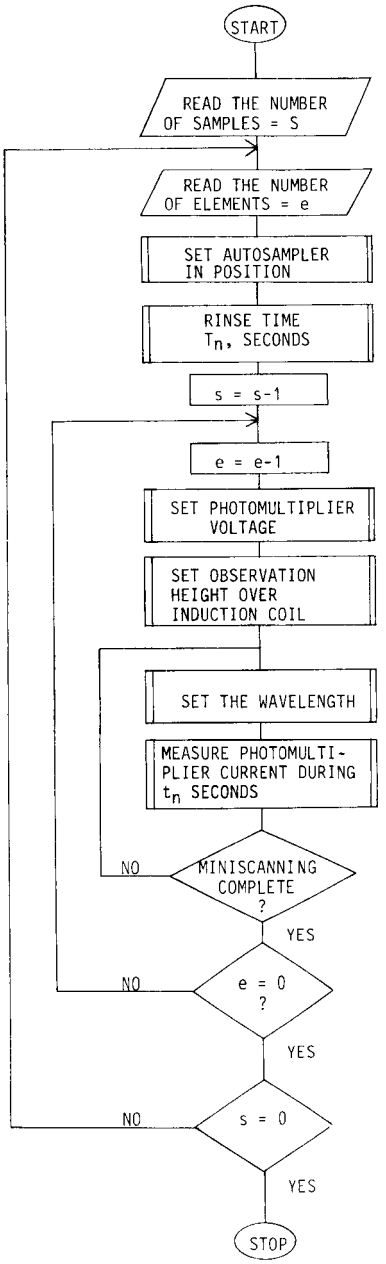

Fig. 7. Flow diagram representing the general working principle for the spectrometer system.

the wavelength found for the intensity maximum is called λ_f. The difference between λ_f and λ_t, the value from the wavelength table, will form an offset which is used to decide if the right peak has been found. The results are presented routinely during each analytical cycle (Fig. 8). The procedure is repeated at every emission line and in every sample or calibration solution.

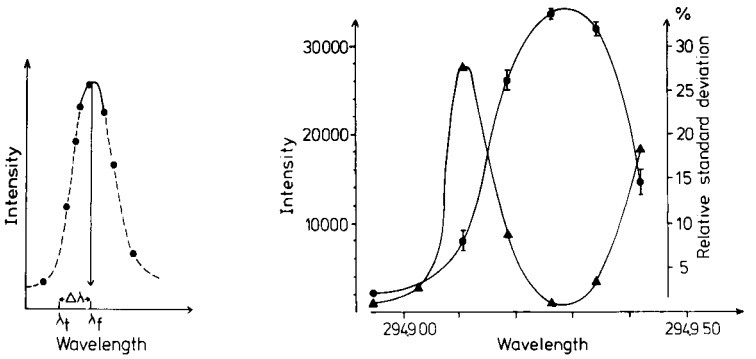

Fig. 8. The three highest intensities are used to estimate the intensity maximum and corresponding wavelength (λ_f).

Fig. 9. Ten different emission lines are read ten times during a period of 50 min; the 294.920-nm line is one of them. Accuracy and reproducibility of both wavelength and intensity are good. (•) Mean intensity (n = 10) with the bar representing standard deviation; (▲) relative standard deviation.

A sudden change in the offset value indicates that some other peak has fallen within the spectral window which is examined. Weak signals in spectral regions with steep background slopes can be hard to detect. Even if the mathematical criterion fails to resolve the right peak, the offset value gives an indication. The wavelength offset is generally less than ±0.02 nm over the whole spectral range and the reproducibility in offset during one measuring cycle is good, always within ±2 pm.

Background correction. Disturbances from stray light and line broadening sometimes demand corrections. The profile plots from the method development give the information needed to select the best site for background measurements; this background intensity is subtracted from the intensity maximum. The operator can choose any position around the emission line; this is an improvement over systems with rotating refractory plate, which can make background measurements only at fixed distances from the emission line. The refractory plate technique may result in false background corrections because of adjacent emission lines or sudden background changes. The flexibility of the proposed system makes proper background correction possible even when other background correction techniques fail. Long-term drift is also minimized because the difference between the top of the peak and the background is always measured and in a very short period of time, normally 1—20 s. The net intensity is generally not influenced by the long-term drift of a few percent per hour, but all absolute intensity measurements are sensitive to this kind of drift.

Calibration. The chemical calibration and evaluations of concentrations are made automatically. The operator informs the system about the concentrations in the calibration solutions and the corresponding positions in the

TABLE 2

Example of tabulated emission lines from each calibration and sample run

Wavelength (nm)	Intensity
408.647	1615
408.654	1685
408.662	2531
408.670	3200
408.678	3269
408.686	2541
408.693	1810
Element	La
Searched wavelength (λ_t)	408.671
Found wavelength (λ_f)	408.675
Offset	0.004
Maximum intensity[a]	1757
Background wavelength	4087
Background intensity	1580

[a]After subtraction of background.

autosampler as well as the sample number and position of the unknown samples; the only limit is that the number of solutions cannot exceed 24. Several calibration groups can be distributed in the sample holder if frequent recalibration is needed. Generally, however, the i.c.p. has proved stable, occasional fluctuations being compensated for by the background correction described above, so that frequent recalibration is required only in high-precision studies.

A graph is plotted for the analytical results of each element; calibration solutions and unknown samples are identified by different symbols. The calibration function is obtained by a least-squares linear regression. The absolute, background and net intensities are presented for all measurements, as well as calculated slope, intercept, standard error of slope and intercept and $S_{y.x}$, and the results are also presented in the plot. It is important to print not only the tables but also the graphs, because they can reveal sources of errors in the analytical procedures, such as disturbances in the calibration procedure, erroneous sample digestions and poor standard samples.

RESULTS AND DISCUSSION

Accuracy and reproducibility

Wavelength regulation and measurement of photomultiplier current are two essential functions of a spectrometer system. The first test of these important functions was performed by reading 10 different emission lines, spread in the interval 200.0—430.0 nm, ten times in the same solution. The miniscans were made in 6 steps, each step being 8.1 pm. The integration time

was 3 s; all measurements took 50 min. No background correction was applied. The results for the Mn 294.920-nm line are illustrated in Fig. 9; the wavelength was found to have an offset of +9 pm. As can be seen, the relative standard deviation on top of the peak was almost as good as beside the peak. The results are surprisingly good and prove that the total error including both mechanic and electronic contributions are under control.

Analytical results

Lanthanum in manganese nodules sampled in the Gulf of Bothnia is a typical example of a sample type and an element which is rarely represented among standard reference samples. Lanthanum emission was measured at three different lines. The background correction reduced the intensity by 2—25%, depending on the concentration of interfering element. The need for background correction varied much for the different emission lines, but the results reproduced in Table 3 indicate that the procedure works well. A number of applications has been developed, e.g., determinations of rare earth elements in geological and biological samples.

Conclusions

A polychromator and an automated monochromator attached to the same i.c.p. is an almost ideal spectrometer configuration. The system described in this paper has proved to be a very valuable complement to the polychromator used previously. Experience in this small laboratory running many routine analyses indicates that automated monochromators have great potential. The cost—flexibility—performance relation makes it an interesting alternative even for small laboratories dealing with metal determinations in liquid samples.

A comparison of the performance of the manually operated spectrometer with the automatic system is rather unfair, but it has been found that the production per unit time is increased by a factor of 10—50 depending on the type of application, and that the accuracy has increased because of the flexibility of line selection in combination with the background correction. The system described has been used routinely for almost two years.

TABLE 3

Determination of lanthanum in manganese nodules

Sample	Lanthanum concn. (ppm) at		
	384.902 nm	498.671 nm	442.990 nm
1321	44.5	45.4	45.9
1519	41.2	39.2	39.7
1535	28.9	29.6	30.2
1537	25.4	25.3	28.0

Financial support of this project by the National Swedish Board for Technical Development (STU) under a grant to Kurt Boström, is greatly appreciated. We thank K. Boström for valuable discussions during the project, M-B. Anttila for typing, A-B. Malkan for drawing the figures, T. Westin for contributing to the software and the Department of Applied Geophysics for the loan of equipment.

REFERENCES

1 V. A. Fassel and R. N. Kniseley, Anal. Chem., 46 (1974) 1155 A.
2 V. A. Fassel, Science, 202 (1978) 163.
3 A. L. Robinsson, Science, 199 (1978) 1324.
4 P. W. J. M. Boumans, Fresenius Z. Anal. Chem., 179 (1976) 1.
5 V. A. Fassel and R. N. Kniseley, Anal. Chem., 46 (1974) 1110 A.
6 R. M. Barnes, Anal. Chem., 50 (1978) 100 R.
7 P. W. J. M. Boumans, L. C. Bastings, F. J. de Boer and L. W. J. van Kollenburg, Fresenius Z. Anal. Chem., 291 (1978) 10.
8 V. A. Fassel, Anal. Chem., 51 (1979) 1290 A.
9 R. K. Winge, V. J. Peterson and V. A. Fassel, Appl. Spectrosc., 33 (1979) 206.
10 H. Kawaguchi, M. Okada, T. Ito and A. Muzvike, Anal. Chim. Acta, 95 (1977) 145.
11 D. J. Johnsson, F. W. Plankey and J. D. Winefordner, Anal. Chem., 47 (1975) 145.
12 R. W. Spillman and H. V. Malmstadt, Anal. Chem., 48 (1976) 303.
13 T. Catterick and D. A. Hickman, Analyst, 104 (1979) 516.
14 P. W. J. M. Boumans, G. H. van Gool and J. A. J. Jansew, Analyst, 101 (1976) 585.
15 M. A. Floyd, V. A. Fassel, R. K. Winge, J. M. Katzenberger and A. P. D. Silva, Anal. Chem., 52 (1980) 431.
16 J-O. Burman, B. Boström and K. Boström, Geol. Fören. Stockholm, Förh., 99 (1977) 102.
17 J-O. Burman, C. Pontér and K. Boström, Anal. Chem., 50 (1978) 679.
18 J-O. Burman and K. Boström, Anal. Chem., 51 (1979) 516; Kem. Tidskr., 90 (1978) 18; 92 (1980) 28.
19 J-O. Burman, B. Johansson, B. Morefält and K-H. Närfelt, Modern Elektronik, 19 (1979) 32.
20 J-O. Burman, in R. M. Barnes (Ed.), Applications of Plasma Emission Spectroscopy, Heyden, London, 1980, pp. 15—22.
21 K. Boström, J-O. Burman, B. Boström, C. Pontér and S. Brandlöf, Finn. Mar. Res., 244 (1978) 8.
22 K. Boström, J-O. Burman, C. Pontér and J. Ingri, Mar. Chem., 10 (1981) 335.
23 B. Johansson, B. Morefält and K-H. Närfelt, M.Sc. Thesis University of Luleå, No. 080E, 1979.
24 K. L. Bowels, Microcomputer Problem Solving Using Pascal, Springer-Verlag, Berlin, 1977.
25 G. F. Larsson, V. A. Fassel, R. K. Winge and R. N. Kniseley, Appl. Spectrosc., 30 (1976) 384.

Analytica Chimica Acta, 133 (1981) 393—408
Computer Techniques and Optimization
Elsevier Scientific Publishing Company, Amsterdam — Printed in The Netherlands

CHARACTERIZATION OF NOISE IN INDUCTIVELY-COUPLED PLASMA EMISSION SPECTROMETRY

R. P. J. DUURSMA[a], H. C. SMIT* and F. J. M. J. MAESSEN

Laboratory for Analytical Chemistry, University of Amsterdam, Nieuwe Achtergracht 166, 1018 WV Amsterdam (The Netherlands)

(Received 9th December 1980)

SUMMARY

The nebulizing process in inductively-coupled plasma emission spectrometry is a major source of the instrumental variability; an attempt has been made to isolate this source so that its influence on the final result could be evaluated. Direct measurements of the time-dependent variations of the sample supply to the plasma were achieved by using a device based on the light-scattering property of nebulized test solutions. The noise from the nebulizer and of the emission signal was characterized by autocovariance functions and power spectral densities. The types of noise observed showed $f^{-1/2}$ and $f^{-1/4}$ character, depending on the concentration of the test elements employed. Cross-covariance revealed a strong correlation between the noise sources considered. The applicability and limitations of possible correction and electronic filtering procedures are indicated.

The combination of the inductively coupled plasma with atomic emission spectrometry (i.c.p.e.s.) gives impressive analytical performance, with ng ml^{-1} detection limits for most metals, linear dynamic ranges of 3—5 orders of magnitude, and precisions at the "few percent" level [1—3]. However, there is no thorough description of the random fluctuations in i.c.p.e.s., required for unambiguous specification of analytical quantities. Filling this gap demands either a description in the time domain by the autocovariance function (ACVF), or in the frequency domain by the power spectral density (PSD). Preliminary experiments [4] indicated that fluctuations originating from the nebulizing process are a major contribution to the uncertainty of the final analytical result.

The main object of the present study was to analyse the noise appearing in i.c.p.e.s., with the eventual aim of improving the signal-to-noise ratio and precision of analysis on the basis of system theoretical principles. Underlying the experimental design was the consideration that if the variation of the sample supply to the plasma is known, then in principle (slow) random fluctuations can be corrected for afterwards. In addition, the approach applied provides the information essential for assessing the applicability of electronic filtering procedures.

---

[a]Present address: Gist-Brocades, Research and Development, P.O. Box 1, 2600 MA Delft, The Netherlands.

General description of i.c.p. spectrometry and elucidation of the experimental approach

The i.c.p. can be considered as an electrical flame. The plasma is generated by transfer of energy to a flowing conducting gas (plasma gas) by inducing a magnetic field around the top of co-axial silica tubes which constitute the burner or torch. Sample solutions are normally introduced into the plasma by means of a pneumatic nebulizer; the very fine mist enters the plasma, and condensed spray drains to waste. Figure 1 shows schematically the principal components of i.c.p.e.s. instrumentation. The property that makes the plasma most suitable as an excitation source in analytical atomic emission spectrometry is its high temperature. Radiation emitted by free atoms or ions of the analyte is measured; and to prevent systematic errors, all processes transforming the analyte to atoms and ions must be experimentally controlled. The different stages of sample transformation [5], are schematically represented in Fig. 2.

The complexity of the process allows many sources of variability to affect the measurement. In order to evaluate the influence of each source of vari-

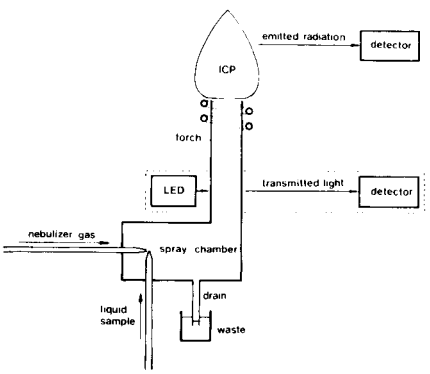

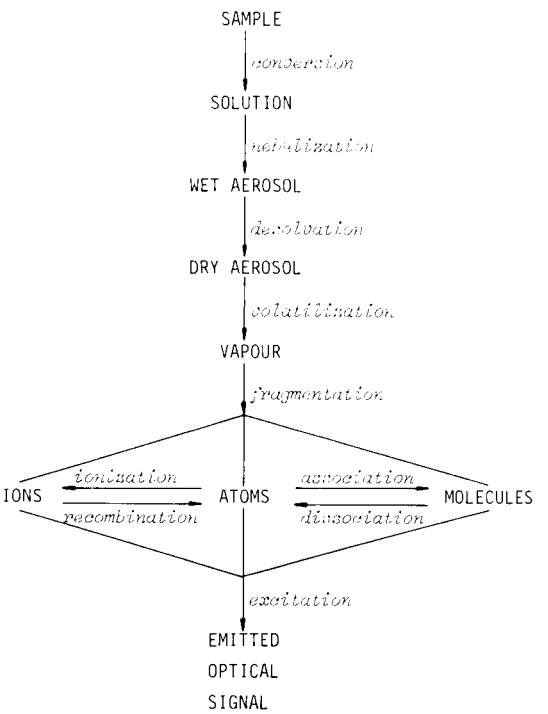

Fig. 1. Principal components of i.c.p.e.s. instrumentation and arrangement of equipment for detection of aerosol density variations.

Fig. 2. Stages in the transformation of sample to analytical signal.

ability on the analytical result, these sources must be separated. To that end, the variability of the complete instrumentation and of the instrumentation without the nebulizer and associated spray chamber was measured. Comparison of the results showed that the total variability increased by a factor of about four when solutions were introduced [4]. Therefore, attempts were made to measure directly the density variations of the stream of mist particles dragged into the plasma, with the aim of testing the applicability of a correction procedure based on the empirical relation between the variations of the mist density and of the emission signals.

Variation of mist density was measured by utilizing the light scattering property of mist particles. For brevity in the subsequent text, the intensity of light transmitted by the aerosol and measured by absorbance is referred to as the "mist signal", whereas the i.c.p. response is denoted by "emission signal". Well-defined nebulizing conditions were realized by setting the flow rate of the nebulizing gas at a fixed value, to ensure a constant Reynolds number. Except for the sample flow rate, the i.c.p. operating parameters were also kept constant. The sample flow rate was adjusted by means of a constant flow pump. These experiments proved the existence of a non-linear relation between sample flow rate and emission signal. A similar relation was found between the sample flow rate and the mist signal. Consequently, the relations considered are affected by the corresponding non-linear processes. However, if all processes after the nebulization step are linear, the relation between mist signal and emission signal will be linear. The fluctuations of the mist signal will then be correlated to the fluctuations of the emission signal, in principle enabling the reduction of noise affecting the i.c.p. response.

THEORY

In terms of system theory, the impulse response of a compound system, $h_c(t)$, fully characterizes a linear system. Provided that the impulse response is known, the output signal $y(t)$ can be calculated from the input signal $x(t)$ with the convolution integral

$$y(t) = \int_0^\infty h_c(\tau)\, x(t-\tau)\mathrm{d}\tau \equiv h_c(t) * x(t) \qquad (1)$$

If the input responses of the individual processes, $h_i(t)$, are known, the impulse response of the complete system is also known because the output signal of each part is the input signal for the next part in the chain. Consequently, for a compound system composed of three components, the following expressions hold:

$$y(t) = h_3(t) * [h_2(t) * \{h_1(t) * x(t)\}] \; ; \; y(t) = h_3(t) * h_2(t) * h_1(t) * x(t) \qquad (2)$$

A system not affecting the input signal shows an impulse response according to a delta Dirac function $\delta(t)$, satisfying the condition [6]: $x(0) \equiv \int_{-\infty}^{\infty} x(t)\delta(t)\mathrm{d}t$.

In general, a stochastic input signal $x(t)$ with a Gaussian probability density function can be described by an ACVF, $C_{xx}(\tau)$:

$$C_{xx}(\tau) = E[x(t)x(t+\tau)] = \lim_{T\to\infty} \frac{1}{T} \int_0^T x(t)x(t+\tau)\mathrm{d}t \tag{3}$$

where E denotes an expected value. The description of the output signal $C_{yy}(\tau)$ is then given [7] by

$$C_{yy}(\tau) = \int_0^\infty \int_0^\infty h(\tau_1)h(\tau_2)C_{xx}(\tau + \tau_1 - \tau_2)\mathrm{d}\tau_1\mathrm{d}\tau_2 \tag{4}$$

or, in alternative notation, $C_{yy}(\tau) = h(\tau)*h(\tau)*C_{xx}(\tau)$. When the system correlation function (SCF) $\psi(\tau)$ is introduced, $\psi(\tau) = \int_0^\infty h(t)h(t+\tau)\mathrm{d}t$, then the ACVF of the output signal can be calculated by

$$C_{yy}(\tau) = \psi(\tau)*C_{xx}(\tau) \tag{5}$$

Hence, the variance of the output signal, $C_{yy}(0)$ can be calculated from the ACVF of the input signal.

The ACVF contains all statistical data which can also be represented by the PSD, usually referred to as the power spectrum, $P(\omega)$. A power spectrum is the Fourier transform of the corresponding ACVF (Wiener—Khinchin relations): $P(\omega) = F\{\mathrm{ACVF}(t)\}$, where F is the Fourier transform. This unambiguous relation can be used to determine noise. An ACVF can be described properly by a series of exponentials whereas power spectra can, within a certain frequency range, be described by $P(\omega) \simeq 1/\omega^\alpha$, $|\alpha| \geqslant 0$; here α is a constant depending on the behaviour of the random variable in the time domain. The statistical properties of a variable are then conveniently described by the value of the ACVF(t) at $t = 0$, and the value of α. When integrating techniques are used, it is possible to calculate the standard deviation of the integrated signal from the ACVF of the output signal [8].

Impulse responses can be calculated from the ACVF of the input signal and the CCVF (crosscovariance function) of input and output signals by means of Fourier transforms:

$$h(t) = F^{-1}(H(\omega)) = F^{-1}\left\{\frac{P_{xy}(\omega)}{P_{xx}(\omega)}\right\} = F^{-1}\left\{\frac{F[\mathrm{CCVF}(t)]}{F[\mathrm{ACVF}(t)]}\right\} \tag{6}$$

where F^{-1} is a reverse Fourier transformation.

To enable the i.c.p.e.s. instrumentation to be described in terms of a system theory, the compound system was subdivided (see Fig. 3) into the following component parts and corresponding processes: nebulizer/spray chamber (formation of mist particles capable of reaching the plasma); torch system (transport); argon plasma (excitation); monochromator/chopper (spectral selection and modulation); photomultiplier tube/shot noise generator (detection of random photon arrival); lock-in amplifier (demodulation and amplification). Each of these parts can be described by an impulse response. Calculation of the response of the compound system is possible irrespective of the physical nature of the parameters and variables involved.

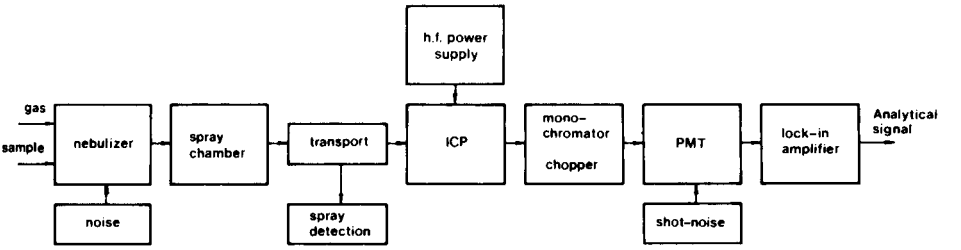

Fig. 3. Block diagram of system theoretical approach of the i.c.p.e.s. technique.

Although the i.c.p.e.s. operating conditions were kept constant, the nebulizer appeared to produce an aerosol with notable density fluctuations as was observed from the time-dependent fluctuations of the mist signal. In order to circumvent the effect of non-linearity of the nebulizer, the produced mist is considered as the input of the i.c.p.e.s. system, whereas the operating conditions are considered as parameters. For convenience, the effects of diffusion and mixing were neglected and attention was focused on delays and on the statistical properties of the fluctuations of the sample supply to the plasma and the corresponding PMT output.

The first process, i.e., transport of the nebulized sample via the torch to the plasma, was described with a delay time τ_d

$$h_1(t) = \delta(t - \tau_d) \tag{7}$$

The second process, excitation, was separated into two parallel processes describing the background and the line intensity, respectively

$$h_2(t) = \{(K_B + K_C C_i)f + B\}\delta(t) \tag{8}$$

In eqn. (8) it is assumed that variations in the emitted intensity mainly depend on variations in the quantity of test element introduced into the plasma under the experimental conditions considered (Figs. 6 and 7). Here, K_B (counts l^{-1}) expresses the change of the background intensity with the quantity of water introduced into the plasma. K_B is calculated from the experimentally established relation between the intensity of the background and the light intensity from the LED, assuming that the scattered LED light is a measure of the density of the mist stream entering the plasma. K_C (counts g^{-1}) is an excitation parameter, expressing the relation between line intensity and the mass of test element introduced into the plasma; K_C is considered constant for the sets of operating conditions employed. In the experiments, extremely dilute aqueous test solutions were introduced at varying sample flow rates, keeping the remaining i.c.p.e.s. operating parameters at pre-set fixed values. Consequently, the excitation conditions can only be changed by changing the quantities of water reaching the plasma, i.e., the sample flow rate. C_i (g l^{-1}) is the concentration of test element in the aerosol transported to the plasma, and f (l s^{-1}) is the flow rate of aerosol introduced into the plasma. B (counts s^{-1}) is the intensity of the spectral background radiation when no liquid is nebulized.

Because the average residence time of an atom or ion of a test element in

the plasma is small compared to the time delay in transporting the aerosol from the spray chamber to the plasma, the behaviour in the time domain of the emission signal can be described by a δ-function. This means that the plasma is considered as a zero-order process.

In the third process, i.e. spectral selection by the monochromator, the effects of stray light and misalignment [9] on the light intensity at the PMT are neglected. Consequently $h_3(t) = \delta(t)$. Photons reaching the detector generate electrical impulse charges which are filtered by the combined action of the termination resistor and the cable capacitance. The impulse response of this filter was described by

$$h_{4(\mathrm{PMT})}(t) = (K_1/T_{\mathrm{RC}})\exp(-t/T_{\mathrm{RC}}) \tag{9}$$

where T_{RC} is the time constant of the filter and K_1 is the gain of the PMT-resistor combination.

Shot noise originates from the random arrival of photons at the PMT, resulting in pulse distributions with uniform height and average frequency ν. The impulse response is given by the addition of a number of time-separated impulses. This means that the shot noise contribution to the fourth process ($h_{4(s-n)}(t)$) can be described by

$$h_{4(s-n)}(t) = K_1 \sum_i \delta(t - t_i) \tag{10}$$

where t_i is random time [6].

Campbell's theorem [7] states that when the average frequency of the pulses from a PMT is ν, the average component of the result, $E\{y(t)\}$, is given by $E\{y(t)\} = \nu \int_{-\infty}^{+\infty} h_{4(\mathrm{PMT})}(t)\mathrm{d}t$. For the power spectrum $P(\omega)$ of the shot-noise process,

$$P(\omega) = 2\pi\nu^2 H^2(0)\delta(0) + |H(j\omega)|^2 \tag{11}$$

where $H(\omega)$ is the Fourier transform of $h(t)$: $H(\omega) = F\{h(t)\}$. Thus, the first part of the sum in eqn. (11) represents the average component, whereas the second part is equivalent to a white noise source with an amplitude of $\nu^{1/2}$ in the time domain, filtered by a filter with the impulse response $h(t)$. The standard deviation, σ_{RV}, of such a noise source is given by $\sigma_{\mathrm{RV}} = [C(0)]^{1/2} = \nu^{1/2}\left[\int_{-\infty}^{+\infty} h(\alpha)h(t + \alpha)\mathrm{d}\alpha\right]^{1/2}$.

The supply of test element to the plasma is not a stationary process, because the number of emitting particles is a function of time. Therefore, the corresponding frequency of the pulses from the PMT, $\nu(t)$, is also a function of time, resulting in the following expressions for the average output and its variance

$$E\{y(t)\} = \int_{-\infty}^{+\infty} \nu(t)h(t - \tau)\mathrm{d}\tau = \nu(t) * h(t) \tag{12}$$

$$\sigma_y^2 = C(t_1, t_2) = \left[\int_{-\infty}^{+\infty} \nu(\tau)h(t_1 - \tau)h(t_2 - \tau)\mathrm{d}\tau\right]_{t_1 = 0,\, t_2 = 0} \tag{13}$$

$$\int_{-\infty}^{+\infty} \nu(\tau)h(-\tau)h(-\tau)\mathrm{d}\tau \tag{14}$$

The fifth process, lock-in amplifier demodulation, includes filtering with a second-order system. The impulse response of this process can be expressed by

$$h_5(t) = (tg/T_L^2)\exp(-t/T_L) \tag{15}$$

where T_L is the time constant of the filter, and g is the amplifier gain.

Because the shot noise constitutes an additional signal source, the input response was split into two parts: one describing an average output signal, to be expressed with a repeated convolution of the impulse response, and the other describing input-dependent random fluctuations. The first part, $h_I(t)$, is given by $h_I(t) = h_1(t) * h_2(t) * h_{4(PMT)}(t) * h_5(t)$ and after substituting eqns. (7), (8), (9) and (15), by

$$h_I(t) = \delta(t - \tau_d) * [\{(K_B + K_C C_i)f + B\}\delta(t)] * [(K_1/T_{RC})$$
$$\exp(-t/T_{RC})] * [(tg/T_L^2)\exp(-t/T_L)]$$

finally yielding

$$h_I(t) = [(K_B + K_C C_i)f + B]\{(K_1/T_{RC})\exp[-(t - \tau_d)/T_{RC}] * (tg/T_L^2)$$
$$\exp[-(t - \tau_d)/T_L]\} \tag{16}$$

Because in practice $T_L \gg T_{RC}$ (see Experimental), the convolution can be neglected:

$$h_I(t) = \{(K_B + K_C C_i)f + B\}K_1 g(t/T_L^2)\exp[-(t - \tau_d)/T_L] \tag{17}$$

When average values are observed, $h_I(t)$ is expressed by the static amplification factor K:

$$K = \int_{-\infty}^{\infty} h_I(t)dt = \{(K_B + K_C C_i)f + B\}K_1 g \tag{18}$$

The second part of the impulse response, $h_{II}(t)$, is subsequently subdivided into a part before and a part after shot noise is generated, i.e., in $h_{II}^{B(s-n)}(t)$ and $h_{II}^{A(s-n)}(t)$, respectively: $h_{II}^{B(s-n)}(t) = h_1(t) * h_2(t)$. After substitution of eqns. (7) and (8) this yields

$$h_{II}^{B(s-n)}(t) = \delta(t - \tau_d) * \{(K_B + K_C C_i)f + B\} \tag{19}$$

Equation (16) expresses the amount of test element entering the plasma, and so determines the average frequency of photon arrival, $\nu(t)$. On the basis of $h_{II}^{A(s-n)}(t)$, an expression for the fluctuations of the output signal can be derived (cf. eqns. 2—4):

$$C_{yy}(t) = \nu(t) * (h_{4(PMT)}(t) * h_{4(PMT)}(t)) * (h_5(t) * h_5(t)) \tag{20}$$

and, because $T_L \gg T_{RC}$, $h_{4(PMT)}(t)$ can be replaced by the static gain K_1: $C_{yy}(t) = \nu(t) * \{K_1^2(h_5(t) * h_5(t))\}$. Or when the SCF $\psi(t)$ is introduced, $C_{yy}(t) = K_1^2\nu(t) * \psi_5(t)$. After substitution of eqn. (15) this becomes

$$C_{yy} = [K_1^2 g^2 \nu(t)] * [\exp(-t/T_L)]/4T_L \tag{21}$$

yielding for the standard deviation of the output signal, σ_{yy}, the expression:

$$\sigma_{yy} = [C_{yy}(0)]^{1/2} = K_1 g[\nu(t)/4T_L]^{1/2} \quad (22)$$

Considering i.c.p.e.s., two sources causing fluctuations of the output signal were assumed, namely, shot noise and density variations in the stream of mist particles entering the plasma. The relative importance of the sources can be established by comparing the power spectrum of the PMT output with the power spectrum of the input of the aerosol. If the system is linear and the power spectra show a similar appearance, shot noise contributions are small. In that case, input fluctuations are negligible if the condition $K_B = K_C C_i$ (cf. eqn. 7) is approximated. Such a situation gives rise to flat output power spectra dominated by shot noise. It must be borne in mind, however, that the implicity assumed strong correlation between the fluctuations of K_B and $K_C C_i$ does not necessarily exist in i.c.p. excitation.

An attempt is made to cover eqn. (7) with the experimental results presented in the following paragraphs. Important features to be discussed in relation to theory are the existence of delays, the shapes of PSDs in the frequency domain, and the correlations appearing between input and output signal.

EXPERIMENTAL

Aerosol density measurement equipment

Density variations of the stream of mist particles entering the plasma were derived from intensity variations of light irradiating the aerosol. A light-emitting diode (LED) served as the radiation source (λ_{max} = 920 nm); this wavelength corresponds to the maximum of the droplet size distributions [10]. Although other methods are possible for detecting the fluctuations in the mist [11], the method used was preferred because of the size of the detector and the availability of the components. A photosensitive transistor was used for detection of the light transmitted by the mist particles. Figure 1 shows the positioning of the arrangement in the instrumental set-up; a diagram of the components used is shown in Fig. 4. The LED was 100% modulated with a square wave to avoid interference with the light of the plasma. The transistor response was demodulated using a PAR-128 lock-in amplifier; the −3 dB/45° shift frequency was 70 kHz. The amplitude of the lock-in amplifier response appeared to decrease with increasing frequency according to a first-order model. A modulation frequency of 10 kHz was used throughout the experiments. All active components were thermostatted to 30.2°C. The nebulizer was fed by a Gilson Minipuls-2 peristaltic pump. Aqueous test solutions were used, containing eight elements at various concentrations in 2% (w/v) nitric acid.

Conditions for i.c.p.e.s.

Tables 1 and 2 summarize the instrumentation and operating conditions used. Light emitted by the plasma was chopped (273 Hz) and the PMT

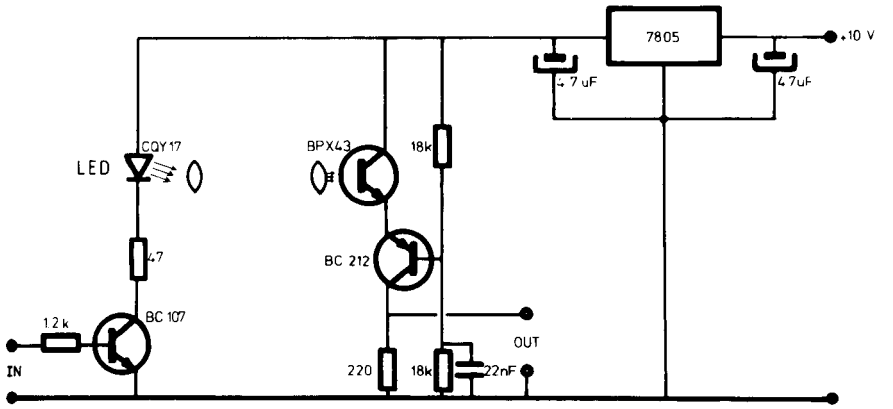

Fig. 4. Electronic circuit of the LED—detector arrangement.

response was converted to electrical tension using a 1 MΩ resistor. The cable capacitance was 160 pF, yielding a time constant of 160 μs. After amplification (PAR-118) and filtering (100—1000 Hz), the response was demodulated with a PAR-126 lock-in amplifier. The output filter was a second-order low-pass type with identical time constants of 10 ms.

Computer and software

Lock-in amplifier outputs were fed to the laboratory micro-mini-computer system consisting of the following principal components: a 12-bit A/D con-

TABLE 1

Specification of i.c.p.e.s. instrumentation

Generator	
R.f. generator	Plasma-Therm, Inc., Kresson, N.J. Model No. HSF-2000D
Frequency	27.12 MHz ± 0.05% stability
Oscillator	Electron-coupled Pierce oscillator with crystal operating at 13.56 MHz. This frequency is doubled in the oscillator plate circuit
Power output	0.5—2.0 (nominal) kW
Envelope ripple	5% maximum at 2.0 kW
R.f. output impedance	50 ohms
Coil	Three-turn, copper, water-cooled, i.d. 25 mm, elliptical 2 × 4 mm, short diameter of the ellipse along the axis of the coil
Monochromator	
Mounting	0.5-m Ebert
Grating	Aluminized replica from interferometrically ruled master on fused quartz, 2360 grooves mm^{-1} on 58 × 58 mm ruling area, 300 nm blaze
Wavelength coverage	185—450 nm
Reciprocal linear dispersion	0.8 nm mm^{-1}
Entrance and exit slit width	5—2000 μm (in this study: 10 μm)
Detector	Hamamatsu R 456 photomultiplier

TABLE 2

Operating conditions and torch assembly, external optics, and gas and sample introduction system

Sample carrier gas flow rate	0.8 l min^{-1}
Solution uptake rate	0—1.33 ml min^{-1}
Plasma gas flow rate	19 l min^{-1}
Auxiliary gas flow rate	not used
RF power output	1.1 kW
Reflected power	< 25 W
Plasma tube	18 mm i.d., concentricity[a] 0.1 mm
Auxiliary tube	13 mm i.d. reducing to 9 mm, concentricity 0.1 mm
Aerosol tube	7 mm o.d. tapered to 3.3 mm ± 0.8 mm; 1.0 mm i.d. ± 0.1 mm; non-capillary type tube
Tube material	Clear fused quartz, General Electric Type 204
Optics	Off axis, concave, focusing mirror, 3.66 magnification
Nebulizer	Cross-flow (Jarrell-Ash)
Capillaries	Glass in stainless-steel jackets
Orifice diameter	220 μm (solution and gas capillaries)

[a]The term concentricity refers to the extent to which the tubes are concentrically aligned.

verter connected to an 8080 microcomputer with 16K RAM and a V75 minicomputer (Sperry Univac). The software used was laboratory-basic interpreter (in micro) and Vortex II + TSS + real-time routines (in mini). The complete system and the software used will be described elsewhere [12].

The responses of the lock-in amplifier were sampled every 10 ms over a period of 90 s and either stored on digital cassette or directly converted to a PDF. The calculated ACVF's, CCVF's and impulse responses were based on the stored data. The maximal delay was 127 samples or 1.27 s. To estimate long-term stability, a separate recording with 2-Hz sample frequency was made. Figure 5 summarizes the calculation procedures applied, together with the computers used.

RESULTS

Evaluation of results was started by verifying whether the distribution of the recorded lock-in amplifier response and the absorption of the light irradiating the aerosol differed from the normal distribution. Probability density functions, calculated from the results obtained for various combinations of sample flow rates and analyte concentrations, indicated that the experimental distributions of mist signals and emission signals were close to normal.

Plots of sample flow rate versus mist signal and copper emission signal for concentrations of 10 μg ml^{-1} and 0 μg ml^{-1} are shown in Fig. 6. From the complete results, including all spectral lines and concentrations of the test element considered, the following properties of the plots became apparent. First, the mist signal reaches a plateau level when the sample flow rate is

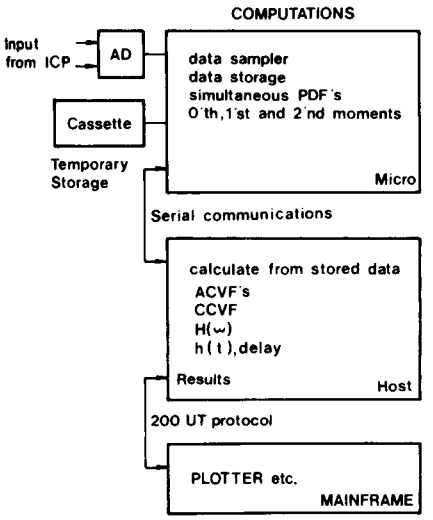

Fig. 5. Calculation procedures applied and computers used.

increased beyond 1 ml min^{-1}. Second, when the analyte concentration is relatively high, both mist signal and emission signal increase with increasing sample flow rate. Third, the emission signal (spectral background at the wavelength corresponding to the wavelength of the emission line considered) decreases with increasing flow rate of the blank solution.

Figure 7 shows the calculated direct relations between the mist signal and the emission signal at the Cu I 324.754-nm line. As can be seen, fairly straight lines resulted for all concentrations considered. The least-squares estimates are listed in Table 3. Fitting, in turn, the b values (i.e., the slopes of the lines in Fig. 7) with $b = a' + b'x$, where x is the concentration of the

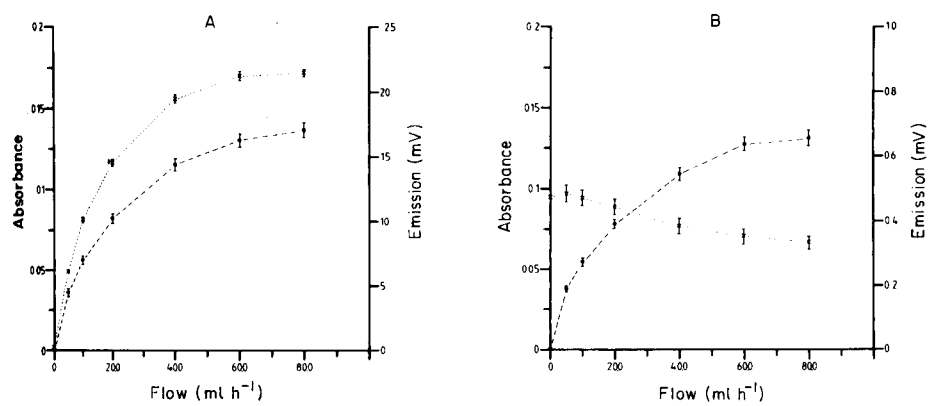

Fig. 6. Examples of the variation of emission signal (·····) and mist signal (---) as a function of sample flow rate. (A) Aqueous solution of $Cu(NO_3)_2$ in 2% (w/v) HNO_3 containing 10 μg Cu ml^{-1}; (B) 2% (w/v) HNO_3 alone. Observed spectral area corresponded to monochromator adjustment for measuring the Cu I 324.754-nm line.

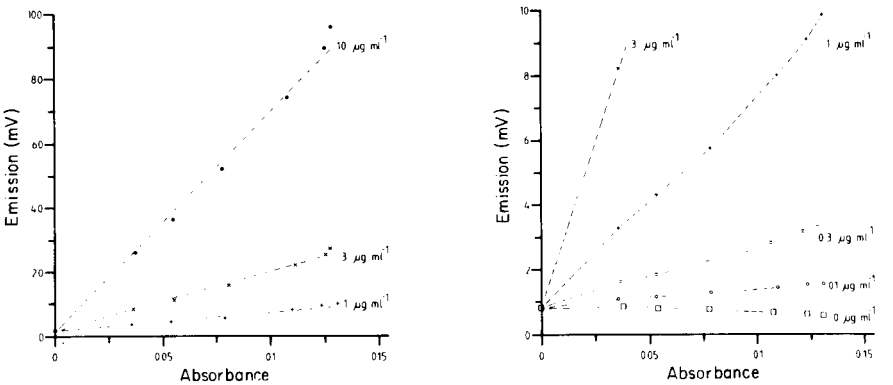

Fig. 7. Relations between the emission signal Cu I 324.754-nm line and the mist signal for various concentrations of copper. The experimental conditions were constant throughout Fig. 7, but differ from those in Fig. 6.

test element, gave the following results: $a' = -1.86$ mV, $b' = 67.7$ mV ml μg^{-1}, and $r = 0.99997$. Similar results were observed for all remaining spectral lines examined, i.e. Cu I 324.754, Cr II 267.716, Mn II 257.610 and Si I 251.611 nm.

Typical nebulizer and total system variabilities are indicated by the run sequences in Fig. 8. The data were measured at successive 10-ms intervals. It is evident that the shape of the pseudo non-random pattern, present in both diagrams, matches closely.

In order to investigate the correlation between the fluctuations of mist and emission signal, CCVFs were calculated. From the CCVFs, the delay time arising from transportation of the aerosol (cf. eqn. 6) was found to be 0.28 s (see Fig. 9). For different sample flow rates but fixed test element concentrations, equal CCVF non-zero values were found for $t = 0.28$ s.

The standard deviation of the emission signal, $[ACVF_{yy}(0)]^{1/2}$ appeared to be dependent on the concentration of the test element. As an example,

TABLE 3

Least-squares estimates of the relation between the mist signal and the emission signal (Cu I 324.754 nm). Unweighted estimates of $y = a + bx$, where x = mist signal (extinction) and y = emission signal (mV)

Concentration (μg ml^{-1})	Range of sample flow rate (ml min^{-1})	No. of measure-ments	a (mV)	b (mV)	Linear correlation coefficient
10	0—1	6	1.508	675.6	0.9978
3	0—1	6	0.286	198.3	0.9972
1	0—1.333	7	0.742	67.69	0.9976
0.3	0—1.333	7	0.888	18.25	0.935
0.1	0—1.333	7	0.861	5.41	0.9935
0	0—1.333	7	0.866	−1.81	−0.929

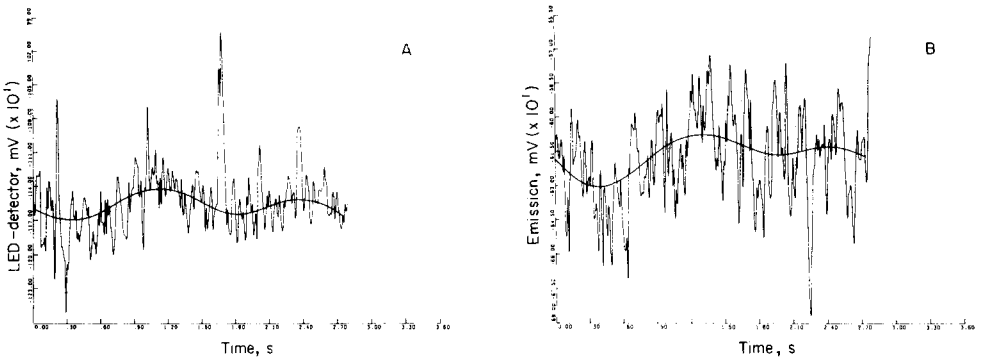

Fig. 8. Run-sequence plots measured at 10 ms intervals of (A) the mist signal and (B) the corresponding Cu I 324.754-nm emission signal.

numerical values pertaining to the Cu I 324.754-nm spectral line are listed in Table 4.

Long-term stability measurements were used as input to a program [8] yielding the standard deviation of the integrated signal as a function of the integration time. Results are shown in Fig. 10, from which the minimum integration times required to satisfy pre-set variances can be easily derived: $\sigma_T = (\sigma_I^2/T)^{1/2}$, where σ_T is the maximal acceptable variance, σ_I^2 is the variance of the integrated signal, and T is the integration time.

For a sample flow rate of 1 ml min^{-1}, the power spectra of the fluctuations of the mist and emission signals were calculated by applying a Fourier transformation to the corresponding ACVFs. The power spectra of the mist signal fluctuations showed an $f^{-1/2}$ character in the frequency range 0.1—30 Hz. Examples of results are shown in Fig. 11. The power spectra of the

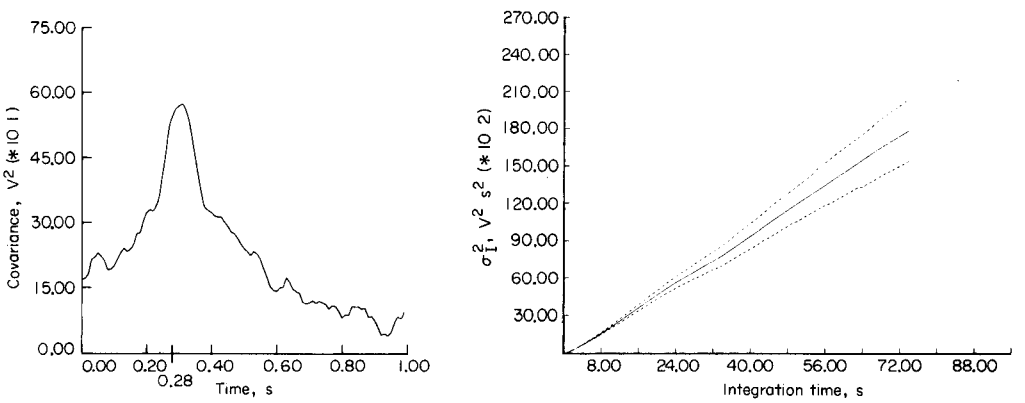

Fig. 9. Example of a CCVF, calculated from mist signal and corresponding emission signal (Cu I 324.754 nm; 10 μg Cu ml^{-1}), showing a maximal correlation corresponding to a delay of 0.28 s.

Fig. 10. Variance of integrated emission signal (σ_I^2) as a function of integration time (Cr II 267.716 nm; 10 μg Cr ml^{-1}). The dashed curves show 90% confidence intervals.

TABLE 4

Standard deviation of the emission signal as a function of the concentration of the test element (Cu I 324.754), at a sample carrier flow rate of 1 ml min^{-1}

Conc. ($\mu g\ ml^{-1}$)	10	3	1	0.3	0.1	0
S.d. (mV)	41.2	11.1	3.8	1.25	0.59	0.37

emission signal fluctuations calculated for all test element concentrations considered are: 0 $\mu g\ ml^{-1}$, 0.1 $\mu g\ ml^{-1}$, 1 $\mu g\ ml^{-1}$, and 10 $\mu g\ ml^{-1}$. The power spectrum of the emission signal related to the test element concentration of 0.1 $\mu g\ ml^{-1}$ showed an $f^{-1/4}$ character, whereas the remaining spectra displayed a character similar to the spectrum of the mist signal fluctuations. From the power spectra obtained, impulse responses were calculated using eqn. (6). Results are presented in Fig. 12.

DISCUSSION AND CONCLUSIONS

Because the relations depicted in Fig. 7 are almost linear, and because the emission signals are proportional to the amount of analyte introduced into the plasma, an important conclusion can be drawn. The absorbance of the LED radiation by the mist particles appears to be an excellent measure of the amount of material entering the plasma. The linearity of the relations is illustrated by Table 3. This demonstrates the general validity of eqn. (8); the linearity of this equation is demonstrated by the proportionality of concentrations (Table 3) and slopes of the plots in Fig. 7.

The calculated CCVFs showed that a delay of 0.28 s occurred between a variation in the density of the mist and the corresponding variation in the emission signal. This delay is easily derived from the maximum value of the

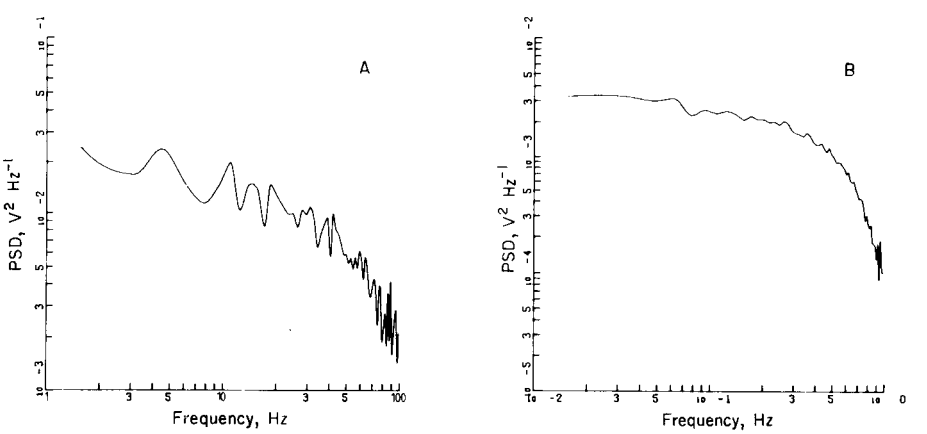

Fig. 11. Power spectral density functions of the variations of the mist signal for various sampling conditions: (A) 10000 samples measured at 10-ms intervals; (B) 5000 samples measured at 500-ms intervals.

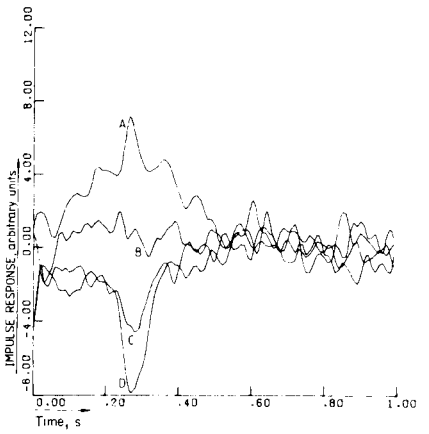

Fig. 12. Impulse response functions of i.c.p.e.s. considering mist and emission signals as input and output signal, respectively. Curves A, B, C and D correspond to blank, 0.1, 1 and 10 μg Cr ml^{-1}, respectively.

CCVF in Fig. 9. Besides, the value of the CCVF was related to the slopes of the lines in Fig. 7. Essentially, these features create the possibility of correcting the emission signal by means of the mist signal.

The variations of the mist signal are conveniently described in the frequency domain by the PSD, showing a behaviour proportional to $f^{-1/2}$ between 0.1 and 30 Hz (see Figs. 8 and 11). The variations of the emission signal can be described in the same fashion and show a PSD of identical shape in most cases. This correspondence of shape is shown by mist and emission signals originating from solutions containing analyte concentrations of 10, 3, 1, 0.3, or 0 μg ml^{-1}, whereas the PSDs of mist and emission signals originating from a solution containing the analyte at 0.1 μg ml^{-1}, are described properly with $f^{-1/2}$ and $f^{-1/4}$, respectively.

Because the PSD of the emission signal can be described by $f^{-1/2}$ down to 0.1 Hz (see Fig. 11), no significant improvement of precision can be anticipated from electronic filtering procedures if applied to the i.c.p. instrumentation considered.

As shown in Table 4, the standard deviation of the emission signal increases with increasing analyte concentrations. In the concentration range beyond 0.3 μg ml^{-1} the relation is proportional. This should be borne in mind when minimum integration periods are derived from the equation $\sigma_T = (\sigma_I^2/T)^{1/2}$ [4].

When the i.c.p. is used as a detector in, e.g., chromatography, it is tempting to use baseline-correcting procedures to remove the slow random fluctuations in the assumed baseline. However, because a non-zero correlation exists between the origin of the baseline fluctuations and the fluctuations in the analytical signal (eqn. 8), demodulation will yield better results. Nevertheless, if baseline corrections are used, integrating techniques must be mistrusted because the fluctuations superimposed on peak-shaped signals constitute a non-stationary signal.

The correlations between the mist signal and the emission signal make it possible to predict fluctuations in the output signal, if the fluctuations in the sample stream are known. Another potential application of the noise analysis could lie in improving the precision of the method by optimum filtering procedures.

Research is now under way to provide a complete prescription usable for improving the precision of i.c.p.e.s., and to indicate the limitations of the proposed corrections.

The authors thank Mr. J. Bosmeyer for his contribution to the development of the aerosol density measurement equipment, Mr. A. van de Werve for calculating the variance functions, and Ir. P. J. H. Scheeren for many useful discussions.

REFERENCES

1 R. M. Barnes, CRC Crit. Rev. Anal. Chem., 7 (1978) 203.
2 S. Greenfield, H. M. McGeachin and P. B. Smith, Talanta, 22 (1975) 1, 553; 23 (1976) 1.
3 R. K. Winge, V. A. Fassel, R. M. Knisely, E. DeKalb and W. J. Haas Jr., Spectrochim. Acta, Part B, 32 (1977) 327.
4 F. J. M. J. Maessen and J. Balke, Int. Winter Conf. Developments in Atomic Plasma Spectrochemical Analysis, Puerto Rico 1980, Paper No. 84.
5 C. Th. J. Alkemade, in J. A. Dean and T. C. Rains (Eds.), Fundamental Aspects of Decomposition, Atomization, and Excitation of the Sample in the Flame, Flame Emission and Atomic Absorption Spectrometry, Vol. I Theory, M. Dekker, New York, 1969, p. 101.
6 A. Papoulis, Probability, Random Variables and Stochastic Processes, McGraw-Hill, New York, 1965.
7 P. M. E. M. van der Grinten and J. M. H. Lenoir, Statistische Procesbeheersing, Het Spectrum, Utrecht, 1973, p. 84.
8 R. P. J. Duursma and H. C. Smit, Anal. Chim. Acta, 133 (1981) 67.
9 P. W. J. M. Boumans, Spectrochim. Acta, Part B, 35 (1980) 57.
10 M. S. Cresser and R. F. Browner, Spectrochim. Acta, Part B, 35 (1980) 73.
11 E. Kranz, Spectrochim. Acta, Part B, 27 (1972) 327.
12 R. P. J. Duursma, H. Steigstra, R. G. Logchies and H. C. Smit, Anal. Chim. Acta (CTO), in press.

Analytica Chimica Acta, 133 (1981) 409—419
Computer Techniques and Optimization
Elsevier Scientific Publishing Company, Amsterdam — Printed in The Netherlands

THE EFFECT OF SAMPLE MATRIX ON SELECTION OF OPTIMUM TIMING PARAMETERS IN CYCLIC NEUTRON ACTIVATION ANALYSIS

R. E. TOUT and A. CHATT*

Trace Analysis Research Centre, Department of Chemistry, Dalhousie University, Halifax, Nova Scotia, B3H 4J1 (Canada)

(Received 20th August 1980)

SUMMARY

Cyclic instrumental neutron activation analysis can be used to improve detection limits for short-lived nuclides. The detection limit for a given nuclide is a function of the activity arising from the sample matrix and the various timing parameters used in the analysis. An easily operated computer program, based on the cyclic activation equation, has been developed to estimate theoretically the optimum timing parameters for a number of short-lived nuclides in four different types of simulated sample matrix. The computed results are discussed with reference to the change in maximum sensitivity when optimum conditions are not used, and a comparison is made with the experimentally determined results for the measurement of selenium in NBS Bovine Liver.

During the last few years, the cyclic instrumental neutron activation (c.i.n.a.) technique has been added to the conventional instrumental nuclear activation procedures in a small number of nuclear analytical laboratories, principally to improve the sensitivities and detection limits of elemental measurements by short-lived nuclides. Applications [1—4] of c.i.n.a. include the use of the following short-lived nuclides: ^{20}F ($t_{1/2}$ = 11 s), ^{46m}Sc (20.0 s), ^{77m}Se (17.5 s), ^{179m}Hf (18.6 s) and ^{207m}Pb (0.8 s). There are no alternative long-lived thermal neutron activation products for the determination of certain elements, such as fluorine and lead. However, even when such alternatives do exist, e.g. ^{46}Sc (84 d), ^{75}Se (120.4 d) and ^{181}Hf (42.5 d), the use of the short-lived nuclide has the obvious advantage of a reduction in total experimental time [5]. Several methods have been described for calculating optimum and near-optimum c.i.n.a. conditions to obtain the maximum number of counts under a given photopeak [6—9].

In order to use a c.i.n.a. system at its optimum efficiency, a computer simulation study was initiated. The objectives of this study were: (a) to determine the optimum timing parameters (times of irradiation, decay, counting and transfers) for a given element in a specific type of sample matrix: (b) to evaluate the variation of timing parameters with changes in sample matrix; and (c) to predict the optimum timing parameters for simultaneous determination of several short-lived nuclides in a sample matrix.

Preliminary results have been abstracted [10]. Detailed descriptions of the computer program, experiments and results are given below.

THEORETICAL CONSIDERATIONS

The c.i.n.a. technique involves repeated cycling of a sample between the irradiation and counting positions. The measured activity is accumulated by the analyzer system. Because of the build-up in residual activity of the short-lived nuclides from each successive irradiation segment of the cycle, each counting period produces an increased contribution to the detector signal from the nuclide of interest. At the same time the background activity from long-lived nuclides in the sample increases at an approximately linear rate. A detailed account of the theory of c.i.n.a. has been reported by Spyrou and Kerr [11]. An expression for the cumulative detector response (D_c), for a nuclide after n cycles of irradiation and counting periods, can be derived from the detector response (D_1) of the first cycle. Thus from $D_1 = N\sigma\phi\epsilon I \lambda^{-1} (1 - e^{-\lambda t_i}) (e^{-\lambda t_d}) (1 - e^{-\lambda t_c})$, it can be shown that

$$D_c = N\sigma\phi\epsilon I\lambda^{-1} (1 - e^{-\lambda t_i}) (e^{-\lambda t_d}) (1 - e^{-\lambda t_c}) [n(1 - e^{-\lambda T})^{-1} - e^{-\lambda T} (1 - e^{-n\lambda T}) (1 - e^{-\lambda T})^{-2}]$$

where N is the number of target nuclei in sample, σ the reaction cross-section, ϕ the neutron flux, ϵ the efficiency of the detector, λ the decay constant, I the number of γ-rays per disintegration, t_i the length of each irradiation period, t_d the time between end of irradiation and start of counting period, and t_c the length of each counting period; $T = t_i + t_d + t_c + t_{d'}$ where $t_{d'}$ is the time between end of counting and start of next irradiation period. These timing parameters are illustrated in Fig. 1.

The significance (S) of a peak of accumulated counts (D_p) in a γ-ray spectrum is generally (because of counting statistics) taken as proportional to the square root of the number of background counts (D_b) under the peak, i.e. $S = kD_pD_b^{-1/2}$, where k is a proportionality constant. For m number of nuclides contributing to D_b, the expression for S becomes:

$$S = kD_p \left(\sum_{b=1}^{m} D_b \right)^{-1/2}$$

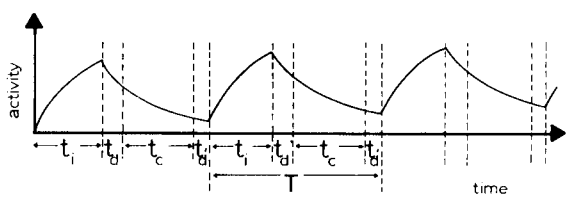

Fig. 1. Timing parameters in c.i.n.a.

Thus S for a particular photopeak of a given short-lived nuclide in a sample can be evaluated from the calculation of D_p, and the component of D_b by using the cyclic activation equation. A computer program has been developed to determine S and its maximum attainable value (S_{max}).

PROGRAM DESCRIPTION AND APPLICATION

The cyclic optimization program is written in FLEXTRAN [12] and is run on a PDP 11/05 minicomputer, through an interactive terminal. After initialization, the program goes through an interrogation sequence in which it requests the following information: total experiment time, the initial values of t_i, t_d, t_c and $t_{d'}$, and the number of elements in the sample matrix to be included in the calculation of D_b. The mass of each element (nuclide) contributing to the background activity, and their relevant nuclear data, then have to be entered by the operator. Since the objective is to determine only the timing parameter that will produce S_{max} and not the absolute value of S, the only parameter required for the nuclide of interest is its decay constant, λ.

After this information has been completed, the program calculates an integer value of n from the given value of total experiment time and the various components of T. A value proportional to S obtained at the end of such a simulated experiment is evaluated for each nuclide contributing to the background activity, and then for the matrix as a whole. The values of t_i and t_c are then incremented by one second (or by any other predetermined quantity of time) and the calculations are repeated. The magnitudes of S for each nuclide contributing to the background can thus be compared and those with minimal contribution are eliminated from further computations. The calculation of S for the combined background effect and its variation over a given range of t_i and t_c determine the timing parameters which produce S_{max}. Two practical limitations prevent the highest theoretical value of S being obtained in any cyclic activation system. Although S always increases with increasing total experimental time, the rate of increase of S diminishes (see Fig. 2) until a point is reached at which the small increase in S with each cycle does not warrant the additional experiment time. Thus one limitation is a practicable total experimental time per sample, i.e. the time from the start of the first irradiation to the end of the last counting period ($nT - t_{d'}$). For a given total time, it can be seen from the cyclic activation equation that D_p is maximized if $t_d = t_{d'} = 0$ and $t_i = t_c = T/2$. Zero values of t_d and $t_{d'}$ are not attainable in a real system, so that the finite transfer time from irradiation to counting position and back, is the second practical limitation which must be considered so that the computer-based experiments produce results comparable to those of a real system.

The results obtained from the computer program described above were produced in order to make the most efficient use of the Dalhousie SLOWPOKE cyclic activation system [13]. The most reliable transfer time of this system is of the order of one second, and this is the value used for t_d and $t_{d'}$ in this

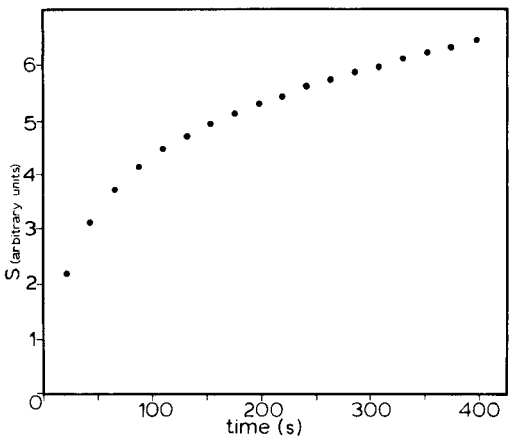

Fig. 2. Variation of S with total experimental time for determining ^{77m}Se in a simulated coal matrix (conditions: $t_i = t_c = 10$ s and $t_d = t_{d'} = 1$ s).

work unless otherwise stated. The total time used for all computations was 300 s. This is an arbitrary value; but for short-lived nuclides ($t_{1/2} < 25$ s) and $t_i = t_c \approx t_{1/2}$, at the end of 300 s the rate of increase in S with additional cycles is relatively small. A 300-s time is also consistent with the aim of a high sample through-put.

The four simulated sample matrices used here are based on four standard reference materials (SRM) supplied by the U.S. National Bureau of Standards (NBS): Bituminous Coal (SRM 1632a), Sub-bituminous Coal (SRM 1635), Bovine Liver (SRM 1577) and Orchard Leaves (SRM 1571). The elemental concentrations of the SRM were taken from the NBS certificates of analysis [14—17] and from the literature [18], and the related nuclear parameters from appropriate tables [19, 20].

RESULTS AND DISCUSSION

The computer-predicted rate of increase in the significance of the selenium signal at the 162-keV peak of ^{77m}Se in a simulated SRM 1632a coal matrix is shown in Fig. 2. It can be seen that the largest increases in the value of S occur during the first 100 s of the experiment and that the rate of increase in S is reduced substantially before a total time of 300 s is reached. Doubling the total time from 300 to 600 s results only in a predicted increase in S of less than 23%.

The nuclides considered to be contributing to the background activity in each of the simulated matrices described above are listed in Table 1, in order of increasing contribution to the total matrix effect. It is evident that ^{28}Al produces the greatest background contribution in all four matrices. Figure 3 shows the variation of S with t_i and t_c for ^{77m}Se in a matrix containing the appropriate amounts of Al, V and Mn present in SRM 1635 coal. The

TABLE 1

Nuclides contributing to background activity of different sample matrices

Computer-simulated matrix	Contribution to background activity
SRM 1571	$^{37}S < {}^{139}Ba < {}^{66}Cu < {}^{80}Br < {}^{24}Na < {}^{86m}Rb < {}^{32}P < {}^{42}K < {}^{38}Cl < {}^{27}Mg < {}^{49}Ca < {}^{56}Mn < {}^{28}Al$
SRM 1577	$^{42}K < {}^{27}Mg < {}^{56}Mn < {}^{66}Cu < {}^{32}P < {}^{24}Na < {}^{38}Cl < {}^{28}Al$
SRM 1632a	$^{38}Cl < {}^{66}Cu < {}^{56}Mn < {}^{52}V < {}^{28}Al$
SRM 1635	$^{24}Na < {}^{66}Cu < {}^{56}Mn < {}^{52}V < {}^{28}Al$

contribution of ^{28}Al to the background is so great that the variation of S with a background resulting from ^{28}Al alone is indistinguishable from the combined effect of all other nuclides. Similar results were obtained for the matrix based on SRM 1632a coal with an aluminium content about 10 times greater than the SRM 1635 coal.

Although ^{28}Al is the single largest contributor to background activity in the Bovine Liver and Orchard Leaves simulated matrices (Table 1), its concentration is not so high that contributions from other nuclides can be ignored. In Fig. 4 the variation of S with t_i and t_c is shown for the detection of ^{77m}Se in a Bovine Liver matrix composed of Al, Cl, Na, P and Cu; values of S are plotted for the individual nuclides as well as the matrix as a whole. Figure 4 shows that S_{max} can be attained with integer values of t_i and t_c equal to either 12 or 13 s. It is also evident that the peaks are relatively broad and

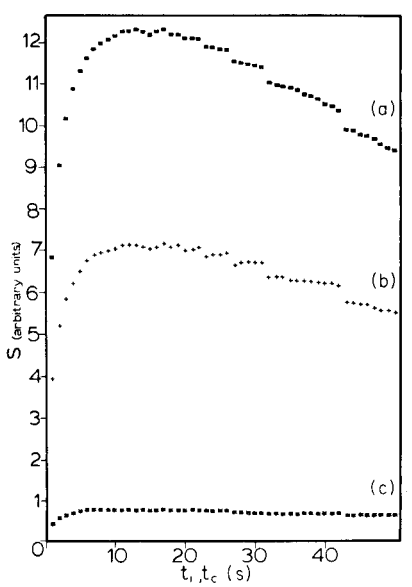

Fig. 3. Optimization of S with t_i and t_c for measuring ^{77m}Se in a simulated coal matrix (SRM 1635). (a) Mn background; (b) V background; (c) Al and total background.

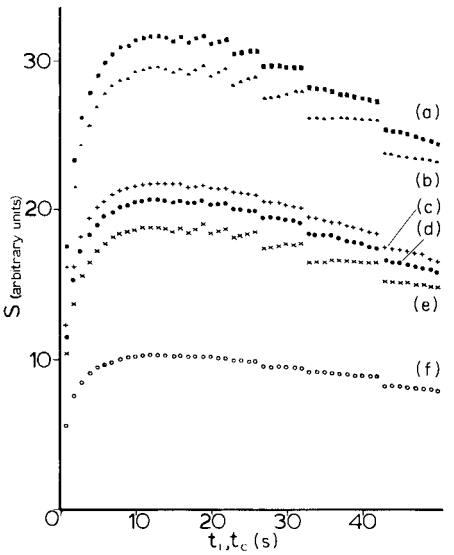

Fig. 4. Optimization of S with t_i and t_c for detecting ^{77m}Se in a simulated liver matrix (SRM 1577). (a) Cu background; (b) P background; (c) Na background; (d) Cl background; (e) Al background; (f) total background.

that values of S close to S_{max} can be produced by a range of values of t_i and t_c. In quantitative terms, for the detection of ^{77m}Se in the simulated Bovine Liver matrix, the computer results predict that a value of S greater than 90% of S_{max} could be obtained by using values of t_i and t_c in the range 5—32 s.

In order to evaluate the agreement between computer-predicted results and the experimental situation, three samples (1 g each) of Bovine Liver were analysed for selenium using the Dalhousie SLOWPOKE cyclic activation system; values for $t_i = t_c$ of 5, 12 and 32 s, and for $t_d = t_{d'} = 1$ s, were used. The resulting significance of the 162-keV γ-ray of ^{77m}Se was determined relative to the value obtained for t_i and t_c equal to 12 s; the results are shown in Table 2. There is good agreement as the experimental values differ from the computed results by 5% or less.

TABLE 2

Comparison of computer-predicted and experimentally determined significance values for detecting the 162-keV peak of ^{77m}Se

Significance ratio	Predicted	Experimental
$S(t_i = t_c = 5\text{ s})/S(t_i = t_c = 12\text{ s})$	0.91	0.86
$S(t_i = t_c = 32\text{ s})/S(t_i = t_c = 12\text{ s})$	0.94	0.90

The predicted optimum values of t_i and t_c for a number of short-lived nuclides of interest in c.i.n.a. are listed in Table 3 for the simulated sample matrices of Bovine Liver, Orchard Leaves and Coal (^{28}Al background only). It can be seen that many of the optimum predicted times for t_i and t_c are common to the three types of matrix; and even where there is not an exact agreement the differences in the resulting value of S, if the optimum timing parameters predicted for another matrix are used, are minimal. For example, the optimum value of t_i and t_c for ^{77m}Se in Bovine Liver is calculated as 12 or 13 s, while for Orchard Leaves and Coal these values are 19 s. The change in S if t_i and t_c for the Bovine Liver are equated to 19 s is a reduction in S_{max} of less than 1%. Similarly, the contributions from the individual nuclides to the background show that approximately the same optimum value of t_i and t_c is required for each nuclide as that necessary because of the total background effect. This can be seen (Table 4) in the optimum values of t_i and t_c required for the detection of silver using the nuclide ^{110}Ag ($t_{1/2}$ = 24.5 s) in the simulated Bovine Liver matrix. Thus, effectively the optimum t_i and t_c values could have been obtained by approximating the background activity to just one longer-lived nuclide, even if that nuclide has a half-life as short as 2.3 min (^{28}Al). Hence, if the half-life of the nuclide of interest is less than 0.18 of that of the shortest-lived nuclide producing a major contribution to the background (0.18 is the ratio of half-lives of ^{110}Ag to ^{28}Al,

TABLE 3

Optimum timing parameters for several short-lived nuclides and effect of changes in timing parameters on significance values

Computer-simulated matrix	Nuclide	$t_{1/2}$ (s)	Optimum value of t_i and t_c (s)	90% S_{max} range of t_i and t_c (s)	% Reduction in S_{max} if $t_i = t_c = t_{1/2}$
SRM 1571	^{183m}W	5 3	6	3—12	1.2
	^{77m}Se	17.5	19	5—32	2.0
	^{179m}Hf	18.6	19	5—32	0
	^{110}Ag	24.5	19	6—42	1.5
	^{75m}Ge	49	42	10—>99	5.3
SRM 1577	^{183m}W	5.3	6	3—12	1.1
	^{77m}Se	17.5	12 or 13	5—32	0.8
	^{179m}Hf	18.6	19	5—34	0
	^{110}Ag	24.5	19	6—42	1.4
	^{75m}Ge	49	42	10—>99	5.0
SRM 1632a[a]	^{183m}W	5.3	6	3—12	1.3
	^{77m}Se	17.5	19	5—32	1.2
	^{179m}Hf	18.6	19	6—32	0
	^{110}Ag	24.5	19 or 22	6—42	1.5
	^{75m}Ge	49	59	11—>99	6.2

[a]Al background.

TABLE 4

Optimum value of t_i and t_c for detecting ^{110}Ag in Bovine Liver

Nuclide contributing to background	Optimum value of t_i and t_c	Nuclide contributing to background	Optimum value of t_i and t_c
^{28}Al	19 or 22	^{32}P	19 or 22
^{38}Cl	19	^{66}Cu	19
^{24}Na	19	Total background[a]	19

[a]From these 5 nuclides.

the worst case in this study), the matrix effect can be well approximated as resulting from just that one major contributing nuclide. Since ^{28}Al (even at its low concentration of 35.5 μg g^{-1} in Bovine Liver) would appear to be the major background activity for various matrix types, and since the nuclides under investigation by c.i.n.a. generally have $t_{1/2} < 25$ s, the one nuclide background approximation can be made for all optimization computations. The values of ϵ, I and σ can thus be included in the proportionality constant; therefore, the only data required are λ for the nuclide of interest, and λ for the background nuclide which as explained above can be almost any value (even up to that of ^{28}Al). Thus optimum time parameters can be evaluated without reference to a specific detector, a particular type of elemental composition and with only two pieces of nuclear data of which only one has to be accurately known.

Table 3 shows that the magnitude of the range over which $S \geqslant 90\%\ S_{max}$ decreases as the half-life of the nuclide decreases. For example, the 90% S_{max} range for ^{77m}Se ($t_{1/2}$ = 17.5 s) in simulated Bovine Liver matrix is 5—32 s while the range is 3—12 s for ^{183m}W ($t_{1/2}$ = 5.3 s) in the same matrix. Thus, the shorter the half-life of the nuclide of interest (comparison with those of the background nuclides), the more unimportant the matrix composition becomes; however, the range of the near-optimum timing parameters is considerably reduced, which means that t_i and t_c must be chosen with great accuracy. The variation of the optimum values of t_i and t_c and the range of 90% S_{max} for nuclides with half-lives between 1 and 22 s in a simulated Bovine Liver matrix are shown in Fig. 5. It can be seen that the optimum value of t_i and t_c initially increases in direct proportion to the increase in half-life; however, for $t_{1/2}$ = 10—17 s and for $t_{1/2}$ = 18—22 s the optimum values of t_i and t_c remain almost constant. This step-like variation is also present in the plot of S with t_i and t_c (e.g., in Fig. 4 and to a lesser extent in Fig. 6). This is a result of the integer value of n, which means that although the total experimental time is designated as 300 s, it usually has to be slightly larger or smaller to accommodate a whole number of cycles. Even though the integer value of n results in a step-like variation in the optimum timing parameters that will produce S_{max}, the variation of S_{max} with increasing half-life is smooth (Fig. 7). Moreover, for all nuclides with

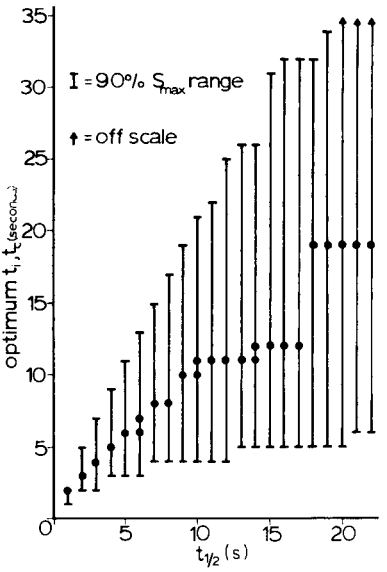

Fig. 5. Variation of optimum t_i and t_c for nuclides with $t_{1/2}$ between 1 and 22 s in a simulated liver matrix (SRM 1577).

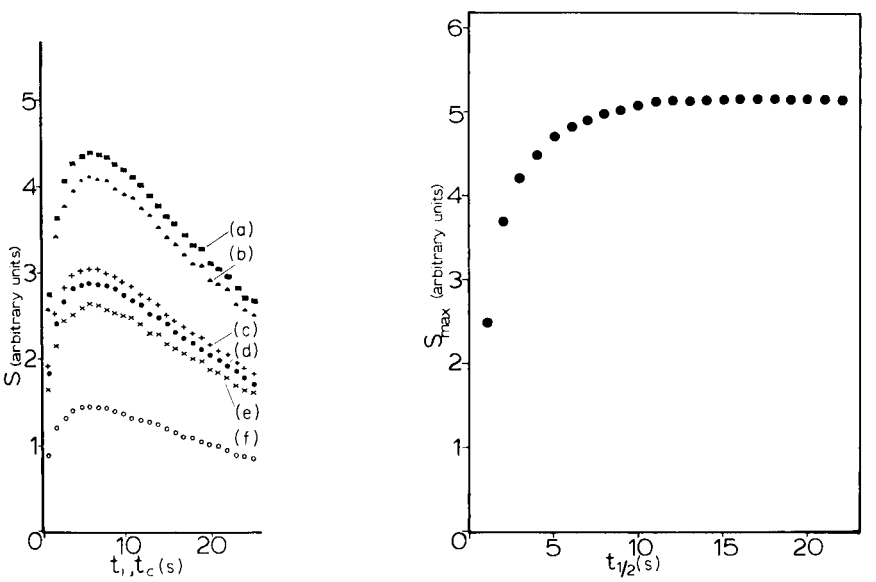

Fig. 6. Optimization of S with t_i and t_c for detecting ^{183m}W in a simulated liver matrix (SRM 1577). Curves (a–f) have the same meaning as in Fig. 4.

Fig. 7. Variation of S_{max} with $t_{1/2}$ of nuclides.

half-lives ranging from 13 to 22 s (or possibly more), the computer program predicts that S_{max} will be approximately constant (if the nuclear parameters of the nuclides are similar) with only a 0.26% deviation from its largest value.

Although the optimum timing parameters for the range of half-lives shown in Fig. 5 have been calculated for a simulated Bovine Liver matrix, from the results presented above (i.e., widely different matrix activities can be approximated to one background nuclide) it should be clear that these parameters can also be applied in the analysis of all samples except any which may have a very significant background contribution from a nuclide with a half-life less than that of ^{28}Al. When data are extracted from Fig. 5, it must be noted that the condition of $t_d = t_{d'} = 1$ s has been used. Changes in the optimum value of t_i and t_c for ^{77m}Se in a simulated Bovine Liver matrix as a function of t_d and $t_{d'}$ are shown in Table 5.

Figure 7 shows that the 90% S_{max} increases at a greater rate than either half-life or optimum time parameters (so that t_i and t_c have to be known accurately only for nuclides of comparatively short half-life); Fig. 7 also indicates that a single value of t_i and t_c can be chosen to produce results close to S_{max} for nuclides with a large range of half-lives. It can be seen from Fig. 5 that $t_i = t_c = 6$ or 7 s will produce values of $S \geqslant 90\%\ S_{max}$ for half-lives in the range 3—22 s (or possibly more). This means that for nuclides within this range of half-lives only one c.i.n.a. experiment is needed to produce close to optimum results for all short-lived nuclides of interest.

Figure 7 provides a guide to the value of optimum timing parameters for the c.i.n.a. measurement of short-lived nuclides. However, this study also shows that a "general rule-of-thumb" equating t_i and t_c to the half-life of the nuclide of interest will produce values of S close to S_{max}. From Table 3 it can be seen that by following this rule, the deviation of S from S_{max} is less than 2% for nuclides with $t_{1/2} < 25$ s.

Conclusions

Computer-based experiments have shown that for the determination of short-lived nuclides ($t_{1/2} < 25$ s) by c.i.n.a., the individual matrix effects due to the major constituents of a sample are not important in determining the optimum timing parameters. Also, a number of short-lived nuclides can be studied at close to their best detection limits by only using one set of c.i.n.a.

TABLE 5

Changes in optimum t_i and t_c with variations in t_d and $t_{d'}$ for determining ^{77m}Se in Bovine Liver

Value of t_d and $t_{d'}$	Optimum value of t_i and t_c	Value of t_d and $t_{d'}$	Optimum value of t_i and t_c	Value of t_d and $t_{d'}$	Optimum value of t_i and t_c
0.5	12	2.0	18	3.5	20
1.0	12	2.5	19	4.0	23
1.5	16	3.0	19		

timing parameters. The agreement between the computer-predicted results and the experimental results was within 5% for ^{77m}Se in Bovine Liver.

The authors acknowledge the cooperation of the Operations Group, Dalhousie University SLOWPOKE-2 Reactor, with irradiations. This research was supported by a research operating grant (A-9977) and a strategic grant (G-0054) from the Natural Sciences and Engineering Research Council of Canada.

REFERENCES

1 S. A. Kerr and N. M. Spyrou, J. Radioanal. Chem., 44 (1977) 159.
2 A. Chatt and K. N. DeSilva, Proc. 4th Int. Conf. Nucl. Meth. Environ. Energy Res., University of Missouri-Columbia, U.S.A., 1980, in press.
3 A. Egan and N. M. Spyrou, Anal. Chem., 48 (1976) 1959.
4 A. Egan, S. A. Kerr and M. J. Minski, Radiochem. Radioanal. Lett., 28 (1977) 369.
5 R. E. Tout and A. Chatt, Anal. Chim. Acta, 118 (1980) 341.
6 J. Janczyszyn and L. Gorski, Radiochem. Radioanal. Lett., 8 (1971) 297.
7 Y. Maki and T. Nojiri, Radioisotopes, 27 (1978) 27.
8 S. J. Gage, G. D. Atkinson, Jr. and G. D. Bouchey, Nucl. Technol., 17 (1973) 247.
9 H. Tominaga and N. Tachikawa, Radiochem. Radioanal. Lett., 37 (1979) 55.
10 R. E. Tout and A. Chatt, Trans. Am. Nucl. Soc., 33 (1979) 233.
11 N. M. Spyrou and S. A. Kerr, J. Radioanal. Chem., 48 (1979) 169.
12 F. H. Shamber, Flextran, Tracor Northern, Wisconsin, U.S.A. (1975).
13 A. Chatt, K. N. DeSilva, J. Holzbecher, D. C. Stuart, R. E. Tout and D. E. Ryan, Can. J. Chem., (1981) accepted for publication.
14 NBS Certificate of Analysis, SRM 1571, Orchard Leaves, Washington, DC, 1976.
15 NBS Certificate of Analysis, SRM 1577, Bovine Liver, Washington, DC, 1977.
16 NBS Certificate of Analysis, SRM 1632a, Bituminous Coal, Washington, DC, 1978.
17 NBS Certificate of Analysis, SRM 1635, Subbituminous Coal, Washington, DC, 1978.
18 R. A. Nadkarni and G. H. Morrison, J. Radioanal. Chem., 43 (1978) 347.
19 C. M. Lederer, J. M. Hollander and I. Perlman, Table of Isotopes, 6th edn., Wiley, New York, 1967.
20 F. Adams and D. Dams, Applied Gamma-ray Spectrometry, Pergamon Press, Oxford, 1970.

Analytica Chimica Acta, 133 (1981) 421—431
Computer Techniques and Optimization
Elsevier Scientific Publishing Company, Amsterdam — Printed in The Netherlands

COMPUTER-AIDED MEASUREMENT OF KINETIC PARAMETERS OF ELECTRODE REACTIONS OF COBALT(III)—AMMINE COMPLEXES AT MERCURY ELECTRODES

A. YAMADA,* T. YOSHIKUNI, Y. KATO and N. TANAKA
Department of Chemistry, Faculty of Science, Tohoku University, Sendai 980 (Japan)
(Received 20th August 1980)

SUMMARY

A computer-aided technique based on Tast polarography is examined for the determination of kinetic parameters of electrode reactions. It is particularly useful for the investigation of unstable species because of the simple and rapid processing of data. Kinetic parameters of cobalt(III)—ammine complexes at mercury electrodes are given for $[Co(NH_3)_6]Cl_3$, $[Co(H_2O)(NH_3)_5](ClO_4)_3$, $[Co(NO_3)(NH_3)_5](NO_3)_2$, $[CoF(NH_3)_5](ClO_4)_2$, $[Co(CO_3)(NH_3)_5]NO_3$, *cis*-$[Co(H_2O)_2(NH_3)_4](ClO_4)_3$, $[Co(CO_3)(NH_3)_4]NO_3 \cdot 0.5H_2O$, $[Co(ox)(NH_3)_4]Cl \cdot H_2O$, and $NH_4[Co(ox)_2(NH_3)_2] \cdot H_2O$, which are obtained in solutions containing 0.1 M acetate buffer and 0.005% gelatin at 25°C.

During the past ten years, several kinetic parameters of electrode reactions have been reported [1] with a variety of methods of measurement. Most of the kinetic parameters have been relevant to stable species. With regard to kinetic parameters of metal—ammine complexes, few data have been reported, largely because of the instability of the metal complexes in solutions: even if the complexes are stable in the solid state, they often undergo reactions such as aquation and dissociation in solution [2]. Fast computer-aided data acquisition and data processing techniques are useful in such situations, as the effect of side-reactions may be reduced.

In a previous paper [3], a laboratory minicomputer system, RETDAS (Real Time Data Analysis System), was successfully used for the measurement of diffusion coefficients of metal complexes. This system was also used in the present study to determine the kinetic parameters of electrode reactions of unstable cobalt(III)—ammine complexes.

Fundamental equation for determination of kinetic parameters

In this theoretical development, the kinetic parameters for the electrode reaction involving n electrons, O + ne = R, are considered, and specific adsorption and charging current are assumed to be absent. Only the oxidized species O is initially present and both O and R are considered to be soluble in either the solution or the electrode. Tast (current-sampled) polarography and d.c. polarography were used to obtain kinetic parameters such as trans-

0378—4304/81/0000—0000/$02.50

fer coefficient, half-wave potential, standard rate constant, specific rate constant, etc. The current—potential relationship is given [4, 5] by

$$I/I_d = [1 + \exp(\zeta)]^{-1} \cdot (\lambda t^{1/2})^{1.04} [1.63 + (\lambda t^{1/2})^{1.04}] [1.13 + (\lambda t^{1/2})^{1.04}]^{-2} \quad (1)$$

$$\text{where } \lambda = k_s [D_O{}^{(\alpha-1)/2} D_R{}^{-\alpha/2}] \{\exp[(1-\alpha)\zeta] + \exp(-\alpha\zeta)\} \quad (2)$$

$$\text{and } \zeta = (nF/RT)(E - E^r_{1/2}) \quad (3)$$

Here I_d is the diffusion current at time t; k_s, the standard rate constant; α, the transfer coefficient; D_O and D_R are the diffusion coefficients of substances O and R, respectively; F, R and T have their usual meanings. The reversible half-wave potential $E^r_{1/2}$ is related to the standard potential E_0 by the relation $E^r_{1/2} = E_0 + (RT/nF)\ln(D_R/D_O)^{1/2}$, and can be determined by procedures reported earlier [6—8].

Since I, I_d, t and ζ in eqn. (1) are measurable, λ at various potentials can be determined. Then, from eqn. (2):

$$\ln\lambda - \ln[1 + \exp(\zeta)] = \ln k_s [D_O{}^{(\alpha-1)/2} D_R{}^{-\alpha/2}] - \alpha\zeta \quad (4)$$

If the left-hand side of eqn. (4) is plotted against ζ, a straight line should be obtained. A transfer coefficient (α) can then be computed from the slope obtained, and a standard rate constant (k_s) from the intercept.

There are cases, however, in which the standard potential is unknown (totally irreversible case) and in these cases it may be of value (e.g. in comparing rate constants for reactions involving a series of related compounds) to determine the rate constant k_r for reduction at some convenient reference potential E_r. For a totally irreversible electroreduction, the following relations [9] can be used instead of eqns. (1—3):

$$(RT/\alpha nF)\ln[2x(3-x)/5(1-x)] = E_{1/2} - E \quad (5)$$

$$E_{1/2} = (RT/\alpha nF)\ln[1.35k_r(t/D_O)^{1/2}] \quad (6)$$

where $x = I/I_d$. In this case a plot of $\ln[2x(3-x)/5(1-x)]$ vs. E should give a straight line. The transfer coefficient (α) and the rate constant (k_r) can be obtained if the reference potential (E_r) is given. Usually E_r is chosen as $E_r = 0$ on a given reference electrode and the rate constant will hereafter be referred to as k^0_c.

EXPERIMENTAL

System description

The computer-aided electrochemical system used was essentially the same as that described previously [3], except for some minor modifications. A commercial potentiostat (Model 312, Fuso Co. Ltd.) was modified for use in the computer-assisted system. Polarographic signals were fed to the analog/digital converter.

The system for the determination of kinetic parameters of electrode reac-

tions was developed on the Real Time Data Analysis System (RETDAS) [3, 10] which is built around a CPU TACC 1200M NOVA 01 with a 24 KW core memory. This system was named MKIPER (Measurement of Kinetic Parameters of Electrode Reactions). A schematic diagram of the MKIPER system is shown in Fig. 1. The system is composed of two subsets MKIPER/phase-1 and MKIPER/phase-2. The subset MKIPER/phase-1 was developed for real-time control and data acquisition, and comprises a group of modules. The subset MKIPER/phase-2 performs data analysis according to the fundamental equations described above. This subset also includes the KINET program [11], developed for the calculation of kinetic parameters of electrode reactions.

The system MKIPER is supported by the CORKIPER system (Computer Retrieval of Kinetic Parameters of Electrode Reactions) [12, 13], and also with the COGS (Conversationally Organized Graphic System). Both have been developed on the RETDAS. The CORKIPER is the information retrieval and file management system. The kinetic parameters obtained with MKIPER can be easily stored in CORKIPER. The CORKIPER retrieves data in a question and answer mode and the researcher can obtain the desired electrochemical data. The detail of system CORKIPER has already been described [12, 13].

Figure 2 shows a schematic diagram of the COGS, which is a general-purpose, application-independent computer graphic system. It is designed

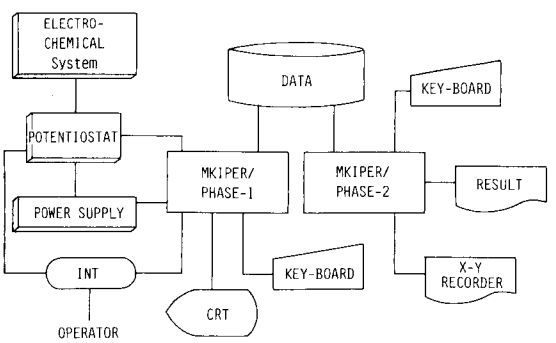

Fig. 1. Configuration of the MKIPER system.

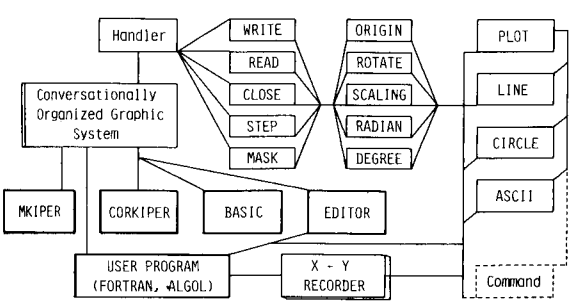

Fig. 2. Block diagram of Conversationally Organized Graphic System (COGS).

to plot experimental and simulated data onto an x—y recorder since RETDAS has no plotter. Basically, COGS comprises two sets of parallel programs, one written for the handler of x—y recorder and one for the user's support program including MKIPER, CORKIPER, BASIC and EDITOR. There are about 40 commands in COGS. The system can, therefore, be used by simply issuing the appropriate COGS command from the key board or from the data file.

These utilities are convenient for the production of individual files in the laboratory minicomputer system.

Reagents

Zinc(II) nitrate was prepared by dissolving a known amount of the metal (99.999%) in reagent-grade nitric acid. Cobalt(III) complexes were prepared by established methods; their purity was confirmed by elemental analysis. All other chemicals used were of analytical reagent grade. A small amount of gelatin, polyacrylamide (PAA; mean molecular weight, 850 000) or polyoxyethylene lauryl ether (LEO; mean molecular weight, 862) was used as maximum suppressor. Redistilled water was used throughout.

Electrode system

The DME and the electrolytic cell system are shown schematically in Fig. 3. The cell had a volume of ca. 40 ml. The temperature of the mercury was kept constant by encasing part of the tubing in a small Liebig condenser (about 10 cm long) through which water was circulated at 25 ± 0.1°C. A normal dropping mercury electrode (DME) with a drop time of 4 s (mercury flow rate, 1.16 mg s^{-1}) was used. Dissolved oxygen was removed by bubbling purified nitrogen gas through the solution. All measurements were made at 25 ± 0.1°C.

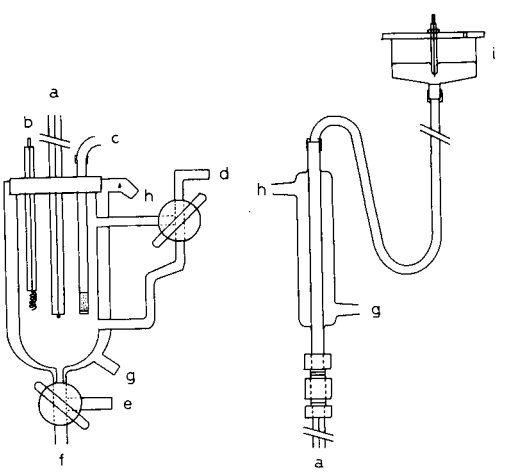

Fig. 3. Electrolytic cell and dropping mercury electrode. a, DME; b, counter electrode (Pt); c, reference electrode (SCE); d, N_2 gas inlet; e, solution inlet; f, solution outlet; g, circulatory water inlet; h, circulatory water outlet; i, mercury reservoir.

Procedures

The parameters required for the experiment to proceed were input through the communication module in a question/answer mode. There are two types of control mode: direct current polarographic mode (DCP) and Tast polarographic mode (TAST). Data acquisition was done by indicating one of these control modes. Electrode potentials were applied to the electrolytic cell from the ramp generator of the potentiostat, the programmable power supply (Model TR-6120, Takeda Riken Co. Ltd.) or the digital/analog converter in the RETDAS.

After measurements of residual current of 40 ml of supporting electrolyte solution, a solid sample of the cobalt complex under test was added to the solution. The current was then measured. The data acquired in core memory by MKIPER/phase-1 were stored in a disk file.

Experimental data in the disk file were used for further data analysis by MKIPER/phase-2 and by COGS for graphic display. An example (TAST mode) of the result by the MKIPER/phase-1 is given in Table 1. Kinetic parameters of electrode reactions thus obtained are stored in the CORKIPER system to initiate further retrieval of those data. An example of the storage of kinetic parameters is shown in Fig. 4, and that of the retrieval, in Fig. 5.

RESULTS AND DISCUSSION

Several key reactions for kinetic parameters of electrode reactions have been proposed [14]. Kinetic parameters of several species were determined as a test of the proposed polarographic method. The results are summarized in Table 2. Literature values are also given. The addition of a little surface-active substance did not affect the kinetic parameters. The presence of large amounts of surface-active substances tends to distort polarographic waves [19, 20]. The concentrations used here were carefully selected and are considered to have no effect on the kinetic parameters. There are no significant differences between the values obtained in this work and those obtained by other electrochemical methods. These results clearly indicate that the MKIPER system works well.

TABLE 1

An example of the application of subset MKIPER/phase-1

```
MKIPER $TTI/I $TTO/O
* ACQUISITION MODE ?                TAST
* SCANNING MODE ?                   PRESET
* GAIN OF AMP (POTENTIAL) ?          5
* GAIN OF AMP (CURRENT) ?            5
* NUMBER OF MEASUREMENT ?           14
* DATA FILENAME ?                   DATA05.DT
ENTER MESSAGES FROM CRT!
INTERRUPT CHANNEL: START = 1, STOP = 2
DATA ACQUISITION END
```

```
CORED  $TTI/I $TTO/O

CORKIPER FILE EDITOR (REV. 00-01)

TYPE  BEGIN  END    OUTPU  REGIS
      REFER  COMME  ELECT  SYSTE
      METAL  METHO  MEDIU  HEAT
      TEMPE  TRANS  RATE   POTEN
      PUNCH  LOAD   EQUIV  SYMBO

* METHOD  : 1
   TEXT   ? TAST POLAROGRAPHY
   SYMBOL ? TAST
    ..SYMBOL ALREADY IN SYSTEM, OK ? YES

* MEDIUM  : 1
   TEXT   ? 0.1M ACETATE BUFFER
   VALUE  ? 0.1
   SYMBOL ? ACETATE-BUFFER
    ..SYMBOL ALREADY IN SYSTEM, OK ? YES

* TEMP    : 1
   TEXT   ? TP = 25 DEG.
   VALUE  ? 25
   SYMBOL ? TP
    ..SYMBOL ALREADY IN SYSTEM, OK ? YES

* TRANS   : 1
   TEXT   ? CT = 0.51
   VALUE  ? 0.51
   SYMBOL ? CT
    ..SYMBOL ALREADY IN SYSTEM, OK ? YES

* RATE    : 1
   TEXT   ? KC = 5.48E-5 CM/SEC
   VALUE  ? 5.48E-5
   SYMBOL ? KC
    ..SYMBOL ALREADY IN SYSTEM, OK ? YES

* POTEN   : 1
   TEXT   ? EH = -0.153 V VS. SCE
   VALUE  ? -0.153
   SYMBOL ? EH
    ..SYMBOL ALREADY IN SYSTEM, OK ? YES

* SYSTEM  : 1
   TEXT   ? DME/1MM [COF(NH3)5](CL04)2
   SYMBOL ? [COF(NH3)5](2+)/[COF(NH3)5](+)
    ..SYMBOL IS NEWLY DEFINED , OK ? YES

* REFER.  : 1
   LITR.1 ?
     TEXT/1 DOCTORAL THESIS OF T. YOSHIKUNI
     AUTR/1 T.YOSHIKUNI
     JRNL/1 PRIVATE-COMMUNICATION
     YEAR/1 1980

* REGIST
* ARE YOU SURE ? YES
  REGIS ITEM (A,C,R,J,M) : A
  REGISTRATION FINISHED.

* END
STOP EDITING.
```

Fig. 4. An example of storage with the COREDITOR system.

```
CORKIPER $TTI/I $TTO/O

* METAL  (1) ? COBALT
* METHOD (2) ? NO
* MEDIUM (3) ? ACETATE-BUFFER EQ 0.1
* TEMP.  (4) ? TP EQ 25.0
* TRANS. (5) ? NO
* RATE   (6) ? NO
* HEAT   (7) ? NO
* ELECT. (8) ? DME
* POTEN. (9) ? NO
* SYSTEM (S) ? NO
* AUTHOR (A) ? A.YAMADA
* JOURNL (J) ? NO
* YEAR   (Y) ? NO

*** WAIT! PROGRAM IS RUNNING. ***

NUMBER OF FILE ...   5

NUMBER OF FILE ...   9

* SORT END, TYPE L TO LIST:  LIST

SYSTEM ... DME/1.0MM CO(III)EDTA
MEDIUM ... 0.1M ACETATE-BUFF. + 0.4M NANO3
TEMP.  ... 25.0              TRANS. ... CT=0.51
RATE   ... KS=2.9E-2         HEAT   ... ---
METHOD ... PS                POTEN. ... ES=0.135
ELECT. ... SDME              METAL  ... COBALT

REF. ... A. YAMADA AND N. TANAKA, ANAL. CHEM.
         45, 167 (1973).

SYSTEM ... DME/1MM [CO(NO3)(NH3)5](NO3)2
MEDIUM ... 0.1M ACETATE-BUFF. + 0.005% GEL.
TEMP.  ... 25.0              TRANS. ... CT=0.62
RATE   ... KC=3.61E-5        HEAT   ... ---
METHOD ... TAST              POTEN. ... EH=-0.142
ELECT. ... DME               METAL  ... COBALT

REF. ... A. YAMADA, T. YOSHIKUNI, Y. KATO AND
         N. TANAKA PRIVATE COMMUNICATION.
```

Fig. 5. An example of retrieval with the CORKIPER system. Only two outputs of 14 data are shown.

Many mixed cobalt(III) complexes with various ligands have been prepared, but the kinetic parameters of electrode reactions have been studied for only a few [21]. This is mainly due to instability of the complexes and the complexity of the electrode process. The computer-assisted Tast polarographic technique was therefore examined for several cobalt(III)—ammine complexes.

The cobalt(III)—ammine complexes studied are reduced in two steps: Co(III) → Co(II) and Co(II) → Co(0). From a polarographic log-plots analysis [22] and other preliminary experiments, both steps are considered to be totally irreversible. Examples of the current—potential curves of the cobalt(III) complexes are shown in Fig. 6. The diffusion coefficients required for the calculation of kinetic parameters were taken from earlier work [3].

Table 3 summarizes the kinetic parameters of the electrode reactions corresponding to the first wave for various cobalt(III)—ammine complexes, which were determined by application of eqn. (4). Few data are available on

TABLE 2

Kinetic parameters of electrode reactions determined by the MKIPER system at 25°C

Ions	Solution	E_0 (V vs. SCE)	k_s (cm s^{-1})	α	Reference
Cu^{2+}	1 M $NaNO_3$ + 5 mM HNO_3[a]	0.022	2.8×10^{-2}	0.29	This study
		0.022	3.1×10^{-2}	0.23	[15]
Cd^{2+}	0.5 M $(NH_4)_2SO_4$	−0.617	3.6×10^{-2}	0.20	This study
	0.5 M Na_2SO_4	−0.604	7.6×10^{-2}	0.21	[16]
Zn^{2+}	0.5 M $NaNO_3$ + 0.5 mM HNO_3	−0.995	4.3×10^{-3}	0.38	This study
		−0.994	4.4×10^{-3}	0.34	[17]
	0.1 M $NaClO_4$[b]	−0.996	1.5×10^{-3}	0.31	This study
		−0.998	1.7×10^{-3}	0.32	[18]
	0.3 M $NaClO_4$[b]	−0.997	9.0×10^{-3}	0.30	This study
		−0.995	1.2×10^{-2}	0.34	[18]
	0.5 M $NaClO_4$[b]	−0.998	5.4×10^{-3}	0.27	This study
		−0.998	5.4×10^{-3}	0.29	[18]
	1.0 M $NaClO_4$[b]	−0.998	2.6×10^{-3}	0.30	This study
			2.6×10^{-3}	0.30	[18]

[a]Solutions contained 0.001% polyacrylamide.
[b]Solutions contained 0.1 mM $HClO_4$ and 2 μM polyoxyethylene lauryl ether.

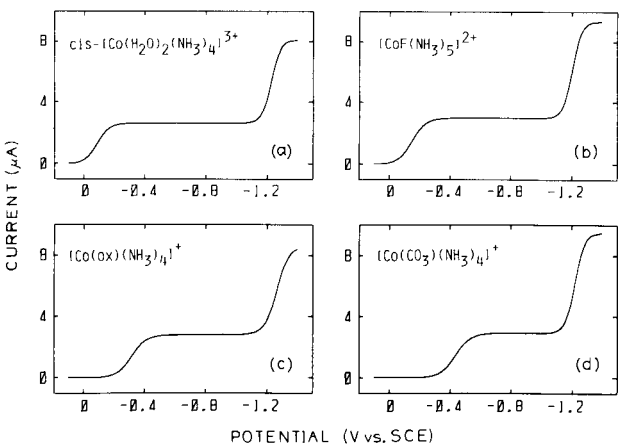

Fig. 6. Examples of Tast polarograms for (a) 1 mM *cis*-$[Co(H_2O)_2(NH_3)_4]^{3+}$, (b) 1 mM $[CoF(NH_3)_5]^{2+}$, (c) 1 mM $[Co(ox)(NH_3)_4]^{+}$, and (d) 1 mM $[Co(CO_3)(NH_3)_4]^{+}$, obtained in 0.1 M acetate buffer and 0.005% gelatin at 25°C.

the kinetic parameters for such complexes. Vlček [32] reported apparent heat of activation and other kinetic parameters (α and $k_c^0/D^{1/2}$) for the cathodic reduction Co(III) → Co(II) at the dropping mercury electrode. The transfer coefficients given by Vlček are 0.67 for $[Co(NH_3)_6]^{3+}$, 0.56 for $[Co(H_2O)(NH_3)_5]^{3+}$, 0.53 for $[Co(NO_3)(NH_3)_5]^{2+}$, 0.51 for $[CoF(NH_3)_5]^{2+}$, and 0.55 for *cis*-$[Co(H_2O)_2(NH_3)_4]^{3+}$, which were measured in solutions con-

TABLE 3

Kinetic parameters of electrode reactions of the first reduction wave, Co(III) → Co(II), for the cobalt(III)—ammine complexes obtained in 0.1 M acetate buffer (pH 5.0) containing 0.005% gelatin at 25°C

Complex		$E_{1/2}$ (V vs. SCE)	D^a ($\times 10^6$ cm^2 s^{-1})	α	k_c^0 (cm s^{-1})
$[Co(NH_3)_6]Cl_3$	[23]	−0.403	8.06	0.82	2.77×10^{-9}
$[Co(H_2O)(NH_3)_5](ClO_4)_3$	[24]	−0.248	7.76	0.63	2.41×10^{-6}
$[Co(NO_3)(NH_3)_5](NO_3)_2$	[25]	−0.142	8.46	0.62	3.61×10^{-5}
$[CoF(NH_3)_5](ClO_4)_2$	[26]	−0.153	9.21	0.51	5.48×10^{-5}
$[Co(CO_3)(NH_3)_5]NO_3$	[27]	−0.248	7.09	0.68	1.46×10^{-6}
cis-$[Co(H_2O)_2(NH_3)_4](ClO_4)_3$	[28]	−0.087	7.11	0.59	1.33×10^{-4}
$[Co(CO_3)_2(NH_3)_4]NO_3 \cdot 0.5H_2O$	[29]	−0.439	9.04	0.47	3.65×10^{-7}
$[Co(ox)(NH_3)_4]Cl \cdot H_2O$	[30]	−0.322	8.19	0.50	2.10×10^{-6}
$NH_4[Co(ox)_2(NH_3)_2] \cdot H_2O$	[31]	—	7.58	—	—

[a]Taken from the literature [3].

taining 0.14 M $HClO_4$ and 1.26 M $NaClO_4$. Since the composition of the solution is quite different, it is difficult to compare the rate constants (k_c^0) in this study with those listed by Vlček.

The electrode reactions of $[Co(NH_3)_6]^{3+}$ in ammoniacal buffer solutions have been examined by several authors at platinum electrodes [33—36] and at a mercury electrode [37]. The rate constants reported scatter, while the transfer coefficient lies in the range 0.6—0.75. In acidic media, previous experiments [38] gave E_0 = −0.241 to −0.249 V vs. SCE, α = 0.69—0.71 and $k_s = 1.5 \times 10^{-3}$—1.9×10^{-3} cm s^{-1} for the kinetic parameters of $[Co(NH_3)_6]^{3+}$ in 0.9 M $NaNO_3$ − 0.1 M acetate buffer (pH 4.9) at 25°C.

The electrode reaction of $[CoF(NH_3)_5]^{2+}$ has been studied to assess the experimental double-layer effects in the presence of anion-specific adsorption [39] and to evaluate the effects of ion pairing between $[CoF(NH_3)_5]^{2+}$ and sulfate [40]. $[Co(H_2O)(NH_3)_5]^{3+}$ ions have also been used to examine ion-pairing effects with sulfate ions in electrode kinetics [40]. However, no precise kinetic parameters are available from these studies.

When the aquo—ammine complexes are arranged by the number of water molecules ($[Co(NH_3)_6]^{3+} < [Co(H_2O)(NH_3)_5]^{3+} < [Co(H_2O)_2(NH_3)_4]^{3+}$), it can be seen that both the half-wave potentials and the rate constants of the complexes increase whereas the transfer coefficients decrease. This suggests that $[Co(NH_3)_6]^{3+}$ is more stable than the complexes in which ammonia is replaced by water. This is in good agreement with the order expected on the basis of the acid-hydrolysis rate of the complexes [2]. Analogously, the complex $[Co(CO_3)(NH_3)_4]^+$ is more stable than $[Co(CO_3)(NH_3)_5]^+$, the carbonate being bidentate in the former and monodentate in the latter. Furthermore, the experimental data obtained for the various cobalt(III)—ammine complexes show transfer coefficients above 0.5, indicating that the electrode process follows outer-sphere pathways [41].

Among the cobalt complexes used here, cobalt(III) is substitution-inert towards solvolysis, while cobalt(II) is substitution-labile. In general, dissociation of the inert cobalt(III) complexes can be neglected from the standpoint of polarography, whereas that of the labile cobalt(II) complexes occurs rapidly compared with the scanning rate of the applied potential. Therefore, the cobalt(II) complex results in the formation of an aquo cobalt(II) mixture in an equilibrium state with water molecules in aqueous solutions. The overall electrode reactions are considered to be as follows. With the pentaammine complex:

$$[Co^{III}L(NH_3)_5]^{(3-n)+} + e \rightarrow [Co^{II}L(NH_3)_5]^{(2-n)+} \quad (7a)$$

$$[Co^{II}L(NH_3)_5]^{(2-n)+} + pH_2O \rightarrow [Co^{II}(H_2O)_p(NH_3)_{6-p}]^{(2-n)+} + (p-1)NH_3 + L^{n-} \quad (7b)$$

$$[Co^{II}(H_2O)_p(NH_3)_{6-p}]^{(2-n)+} + 2e \rightarrow Co(0) + (6-p)NH_3 + pH_2O$$

($L = NH_3$, H_2O, F^-, NO_3^- and CO_3^{2-}) (7c)

With the tetraammine complex:

$$[Co^{III}(L)_2(NH_3)_4]^{(3-n)+} + e \rightarrow [Co^{II}(L)_2(NH_3)_4]^{(2-n)+} \quad (8a)$$

$$[Co^{II}(L)_2(NH_3)_4]^{(2-n)+} + 2pH_2O \rightarrow [Co^{II}(H_2O)_{2p}(NH_3)_{6-2p}]^{(2-n)+} + (2p-2)NH_3 + (L)_2^{n-} \quad (8b)$$

$$[Co^{II}(H_2O)_{2p}(NH_3)_{6-2p}]^{(2-n)+} + 2e \rightarrow Co(0) + (6-2p)NH_3 + 2pH_2O$$

($(L)_2 = (H_2O)_2$, CO_3^{2-} and oxalate) (8c)

The electrode reaction of the dioxalatodiamminocobalt(III) complex may be:

$$[Co^{III}(ox)_2(NH_3)_2]^- + e \rightarrow [Co^{II}(ox)_2(NH_3)_2]^{2-} \quad (9a)$$

$$[Co^{II}(ox)_2(NH_3)_2]^{2-} + (2p+q)H_2O \rightarrow [Co^{II}(H_2O)_{2p+q}(ox)_{2-p}(NH_3)_{2-q}]^{(2p-2)-} + pox + qNH_3 \quad (9b)$$

$$[Co^{II}(H_2O)_{2p+q}(ox)_{2-p}(NH_3)_{2-q}]^{(2p-2)-} + 2e \rightarrow Co(0) + (2-p)ox + (2-q)NH_3 + (2p+q)H_2O \quad (9c)$$

The kinetic parameters given in Table 3 correspond to the electrode reactions Co(III) → Co(II) (eqns. 7a, 8a and 9a).

The interpretation of the second polarographic wave becomes more difficult because the labile cobalt(II) complex undergoes some further chemical reaction prior to electron transfer (eqns. 7b, 8b and 9b). If the dissociation reactions (eqns. 7b, 8b and 9b) in the cobalt(II) complex occur completely, only one product appears in noncomplexing media, i.e. $[Co(H_2O)_6]^{2+}$, because cobalt(II) is octahedral and the species $[Co(H_2O)_6]^{2+}$, is most stable [42]. Thus, the second step corresponds to

$$[Co^{II}(H_2O)_6]^{2+} + 2e \rightarrow Co(0) + 6H_2O \quad (10)$$

TABLE 4

Kinetic parameters of electrode reactions of the second reduction wave, Co(II) → Co(0), for the cobalt(III)—ammine complexes obtained in 0.1 M acetate buffer (pH 5.0) containing 0.005% gelatin at 25°C

Complex	$E_{1/2}$ (V vs. SCE)	α	k_c^0 (cm s^{-1})
$[Co(NH_3)_6]Cl_3$	−1.225	0.38	1.74×10^{-19}
$[Co(H_2O)(NH_3)_5](ClO_4)_3$	−1.223	0.38	2.42×10^{-19}
$[Co(NO_3)(NH_3)_5](NO_3)_2$	−1.225	0.41	1.71×10^{-20}
$[CoF(NH_3)_5](ClO_4)_2$	−1.224	0.39	1.45×10^{-19}
$[Co(CO_3)(NH_3)_5]NO_3$	−1.224	0.39	6.83×10^{-20}
cis-$[Co(H_2O)_2(NH_3)_4](ClO_4)_3$	−1.223	0.39	6.53×10^{-20}
$[Co(CO_3)(NH_3)_4]NO_3 \cdot 0.5H_2O$	−1.221	0.37	5.91×10^{-19}
$[Co(ox)(NH_3)_4]Cl \cdot H_2O$	−1.256	0.30	1.57×10^{-16}
$NH_4[Co(ox)_2(NH_3)_2] \cdot H_2O$	−1.287	0.26	6.36×10^{-15}
$[Co(H_2O)_6](NO_3)_2$	−1.252	0.27	2.74×10^{-15}

The kinetic parameters of the electrode reactions corresponding to the second step were examined by applying eqn. (4); the results are given in Table 4 together with those for $[Co(H_2O)_6]^{2+}$. The kinetic parameters obtained are significantly different from those for $[Co(H_2O)_6]^{2+}$. This clearly indicates that bond rupture in the cobalt(II) complex is incomplete, as would be expected from other considerations.

The authors thank the Ministry of Education for financial support.

REFERENCES

1 R. Tamamushi, Kinetic Parameters of Electrode Reactions of Metallic Compounds, Butterworths, London, 1975.
2 F. Basolo and R. G. Pearson, Mechanism of Inorganic Reactions. A Study of Metal Complexes in Solutions, J. Wiley, New York, 1967.
3 A. Yamada, T. Yoshikuni, Y. Kato and N. Tanaka, Anal. Chim. Acta, 112 (1979) 55.
4 H. Matsuda, Ber. Bunsenges. Phys., 61 (1957) 489; 62 (1958) 977.
5 H. Matsuda and Y. Ayabe, Ber. Bunsenges. Phys. Chem., 63 (1959) 1164.
6 R. Tamamushi, K. Ishibashi and N. Tanaka, Z. Phys. Chem., Frankfurt am Main, 35 (1962) 117.
7 R. Tamamushi and N. Tanaka, Z. Phys. Chem., Frankfurt am Main, 39 (1963) 117.
8 P. J. Gellings, Ber. Bunsenges. Phys. Chem., 66 (1962) 477, 481, 799; 67 (1963) 167.
9 K. B. Oldham and E. P. Parry, Anal. Chem., 40 (1968) 65.
10 A. Yamada, M. Sakata, Y. Kato and N. Tanaka, Sci. Rep. Tohoku Univ. Ser. I, 58 (1975) 94.
11 A. Yamada and N. Tanaka, Sci. Rep. Tohoku Univ. Ser. I, 53 (1970) 110.
12 A. Yamada, Y. Kato, M. Sato, M. Sasaki and N. Tanaka, Bunseki Kagaku, 25 (1976) 69.
13 A. Yamada, Y. Kato, I. Doi, K. Saito, Y. Tanaka and N. Tanaka, Sci. Rep. Tohoku Univ. Ser. I, 60 (1977) 41.
14 Promotion Bureau Science and Technology Agency (Japan), Report of the Physical and Chemical Property Data, Chemical Kinetics Data, Vol. 4, 1978, Chap. 5.

15 A. Yamada and N. Tanaka, Anal. Chem., 45 (1973) 167.
16 J. K. Frischmann and A. Timnick, Anal. Chem., 39 (1967) 507.
17 N. Tanaka and A. Yamada, Electrochim. Acta, 14 (1969) 491.
18 N. Tanaka, Y. Aoki and A. Yamada, Electrochim. Acta, 14 (1969) 1155.
19 R. Tamamushi, S. Yamamoto, A. Takahashi and N. Tanaka, Anal. Chim. Acta, 20 (1959) 486.
20 N. Tanaka, R. Tamamushi and A. Takahashi, Collect. Czech. Chem. Commun., 25 (1960) 3016.
21 A. J. Bard (Ed.), Encyclopedia of Electrochemistry of Elements, Vol. 3, M. Dekker, New York, 1975, Chap. III-2.
22 I. M. Kolthoff and J. J. Lingane (Eds.), Polarography, Vol. 1, Interscience, New York, 1964, Chap. 11.
23 W. C. Fernelius (Ed.), Inorganic Syntheses, Vol. 2, McGraw-Hill, New York, 1946, p. 216.
24 A. Benrath and A. Miens, Z. Anorg. Allg. Chem., 177 (1929) 289.
25 S. M. Jørgensen, Z. Anorg. Allg. Chem., 17 (1898) 463.
26 M. Linhard and G. Stirn, Z. Anorg. Allg. Chem., 268 (1952) 105.
27 J. C. Bailar, Jr., Inorganic Syntheses, Vol. 4, McGraw-Hill, New York, 1953, p. 171.
28 R. G. Jørgensen, Z. Anorg. Allg. Chem., 2 (1892) 294.
29 S. M. Jørgensen, Z. Anorg. Allg. Chem., 2 (1892) 279.
30 W. Schramm, Z. Anorg. Allg. Chem., 180 (1929) 167.
31 E. H. Riesenfeld and R. Klement, Z. Anorg. Allg. Chem., 124 (1922) 1.
32 A. A. Vlček, Proc. Int. Conf. Coord. Chem., Pergamon, Haifa-Jerusalem, 1961, p. 590.
33 H. Bartelt and S. Landazury, J. Electroanal. Chem., 22 (1969) 105.
34 H. Bartelt, Electrochim. Acta, 16 (1971) 307.
35 L. N. Klatt and W. J. Blaedel, Anal. Chem., 39 (1967) 1065.
36 J. Suzuki, Bull. Chem. Soc. Jpn., 43 (1970) 755.
37 H. A. Laitinen and P. Kivalo, J. Am. Chem. Soc., 75 (1953) 2198.
38 N. Tanaka, A. Kitani, A. Yamada and K. Sasaki, Electrochim. Acta, 18 (1973) 675; Sci. Rep. Tohoku Univ. Ser. I, 55 (1972) 201.
39 M. J. Weaver, J. Electroanal. Chem., 93 (1978) 231.
40 A. A. Vlček, Nature, 197 (1963) 786.
41 F. C. Anson, M. G. Finn and A. Yamada, Inorg. Chem., 16 (1977) 2124.
42 F. A. Cotton and G. Wilkinson, Advanced Inorganic Chemistry, Interscience, New York, 1966.

Analytica Chimica Acta, 133 (1981) 433—441
Computer Techniques and Optimization
Elsevier Scientific Publishing Company, Amsterdam — Printed in The Netherlands

STATISTICAL DECISION THEORY APPLIED TO ANALYTICAL CHEMISTRY
Part 1. The Statistical Decision Model and its Relation to Branches of Mathematical Statistics

I. E. FRANK, E. PUNGOR and G. E. VERESS*
Technical University, Department of Analytical Chemistry, Budapest (Hungary)
(Received 23rd September 1980)

SUMMARY

Statistical decision theory can be considered as an extension of point estimation, interval estimation and hypotheses testing. Basic elements of statistical decision models are discussed and the relation between decision theory and other branches of mathematical statistics is indicated. Some illustrative examples of application to analytical chemistry are given.

Several theories of mathematical statistics, particularly those concerned with testing hypotheses and with estimation, are widely applied in analytical chemistry, but statistical decision theory, which can be considered as an extension of these theories, has received little attention. The main point of statistical decision theory is to formalize actions and consequences in different decision problems by introducing the concept of the loss function. This offers possibilities for a general and uniform treatment of different decisions, independent of the actual problem. In this paper, the relevance of this branch of mathematical statistics to analytical chemistry is discussed. First, the basic concepts are introduced, then the relation between decision theory and other branches of mathematical statistics is outlined, and finally the applicability of the theory in analytical chemistry is demonstrated by some illustrative examples. Statistical decision theory is applied in several branches of science, especially in economics, and it seems to be a useful mathematical technique for treating results of analytical decisions in order to solve problems of optimization. Statistical decision theory has been described in several books [1—7]. Its relation to estimation theory has been discussed [1], and its relevance to testing hypotheses and classification has been outlined [2—4]. Decision theory also plays an important role in statistical quality control [2].

BASIC ELEMENTS OF STATISTICAL DECISION THEORY

The selection of one of several possibilities or actions means a decision. The outcome of the decision depends on two factors: the actual state of the

0378—4304/81/0000—0000/$02.50

system and the quality of the decision. The consequences of decision can be predicted only if these factors are known. The decision itself is, of course, a known factor, but the state of the system is generally unknown and can be described by a random variable. If the aim is to optimize the outcome of the decision, then information concerning the state of the system is needed.

If the decision is made on the basis of information obtained from statistical samples of the system, it is called a statistical decision. If the state of the system is well defined, then the decision is a deterministic decision.

Statistical decision theory, founded by A. Wald in the fifties, deals with statistical decisions. If the decision is related to a change of the system, and the state of the system is to be optimized, then the decision process is called control. From this point of view, control is a series of statistical decisions, and before each decision step, information concerning the changed state of the system is obtained.

State space, sample space, decision space, decision function

Three spaces are interpreted in statistical decision theory: state or parameter space, sample space, and decision or action space. All three are finite, discrete or continuous; as will be seen, two of them or all three in a special case can be equal.

The parameter space is connected with the state of the system, which can be described by a random variable, and the elements of the parameter space range over the possible values of the random variable. This variable can be scalar or vector and is characterized by its distribution function. Information concerning the state of the system, which decreases uncertainty regarding the true value of the random variable describing the system, is obtained by statistical evaluation of sample space. Elements of the sample space are observed, and this is also described by a random variable. The distribution function of this variable is a conditional distribution function because the distribution depends on the value of the state variable. The decision space is constructed of the possible actions, i.e. decisions.

The three spaces can be denoted by: $\upsilon \in \theta$ (state space), $x \in \mathrm{X}$ (sample space), and $d \in \mathrm{D}$ (decision space). The connection between decision space D and sample space X is given by the decision function δ, which is defined for the sample and takes its values from the decision space. This means that elements of the sample space are related to an element of the decision space according to the decision function δ. Decision is made on the basis of observed sample values x by the decision function: $\delta(x) = d$. The main point of statistical decision theory is to determine an optimal decision function from the point of view of the consequence of the decision.

Loss function

The consequence of decision is formalized by the loss function, $l(\upsilon, d)$. This is a real non-negative function defined on the $\theta \mathrm{D}$ space; i.e., the func-

tion depends on the parameter variable ν and the decision variable d, and its range is a set of non-negative real numbers. The loss function is also a random variable. Because of the relation $\delta(x) = d$, the loss function can be given as $l[\upsilon, \delta(x)]$. In this case, it is defined on the XD space, and the loss is a composite function of the random variables υ and x. In this paper, the loss is only a formal quantity; its economic interpretation will be discussed later.

There are several types of loss function. In the case of discrete parameter and decision spaces, the loss function can be given as the loss matrix L

$$L = \begin{pmatrix} l(\upsilon_1, d_1) & \cdots \\ \vdots & \\ & l(\upsilon_n, d_m) \end{pmatrix}$$

If υ and d are continuous variables, then the loss function can be represented by a surface. If θ and D are equal, then a new variable can be introduced: $z = \upsilon - \mathrm{d}$. The following loss functions can then be interpreted (Fig. 1, a–d): (a) The squared loss, $l(z) = kz^{2n}$; (b) the difference loss, $l(z) = k|z|$; (c) a simple loss, $l(z) = 0$ if $z = 0$ or $l(z) = a$ if $z \neq 0$; and (d) a modified loss, $l(z) = a$ if $|z| > \epsilon$ or $l(z) = 0$ if $|z| \leqslant \epsilon$. In all these expressions, k, n, a and ϵ are positive real numbers.

These loss functions are symmetric convex functions, and their minimum is at $z = 0$, where $l(0) = 0$.

Risk function

The expected value of the loss function according to the variable x is called the risk function:

$$R_\delta(\nu) = \underset{x}{E}\{l[\upsilon, \delta(x)]\}$$

To calculate it, the conditional distribution function $F(x|\upsilon)$ of the random variable x, or the conditional probabilities $p(x_i|\upsilon_j)$ for $i = 1, .., n$ and $j = 1, .., m$, must be known. For a certain decision function δ, the risk is a function of parameter υ. If the variables υ and x are continuous, then the risk is

$$R_\delta(\upsilon) = \int_x l[\upsilon, \delta(x)]\,\mathrm{d}\,F(x|\upsilon)$$

and if they are discrete,

$$R_\delta(\upsilon_j) = \sum_i l[\upsilon_j, \delta(x_i)]\,\mathrm{p}(x_i|\upsilon_j)$$

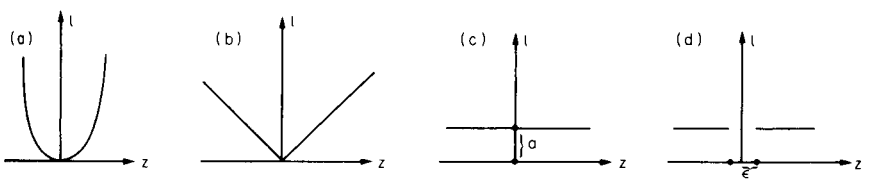

Fig. 1. Loss functions. For explanation, see text.

Determination of decision function

For the same ν parameter, the values of the risk function may differ when different decision functions are used. This can be used, therefore, to optimize the decision function, and so the optimization criterion should include the risk function. If the relation $R_{\delta_1}(\upsilon) < R_{\delta_2}(\upsilon)$ holds for a certain parameter υ when two risk functions are compared, then the decision function δ_1 is better than δ_2 for a given value υ. Decision function δ_1 is uniformly better than δ_2, if the relation $R_{\delta_1}(\upsilon) \leqslant R_{\delta_2}(\upsilon)$ holds for each value of parameter υ. If equality holds for each value of υ, decision functions δ_1 and δ_2 are equivalent. If there exists a decision function δ_0, which satisfies this expression, compared with any other decision function δ, then δ_0 is the uniformly best decision function, and all others are unacceptable. A decision function is acceptable if no uniformly better function exists when they are compared. When two decision functions are compared, it is possible that one will be better for a certain value of υ whereas the other will be better for another value of υ (see Fig. 2). There are different criteria for choosing the optimal decision function.

If a *uniformly best decision function* exists, then it must be chosen as the optimal decision function. If a uniformly best function does not exist, then a "good" decision function can be used to calculate the expected value of the risk function, i.e., the so-called average risk function, $\bar{R}_\delta = E_\nu[R_\delta(\upsilon)]$. This is affected by the decision function δ only.

Bayes risk method. The average risk can also be calculated as an expected value of the loss function from the variables x and υ:

$$\bar{R}_\delta = \underset{\nu}{E}\{\underset{x}{E}[l(\upsilon, \delta(x))]\}$$

For this calculation the distribution function of parameter υ, $F(\upsilon)$ or in the discrete case its probabilities $p(\upsilon_j)$, for $j = 1, \ldots, m$, must be known. The average risk in a discrete case is $\bar{R}_\delta = \Sigma_j R_\delta(\upsilon_j)p(\upsilon_j)$; and in a continuous case, it is $R_\delta = \int_\nu R_\delta(\upsilon)\mathrm{d}F(\upsilon)$. The decision function δ which minimizes this average risk, $\min_\delta \bar{R}_\delta$, will be the optimal function. This minimum of the average risk is called Bayes risk.

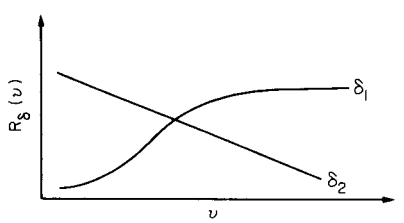

Fig. 2. Risk functions.

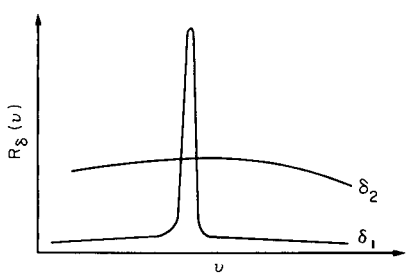

Fig. 3. Risk functions comparing the Bayes and minimax methods.

Minimax method. If the distribution function $F(v)$ or the probabilities $p(v_j)$ are unknown, i.e. the Bayes risk cannot be calculated, the minimax method can be used. This method is current in games theory, where it is assumed that the opponent of the decision maker tries to maximize the loss of the decision maker, i.e., v will be the parameter worst from the point of view of loss. However, in decision theory, the opponent is nature itself, and so the worst value of parameter v cannot properly be regarded as most probable. Nevertheless, the minimax method is also used in decision theory to look for a decision function which minimizes either the maximum loss or its expected value.

This method gives the greatest security against high losses, but as the estimation of the distribution function $F(v)$ ignores the information obtainable from the system, a certain value being assumed, false results may be obtained. In the example on Fig. 3 the minimax method indicates that decision function δ_2 should be chosen, although decision function δ_1 proved to be the better on the basis of Bayes risk for most distribution functions.

RELATION BETWEEN STATISTICAL DECISION THEORY AND OTHER MATHEMATICAL STATISTICAL METHODS

Statistical decision theory can be considered as an extension of hypothesis testing, point estimation and interval estimation.

Point estimation as a statistical decision

In point estimation, the true value of a parameter v is estimated by a value $\hat{v}$. The elements of the statistical decision model in this case are as follows: the elements of parameter space θ are the possible values of parameter v, i.e., $v \in \theta$; the elements of sample space X are the values of the statistical sample x concerning parameter v, i.e., $x \in X$; the elements of decision space D are the estimated values of parameter v, i.e., $\hat{v} \in D$. Spaces θ, D, and X are of the same physical dimension, and all three contain possible values of parameter v. Decision function δ is a statistic from sample values x, and parameter v is estimated by the decision function δ, i.e., $d = \delta(x) = \hat{v}$.

If sufficient statistics exist for estimation, then the optimal decision function is a function of these statistics [2]. Considering a random variable v (with normal distribution) of the expected value μ, and variance σ^2, sufficient statistics of v are provided by the sample average $\bar{x} = \Sigma_i x_i/n$, thus the optimal decision function is $\delta(x) = v = \bar{x}$.

Loss function is generally given as a function of the difference $(v - \hat{v})$, the most widely used one being the square loss function $l(v, \hat{v}) = (v - \hat{v})^2$. In this case, the risk function gives the variance of estimation

$$R_\delta(v) = \int_x (v - \hat{v})^2 \, \mathrm{d}\, F(x|v) = \sigma^2.$$

Testing statistical hypotheses as a statistical decision

In testing statistical hypotheses, the so-called null hypothesis H_0 is made concerning a distribution or its parameters, and there is an alternative

hypothesis H_1. On the basis of the sample, the validity of the null hypothesis is investigated at a certain confidence level, i.e., a decision is made on acceptance or rejection of the null hypothesis.

In this case the elements of the decision model are as follows: the elements of parameter space θ are the possible values of parameters related to the hypothesis, i.e. $\upsilon \in \theta$; the elements of sample space X are values of the statistical sample for testing statistical hypotheses, i.e., $x \in X$; the decision space has two elements, acceptance of null hypothesis H_0 ($d = 1$) at a certain confidence level, or rejection of H_0 ($d = 0$), i.e., $d \in D$.

Spaces θ and X are equal, and the elements of decision space D consist of two values. Interval estimation is closely related to hypothesis testing. Conif hypothesis H_0 is rejected. The decision is made on the basis of sample space X according to decision function δ, and its value is defined by comparing the statistic $t(x)$ made from samples x with a given value c, depending on the confidence level, i.e., $\delta(x) = 1$ if $t(x) \geqslant c$, and $\delta(x) = 0$ if $t(x) < c$. The decision function is a function not only of samples x but also of value c affected by the confidence level.

An error of the first kind is made when hypothesis H_0 is valid but is rejected, and an error of the second kind is made when the hypothesis H_0 is not valid but is accepted. The loss consists of errors of both kinds. If the hypotheses are H_0: $\upsilon = \upsilon_0$ and H_1: $\upsilon \neq \upsilon_0$, and the binary decision space is $D = \{1, 0\}$, then when the following simple loss function

$$l(\upsilon, 0) = \begin{cases} 1, \text{ if } \upsilon = \upsilon_0 \\ 0, \text{ if } \upsilon \neq \upsilon_0 \end{cases} \qquad l(\upsilon, 1) = \begin{cases} 1, \text{ if } \upsilon \neq \upsilon_0 \\ 0, \text{ if } \upsilon = \upsilon_0 \end{cases}$$

is introduced, the risk is

$$R_\delta(\upsilon) = l(\upsilon, 0)\, p(d = 0) + l(\upsilon, 1)\, p(d = 1)$$

where $p(d = 0)$ is the probability of rejection of hypothesis H_0, and $p(d = 1)$ is the probability of acceptance of H_0. If $\upsilon = \upsilon_0$, then the numerical value of the risk is equal to the probability of first-kind error and if $\upsilon \neq \upsilon_0$, then it is equal to the probability of second-kind error.

Interval estimation as a statistical decision

In interval estimation, instead of estimating parameter ν with one value $\hat{\upsilon}$, a confidence interval $[\alpha_1, \alpha_2]$ is given which contains the true value of υ with probability $1 - \epsilon$: $P(\alpha_1 \leqslant \upsilon < \alpha_2) = 1 - \epsilon$. The elements of the statistical decision model are as follows: the elements of parameter space θ are the possible values of the unknown parameter υ, i.e., $\upsilon \in \theta$; the elements of sample space X are values of the statistical sample concerning parameter υ, i.e., $x \in X$; the elements of decision space D are the values $[\alpha_1, \alpha_2]$ that give the confidence interval, i.e., $[\alpha_1, \alpha_2] \in D$.

Spaces θ and X are equal, and the elements of decision space D consist of two values. Interval estimation is closely related to hypothesis testing. Considering H_0: $\upsilon = \upsilon_0$ and H_1: $\upsilon \neq \upsilon_0$, hypothesis H_0 is accepted on confidence

level $1 - \epsilon$ if the confidence interval of the same probability contains the value v_0. Thus, the decision space $D = \{d = [\alpha_1, \alpha_2]\}$ of the interval estimation is replaced by a binary decision space $D = \{d = 1, d = 0\}$ in hypothesis testing.

The decision function of interval estimation is a function of sample x, the value set of which consists of the boundary values of the interval, i.e., $d = \delta(x) = [\alpha_1, \alpha_2]$, where $\alpha_1 = \alpha_1(x)$, $\alpha_2 = \alpha_2(x)$. In the case of the normal distribution $N(a, \sigma)$, the confidence interval for parameter a is

$$\delta(x) = \begin{cases} \alpha_1 = \bar{x} - t_{\epsilon, n-1}\, s^* n^{-1/2} \\ \alpha_2 = \bar{x} + t_{\epsilon, n-1}\, s^* n^{-1/2} \end{cases}$$

where n is the number of samples, x_i, $\bar{x}$ is the sample mean $\bar{x} = \Sigma_i x_i / n$, s^* is the standard deviation, and $t_{\epsilon, n-1}$ is the value of the Student distribution for confidence level $(1 - \epsilon)$ with $(n - 1)$ degrees of freedom.

A possible loss function is, for example;

$$l(v, \mathrm{d}) = \begin{cases} \mathrm{O} \text{ if } \alpha_1 \leqslant v < \alpha_2 \\ A \text{ if } v < \alpha_1 \\ B \text{ if } v \geqslant \alpha_2 \end{cases}$$

Assuming a symmetric distribution, the risk function is:

$$R_\delta(v) = (1 - \epsilon)\,\mathrm{O} + (\epsilon/2)\,A + (\epsilon/2)B$$

where $1 - \epsilon$ is the probability that interval $[\alpha_1, \alpha_2]$ contains the true value of v, and $\epsilon/2$ is the probability that v is less than α_1 or that v is greater than α_2.

Classification as statistical decisions

In classification problems belonging to pattern recognition, patterns characterized by n-dimensional vectors (pattern vectors) must be classified into different categories. The elements of a decision model in a classification problem are as follows: the elements of parameter space θ are the true categories of patterns, i.e., $v \in \theta$; the elements of sample space X are pattern vectors, i.e., $\mathrm{x} \in \mathrm{X}$; the elements of decision space D are categories in which patterns are classified, i.e., $\hat{v} \in \mathrm{D}$.

The decision function assigns a certain category $\hat{v}$ to each pattern vector: $\delta(\mathrm{x}) = \hat{v}$. Spaces θ and D are equal, and space X is a vector space. In supervised pattern recognition, the decision function is determined by training. In the case of binary classification, the decision function is given by a hyperplane. Depending on whether the pattern lies on one side of the plane or the other, it is placed in class 1 or class 2. The distribution function of patterns belonging to the same category is denoted by $F(\mathrm{x}|v)$, while distribution of categories is denoted by $F(v)$. The value of the loss function $l(v, \hat{v})$ gives the loss occurring if the pattern is wrongly classified.

STATISTICAL DECISION PROBLEMS IN ANALYTICAL CHEMISTRY

Applications of statistical decision theory in analytical chemistry are illustrated below.

Example 1. Point estimation

The chlorine content of waste water was determined. Parallel measurements gave the values 3.50, 3.45, 3.42, 3.40, 3.48 mg l^{-1}. The decision model is as follows: v = true value of chlorine content; x = measured values of chlorine content; $d = \hat{v}$ = estimated value of chlorine content. The decision function, according to the statistics, is $\hat{v} = \delta(x) = \bar{x} = 3.45$. A square loss function, $l(v, \hat{v}) = (v - \hat{v})^2$, is assumed. The risk is equal to the variance of the estimation, which characterizes the precision of the estimation. The greater the risk, the worse the estimate: $R_\delta(v) = s^2 = 0.134$. Of course, the goodness of the estimation is relative, depending on the given problem.

Example 2. Hypothesis testing

It is necessary to decide whether or not a chemical product is of good quality. The criterion is that the concentration of component A of the product has a certain value. Product quality control gave the following measurements for the concentration of A: 0.46, 0.40, 0.46, 0.44 g l^{-1}.

The decision model is: v = the true unknown value of concentration of component A, while the given requested value is v_0; x = measured values of concentration; $d = 1$, if the product is good, and $d = 0$, if the product is unsuitable.

The null hypothesis concerning the concentration of compound A is H_0: $v = v_0$, where $v_0 = 0.45$; the alternative hypothesis is H_1: $v \neq v_0$. The decision function is that $\delta(x) = 1$ if H_0 is accepted at the confidence level 0.95, and $\delta(x) = 0$ if H_0 is not accepted at this confidence level.

The sample mean is $\bar{x} = 0.44$ with the standard deviation $s^* = 0.028$. Hypothesis testing is done by using the t test, i.e., $t = (\bar{x} - v_0)(s^* n^{-1/2})^{-1}$ is calculated. When concrete values are used, the value is $t = (0.44—0.45)(0.028/2)^{-1} = -0.714$.

If the expression $P(|t| < t_{\epsilon, n-1}/H_0) = 1 - \epsilon$ holds, the hypothesis H_0 at the confidence level, 0.95 is accepted. If $1 - \epsilon = 0.95$, then $t_{\epsilon, n-1} = 3.18$, i.e., $-0.714 < 3.18$, and so hypothesis H_0 is accepted; the decision is therefore that the product is good.

Example 3. Pattern recognition

A decision is needed on whether or not a material belongs to a certain compound group A. The decision is based on the existence of a peak at wavenumber v in the infrared spectrum. The decision model is as follows: θ = {A, not A} = $\{v_1, v_2\}$ = {1, 0}; X = {peak, no peak} = $\{x_1, x_2\}$ = {1, 0}; D = {A, not A} = {1, 0} = $\{d_1, d_2\}$. All three spaces are binary; θ and D are equal. The possible decision functions and the simple loss function $l(v, d)$ for the four different cases are as follows:

Decision functions

	$\delta_1(x)$	$\delta_2(x)$	$\delta_3(x)$	$\delta_4(x)$
x_1	d_1	d_2	d_1	d_2
x_2	d_1	d_2	d_2	d_1

Loss functions

	v_1	v_2
d_1	0	a
d_2	a	0

Here a is an arbitrary value, $P(x_i|v_j)$ denotes the probability of the existence of a peak if the material belongs to compound group v_j. This probability can be taken from a spectral library or from the literature. For example,

	x_1	x_2
v_1	0.8	0.2
v_2	0.3	0.7

The risk as a function of v and δ is

	δ_1	δ_2	δ_3	δ_4
v_1	0	a	$0.2\,a$	$0.8\,a$
v_2	a	0	$0.3\,a$	$0.7\,a$

In this case, there is no uniformly best decision function, because both function δ_1 at v_1 and function δ_2 at v_2 give zero risk. To calculate the Bayes risk, it is supposed that the probability of occurrence of the compound group is $p(v_1) = 0.4$ and $p(v_2) = 0.6$. Consequently, the average risks for the four decision functions are: $\bar{R}_{\delta_1} = 0.6\,a$; $\bar{R}_{\delta_2} = 0.4\,a$; $\bar{R}_{\delta_3} = 0.26\,a$; $\bar{R}_{\delta_4} = 0.74\,a$. According to the Bayes method, decision function δ_3 must be chosen, i.e., detection of a peak at wavenumber v means that the material belongs to compound group A, otherwise it does not. According to the minimax method, either decision function δ_1 or δ_2 must be chosen, i.e. in the first case the material is assumed to be A and in the second case not A, the result being independent of the occurring peak in both cases.

REFERENCES

1 R. Deutsch, Estimation Theory, Prentice-Hall, London, 1965.
2 K. Sarkadi and I. Vincze, Mathematical Methods of Statistical Quality Control, Akadémiai Kiadó, Budapest, 1974.
3 T. Ferguson, Mathematical Statistics, A Decision Theoretic Approach, Academic Press, New York, 1967.
4 P. J. Bickel and K. A. Doksum, Mathematical Statistics, Basic Ideas and Selected Topics, Holden-Day, San Francisco, 1977.
5 L. Weiss, Statistical Decision Theory, McGraw-Hill, New York, 1961.
6 N. L. Hays and R. L: Winkler, Statistics (I), Holt, Rinehart and Winston, New York, 1962.
7 A. Wald, Statistical Decision Functions, Wiley, New York, 1950.

Analytica Chimica Acta, 133 (1981) 443—450
Computer Techniques and Optimization
Elsevier Scientific Publishing Company, Amsterdam — Printed in The Netherlands

STATISTICAL DECISION THEORY APPLIED TO ANALYTICAL CHEMISTRY
Part 2. Information and Decision in Analytical Measuring Systems

I. E. FRANK, E. PUNGOR and G. E. VERESS*
Institute for General and Analytical Chemistry, Technical University, Budapest (Hungary)
(Received 23rd September 1980)

SUMMARY

A uniform treatment of analytical measuring systems using information theory and statistical decision theory is considered. There are two levels in the description. In the first, decision is made in the analytical measurement system where the information is obtained; the analytical measuring system is then considered as a part of a higher-level system where decision is made. The latter description makes it possible to determine the value of the information and to optimize its quantity.

Classical chemical analysis, rather uniform in aspect, has become replaced increasingly by instrumental techniques closely connected with metrology, electronics and cybernetics, and certain analytical methods are slowly becoming independent branches of analytical chemistry. Uniform treatment of the different methods is very difficult because of increasing specialization. Not only does the number of techniques grow but their aims also differ. In addition to research, special analytical problems, and measurements of small sample series, chemical analysis has an important role in the control and regulation of industrial processes, and in the quality control of products.

Few attempts have been made to treat analytical measuring systems uniformly, although descriptions from the aspects of measuring techniques, mathematical statistics, semeiotics and systems theory are plentiful. In Part 1 of this series [1], statistical decision theory was outlined and its relation to some mathematical statistical methods was discussed. The present paper is concerned with the relationships between models of analytical measuring systems based on information theory or statistical decision theory. The aim is to provide a uniform interpretation of analytical chemical methods as information-producing and decision processes.

In the following paragraphs, some basic concepts and equations of information theory and statistical decision theory are summarized. Detail can be found in some basic monographs [2—7].

0378—4304/81/0000—0000/$02.50

Information and entropy

In the Kolmogorov probability field (Ω, X, P), Ω denotes the set Ω of elementary events $\omega(\omega \in \Omega)$, X is the set of subsets of $\Omega(x \in X)$ where x is the "event", and P denotes the probability of these events. If X if a finite set, the quantity of specific information on event x_i is denoted by $I(x_i)$ and is defined as $I(x_i) = -\log_2 p(x_i)$. The dimension of all the information and entropy quantities is the bit, because of $\log_2$.

The set X can be characterized by the average information of the events x_i, i.e., by the so-called entropy $H(x)$: $H(x) = -\Sigma_i\, p(x_i) \log_2 p(x_i)$. If the event space is continuous, then instead of probability distribution, the distribution function or the density function, $f(x)$, is used to calculate the quantity of the information:

$$I(x) = -\log_2 f(x) \text{ and } H(x) = -\int_{-\infty}^{+\infty} f(x) \log_2 f(x)\, dx$$

Considering two event spaces X and Y together, the common entropy $H(X,Y)$ and the conditional entropies $H(X|Y)$ and $H(Y|X)$ can be defined. Their relationships are as follows:

$$H(X,Y) = H(Y|X) + H(X) \text{ and } H(X,Y) = H(X|Y) + H(Y)$$

The mutual information describes the relation between the two event spaces. The specific mutual information $I(x_i;y_j)$ in the discrete case is

$$I(x_i;y_i) = \log_2 [p(x_i,y_i)/p(x_i)p(y_j)]$$

and in the continuous case it is

$$I(x;y) = \log_2 [f(x,y)/f(x)f(y)]$$

The average mutual information $I(X;Y)$, the transinformation, in the discrete case is

$$I(X;Y) = \sum_i \sum_j p(x_i,y_i) \log_2 [p(x_i,y_j)/p(x_i)p(y_j)]$$

and in the continuous case is

$$I(X;Y) = \int_{-\infty}^{+\infty} \int_{-\infty}^{+\infty} f(x,y) \log_2 [f(x,y)/f(x)f(y)]\, dx\, dy$$

If the two sets are independent, then: $I(X;Y) = I(Y;X) = 0$. If there is a well-defined functional relationship between the two event spaces, then $I(X;Y) = I(Y;X) = H(X) = H(Y)$.

The equations describing the relations among the different entropies and the mutual information are as follows:

$$\begin{aligned} I(X;Y) &= H(X) - H(X|Y) \\ I(X;Y) &= H(Y) - H(Y|X) \\ I(X;Y) &= H(X) + H(Y) - H(X,Y) \end{aligned} \qquad (1)$$

The statistical decision model

Three different spaces are interpreted in the statistical decision model: the parameter or state space (θ), the sample space (X) and the decision space (D). The elements of the parameter space θ range over the possible values of the random variable v characterizing the state of the system examined. The sample space X comprises the values of the random variable, i.e., the sample x. As the true value of the parameter v is unknown, estimation of v is based on this sample. The decision d, an element of the decision space D, is made on the basis of the observed values of x by the decision function δ, defined on the sample space, which takes its values from the decision space D, i.e., $\delta(x) = d$.

An important element of the decision model is the loss function $l(v,d)$ defined on the product space θD, which has, traditionally, a real, non-negative value. There are many types of loss function: for example, in the case of discrete parameter and decision spaces, the loss function can be given in a matrix form, while in the continuous case, when θ and D are identical spaces, the loss function is often given as some power of the difference $(v - d)$.

The average loss, the so-called risk, or risk function $R_\delta(v)$ is the expected value of the loss according to x: $R_\delta(v) = E_x[l(v,d)] = E_x[l(v,\delta(x))]$. For a given decision function δ, the risk is a function only of the parameter v.

One of the main points of statistical decision theory is to determine an optimal decision function. If the relation $R_{\delta_o}(v) \leqslant R_\delta(v)$ holds for each value of parameter v and for each decision function $\delta(x)$, then $\delta_o(x)$ is called the uniformly best function [1].

If a uniformly best decision function does not exist, then the Bayes solution can be applied [1]. For this, the average risk according to the parameter v is calculated from $\bar{R}_\delta = E_v[R_\delta(v)] = E_v\{E_x[l(v,\delta(x))]\}$. In the Bayes method, the decision function δ minimizing this average risk is optimal, and the minimum of the average risk is called Bayes risk.

In the minimax method, a decision function is optimal if it minimizes the maximum risk, i.e., $\min_\delta \max_v R_\delta(v)$.

THE ANALYTICAL MEASUREMENT SYSTEM AS AN INDEPENDENT SYSTEM

Characterization of the analytical measurement system requires a decision on whether it is to be considered as a unit independent of other systems, or as part of a higher-level system. Figure 1 shows a simplified scheme of the measurement system together with the information theory and decision models. The relation of these models and analogies among the elements are discussed below.

In information theory, the analytical measurement system is a communication system (Fig. 1B) where the transmitter is the material being analyzed, the coder is the measuring instrument or a classical analytical method by

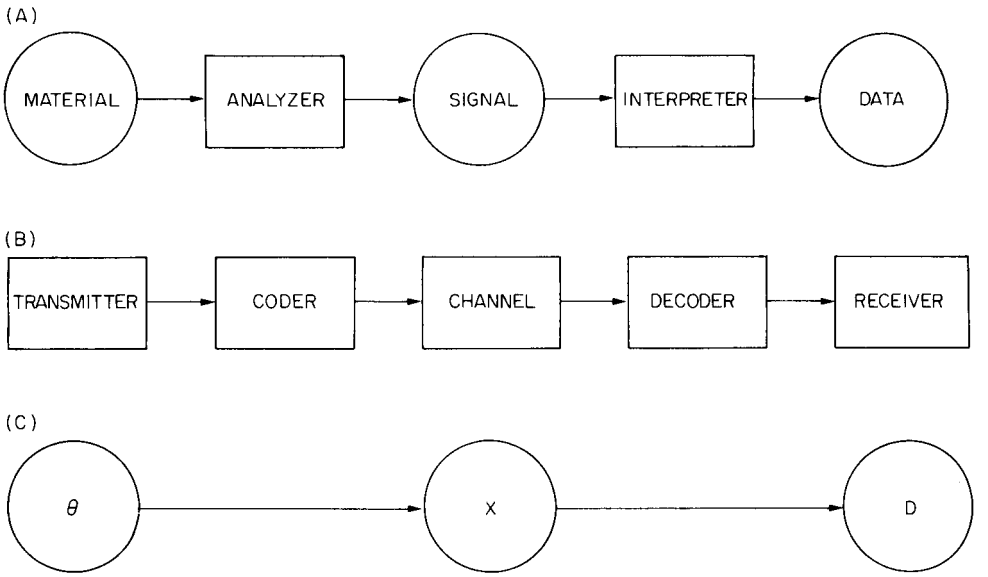

Fig. 1. The analytical measurement system as an independent system. (A) The analytical measurement system; (B) the information theory system; (C) the decision theory system.

which the analytical information of the material is coded into a signal (spectrum, potentiometric curve, chromatogram, formation of precipitation, etc.), the decoder is the signal interpretation (e.g., calibration curve, data bank) that produces the qualitative or quantitative chemical information from the signal, and the receiver is the operator or user. The system can also be described by decision theory model (Fig. 1C). The material is characterized by values of parameter space θ, i.e., by qualitative or quantitative parameters. The purpose of the measurements is to determine the value of this parameter. Therefore an element of sample X is observed, which is connected to v. On the basis of this observed element, which is usually a physical signal, a statement is made concerning the quality of the material. The possible statements create the decision space D. Spaces θ and D are equivalent, both containing qualitative or quantitative parameters of the material, and the sample space X is the signal space. An important part of the decision theory model is the decision function, which corresponds to signal interpretation. The chemical information is a function of the analytical signal, and the qualitative or quantitative parameter of the material can be determined only if the decision function is known. The decision function is established by calibration and training.

For the calibration method, both the analytical signal and the qualitative or quantitative parameter must be known. The unknown parameter can be determined in a reverse manner, i.e., the qualitative or quantitative parameter is estimated from the known analytical signal and from the known decision

function. The analysis of a material with an unknown parameter is simply a reproduction of decisions concerning materials with known parameters. This means, for example, that every qualitative analysis of an unknown material must be preceded by a qualitative analysis of the same known material. The training or calibration must extend over all materials because the decision function varies from material to material. Accordingly, with this model, it is impossible to detect on the basis of the analytical signal any chemical species that has not been detected previously by the given measurement system. This means that without the decision function, the chemical information cannot be extracted from the analytical signal.

In the case of quantitative analysis, it is not necessary to determine the signal for each concentration value during the calibration, because there is generally a simple mathematical relationship (linear, logarithmic, etc.) between the analytical signal and the concentration. The decision function can then be considered as a continuous function of known type over a given concentration interval, and so can be determined by a few points, with interpolation of other values.

Any chemical analysis is done to decrease the uncertainty of knowledge concerning a parameter v characterizing the material qualitatively or quantitatively. In information theory, the uncertainty of knowledge can be characterized by the entropy of the relevant knowledge, and hence decreased uncertainty, i.e., analytical efficiency, can be characterized by decreased entropy, i.e., by the difference between the entropies before and after the analysis (the transinformation). The signal-producing unit can be characterized by the transinformation $I(\theta;\mathrm{X})$, the signal interpretation unit by the transinformation $I(\mathrm{X};\mathrm{D})$, and the whole analytical system by the transinformation $I(\theta;\mathrm{D})$.

The error of the measurement system can also be characterized by the decision theoretical model. The uncertainty of the signal production mapping $\theta \rightarrow \mathrm{X}$ can be characterized by the distribution function $F(v,x)$. The signal interpretation mapping $\mathrm{X} \rightarrow \mathrm{D}$ (i.e., the decision function) contains further errors that depend on the training. Because of these errors, the decision d concerning the required quality or quantity is only an estimate of the true value of the parameter v.

The validity of this estimate can be characterized by the loss function $l(v,d)$. Like the transinformation, the risk $R_\delta(v)$ is a measure of the validity of the measurement system. If $I(\theta;\mathrm{D}) = H(\theta)$ or $R_\delta(v) = 0$, the information transfer is perfect, or the decision is a deterministic one, respectively. The less the transinformation, or the bigger the risk the worse will be the analysis. If there is no information transfer, i.e. the measurement system does not work, then $I(\theta\mathrm{D}) = 0$, and the risk takes its maximum value. Thus the concepts of transinformation and risk are equivalent in characterizing the validity of the analytical system.

THE ANALYTICAL MEASUREMENT SYSTEM AS A SUB-SYSTEM

The analytical measurement system is not generally independent, but forms part of a higher-level system, e.g., participating in the control of a process, producing information (Fig. 2). This measurement system can be regarded as an information channel: information passes from the controlled process (i.e., from the transmitter) to the measurement system to the control element to the receiver. In the decision model, the parameter space θ describes the state of the controlled process, the measurement system is the sampling process (i.e., the mapping of θ into X) and the decision space D contains the decisions of the control. In this model, spaces θ and X are equal and space D is different.

In the model treated in the previous section, the information-producing and decision processes were both parts of the analytical system, while in this case the decision process takes place on a higher level than the analytical measurement process which therefore forms a sub-system of the control process. Accordingly, the goal of this measurement sub-system will be determined by the goal of the whole system, and the value of the analytical information can be determined only by considering the control problem.

Information theory deals only with the quantity of information and does not consider its quality, value and utility; it treats the information system itself, unrelated to a higher-level control system (i.e., a receiver). Statistical decision theory can be used to characterize more completely the information obtained by the analytical measurement.

The aim of obtaining the analytical information here is to optimize the decision process in a higher-level control system. The control decision must be taken without knowing the exact value of the parameter v characterizing the state of the controlled process. The measure of the uncertainty in the knowledge concerning v is the entropy $H(\theta)$. To decrease $H(\theta)$, chemical

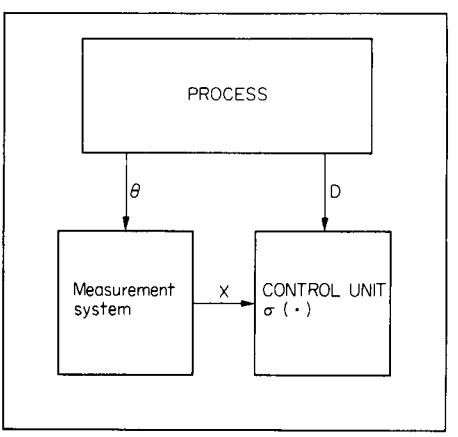

Fig. 2. The measurement system as a subsystem of a controlled system. The process is considered as the transmitter, the measurement system as the information channel and the control unit as the receiver.

analysis is done to provide an estimate of parameter υ by the observed values x of sample space X. After the variable x has been measured a conditional entropy $H(\theta|X)$ can be given for θ. The quantity of the information produced by the analytical measurement is the average mutual information, i.e., $I(\theta;X) = H(\theta) - H(\theta|X)$. Calculation on the average mutual information establishes only the quantity of information obtained by the analysis; its value and utility can be treated only in connection with the loss function concerning the decision. The same quantity of information can have different values in different decision problems, e.g., the value of the information is obviously greater in controlling pharmaceutical production than a pesticide.

The value of information can be defined on the basis of the decrease or risk caused by the information. The value of the information as a function of parameter υ is defined as the differences between the risks with and without analysis, using a certain decision function δ.

The risk without analysis is the expected loss value according to the variable x:

$$R_\delta^b(\upsilon) = \underset{x}{E}[l(\upsilon,\delta(x))] = \int_{x\in X} l(\upsilon,\delta(x))f_b(x|\upsilon)\,dx$$

where the density function $f_b(x|\upsilon)$ denotes the distribution of the estimate of parameter υ relative to the true value of υ.

If it can be assumed that the analytical measurements are without error, then the value of x is known (x_a) and the risk with the analysis is $R_\delta^a(\upsilon) = l(\upsilon,\delta(x_a))$. In this case, the value of the information obtained by the analytical measurement is

$$V_\delta(\upsilon) = \int_{x\in X} l(\upsilon,\delta(x))f_b(x|\upsilon)dx - l(\upsilon,\delta(x_a))$$

If the analytical result is stochastic, then the risk with analysis is

$$R_\delta^a(\upsilon) = \underset{x}{E}[l(\upsilon,\delta(x))] = \int_{x\in X} l(\upsilon,\delta(x))f_a(x|\upsilon)\,dx,$$

where $f_a(x|\upsilon)$ denotes the conditional density function of the variable related to the parameter value υ. Consequently the value of information obtained by the analysis is generally

$$V_\delta(\upsilon) = R_\delta^b(\upsilon) - R_\delta^a(\upsilon) = \int_{x\in X} l(\upsilon,\delta(x))f_b(x|\upsilon)dx - \int_{x\in X} l(\upsilon,\delta(x))f_a(x|\upsilon)\,dx$$

The average value of information which is independent of parameter υ can be defined as the difference of average risks with and without analytical measurements. For this calculation, the distributions of υ without analysis $F(\upsilon)$ and with analysis $F(\upsilon|x)$ must be known. The average value of information for a given decision function δ is

$$\bar{V}_\delta = \bar{R}_\delta^b - \bar{R}_\delta^a \doteq \underset{\upsilon}{E}[\underset{x}{E}[l(\upsilon,\delta(x))]] - \underset{\upsilon}{E}[\underset{x}{E}[l(\upsilon,\delta(x))]] = \int_{\upsilon\in\theta}\int_{x\in X} l(\upsilon,\delta(x))f_b(x|\upsilon) \times f(\upsilon)dx\,d\upsilon - \int_{\upsilon\in\theta}\int_{x\in X} l(\upsilon,\delta(x))f_a(x|\upsilon)f(\upsilon|x)dx\,d\upsilon$$

Increasing the quantity of information by analysis does not necessarily involve increasing the value of the information. The connection between these two concepts depends on the loss function. If the form of the loss function means that its expected value cannot be decreased by more precise estimation of parameter v, then it is useless to increase unduly the quantity of information. To obtain information always involves cost, and it becomes necessary to consider whether or not increasing the quantity of information increases its value, and if any increase in value involves excessive costs from an economic point of view.

Obtaining information, i.e. decreasing the entropy of the information about the controlled process, can involve not simply one analysis, but the consecutive steps of the analytical measurement. In this case, the decision space D contains the decision to obtain further information in addition to several possible actions of control and regulation. This is called sequential decision. A practical model, not based on decision theory, has been given by Müskens [8] to optimize sampling frequency, i.e., to optimize the information entropy.

To summarize, the information obtained by the analytical measurements decreases the uncertainty of the true value of parameter v, and also the risk of the decision. But the transinformation describes only the analytical measurement system as a unit, whereas the risk, and so the value of information, characterizes the whole control system. Accordingly, from the economic point of view, the selection of an appropriate analytical measurement system for a certain problem must be decided on the basis of the loss, risk and cost. This leads to a decision on how precisely the true value of parameter v must be estimated.

The loss function was considered only formally in considering the value of information obtained by the analytical measurement and of its average value. These quantities are, however, important if they are expressed in financial terms in connection with the total problem; the real loss, risk and value of information become more obvious, and both the analytical measurement system and the controlled process can be examined together from the point of view of economics.

REFERENCES

1 I. E. Frank, E. Pungor and G. E. Veress, Anal. Chim. Acta, 133 (1981) 433.
2 C. E. Shannon, The Mathematical Theory of Communication; University of Illinois Press, Urbana, 1949.
3 F. M. Rexa, An introduction to Information Theory, McGraw-Hill, New York, 1961.
4 L. P. Hyvärinnen, Information Theory for Systems Engineers, Springer, Berlin, 1968.
5 A. Wald, Statistical Decision Functions, J. Wiley, New York, 1950.
6 P. J. Bickel and K. A. Doksum, Mathematical Statistics, Basic Ideas and Selected Topics, Holden-Day, San Francisco, 1977.
7 T. Ferguson, Mathematical Statistics, A Decision Theoretic Approach, Academic Press, New York, 1967.
8 M. Müskens, Anal. Chim. Acta, 103 (1978) 445.

Analytica Chimica Acta, 133 (1981) 451—456
Computer Techniques and Optimization
Elsevier Scientific Publishing Company, Amsterdam — Printed in The Netherlands

Short Communication

SYSTEMATIC COMPUTER-AIDED INTERPRETATION OF VIBRATIONAL SPECTRA

T. VISSER and J. H. VAN DER MAAS*

Laboratory for Analytical Chemistry, University of Utrecht, Croesestraat 77A, 3522 AD Utrecht (The Netherlands)

(Received 19th November 1980)

Summary. The diagnostic value of an interpretation system for vibrational spectra has been investigated in relation to the number of structural units the system can cope with. For five structural units the correlated wavenumber intervals are derived from three infrared and three Raman files by the CRISE program. The interpretative value of each interval in relation to the intensity threshold is discussed. For most intervals a decrease is found on increasing the number of structural units.

Experience with the development of interpretation systems for infrared and for Raman spectra [1, 2] revealed an essential need for insight into the different relevant factors. The interpretation process was therefore studied in detail [3]. It appeared that the interpretative value of wavenumber intervals correlated with structural units (S_i), and therefore the value of interpretation systems, is determined by only two parameters, the score percentage (*SP*) and the interfering percentage (*IP*). These two parameters lead to three types of interval (specific, pseudo-specific and selective) and systems can be compared objectively. The intervals and the corresponding *SP* and *IP* values can be obtained from a collection of coded spectra by means of the CRISE computer program.

For the development of systems, it is important to know to what extent the interpretative value of a wavenumber interval is related to the structural units in the system. This aspect was therefore investigated further by using the CRISE program.

Experimental

Two collections of spectra (infrared and Raman) were used; both contained the spectra of the same 549 liquid organic compounds. The samples (purity over 98%, g.l.c. checked) were all combinations of the atoms CH (161), CHO (333), CHN (51) and CHON (4).

Infrared spectra were recorded on a Perkin-Elmer 180 spectrometer and the Raman spectra on a Spectra-Physics model 700. For all spectra the accuracy was equal to or better than 2 cm^{-1}. The intensity of the most

0378—4304/81/0000—0000/$02.50

intense band in each spectrum or spectral region was set between 85 and 95 scale divisions. More detailed information about the scanning conditions has been given [3]. From these two collections, two smaller files were assembled for each technique: one with the data of 161 hydrocarbons (I) and one with additionally 172 O—H and C—O compounds (II). The main collection (III) also included carbonyl and nitrogen derivatives.

For all three files and for both techniques the presence of specific (*SP* = 100%, *IP* = 0%), pseudo-specific (SP < 100%, IP = 0%) and selective (*SP* = 100%, *IP* > 0%) intervals was established in relation to the intensity threshold (*IT*) by means of the Fortran Extended IV program CRISE. The number of intervals was restricted by setting a minimum *SP* of 4% and a maximum width of 300 cm^{-1}. For obvious reasons, intervals which are not related to any fundamental vibration of the structural unit (S_a) under consideration were disregarded. Data calculations with CRISE were performed on a Cyber-175 computer requiring 42K words of main memory and a calculation time of 0.5—5 CPU seconds per investigated structural unit.

Discussion and results

For a certain structural unit S_a, the score percentage of a pseudo-specific interval can be altered on changing the intensity threshold. A change of *IT* influences the presence or absence not only of S_a peaks (direct effect), but also of interfering S_i peaks which define the width of the pseudo-specific interval (indirect effect).

If an increase in *IT* results in a decrease of *SP*, then the interfering S_i peaks must be more intense than the S_a peaks. If *SP* increases, this implies that the S_i peaks are weaker than the S_a peaks. For that reason high *SP*-values at low *IT* values indicate the absence of interfering peaks.

For each of the investigated structural units, —C—H, C=C, C≡C, C—O and O—H, the results are discussed below. The slopes of the maximum score percentages reached, SP_{max}, in relation to *IT* are displayed in the Figs. 1—5.

The —C—H group. Specific intervals are not found for this group. Pseudo-specific intervals with $SP_{max} > 90\%$ are present between 2997 and 2821 cm^{-1} for i.r. spectroscopy and between 2967 and 2633 cm^{-1} for Raman spectroscopy. All intervals are related to the —C—H stretching vibration except for one (Raman file I, *IT* = 3%) that bears on the —C—H bending vibrations (1466—1418 cm^{-1}). Selective intervals are found for i.r. spectra in all three files at *IT* < 10% (3007—2887 cm^{-1}, *IP* = 50%); in Raman spectroscopy, such selective intervals are absent from file III because of the absence of C—H bands in some of the spectra.

As can be seen from Fig. 1, SP_{max} for Raman spectra shows little dependence on the files whereas for i.r. spectra a slight decrease shows up for file III compared with I and II. As selective intervals (*SP* = 100%, *IP* > 0%) are found, this effect must be attributed to the increased presence of interfering peaks in i.r. file III.

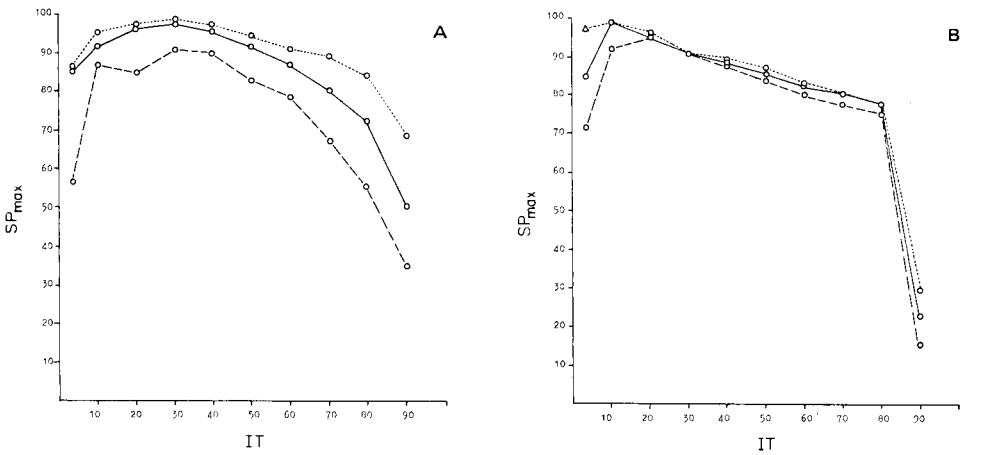

Fig. 1. SP_{max} as a function of IT for the —C—H structural unit: (A) infrared; (B) Raman. (○) —C—H stretching; (△) —C—H bending; (. . .) File I; (—) File II; (- - -) File III.

The C=C group. Specific intervals are absent for two reasons: (i) some vibrations are inactive in i.r., and (ii) C=C=C compounds do not give rise to a peak in the C=C region around 1600 cm^{-1} in i.r. or in Raman spectra. Pseudo-specific intervals are present. As can be seen from Fig. 2A, the shape of the curves for i.r. is rather erratic which is probably due to the appearence of three different SP_{max} intervals: =C—H (3048—3010 cm^{-1}), C=C (1681—1490 cm^{-1}) and $\delta_{=C-H}$, out-of-plane (772—653 cm^{-1}). In the Raman spectra all intervals are related to the C=C band. In the i.r., the decreased SP_{max} for file III is caused by an increase of interferences: the C=O peak(s) in the C=C stretching region and the skeletal modes in the =C—H out-of-plane region. In

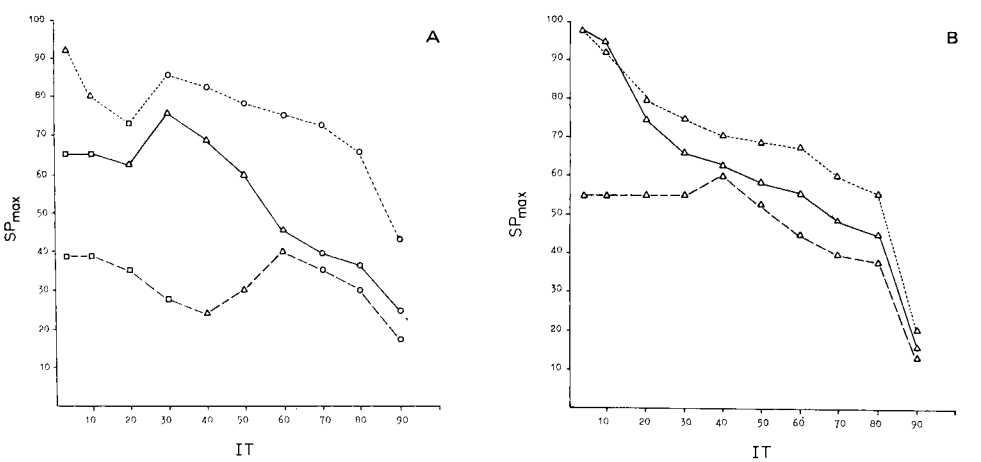

Fig. 2. SP_{max} as a function of IT for the C=C structural unit: (A) infrared; (B) Raman. (△) C=C stretching; (□) =C—H stretching; (○) =C—H out-of-plane; (...) File I; (—) File II; (- - -) File III.

the Raman, the interferences of C=O bands are rather small as in general the intensity of carbonyl bands is low-to-medium compared with most of the C=C bands.

The C≡C group. In Raman spectroscopy, a specific interval is found for all three files as a result of the intense C≡C band (2320—2065 cm^{-1}). In i.r. spectroscopy, there is no specific interval because of the inactivity of some C≡C vibrations. Nevertheless, useful pseudo-specific intervals are found based on the ≡C—H band (3318—3297 cm^{-1}) and the C≡C band (2273—2092 cm^{-1}). As can be seen from Fig. 3A, the SP_{max} for file II for some *IT* values is even higher than for file I, indicating that interferences of O—H bands in the ≡C—H region is very small. In file III the lower SP_{max} values at $IT < 60\%$ are attributed to interference by N—H bands. For obvious reasons there is no selective interval in the i.r. spectra.

The O—H group. As expected, there are no specific intervals. In the i.r. spectra, the ≡C—H and N—H bands interfere in the O—H stretching region around 3300 cm^{-1}; moreover, the O—H group of carboxylic acids seldom gives rise to a peak in that area. For the Raman spectra, an SP_{max} of even 4% is unattainable because of the very small polarizability of the O—H bond. As can be seen from Fig. 4, SP_{max} reaches 94% for i.r. spectra in file II, which indicates that there is little interference from ≡C—H bands. The large decrease to an *SP* value of only 35% in file III is the result of N—H interference and the aberrant behaviour of the carboxylic acids. The latter phenomenon also explains the absence of a selective interval in file III whereas it is present in II (3575—3238 cm^{-1}, $IP = 3\%$).

The C—O group. Specific intervals are absent in the i.r. spectra because of skeletal modes which coincide with the C—O stretching around 1100 cm^{-1}, and in the Raman spectra because of the small activity of the C—O vibration(s). As can be seen in Fig. 5, there are pseudo-specific intervals, e.g., at 1248—1018 cm^{-1} with an SP_{max} value of 70% for file II but of only 14% for

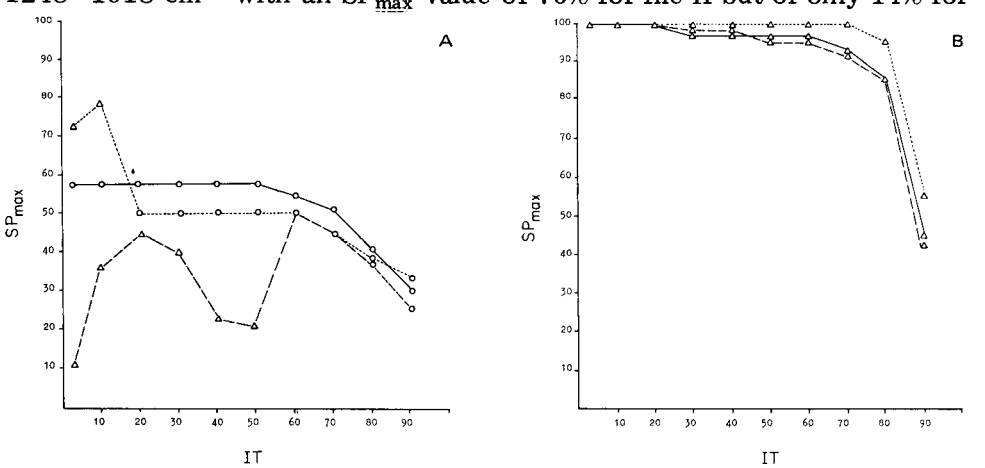

Fig. 3. SP_{max} as a function of *IT* for the C≡C structural group: (A) infrared; (B) Raman. (○) ≡C—H stretching; (△) C≡C stretching; (. . .) File I; (—) File II; (- - -) File III.

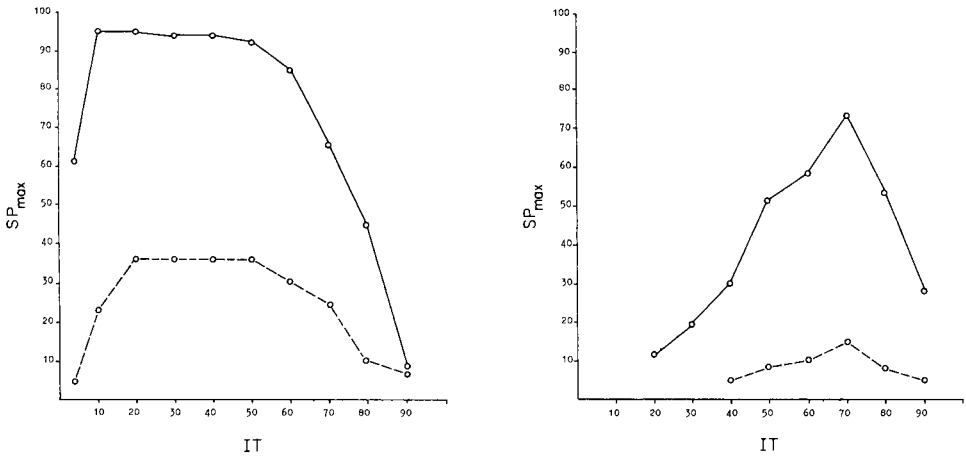

Fig. 4. SP_{max} as a function of IT for the O—H group (infrared): (○) O—H stretching; (—) File II; (- - -) File III.

Fig. 5. SP_{max} as a function of IT for the C—O group (infrared): (○) C—O stretching; (—) File II; (---) File III.

file III. This large difference is attributed to an increased influence of skeletal vibrations in the latter file. For the same reason, the interfering percentage (IP) of the selective interval for file II (1228—997 cm^{-1}) has increased from 16 to 77% in file III (1285—985 cm^{-1}). Obviously there is no selective interval for Raman spectroscopy.

Conclusions

The number of selective intervals proves to be very small; some structural units have none. Most of the available intervals are attended by a high interfering percentage. Therefore it can be concluded that the usefulness of selective intervals is limited.

In a spectrum, the intensities of all peaks are related to the strongest peak, because of the scanning conditions chosen. Changes of these conditions as far as peak intensities are concerned are equivalent to changes of the intensity threshold IT. As is clear from Figs. 1—5, either the SP_{max} versus IT curves for all structural units show a maximum (between IT = 3% and IT = 90%) or the highest SP_{max} value is found at the lowest IT and close to 100%. It follows that alteration of the scanning conditions will lead neither to different, nor to (much) better results. This indicates that the scanning conditions used were chosen quite well. From Figs. 1—5, it also appears that extending the number of structural units leads to a decrease of the SP_{max} values for almost every unit. Therefore it can be concluded that the diagnostic value (SP_{max}) of an interval in a system will be larger the fewer the structural units that the system can cope with.

REFERENCES

1 T. Visser and J. H. van der Maas, J. Raman Spectrosc., 7 (1978) 291.
2 C. G. A. van Eijk and J. H. van der Maas, Fresenius Z. Anal. Chem., 291 (1978) 291.
3 T. Visser and J. H. van der Maas, Anal. Chim. Acta, 122 (1980) 363.

Analytica Chimica Acta, 133 (1981) 457—462
Computer Techniques and Optimization
Elsevier Scientific Publishing Company, Amsterdam — Printed in The Netherlands

Short Communication

CONSTRUCTION OF SMALL DATA BASES FOR TRACE ELEMENT DETERMINATIONS

KIYOKATSU JINNO* and TATSUNORI KOIZUMI
School of Materials Science, Toyohashi University of Technology, Toyohashi 440 (Japan)
(Received 7th July 1980)

Summary. Construction of a small data base intended as a model for personal use in the area of trace element determinations is described. A MELCOM 7000 computer is used and several types of on-line conversational retrieval systems are discussed.

Many large-scale data banks are now available in different areas of information. Because these usually contain excess of information for particular purposes and are increasingly in demand, smaller data bases for individual use have become important [1]. The present communication describes the construction of a model data base for trace element determinations. The aims were to provide a source of primary information on trace characterization and to create an on-line system for remote users. The problems arising in the construction of a small data base with the data base management system of a commercial computer are also discussed.

Data collection

In trace element characterization, the detection limit, especially in terms of the absolute amount, available with an analytical technique, is of particular interest. Such information was collected in two ways. First, data were collected from the main journals of analytical chemistry over the past 2 years, from papers concerned with inductively-coupled plasma emission spectrometry (i.c.p.e.s.), atomic absorption spectrometry, atomic emission spectrometry, neutron activation, etc. Secondly, laboratory measurements, mainly by i.c.p.e.s., were utilized. At present, about 650 data records have been collected, and these form the data base. The number will be increased in the future.

*Present address: Department of Chemistry, University of California, Irvine, CA 92717, U.S.A.

0378—4304/81/0000—0000/$02.50

The data management system

To construct an objective data base, an extended data management system (EDMS; Mitsubishi, MELCOM manuals, NM-SROO-54A(84CO) and NM-SROO-98A(8ZAI)) was used. The EDMS operates under the UTS/VS, the operating system of the MELCOM 7000 COSMO II, and is the general-purpose data management system based on that suggested by CODASYL DBTG. The EDMS has the following support languages: data description language (DDL), data manipulation language (DML), end user language (EUL) and reconstruction process control language (RPCL). The EDMS system consists of the following program modules: file definition processor (DMSFDP), data base management library (DBM Library), data base reconstruction subsystem (REST), interactive data base processor (IDP) and support utilities including an initialization processor (DMSINIT), dump processor (DMSDUMP), load processor (DMSLOAD) and summary statistics processor (DMSSUMS).

The data structures of EDMS data base may be defined from the viewpoints of the logical relationships of data (logical structure), the logical arrangement of data (storage structure), and the physical layout of data (physical structure). These data structures may be collected as a Scheme file by the data base administrator, and the EDMS system manages data by referring to this Scheme. The data base can, however, be used via application programs or the IDP processor; in this case, a Subscheme file, which is subset of the scheme file and is a map of a programmer's view of the data used, is referred to by EDMS. The relationships of these data structures, data base, and application programs are shown in Fig. 1.

In the EDMS data base, a network structure can be attained. The smallest unit of named data is called an item. A group of items is made up after consideration of the data type and user's needs. The group is given a name and is referred to as a whole. Finally, the data set is established between groups of items; the data set is the named collection of logically related items.

Design and construction of data base

The collected data items. A data record contains the data items [2] listed in Table 1. Some of these items deserve comment. Under METHOD, the full name of the analytical method is given; as different names are often applied to the same method, a logical compilation of terms is planned for the future. With regard to detection limits (DETECLIM), numerical values are always

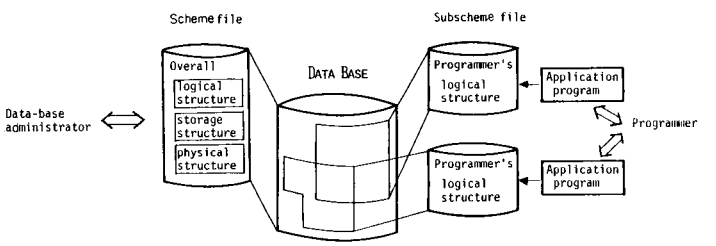

Fig. 1. The relationships of data base, data structure, and application programs.

measured under particular analytical conditions, which can be described under the item DETECCOM. The range available (RANGEMAX) is the maximum range available (in micrograms); if experimental data are not available, NULL is entered as the input data. Matrix size (MATSIZE) must be known in trace analysis, because the minimum detectable concentration is obtained from the detection limit and the sample size. Literature information is then added, with the full title of the paper concerned. Interferences with the analytical measurements are listed under INTERFER. Any additional information is entered under COM.

To store a complete data record containing these items in the EDMS data base, DDL items are of variable type and size, as shown in Table 1. An example of a typical data record is shown in Table 2.

Retrieval key items and item grouping. It is very important in defining the data structures to designate retrieval key items. The following nine items were chosen as the retrieval keys: NO, ELECON, METHOD, MATRIX, DETECLIM, AUTHOR, JNL, CODEN and YEAR.

After careful consideration of the type of data, the flow of retrieval, and the frequency of use of key items, data items were grouped into several sets as shown in Fig. 2. DATAJ and DATAM are grouped by the consideration that these data (reference information and analytical information, respectively), are frequently required and are conveniently divided into two groups. DATAD provides the numerical information. DATAT is separated from DATAJ because it is not a key item. DATAC is a subinformation group.

The logical relationships between the group items were established by data sets (e.g., SETMD, SETMD). Several support groups were also con-

TABLE 1

The list of data items

DDL items	Variable type and size	Explanation
NO	A 4	Serial number
ELECON	A 16	Element
METHOD	A 72	Method
MATRIX	A 40	Matrix
DETECLIM	A 12	Detection limit (μg)
DETECCOM	A 4	Notation of detection limit
RANGEMAX	A 12	Range available (μg)
RANGECOM	A 4	Notation of range available
MATSIZE	A 8	Matrix size
AUTHOR (8)	A 20	Author
YEAR	I 4	Year of publication
CODEN	A 8	CODEN
JNL	A 72	Journal
TITLE (3)	A 80	Title
INTERFER	A 80	Interference
COM (3)	A 72	Comments

TABLE 2

A typical data record

NO	: 1
ELEMENT	: ALUMINUM
METHOD	: LASER-ATOMIC FLUORESCENCE
MATRIX	: SOLUTION
DETECTION LIMIT	: 0.0004 ⋆
RANGE AVAILABLE	: 6200.
AUTHOR	: WEEKS, S. J. HARAGUCHI, H. WINEFORDNER, J. D.
YEAR	: 1978
CODEN	: ANCHEM
JOURNAL	: ANALYTICAL CHEMISTRY, VOL 50, P360
TITLE	: IMPROVEMENT OF DETECTION LIMITS IN LASER-EXCITED ATOMIC FLUORESCENCE FLAME SPECTROMETRY
INTERFERENCE	:
COMMENT	: ⋆ USING PNEUMATIC NEBULIZATION

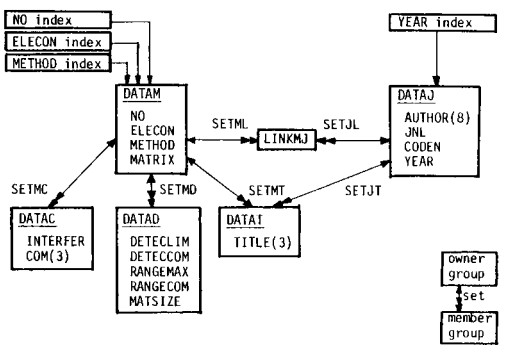

Fig. 2. The logical data structure.

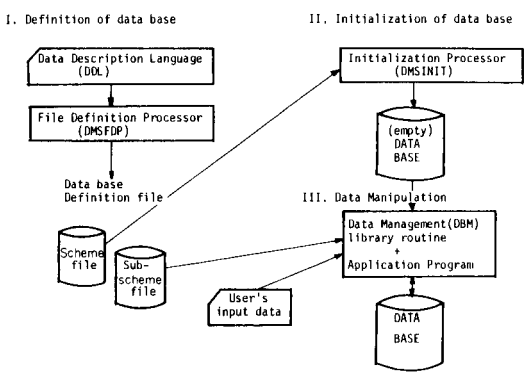

Fig. 3. The construction outline of the EDMS data base.

```
***** WELCOM TO TRAC-DB SYSTEMS *****
PRIMARY KEY ITEM?
    1:LIST UP, 2:NO, 3:ELECON
    4:METHOD, 5:-----
?3
***** RETRIEVE BY KEY ITEM:ELECON *****
* SECONDARY KEY ITEM REQUIRED?
    (0:---, 1:METHOD, 2:DETECLIM)
?1
WHEN ELECON=?
?CADMIUM
***    19  DATA FOUND     ELECON=  CADMIUM
WHEN METHOD=?
?NEUTRON ACTIVATION ANALYSIS
***     1  DATA FOUND
* TERTIARY KEY ITEM REQUIRED?
    (0:---, 1:DETECLIM)
?0
** OUTPUT DATA, YES OR NO?
?Y
** OUTPUT MODE, A,B, or C?
?A
NO                  69
ELEMENT             CADMIUM
METHOD              NEUTRON ACTIVATION ANALYSIS
MATRIX              WATER                                    1 L
DETECTION LIMIT     0.4
RANGE AVAILABLE     NULL
AUTHOR              LEWVIC,K.          STEINNES,E.       PAPPAS,A.C.

YEAR                1978
CODEN               ACACAM
JOURNAL             ANALYTICA CHIMICA ACTA, VOL 97, P295
TITLE               THE SIMULTANEOUS DETERMINATION OF ARSENIC,CADMIUM,COBALT
                    IN FRESH WATER BY NEUTRON ACTIVATION ANALYSIS

INTERFERENCE
COMMENT


** ELEMENT ACCESS CONTINUE? YES OR NO
?N
```

Fig. 4. Example of retrieval (1); key item = ELECON, METHOD.

```
** SYSTEM ACCESS CONTINUE? YES OR NO?
?Y
PRIMARY KEY ITEM?
    1:LIST UP, 2:NO, 3:ELECON
    4:METHOD, 5:-----
?4
***** RETRIEVE BY KEY ITEM:METHOD *****
* SECONDARY KEY ITEM REQUIRED?
    (0:---, 1:ELECON, 2:DETECLIM)
?0
WHEN METHOD=?
?ATOMIC ABSORPTION SPECTROMETRY
***     7  DATA FOUND     METHOD=  ATOMIC ABSORPTION SPECTROMETRY
** OUTPUT DATA, YES OR NO?
?Y
** OUTPUT MODE, A,B, or C?
?C
NO                  50
ELEMENT             BISMUTH
METHOD              ATOMIC ABSORPTION SPECTROMETRY
MATRIX              SOLUTION                                 1 ML
DETECTION LIMIT     0.1
RANGE AVAILABLE     NULL

NO                  10
ELEMENT             ALUMINUM
METHOD              ATOMIC ABSORPTION SPECTROMETRY
MATRIX
DETECTION LIMIT     10.0
RANGE AVAILABLE     NULL

NO                  16
ELEMENT             ANTIMONY
METHOD              ATOMIC ABSORPTION SPECTROMETRY
MATRIX              WATER
DETECTION LIMIT     0.02
RANGE AVAILABLE     1.6

NO                  36
ELEMENT             BARIUM
METHOD              ATOMIC ABSORPTION SPECTROMETRY
MATRIX              SOLUTION                              0.020 ML
DETECTION LIMIT     0.000003    *

(The rest is omitted.)
```

Fig. 5. Example of retrieval (2); key item = METHOD.

structed: the subindex group of NO, ELECON, METHOD and YEAR, and the link group LINKMJ between DATAM and DATAJ. These support groups were built because these items are frequently required together in trace element determinations.

Construction of the data base. Construction of the data base is outlined in Fig. 3. The procedures are roughly divided into three parts. First, the data base is defined; according to the data structures outlined, the DDL description was made up, and then the Scheme and Subscheme files were constructed by DMSFDP. Secondly, for initialization of the data base file, the data base area was initialized by DMSINIT, in accordance with the Scheme file. An empty data base file that had only control information was constructed. Thirdly, data storage, was done by using application programs. Data files were compiled by an Editor from the source data collected. These data on editor files were then stored in the data base area with application programs written in FORTRAN.

Data retrieval

Figures 4 and 5 show the sequence of some retrieval steps. A suitable key item is selected independently in each sequential step, and the output mode of data obtained can be chosen.

Conclusion

The test-scale data base has now been constructed, and application programs have been written for data storage and retrieval. The data base now contains only 650 data records, and several types of retrieval system have been partly achieved. The next steps are to construct practical data bases by increasing the amount of source data and by improving the application programs for retrieval. The actual performance, accuracy and precision of the retrieval system, and reconstruction of the data base also require attention.

The authors thank Dr. N. Tanaka and Dr. T. Matsuda of Tohoku University for their advice in designing the data base, and Dr. S. Sasaki and Dr. H. Abe of Toyohashi University of Technology for the use of the MELCOM 7000 computer. This research was supported by Grants-in Aids for Special Project Research (Grant No. 411701) on Trace Characterization from the Ministry of Education of Japan.

REFERENCES

1 R. E. Dessy and M. K. Starling, Anal. Chem., 51 (1979) 924A.
2 N. Tanaka, private communication.

Analytica Chimica Acta, 133 (1981) 463—467
Computer Techniques and Optimization
Elsevier Scientific Publishing Company, Amsterdam — Printed in The Netherlands

Short Communication

LEARNING-METHOD CONTROL APPLIED TO MICROCOMPUTER-ASSISTED pH TITRATIONS

TOSHIO NISHIKAWA*, ICHIRO OGASAWARA and TAI HARADA

National Chemical Laboratory for Industry, Tsukuba Research Center, Yatabe, Ibaraki 305 (Japan)

(Received 9th December 1980)

Summary. A "learning method" control is proposed, to simplify development of automatic instrumentation. The method consists of LEARN and EXECUTE stages and may eliminate other computer programming. Its capability is demonstrated by application to automatic pH titration.

Microcomputers are useful as controllers for automatic systems as well as for data processing. Recently, however, the software for such systems has tended to become rather complex, which may make it difficult for a chemist to manipulate the computing program. The present communication provides a new algorithm, called a "learning method", to ameliorate such situations. The method is discussed through application to an automatic pH titration system.

Basic principles

When an automatic chemical instrumentation system is to be developed, it is customary to analyze the experiment in detail, design the operating flow, write the computing program, and then proceed with the automatic experiment. If modification is needed, which frequently occurs in research work, the program must be rewritten.

The learning method, presented here, is based on two stages, LEARN and EXECUTE, shown schematically in Fig. 1. In the LEARN stage, the chemist instructs the computer how to manipulate the experiment. Actually, the operator simply does the chemical experiment in his own way with no knowledge of the computing program, while the computer learns the experimental algorithm, i.e., measuring the input and output signals and their time sequences, and simultaneously storing the parameters representing the algorithm in the computer memory. In the EXECUTE stage, the computer executes the chemical experiment, in the same way, according to the time schedule by deciphering the parameters previously stored in the LEARN stage. If any modifications are required, the operator re-instructs the computer instead of rewriting the program.

0378—4304/81/0000—0000/$02.50

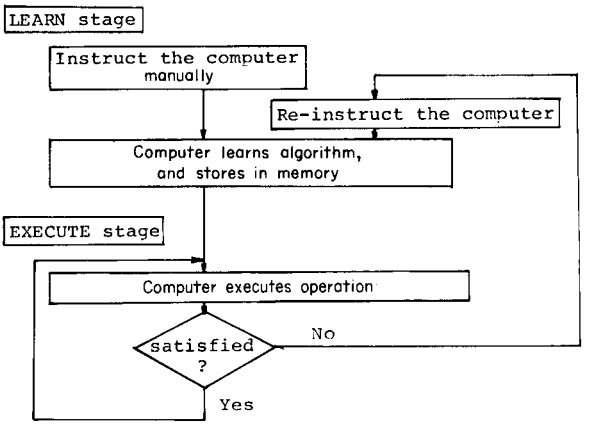

Fig. 1. Schematic flow for development of an automatic system by the "learning method".

Application to automatic pH titration

The pH titration is universally used and the normal manual technique, with slower and slower titrant additions near the end-point, is well-known. Little skill is required with the learning method and this titration was considered appropriate to test its capability.

Hardware. The hardware system consists of a pH meter with an automatic buret (Toa Dempa Co. HSS/HTS 10A) and a microcomputer (Microcomputer Associates Inc.: JOLT system; CPU: 6502, PIA: 6530, 6820, and memories: 4K byte RAM, 2K byte PROM). Figure 2 shows a scheme of the system.

The pH meter with combined glass electrode measures the pH values during the titration, and the signals are fed to the computer in digital form. The input signals to the computer are the pH reading (3 decade BCD) and the buret reading (12-bit binary via A/D converter). The on/off motion of the automatic buret, electrically driven by the stepping motor, is selected either by the manual push-button in the LEARN stage, or by the computer in the EXECUTE stage. The time interval in the buret motion is measured with the internal timer in the 6530 chip.

Software program (AUTIR). The AUTIR (automatic titration) system consists of the following programs: JOB CTRL, which controls job selection, INITIAL, LEARN, EXECUTE, and RESULT, which are integral parts of the system; several subroutines, such as interrupt timer, arithmetic facility, etc.; and the pH/time data, which are the sequences of on/off time parameters corresponding to change of pH. Program storage requires about 2K bytes, coded in the 6502 machine language, and the data area is 1K bytes. Arithmetic is done with the KIMATH floating-point subroutine package.

The INITIAL routine resets the system in hard- and soft-wares, and gets the initial parameters, such as the molarity of the standard solution and the volumes of titrant. The RESULT routine computes by using the buret readings and the above initial parameters, and then types out the titration result.

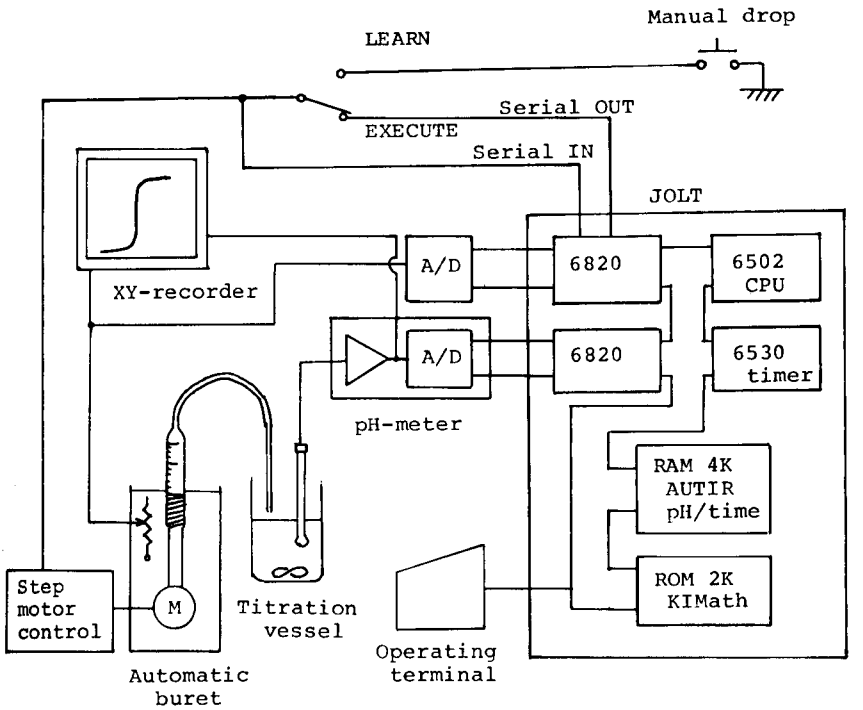

Fig. 2. Block diagram of hardware.

When the LEARN routine is entered, the internal timer starts, and the computer watches whether the buret drive signal is HI or LO, corresponding to working or idle; this reflects the manual manipulation. Whenever the buret drive signal changes its polarity (HI to LO, or LO to HI), the computer reads the pH value and stores it in the pH/time data area, together with the time data when the action occurs. In the EXECUTE routine, the computer picks up the pH/time data, which have been pre-determined in the LEARN stage, and sets the timer start. The buret is controlled (on/off) by the timer interrupt, the interval of which is determined from the pH/time data. When the pH reading exceeds the pH/time value during the titration, the computer retrieves the next pH/time data, and changes the speed of titrant addition. The computer thus does the titration automatically, by driving the buret intermittently. The flow charts of the LEARN and EXECUTE routines are given in Fig. 3.

Operation of the AUTIR system. The AUTIR system was tested in the titration of hydrochloric acid solution with sodium hydroxide solution. An example of the operational messages at the terminal is shown together with the titration curves in Fig. 4. Typical values of the pH/time data are given in Table 1; the values for the time parameters are expressed in hexadecimal.

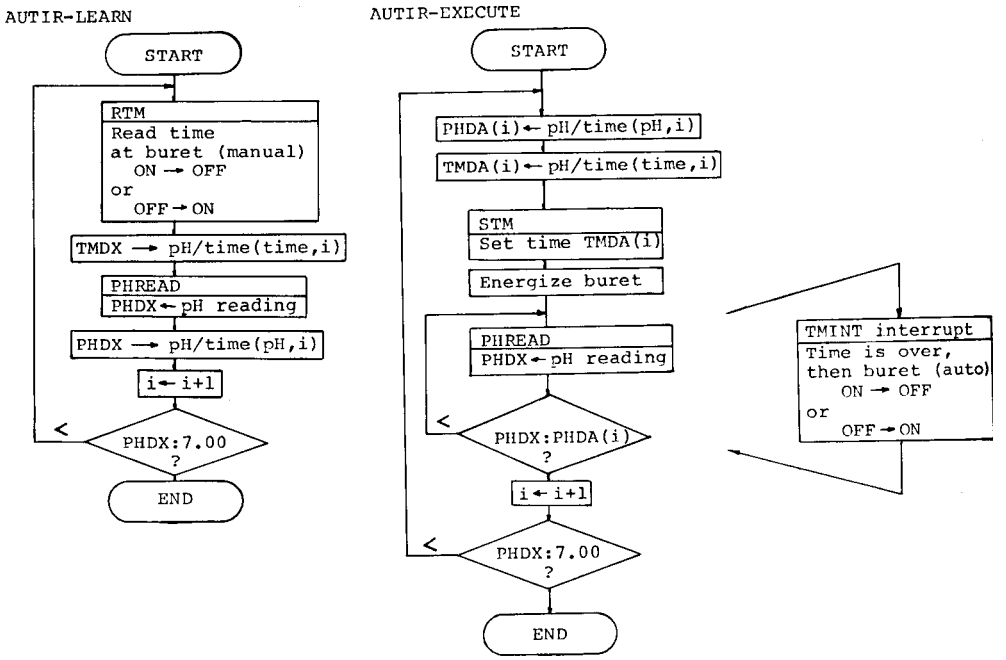

Fig. 3. Flow charts for LEARN and EXECUTE routines of AUTIR.

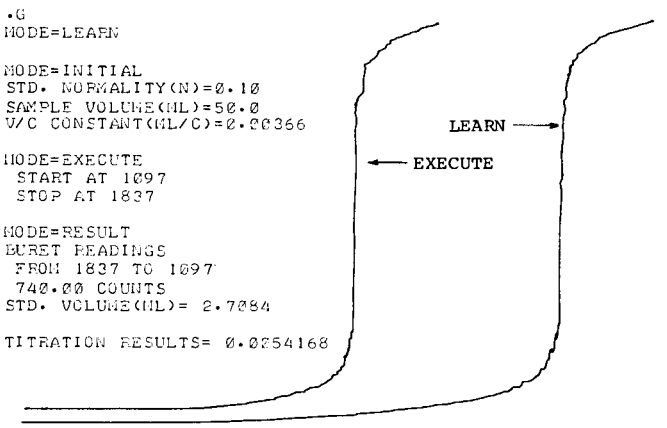

Fig. 4. An example of operation messages and titration curves.

The gradual reduction of time interval can be seen as the end-point is approached. Although the AUTIR system is capable of the titration of strong acid with strong base only, this could be applicable for any combination of acid and base, with some modifications for detecting the end-point in AUTIR program.

TABLE 1

Typical computer output of pH/time data

Time (off)	pH	Time (on)	pH	Time (off)	pH	Time (on)	pH
0E F3	02 76	1B E0	02 87	02 FD	02 90	16 F0	03 02
02 1B	03 03	17 E5	03 24	03 07	03 28	0B 6C	03 42
01 00	03 47	0D 36	03 83	09 D4	04 10	02 84	04 11
04 D6	04 33	01 85	04 37	08 19	04 71	01 15	04 73
0D 3C	05 24	02 83	05 27	03 A9	05 58	01 0E	05 75
03 C2	06 16	00 B5	06 16	04 C9	06 84	00 D4	06 91
03 15	07 28	00 D9	07 34	03 B9	07 54	00 DA	07 58
03 29	07 77	00 C1	07 79	00 00	00 00	00 00	00 00

Conclusions

The learning method, consisting of LEARN and EXECUTE stages, is effective in such automatic titrations, and it should be useful in several fields of chemical instrumentation. The prominent feature of the method is its non-mathematical control, because the instruction algorithm is determined by the operator's intuitive experiment. Possible applications would be in selective data acquisition when infrared or n.m.r. spectral lines are unevenly distributed, or in automation of delicate manipulations such as heating small quantities of chemicals, or cooling in recrystallization.

Vol. 133, No. 3

ACA announcements

ANNOUNCEMENTS OF MEETINGS

SYMPOSIUM ON "FOOD RESEARCH AND DATA ANALYSIS"

The above symposium will be held at the Voksenåsen Hotel, Oslo, Norway, on September 20–23, 1982. The symposium is intended to provide an interdisciplinary meeting ground for scientists interested in the development and use of computer aided analysis of multivariate food research data. Agronomists, microbiologists, chemists, technologists, statisticians, marketing people and psychologists with some experience in data analysis will be able to study the potential of more advanced analytic tools. Specialists in the fields of chemometrics, qualimetrics and psychometrics will have an opportunity to "shake hands".

The programme ranges from reviews of basic philosophy and available computer programmes to reports of practical results obtained by applying multivariate computer analysis to food research data. The oral contributions will be given so that food scientists without advanced knowledge in mathematics or computer science can understand.

All plenary lecturers are invited. Additional contributions are welcome and will be presented in a poster session. Lecture manuscripts and post abstracts will be published in symposium proceedings.

For further information contact: B. Eidstuen, P.O. Box 50, N-1432 Aas-NLH, Norway.

1982 WINTER CONFERENCE ON PLASMA SPECTROCHEMISTRY

The 1982 Winter Conference on Plasma Spectrochemistry, sponsored by the ICP Information Newsletter in cooperation with the Society for Applied Spectroscopy (Florida section) and the American Chemical Society (Tampa section of the Analytical Chemistry Division), will feature developments in atomic plasma spectrochemical analysis by inductively coupled plasma, d.c. plasma, and microwave plasma excitation sources. The meeting will convene on Monday, January 4 through Saturday, January 9, 1982, at the Orlando Hyatt Hotel in Kissimee, FL, U.S.A., adjacent to Walt Disney World.

Papers describing applications, fundamentals, and instrumental developments with atomic plasmas will be presented in lecture and poster sessions. General and special symposia organized and chaired by internationally recognized experts will include the following topics: 1) accuracy, precision, and optimization in plasmas; 2) applications to air, biologicals, chemicals, coal, food, metals, ores, plants, petroleum, soils, rocks, wastes, and water; 3) EPA plasma methods; 4) new instrumentation; 5) plasma detectors for chromatography; 6) plasma interferences and mechanisms; and 7) sample introduction methods. Roundtable discussion sessions will encourage an in-depth evaluation of these topics. Featured speakers will include: P.W.J.M. Boumans (Eindhoven), V.A. Fassel (Ames) and J.D. Winefordner (Gainesville).

A spectroscopic instrument exhibition and manufacturers' seminar program will complement the scheduled sessions. A plasma film festival and plasma photographic contest will also be held.

For information, contact: Dr. Ramon M. Barnes, Chairman, Department of Chemistry, GRC Towers, University of Massachusetts, Amherst, MA 01003, U.S.A.

CALENDAR OF FORTHCOMING MEETINGS

Sept. 4–8, 1981 Tokyo, Japan	**9th International Conference on Atomic Spectroscopy and 22nd Colloquium Spectroscopicum Internationale** Contact: The Japanese Society for Analytical Chemistry, 9th ICAS/22nd CSI, Gotanda Sanhaitsu, 26–2 Nishigotanda –chome, Shinagawa-ku, Tokyo 141, Japan.
Sept. 7–10, 1981 Guildford, Great Britain	**4th International Bioanalytical Forum** Contact: Dr. E. Reid, Wolfson Bioanalytical Unit, Robens Institute, University of Surrey, Guildford GU2 5XH, Great Britain.
Sept. 9–11, 1981 Coventry, Great Britain	**International Conference on Advances in Flow Measurement Techniques** Contact: Conference Organizer, BHRA Fluid Engineering, Cranfield, Bedford, Great Britain.

Sept. 10–11, 1981 Canterbury, Great Britain	**Symposium on "Concepts of Purity"** Contact: P.R.W. Baker, Dept. of Physical Chemistry, Wellcome Research Laboratories, Langley Court, Beckenham, Kent, Great Britain
Sept. 20-25, 1981 Philadelphia, PA, U.S.A.	**8th Annual Meeting of the Federation of Analytical Chemistry and Spectroscopy Societies (FACSS)** Contact: M.A. Kaiser, E.I. du Pont de Nemours & Co., Experimental Station E228/200, CR&D Department, Wilmington, DE 19898, U.S.A.
Sept. 21–24, 1981 Loughbourough, Great Britain	**Particle Size Analysis Conference** Contact: P.J. Lloyd, PSA 81 Conference, Particle Technology Group, Chemical Engineering Department, University of Technology, Loughborough, Leics. LE11 3TU, Great Britain. (Further details published in Vol. 120)
Sept. 28–Oct. 1, 1981 Barcelona, Spain	**16th International Symposium Advances in Chromatography** Contact: Dr. A. Zlatkis, Chemistry Department, University of Houston, Houston, TX 77004, U.S.A. Tel. (713) 749-2623. (Further details published in Vol. 222, No. 2)
Sept. 29–Oct. 2, 1981 Basle, Switzerland	**ILMAC 81; 8th International Exhibition of Laboratory, Chemical Engineering, Measurement and Automation Techniques in Chemistry** Contact: D. Gammeter, Secretariat ILMAC '81, Postfach, CH-4021 Basle, Switzerland. Tel. 061 26 20 20.
Oct. 27–29, 1981 London, Great Britain	**Petroanalysis 81** Contact: Miss I.A. McCann, Conference Officer, Institute of Petroleum, 61 New Cavendish Street, London W1M 8AR, Great Britain. (Tel: 01-636 1004, Telex 264380)
Nov. 23–25, 1981 Barcelona, Spain	**2nd International Congress on Analytical Techniques in Environmental Chemistry** Contact: Dr. Joan Albaigés, General Secretary, Plaza de Espana, Barcelona-4, Spain. Tel. 223 31 01.
Dec. 2–3, 1981 Paris, France	**Journées de Chromatographie en Phase Liquide** Contact: H. Colin, Laboratoire C.A.P., Ecole Polytechnique, Route de Saclay, 91128 Palaiseau Cedex, France.
Jan. 4–9, 1982 Orlando, FL, U.S.A.	**1982 Winter Conference on Plasma Spectrochemistry** Contact: 1982 Winter Conference, c/o ICP Information Newsletter, Chemistry GRC Towers, University of Massachusetts, Amherst, MA 01003, U.S.A. Tel. (413) 545-2294. (Further details published in Vol. 124, No. 2)
March 8–12, 1982 Atlantic City, NJ, U.S.A.	**1982 Pittsburgh Conference and Exhibition on Analytical Chemistry and Applied Spectroscopy** Contact: Mrs. Linda Briggs, Program Secretary, Pittsburgh Conference, Department J-057, 437 Donald Road, Pittsburgh, PA 15235, U.S.A.
March 28–April 2, 1982 Las Vegas, NV, U.S.A.	**National American Chemical Society Meeting** Contact: A.T. Winstead, American Chemical Society, 1155 Sixteenth Street, NW, Washington, DC 20036, U.S.A.
March 30–April 1, 1982 Birmingham, Great Britain	**Royal Society of Chemistry Annual Chemical Congress** Contact: Royal Society of Chemistry, Burlington House, London W1V 0BN, Great Britain.
April 5–8, 1982 Las Vegas, NV, U.S.A.	**International Symposium "Advances in Chromatography"** Contact: Prof. A. Zlatkis, Chemistry Department, University of Houston, Central Campus, 4800 Calhoun, Houston, TX 77004, U.S.A. Tel.: (713) 749-2623.
April 14–16, 1982 Amsterdam, The Netherlands	**12th Annual Symposium on the Analytical Chemistry of Pollutants** Contact: Prof. Dr. Roland W. Frei, The Free University, De Boelelaan 1083, 1081 HV Amsterdam, The Netherlands.

April 15–17, 1982 Tokyo, Japan	**International Symposium "Advances in Chromatography"** Contact: Prof. A. Zlatkis, Chemistry Department, University of Houston, Central Campus, 4800 Calhoun, Houston, TX 77004, U.S.A. Tel.: (713) 749-2623.
April 21–23, 1982 Neuherberg near Munich, G.F.R.	**Second International Workshop on Trace Element Analytical Chemistry in Medicine and Biology** Contact: Dr. P. Schramel, Gesellschaft fuer Strahlen- und Umweltforschung, Institut fuer Angewandte Physik, Physikalisch–Technische Abteilung, Ingolstaedter Landstrasse 1, D–8042 Neuherberg, G.F.R. (Further details published in Vol. 124, No. 2)
April 27–30, 1982 Munich, G.F.R.	**Biochemische Analytic Conference** Contact: Prof. I. Trautschold, Medizinische Hochschule Hannover, Karl-Wiechert-Allee 9, 3000 Hannover 61, G.F.R. (Further details published in Vol. 124, No. 2)
May 2–6, 1982 Interlaken, Switzerland	**2nd International Symposium on Instrumental TLC (HPTLC)** Contact: Dr. R.E. Kaiser, Institute for Chromatography, P.O. Box 1141, D-6702 Bad Dürkheim, G.F.R.
May 11–14, 1982 Ghent, Belgium	**4th International Symposium on Quantitative Mass Spectrometry in Life Sciences** Contact: Prof. A. De Leenheer, Symposium Chairman, Laboratoria voor Medische Biochemie en voor Klinische Analyse, De Pintelaan 135, B-9000 Ghent, Belgium.
June 6–12, 1982 Frankfurt, G.F.R.	**European Meeting on Chemical Engineering and ACHEMA Exhibition Congress 1982** Contact: DECHEMA P.O. Box 970146, D-6000 Frankfurt/M 97, G.F.R.
June 7–11, 1982 Philadelphia, PA, U.S.A.	**VI International Symposium on Column Liquid Chromatography** Contact: R.A. Barford, ERRC – SEA, U.S. Department of Agriculture, 600 Mermaid Lane, Philadelphia, PA 19118, U.S.A.
June 28–30, 1982 East Lansing, MI, U.S.A.	**35th American Chemical Society Annual Summer Symposium** Contact: A.I. Popov, Chemistry Department, Michigan State University, East Lansing, MI 48824, U.S.A.
July 11–16, 1982 Washington, DC, U.S.A.	**6th International Conference on Computers in Chemical Research and Education (ICCCRE)** Contact: Dr. Stephen R. Heller, Chairman, 6th ICCCRE, EPA, MIDSD, PM–218, 401 M Street, S.W., Washington, DC 20460, U.S.A. Tel. (202) 755–4938, Telex: 89–27–58. (Further details published in Vol. 126 and Vol. 133, No. 2)
Aug. 2–7, 1982 Pretoria, South Africa	**13th International Symposium on the Chemistry of Natural Products** Contact: The Symposium Secretariat – S.219, CSIR, P.O. Box 395, Pretoria, 0001 Republic of South Africa.
Aug. 11–13, 1982 Hameenlinna, Finland	**6th European Symposium on Polymer Spectroscopy (ESOPS 6)** Contact: Professor Johan Lindberg, Department of Wood and Polymer Chemistry, University of Helsinki, Meritullinkatu 1 A, SF 00170 Helsinki 17, Finland.
Aug. 15–21, 1982 Perth, Australia	**The 12th International Congress of Biochemistry** Contact: Brian Thorpe, Department of Biochemistry, Faculty of Science Australian National University, Canberra A.C.T. 2600, Australia.
Aug. 29–Sept. 4, 1982 Kyoto, Japan	**5th International Congress of Pesticide Chemistry** Contact: Rikagaku Kenyusho (The Institute of Physical and Chemical Research), 2–1 Hirosawa Wako-shi Saitama Pref. 351, Japan.
Aug. 30–Sept.3, 1982 Vienna, Austria	**9th International Mass Spectrometry Conference** Contact: Interconvention, P.O. Box 105, A - 1014 Vienna, Austria. (Further details published in Vol. 120)

Sept. 12–17, 1982 Kansas City, MO, U.S.A.	**National American Chemical Society Meeting** Contact: A.T. Winstead, American Chemical Society, 1155 Sixteenth Street, NW, Washington DC 20036, U.S.A.
Sept. 13–17, 1982 Petten, The Netherlands	**Practical Applications of Computers and Chemometrics in Analytical Chemistry** Contact: Dr. H.C. Smit, Laboratory for Analytical Chemistry, University of Amsterdam, Nieuwe Achtergracht 166, 1018 WV Amsterdam, The Netherlands.
Sept. 13–17, 1982 London, Great Britain	**14th International Symposium on Chromatography** Contact: The Executive Secretary, Chromatography Discussion Group, Trent Polytechnic, Burton Street, Nottingham, NG1 4BU, Great Britain.
Sept. 15–17, 1982 Petten, The Netherlands	**Chemometrics in Analytical Chemistry** Contact: Dr. H.C. Smit, Laboratory for Analytical Chemistry, University of Amsterdam, Nieuwe Achtergracht 166, 1018 WV Amsterdam, The Netherlands.
Sept. 19–24, 1982 Philadelphia, PA, U.S.A.	**9th National Meeting of the Federation of Analytical Chemistry and Spectroscopy Societies (FACSS)** Contact: Division of Analytical Chemistry, American Chemical Society, Department of Chemistry, Notre Dame, IN 46556, U.S.A.
Sept. 20–23, 1982 Oslo, Norway	**Food Research and Data Analysis** Contact: B. Eidstuen, P.O. Box 50, N-1432 Aas-NLH, Norway. Tel.: 47-2-94 08 60.
Sept. 22–25, 1981 Leipzig, G.D.R.	**Analytiktreffen 1981 – Strukturanalytische Methoden in der Stereochemie** Contact: Sektion Chemie der KMU Leipzig, Liebigstrasse 18, DDR – 7010 Leipzig, G.D.R.
July 17–23, 1983 Edinburgh, Great Britain	**SAC 83: Sixth International Conference on Analytical Chemistry** Contact: Miss P.E. Hutchinson, Royal Chemistry Society, Analytical Division, Burlington House, London W1V 0BN, Great Britain. Tel. 01–734 9971.
Aug. 28–Sept. 2, 1983 Amsterdam, The Netherlands	**9th International Symposium on Microchemical Techniques** Contact: Symposium Secretariat, c/o Municipal Congress Bureau, Oudezijds Achterburgwal 199, 1012 DK Amsterdam, The Netherlands. Tel: (020) 552 3459.

(continued from outside of cover)

Short Communications

Printed in The Netherlands.

VOL. 133. No. 3 ANALYTICA CHIMICA ACTA September 1, 1981

(Computer Techniques and Optimization, Vol. 5, No. 3)

CONTENTS

(continued on inside page of the cover)